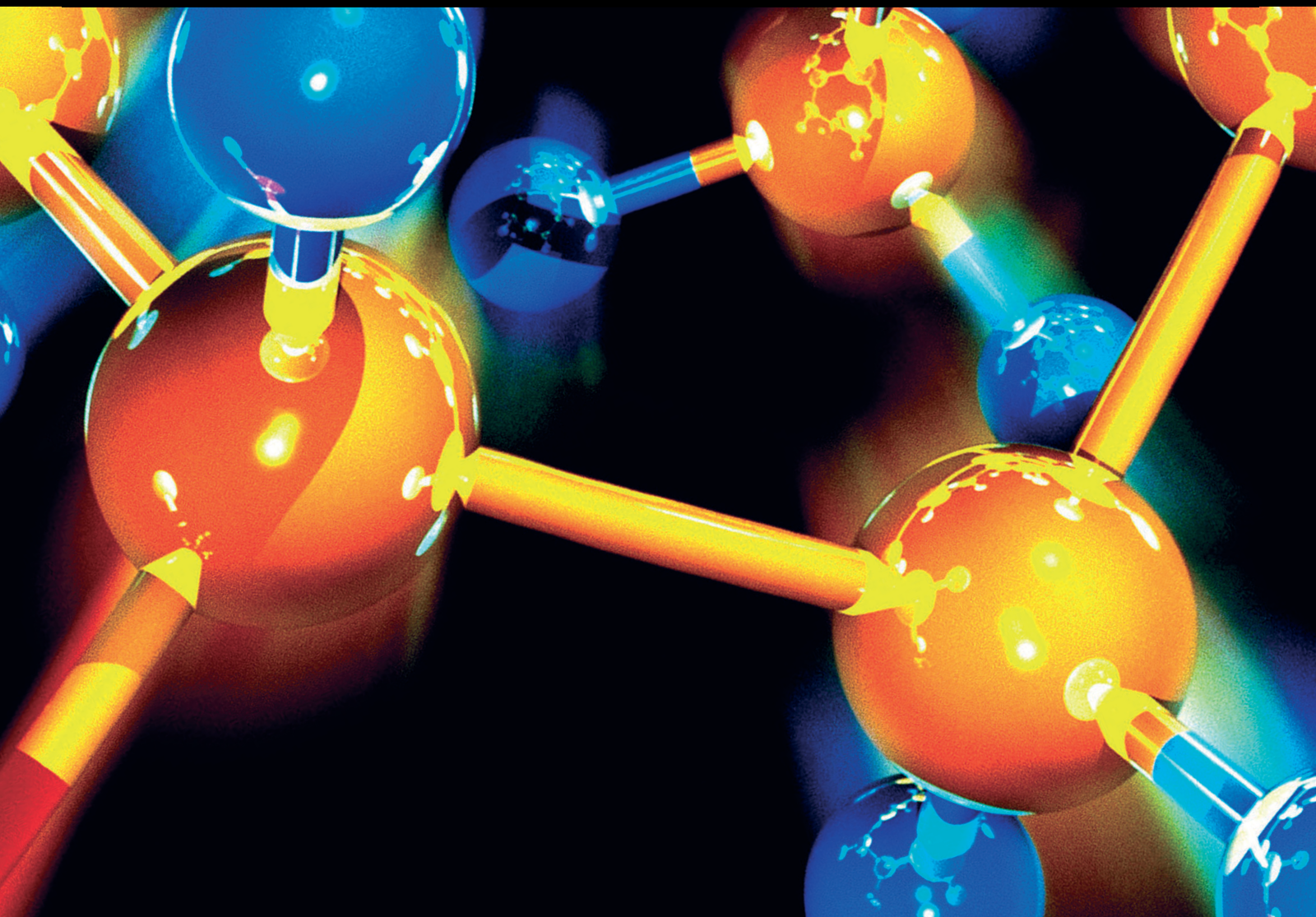


Groundwater Chemistry and Pollution in a Changing Environment: Monitoring, Mechanisms, and Remediations

Lead Guest Editor: Xubo Gao

Guest Editors: Junbing Pu, Xiaoguang Wang, Zhantao Han, and
Chengcheng Li



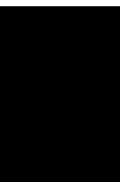


**Groundwater Chemistry and Pollution
in a Changing Environment: Monitoring,
Mechanisms, and Remediations**

**Groundwater Chemistry and
Pollution in a Changing Environment:
Monitoring, Mechanisms, and
Remediations**

Lead Guest Editor: Xubo Gao

Guest Editors: Junbing Pu, Xiaoguang Wang,
Zhantao Han, and Chengcheng Li



Copyright © 2021 Hindawi Limited. All rights reserved.


This is a special issue published in "Journal of Chemistry." All articles are open access articles distributed under the Creative Commons Attribution License, which permits unrestricted use, distribution, and reproduction in any medium, provided the original work is properly cited.

Chief Editor

Kaustubha Mohanty, India

Associate Editors

Mohammad Al-Ghouti, Qatar


Tingyue Gu , USA


Teodorico C. Ramalho , Brazil

Artur M. S. Silva , Portugal


Academic Editors

Jinwei Duan, China

Luqman C. Abdullah , Malaysia

Dr Abhilash , India

Amitava Adhikary, USA

Amitava Adhikary , USA

Mozhgan Afshari, Iran

Daryoush Afzali , Iran

Mahmood Ahmed, Pakistan


Islam Al-Akraa , Egypt


Juan D. Alché , Spain

Gomaa A. M. Ali , Egypt

Mohd Sajid Ali , Saudi Arabia

Shafaqat Ali , Pakistan


Patricia E. Allegretti , Argentina

Marco Anni , Italy

Alessandro Arcovito, Italy

Hassan Arida , Saudi Arabia


Umair Ashraf, Pakistan


Narcis Avarvari , France

Davut Avci , Turkey


Chandra Azad , USA

Mohamed Azaroual, France

Rasha Azzam , Egypt


Hassan Azzazy , Egypt

Renal Backov, France

Suresh Kannan Balasingam , Republic of Korea

Sukanta Bar , USA

Florent Barbault , France

Maurizio Barbieri , Italy

James Barker , United Kingdom

Salvatore Barreca , Italy

Jorge Barros-Velázquez , Spain

THANGAGIRI Baskaran , India

Haci Baykara, Ecuador

Michele Benedetti, Italy

Laurent Billon, France

Marek Biziuk, Poland

Jean-Luc Blin , France

Tomislav Bolanca , Croatia

Ankur Bordoloi , India

Cato Brede , Norway


Leonid Breydo , USA


Wybren J. Buma , The Netherlands

J. O. Caceres , Spain


Patrizia Calaminici , Mexico


Claudio Cameselle , Spain


Joaquin Campos , Spain


Dapeng Cao , China

Domenica Capasso , Italy

Stefano Caporali , Italy

Zenilda Cardeal , Brazil

Angela Cardinali , Italy

Stefano Carli , Italy

Maria F. Carvalho , Portugal


Susana Casal , Portugal


David E. Chavez, USA

Riccardo Chelli , Italy

Zhongfang Chen , Puerto Rico

Vladislav Chrastny , Czech Republic

Roberto Comparelli , Italy

Filomena Conforti , Italy

Luca Conti , Italy


Christophe Coquelet, France

Filomena Corbo , Italy

Jose Corchado , Spain

Maria N. D.S. Cordeiro , Portugal

Claudia Crestini, Italy

Gerald Culioli , France

Nguyen Duc Cuong , Vietnam

Stefano D'Errico , Italy


Matthias D'hooghe , Belgium


Samuel B. Dampare, Ghana

Umashankar Das, Canada

Victor David, Romania


Annalisa De Girolamo, Italy


Antonio De Lucas-Consuegra , Spain

Marccone A. L. De Oliveira , Brazil

Paula G. De Pinho , Portugal

Damião De Sousa , Brazil

Francisco Javier Deive , Spain

Tianlong Deng , China

Fatih Deniz , Turkey
Claudio Di Iaconi, Italy
Irene Dini , Italy
Daniele Dondi, Italy
Yingchao Dong , China
Dennis Douroumis , United Kingdom
John Drexler, USA
Qizhen Du, China
Yuanyuan Duan , China
Philippe Dugourd, France
Frederic Dumur , France
Grégory Durand , France
Mehmet E. Duru, Turkey
Takayuki Ebata , Japan
Arturo Espinosa Ferao , Spain
Valdemar Esteves , Portugal
Cristina Femoni , Italy
Gang Feng, China
Dieter Fenske, Germany
Jorge F. Fernandez-Sanchez , Spain
Alberto Figoli , Italy
Elena Forte, Italy
Sylvain Franger , France
Emiliano Fratini , Italy
Franco Frau , Italy
Bartolo Gabriele , Italy
Guillaume Galliero , France
Andrea Gambaro , Italy
Vijay Kumar Garlapati, India
James W. Gauld , Canada
Barbara Gawdzik , Poland
Pier Luigi Gentili , Italy
Beatrice Giannetta , Italy
Dimosthenis L. Giokas , Greece
Alejandro Giorgetti , Italy
Alexandre Giuliani , France
Elena Gomez , Spain
Yves Grohens, France
Katharina Grupp, Germany
Luis F. Guido , Portugal
Maolin Guo, USA
Wenshan Guo , Australia
Leena Gupta , India
Muhammad J. Habib, USA
Jae Ryang Hahn, Republic of Korea

Christopher G. Hamaker , USA
Ashanul Haque , Saudi Arabia
Yusuke Hara, Japan
Naoki Haraguchi, Japan
Serkos A. Haroutounian , Greece
Rudi Hendra , Indonesia
Javier Hernandez-Borges , Spain
Miguel Herrero, Spain
Mark Hoffmann , USA
Hanmin Huang, China
Doina Humelnicu , Romania
Charlotte Hurel, France
Nenad Ignjatović , Serbia
Ales Imramovsky , Czech Republic
Muhammad Jahangir, Pakistan
Philippe Jeandet , France
Sipak Joyasawal, USA
Sławomir M. Kaczmarek, Poland
Ewa Kaczorek, Poland
Mostafa Khajeh, Iran
Srećko I. Kirin , Croatia
Anton Kokalj , Slovenia
Sevgi Kolaylı , Turkey
Takeshi Kondo , Japan
Christos Kordulis, Greece
Ioannis D. Kostas , Greece
Yiannis Kourkoutas , Greece
Henryk Kozłowski, Poland
Yoshihiro Kudo , Japan
Avvaru Praveen Kumar , Ethiopia
Dhanaji Lade, USA
Isabel Lara , Spain
Jolanta N. Latosinska , Poland
João Paulo Leal , Portugal
Woojin Lee, Kazakhstan
Yuan-Pern Lee , Taiwan
Matthias Lein , New Zealand
Huabing Li, China
Jinan Li , USA
Kokhwa Lim , Singapore
Teik-Cheng Lim , Singapore
Jianqiang Liu , China
Xi Liu , China
Xinyong Liu , China
Zhong-Wen Liu , China


Eulogio J. Llorent-Martínez , Spain
Pasquale Longo , Italy
Pablo Lorenzo-Luis , Spain
Zhang-Hui Lu, China
Devanand Luthria, USA
Konstantin V. Luzyanin , United Kingdom
Basavarajaiah S M, India
Mari Maeda-Yamamoto , Japan
Isabel Mafra , Portugal
Dimitris P. Makris , Greece
Pedro M. Mancini, Argentina
Marcelino Maneiro , Spain
Giuseppe F. Mangiatordi , Italy
Casimiro Mantell , Spain
Carlos A Martínez-Huitle , Brazil
José M. G. Martinho , Portugal
Andrea Mastinu , Italy
Cesar Mateo , Spain
Georgios Matthaiolampakis, USA
Mehrab Mehrvar, Canada
Saurabh Mehta , India
Oinam Romesh Meitei , USA
Saima Q. Memon , Pakistan
Morena Miciaccia, Italy
Maurice Millet , France
Angelo Minucci, Italy
Liviu Mitu , Romania
Hideto Miyabe , Japan
Ahmad Mohammad Alakraa , Egypt
Kaustubha Mohanty, India
Subrata Mondal , India
José Morillo, Spain
Giovanni Morrone , Italy
Ahmed Mourran, Germany
Nagaraju Mupparapu , USA
Markus Muschen, USA
Benjamin Mwashote , USA
Mallikarjuna N. Nadagouda , USA
Lutfun Nahar , United Kingdom
Kamala Kanta Nanda , Peru
Senthilkumar Nangan, Thailand
Mu. Naushad , Saudi Arabia
Gabriel Navarrete-Vazquez , Mexico
Jean-Marie Nedelec , France
Sridhar Goud Nerella , USA
Nagatoshi Nishiwaki , Japan
Tzortzis Nomikos , Greece
Beatriz P. P. Oliveira , Portugal
Leonardo Palmisano , Italy
Mohamed Afzal Pasha , India
Dario Pasini , Italy
Angela Patti , Italy
Massimiliano F. Peana , Italy
Andrea Penoni , Italy
Franc Perdih , Slovenia
Jose A. Pereira , Portugal
Pedro Avila Pérez , Mexico
Maria Grazia Perrone , Italy
Silvia Persichilli , Italy
Thijs A. Peters , Norway
Christophe Petit , France
Marinos Pitsikalis , Greece
Rita Rosa Plá, Argentina
Fabio Polticelli , Italy
Josefina Pons, Spain
V. Prakash Reddy , USA
Thathan Premkumar, Republic of Korea
Maciej Przybyłek , Poland
María Quesada-Moreno , Germany
Maurizio Quinto , Italy
Franck Rabilloud , France
C.R. Raj, India
Sanchayita Rajkhowa , India
Manzoor Rather , India
Enrico Ravera , Italy
Julia Revuelta , Spain
Muhammad Rizwan , Pakistan
Manfredi Rizzo , Italy
Maria P. Robalo , Portugal
Maria Roca , Spain
Nicolas Roche , France
Samuel Rokhum , India
Roberto Romeo , Italy
Antonio M. Romerosa-Nievas , Spain
Arpita Roy , India
Eloy S. Sanz P rez , Spain
Nagaraju Sakkani , USA
Diego Sampedro , Spain
Shengmin Sang , USA

Vikram Sarpe , USA
Adrian Saura-Sanmartin , Spain
St phanie Sayen, France
Ewa Schab-Balcerzak , Poland
Hartwig Schulz, Germany
Gulaim A. Seisenbaeva , Sweden
Serkan Selli , Turkey
Murat Senturk , Turkey
Beatrice Severino , Italy
Sunil Shah Shah , USA
Ashutosh Sharma , USA
Hideaki Shirota , Japan
Cl udia G. Silva , Portugal
Ajaya Kumar Singh , India
Vijay Siripuram, USA
Ponnurengam Malliappan Sivakumar ,
Japan
Tom s Sobrino , Spain
Raquel G. Soengas , Spain
Yujiang Song , China
Olivier Soppera, France
Radhey Srivastava , USA
Vivek Srivastava, India
Theocharis C. Stamatatos , Greece
Athanasios Stavrakoudis , Greece
Darren Sun, Singapore
Arun Suneja , USA
Kamal Swami , USA
B.E. Kumara Swamy , India
Elad Tako , USA
Shoufeng Tang, China
Zhenwei Tang , China
Vijai Kumar Reddy Tangadanchu , USA
Franco Tassi, Italy
Alexander Tatarinov, Russia
Lorena Tavano, Italy
Tullia Tedeschi, Italy
Vinod Kumar Tiwari , India
Augusto C. Tome , Portugal
Fernanda Tonelli , Brazil
Naoki Toyooka , Japan
Andrea Trabocchi , Italy
Philippe Trens , France
Ekaterina Tsipis, Russia
Esteban P. Urriolabeitia , Spain

Toyonobu Usuki , Japan
Giuseppe Valacchi , Italy
Ganga Reddy Velma , USA
Marco Viccaro , Italy
Jaime Villaverde , Spain
Marc Visseaux , France
Balaga Viswanadham , India
Alessandro Volonterio , Italy
Zoran Vujcic , Serbia
Chun-Hua Wang , China
Leiming Wang , China
Carmen W ngler , Germany
Wieslaw Wiczkowski , Poland
Bryan M. Wong , USA
Frank Wuest, Canada
Yang Xu, USA
Dharmendra Kumar Yadav , Republic of
Korea
Maria C. Yebra-Biurrun , Spain
Dr Nagesh G Yernale, India
Tomokazu Yoshimura , Japan
Maryam Yousaf, China
Sedat Yurdakal , Turkey
Shin-ichi Yusa , Japan
Claudio Zaccone , Italy
Ronen Zangi, Spain
John CG Zhao , USA
Zhen Zhao, China
Antonio Zizzi , Italy
Mire Zloh , United Kingdom
Grigoris Zoidis , Greece
Deniz  AHİN , Turkey


Contents

Isotopic Tracing of Perchlorate Sources in the Environment

Mengnan Zhang , Xiaoqian Li, Xuxue Cheng, Xinfeng Wang, Mian Song, Xiaoyan Wang, and Xuemei Ma

Review Article (10 pages), Article ID 9978489, Volume 2021 (2021)

Natural Background Level and Contamination of Shallow Groundwater Salinity in Various Aquifers in a Coastal Urbanized Area, South China

Pan Bi, Dongya Han , Chunyan Liu, Liquan Xiao, Heqiu Wu, and Meng Zhang




Research Article (9 pages), Article ID 2973092, Volume 2021 (2021)

Survey and Risk Assessment of Contaminants in Soil from a Nitrogenous Fertilizer Plant Located in North China

Zizhao Tian , Cunliang Fan, Zhiqiang Gong, Ziting Yuan, Zhiyuan Ma, Xiaosen Xing, Wei He, and Pengfei Jin 

Research Article (13 pages), Article ID 9936652, Volume 2021 (2021)

Hydrogeochemical Characteristics and Formation of Low-Temperature Geothermal Waters in Mangbang-Longling Area of Western Yunnan, China

Xing-Wang Chang, Mo Xu , Liang-Wen Jiang, Xiao Li , and Yun-Hui Zhang 

Research Article (13 pages), Article ID 5527354, Volume 2021 (2021)

Hydrogeochemistry of Fluorine in Groundwater in Humid Mountainous Areas: A Case Study at Xingguo County, Southern China

Jinhui Liu, Xinfeng Wang , Weidong Xu, Mian Song, Lei Gong, Mengnan Zhang, Linbo Li, and Lishan He


Research Article (11 pages), Article ID 5567353, Volume 2021 (2021)

Hydrochemistry and Entropy-Based Groundwater Quality Assessment in the Suining Area, Southwestern China

Yunhui Zhang , Xiao Li , Ming Luo, Changli Wei, Xun Huang, Yong Xiao , Limao Qin, and Qiuming Pei 

Research Article (11 pages), Article ID 5591892, Volume 2021 (2021)

Degradation of High-Concentration Nitrate Nitrogen in Groundwater: A Laboratory Study

Manxi Liu, Lu Xia, Ruinan Liu, Zongjun Gao , Cong Han, Jianguo Feng, Jing Wang, Wanlong Qu, and Tongju Xing


Research Article (13 pages), Article ID 4797946, Volume 2021 (2021)

Hydrogeochemical Features and Genesis of Confined Groundwater and Health Perspectives for Sustainable Development in Urban Hengshui, North China Plain

Yong Xiao , Kui Liu , Qichen Hao , Jianfeng Li , Yunhui Zhang , Weizhe Cui , Limao qin, and Qiuming Pei 

Research Article (15 pages), Article ID 5578192, Volume 2021 (2021)

Hydrochemical Characteristics and Formation Mechanism of Strontium-Rich Groundwater in Shijiazhuang, North China Plain

Duo Li, Shuang Gan, Junfeng Li, Zihan Dong, Qi Long, Shuwei Qiu, Yahong Zhou , and Changyu Lu
Research Article (10 pages), Article ID 5547924, Volume 2021 (2021)

Review Article

Isotopic Tracing of Perchlorate Sources in the Environment

Mengnan Zhang ¹, Xiaoqian Li,² Xuxue Cheng,¹ Xinfeng Wang,¹ Mian Song,¹
Xiaoyan Wang,¹ and Xuemei Ma¹

¹Center for Hydrogeology and Environmental Geology, CGS, Baoding 071051, China

²China University of Geosciences, Wuhan 430074, China

Correspondence should be addressed to Mengnan Zhang; saxilan@163.com

Received 11 March 2021; Accepted 16 September 2021; Published 18 October 2021

Academic Editor: Tingyue Gu

Copyright © 2021 Mengnan Zhang et al. This is an open access article distributed under the Creative Commons Attribution License, which permits unrestricted use, distribution, and reproduction in any medium, provided the original work is properly cited.

Perchlorate (ClO_4^-) is an emerging persistent pollutant that is ubiquitous in the environment at trace concentrations. Perchlorate ingestion poses a risk to human health because it interferes with thyroidal hormone production. The identification of perchlorate sources in groundwater is a primary concern. Chlorine and multi-oxygen isotopic tracing of perchlorate ($\delta^{37}\text{Cl}$, $^{36}\text{Cl}/\text{Cl}$, $\delta^{18}\text{O}$, and $\Delta^{17}\text{O}$) can provide a unique tool for identifying the origin and transport of perchlorate in groundwater. Along with the kinetic fractionation of chlorine and oxygen isotopes, the $\Delta^{17}\text{O}$ value, $^{36}\text{Cl}/\text{Cl}$ ratio, and $\epsilon^{18}\text{O}/\epsilon^{37}\text{Cl}$ (the fractionation coefficient of oxygen and chlorine isotopes) are constant, potentially indicating the biodegradation of perchlorate, without disguising its source information. Therefore, comprehensive characterization of stable chlorine and poly-oxygen isotopes is expected to provide direct evidence for identifying the source of perchlorate in groundwater. However, further studies are needed to increase the amount of isotopic data of different perchlorate sources, to make the end-member model available to broader regions. It is critically important to understand the range of values and differences of isotopes among natural perchlorate sources and the perchlorate formation mechanisms.

1. Introduction

Groundwater is an important water resource, which is of strategic significance to the sustainable development of a country and its people. It has become a hot issue to use water resources rationally, to ensure continued quality and availability, to meet economic and social developmental needs [1]. In some areas, groundwater is an important (or the only) source of drinking water, and water safety issues directly affect residents' health and quality of life [2]. With the rapid development in recent decades of China's economy, groundwater hydrochemistry is affected by natural factors, such as geology, geography, and climate change, and increasingly by anthropogenic inputs [3], making the situation of water shortage severe in China. Groundwater pollution is hard to be found and difficult to reverse; thus, the effective prevention and control of groundwater pollution should first be based on "prevention." That is, identifying the source of the pollutants in groundwater and

determining their migration and transformation paths in groundwater are the primary concerns that should be considered to solve groundwater pollution.

Perchlorate (ClO_4^-) is typically a persistent environmental pollutant, attracting extensive attention for research on its environmental pollution status, ecotoxicological effect, pollution control, and remediation [4–7]. Trace amounts of ClO_4^- can interfere with the normal function of the thyroid, leading to a series of developmental and metabolic diseases in the human body, especially in women of childbearing age and infants [8]. Currently, ClO_4^- widely exists in different environmental media, such as rivers, lakes, groundwater, soil, and sediment [9–11], and is widely found in food, making its way into humans at a fast rate [12–14]; it can be detected in body fluids (such as breast milk, saliva, blood, and urine) [15, 16], constituting a serious threat to human health. In 2008, the US Environmental Protection Agency (EPA) listed ClO_4^- as a level 1 monitoring indicator and recommended a safe reference dose of $0.7 \mu\text{g}/\text{kg}/\text{day}$

exposure to humans, which is likely to be without an appreciable risk of adverse effects. The US EPA in February 2011 officially listed ClO_4^- for regulation under the Safe Drinking Water Act; hence, perchlorate has become an important research topic.

Perchlorate originates from both natural and human sources. Natural perchlorate has been attributed to the earlier use of Chilean nitrate as fertilizer and atmospheric origin. Because perchlorate is a strong and stable oxidant and a strong acid, it is widely used in aerospace, military, and industrial fields, such as in rocket solid fuel, fireworks manufacturing, ammunition equipment, electroplating, desiccants, and oxidants (Table 1). The sources of perchlorate in groundwater vary; the pollution paths are complex and varied and are often affected by the widespread effects of physics, chemistry, and biology. Isotope technology is used to explore the source of material, related migration, and transformation laws at the “atomic” scale, having many unique advantages compared with the content measurement approach at the “molecular” scale. The comprehensive characteristics of the contents of stable chlorine and oxygen isotopes along with the radioactive isotope ^{36}Cl of perchlorate provide an important analytical tool for tracing the source of perchlorate and its migration and transformation in the environment.

China is a large traditional country of fireworks manufacturing and consumption. As the direct products of chemical plants (oxidants and additives of the perchlorate) are widely distributed throughout the country, the potential of perchlorate environmental pollution problems cannot be ignored. A recent investigation shows that 86% of 300 water samples from 13 provinces and cities in China had ClO_4^- detected in them [17]. The concentration of ClO_4^- detected in the blood of adults in Nanchang is more than 10 times higher than that reported in the United States [12]. However, studies on the pollution of ClO_4^- in China have just begun, and the source analysis of ClO_4^- in groundwater has not been reported. Given the present situation of environmental pollution of perchlorate, this paper summarizes and discusses perchlorate isotope testing technology and its application in tracing the source of ClO_4^- in groundwater, providing a reference for effective prevention and control of ClO_4^- pollution in groundwater in China.

2. Environmental Pollution Status of Perchlorate

The United States was the first country to find perchlorate pollution, and existing research has mainly focused on its water pollution; thus far, ClO_4^- has been detected in 44 states [18]. The EPA recommended that the concentration of perchlorate in drinking water be less than $15\ \mu\text{g/L}$ [19]. The Safe Drinking Water Act (SDWA) allows States to establish drinking water standards that are more stringent than EPA’s national standards. California’s latest concentration standard for perchlorate in drinking water is $6\ \mu\text{g/L}$ [18], and Massachusetts’s standard is $2\ \mu\text{g/L}$ [19]. In 2008, the US EPA recommended a safe intake of $0.7\ \mu\text{g/kg/day}$ for the human body. ClO_4^- was detected in high amounts in the southwest

of the United States, including California, Arizona, the highlands of Texas, the East Coast between New Jersey and Long Island, and Massachusetts. In 2008, the US EPA published the test results of 3,865 public water supply samples collected from 2001 to 2005, and the average content value of ClO_4^- was $4\text{--}420\ \mu\text{g/L}$ [20]. Recently, apart from the United States, other countries have begun to investigate the concentration of ClO_4^- in water. The concentration of ClO_4^- was $340\text{--}2,300\ \mu\text{g/L}$ in the upstream and tributary (Usui River) of the Tone River in Japan. Moreover, different concentrations of ClO_4^- were detected in tap water from the Tone River, and a part of the water sample concentration exceeded $10\ \mu\text{g/L}$ [21]. The concentration of ClO_4^- in the Nakdong River in South Korea is as high as $60\ \mu\text{g/L}$, and the concentration in drinking water is as high as $35\ \mu\text{g/L}$ [10]. The average concentration of groundwater samples from six states of India is $1.0\ \mu\text{g/L}$, wherein samples greater than $1.0\ \mu\text{g/L}$ were obtained from central industrial cities [22]. North Korea tested 520 tap water samples from more than 100 areas. The concentration of ClO_4^- was $<1.0\text{--}6.1\ \mu\text{g/L}$, and 80% of the samples exceeded the concentration limit in drinking water [23]. The relevance ratio of ClO_4^- in German groundwater samples is 100%, and the concentration is $0.79\text{--}2.38\ \mu\text{g/L}$ [24] (Table 2).

In the past 10 years, China has also investigated perchlorate environmental pollution. The results show that the environmental pollution problem of perchlorate has been widespread in China, and research on the prevention and control of ClO_4^- pollution in groundwater is imminent. Liu et al. reported the ClO_4^- concentration in factory water and source water of three water plants in Beijing. The results showed that 67% of the samples, with detectable ClO_4^- , were obtained from water plants that used groundwater as their water source. The concentration of ClO_4^- in the source water reached $30.7\ \mu\text{g/L}$ [25–27]. In a recent water survey, covering 13 provinces or autonomous regions in China (including tap water, groundwater, surface water, and bottled water), the detection rate of ClO_4^- is up to 86%, with a concentration of $0.02\text{--}54.4\ \mu\text{g/L}$, where the average concentration of groundwater was the highest, $3.04\ \mu\text{g/L}$ [17]. Severe ClO_4^- pollution exists in Liuyang City, Hunan Province; their fireworks production accounts for more than 60% of that of the world. High concentrations of ClO_4^- are detected in the river water, bottom mud, soil, and groundwater [11, 17], among which ClO_4^- is detected in groundwater, whose concentration is as high as $22.14\ \mu\text{g/L}$. ClO_4^- was also detected in rice and milk samples from 26 cities in China, with concentrations ranging from 0.16 to $4.88\ \mu\text{g/kg}$ and 0.30 to $9.1\ \mu\text{g/L}$, respectively [27]. Furthermore, the results of 131 blood samples from donors in Nanchang showed that the concentration of ClO_4^- in human blood of different age groups (0.4–90 year) was as high as $10.5\ \mu\text{g/L}$, with an average value of $2.68\ \mu\text{g/L}$ [16].

3. Perchlorate Chlorine and Oxygen Isotope Testing Technology

3.1. Isotope Characterization. Chlorine (Cl) and oxygen (O) in perchlorate (ClO_4^-) have multiple isotopes in nature. There are mainly two stable isotopes of Cl on the earth’s

TABLE 1: Applications of perchlorate.

Application field	Raw material
Rocket solid fuel	NH_4ClO_4 , LiClO_4 , NO_2ClO_4 , $\text{NO}\cdot\text{ClO}_4$, $\text{N}_2\text{H}_4\text{HClO}_4$, $(\text{NH}_4)_2\text{N}_2\text{H}_8(\text{ClO}_4)_4$
Fireworks manufacturing	KClO_4 , HClO_4
Electroplating	HClO_4
Oxidant	HClO_4
Desiccant	$\text{Mg}(\text{ClO}_4)_2$

TABLE 2: The global pollution situation of perchlorate.

Area	Sample concentration ($\mu\text{g/L}$)	Drinking water concentration ($\mu\text{g/L}$)
EPA recommend		15
USA	4–420 (public water)	
Japan	340~2300 (river water)	10
South Korea	60 (river water)	35
India	1.0 (groundwater)	
North Korea	<1.0~6.1 $\mu\text{g/L}$ (tap water)	<1.0~6.1 $\mu\text{g/L}$
German	0.79~2.38 (groundwater)	

surface (^{35}Cl and ^{37}Cl) with relative abundances of 75.77% and 24.23% [28], respectively. ^{36}Cl is a trace radioisotope produced by cosmic rays in the stratosphere with a half-life of 301,000 years. There are three stable isotopes of O (^{16}O , ^{17}O , and ^{18}O) with relative abundances of 99.76%, 0.04%, and 0.20% [29], respectively. The composition of a stable isotope is usually expressed by the δ value, that is, $\delta(\text{‰}) = (\text{R}_{\text{sample}}/\text{R}_{\text{standard}} - 1) \times 1,000$, where R_{sample} and $\text{R}_{\text{standard}}$ represent the isotope ratios of the sample and standard, respectively. $\delta^{18}\text{O}$, $\delta^{17}\text{O}$, and $\delta^{37}\text{Cl}$, respectively, can be characterized as $\delta^{18}\text{O}(\text{‰}) = [({}^{18}\text{O}/{}^{16}\text{O})_{\text{sample}}/({}^{18}\text{O}/{}^{16}\text{O})_{\text{VSMOW}} - 1] \times 1,000$, $\delta^{17}\text{O}(\text{‰}) = [({}^{17}\text{O}/{}^{16}\text{O})_{\text{sample}}/({}^{17}\text{O}/{}^{16}\text{O})_{\text{VSMOW}} - 1] \times 1,000$, and $\delta^{37}\text{Cl}(\text{‰}) = [({}^{37}\text{Cl}/{}^{35}\text{Cl})_{\text{sample}}/({}^{37}\text{Cl}/{}^{35}\text{Cl})_{\text{SMOC}} - 1] \times 1,000$. Here, VSMOW and SMOC are the international standards for oxygen and chlorine isotopes, respectively. In general, for many Earth matters, there is a fixed relationship between $\delta^{17}\text{O}$ and $\delta^{18}\text{O}$ ($\delta^{17}\text{O} \approx 0.52 \delta^{18}\text{O}$), following the mass-dependent fractionation, and $\delta^{17}\text{O}$ is not normally reported. Recently, studies have found that atmospheric aerosols, such as sulfate, nitrate, and perchlorate, or surface environmental sediments have ^{17}O anomalies [25–27]. $\Delta^{17}\text{O}$ is typically used to characterize ^{17}O anomalies, that is, $\Delta^{17}\text{O}(\text{‰}) = \delta^{17}\text{O} - 0.52 \delta^{18}\text{O}$ or $\Delta^{17}\text{O}(\text{‰}) = [(1 + \delta^{17}\text{O})/(1 + \delta^{18}\text{O})0.525 - 1] \times 1,000$. The ^{36}Cl content is usually expressed as $^{36}\text{Cl}/\text{Cl}$, which is the ratio of the atoms.

3.2. Testing Technology of Perchlorate Chlorine and Oxygen Isotopes. Research on the sources of perchlorate, geochemical behavior, and isotope kinetic fractionation effect in environmental media is still in its initial stages. The high-precision test method of stable isotope ratio provides the necessary technical support for the mechanism and application of perchlorate environmental pollution. The high-precision stable isotope data of perchlorate ($\delta^{18}\text{O}$, $\Delta^{17}\text{O}$, and $\delta^{37}\text{Cl}$) are usually measured using a gas stable isotope ratio mass spectrometer, and the analysis gases are CO, O₂, and CH₃Cl [30–32]. Ader et al. and Sturchio et al. first

established a test method for the $\delta^{37}\text{Cl}$ value of perchlorate [14, 30–32]. Bao and Gu reported a test method for the simultaneous determination of $\delta^{18}\text{O}$ and $\delta^{17}\text{O}$ and the preparation of O₂ via high-temperature pyrolysis of perchlorate [33]. Furthermore, Böhlke et al. successively reported the preparation of CO via high-temperature carbon reduction of perchlorate, an online measurement $\delta^{18}\text{O}$ value test method [31]. Sturchio et al. established a test method for the simultaneous analysis of $\delta^{37}\text{Cl}$, $\delta^{18}\text{O}$, and $\delta^{17}\text{O}$ based on the above method [30], and this method has been further adapted and developed [29, 34–36]. These methods require the analysis sample to be high-purity perchlorates, such as KClO_4 , RbClO_4 , or CsClO_4 . The ^{36}Cl content is usually determined using an accelerator mass spectrometer (AMS). This article summarizes the current mature testing techniques for perchlorate chlorine and oxygen isotopes.

3.2.1. Oxygen Isotopes. The oxygen isotope composition of perchlorate can usually be determined using two isotope ratio mass spectrometry (IRMS), namely the CO-TC/EA-IRMS high-temperature carbon reduction online continuous flow method, which determines the $\delta^{18}\text{O}$ value and O₂-DI-IRMS pyrolysis; this off-line two-stage method measures the $\delta^{18}\text{O}$ and $\delta^{17}\text{O}$ values simultaneously [31, 32, 34, 35].

The principle of the CO-TC/EA-IRMS high-temperature carbon reduction online continuous flow method can be summarized as follows. Perchlorate (such as CsClO_4) and glassy carbon in a reduction reaction in a high-temperature cracking furnace at 1,325–1,400°C generate CO. After purging pure He carrier gas, CO goes through a gas chromatographic column equipped with a 5 Å molecular sieve for purification. Then, it enters the IRMS in a continuous flow mode and is received by a Faraday cup with m/z of 28 and 30 to determine the $\delta^{18}\text{O}$ value. For high-purity ClO_4^- reagents and samples, the yield of O(CO) was usually $100 \pm 2\%$, and the test accuracy of $\delta^{18}\text{O}$ was $\pm 0.3\text{‰}$ [31, 32, 35, 37]. This method can be used to rapidly and efficiently perform an online test of the perchlorate $\delta^{18}\text{O}$ value, which is especially suitable for batch tests.

For some special samples, it is necessary to measure the $\delta^{18}\text{O}$ and $\delta^{17}\text{O}$ values of perchlorate simultaneously; therefore, O_2 must be used as the mass spectrometry gas. Perchlorate is vacuum cracked into O_2 at 600–650°C using the two-stage method outside the pyrolysis line of O_2 -DI-IRMS; the reaction formula is $\text{CsClO}_4 \longrightarrow \text{CsCl} + 2\text{O}_2$. This cracking reaction can be carried out in a sealed quartz tube or Pyrex heat-resistant glass tube. Then, the produced O_2 enters the IRMS in a two-way mode after purification and is received by the Faraday cups with m/z of 32, 33, and 34 to simultaneously determine the $\delta^{18}\text{O}$ and $\delta^{17}\text{O}$ values [31, 32, 37]. For high-purity ClO_4^- reagents and samples, the yield of $\text{O}(\text{O}_2)$ is usually $100 \pm 5\%$, and the test accuracy of $\Delta^{17}\text{O}$ is $\pm 0.1\%$.

3.2.2. Chlorine Isotopes. The perchlorate stable chlorine isotope composition ($\delta^{37}\text{Cl}$) was determined using the IRMS method, and the radioisotope content ($^{36}\text{Cl}/\text{Cl}$) was determined via the AMS method.

To determine the $\delta^{37}\text{Cl}$ value of perchlorate, first, the perchlorate was vacuum decomposed to produce chloride at 600–650°C. The chloride was dissolved in deionized water, and Cl was precipitated as AgCl by adding AgNO_3 , which reacted with the excess CH_3I in a sealed glass tube at 300°C for 2 h to produce CH_3Cl . The CH_3Cl purified cryogenically by gas chromatography enters IRMS with continuous flow or dual-inlet mode and is measured at m/z of 50 and 52. The accuracy of the $\delta^{37}\text{Cl}$ analysis was $\pm 0.2\%$ [31, 32, 35, 37].

To determine the $^{36}\text{Cl}/\text{Cl}$ content, the same steps as above are used to convert the perchlorate to AgCl precipitate; then, the AgCl precipitate is dissolved in a dilute ammonia (NH_4OH) solution. The AgCl precipitate is prepared again for the AMS measurement using Cl^- , which is purified via anion chromatography or cation exchange chromatography. Typically, seawater is used as a reference substance, and its $^{36}\text{Cl}/\text{Cl} = 0.5 \times 10^{-15}$.

3.2.3. Collection and Preparation of ClO_4^- Samples in Groundwater. The IRMS measurement usually requires a sample amount of at least 0.2 mg ClO_4^- ; thus, an effective sample preparation method is needed to achieve the isotope test of trace environmental ClO_4^- . The most successful and widely used collection and extraction method is based on a highly efficient ClO_4^- selective bifunctional anion-exchange (Figure 1) resin [29, 31, 33, 34, 38]. The principle is that the resin is loaded with numerous exchangeable anions. ClO_4^- replaces the anions on the resin and is adsorbed on the resin because of the difference in the concentration of the two ions in the (Figure 1) resin when water flows through the resin [39]. This anionic resin can efficiently and selectively adsorb ClO_4^- and release ClO_4^- under the elution of a mixed solution of 1M FeCl_3 and 4M HCl . The resin can be reused after activation [39]. The collection and preparation of ClO_4^- samples in groundwater is generally divided into two steps: ClO_4^- adsorption and elution. In the actual sampling process, the water sample usually passes through the filter device to remove interfering ions such as Cl^- , SO_4^{2-} , NO_3^- , and humus, to avoid affecting the adsorption effect of ClO_4^- . The treated water then passes through the A530 E type at a flow

rate of 17 BV/min resin column, comprising bifunctional anion-exchange resin (20–30 mesh). When the entire water sample passes through the resin column, most of the ClO_4^- is adsorbed on the resin and needs to be eluted to prepare the sample. First, a 4–5 BV of 4 mol/L HCl solution or deionized water is passed through the resin column to wash off other adsorbed ions and unadsorbed ClO_4^- . Subsequently, a mixed solution of 1 mol/L FeCl_3 and 4 mol/L HCl is prepared; the solution is passed through the resin column at a flow rate of 0.06–0.13 cm/min. NaOH is added to the obtained eluent and centrifuged to obtain the supernatant. CsCl is added to the supernatant, heated, and evaporated to obtain CsClO_4 precipitation, which is prepared for mass spectrometry tests after purification [29, 40].

4. Isotope Tracing of Chlorine and Oxygen from Perchlorate

4.1. Isotopic Composition Characteristics of Perchlorate from Different Sources. Perchlorates from different sources have characteristic isotopic composition values related to their formation mechanism; perfecting and establishing an end-member model of their sources is a necessary basis for the application of isotope technology to trace the source. The existing natural origin and synthetic perchlorate isotope data show that the comprehensive characteristics of chlorine and oxygen isotopes of perchlorate are expected to provide direct evidence for identifying the source of perchlorate in groundwater.

4.1.1. Synthetic Perchlorate. Synthetic perchlorate is usually produced by the electrolytic oxidation of NaCl . The perchlorate production process largely depends on the content of the raw material Cl, while the electrolyzed water provides an O source for the synthesis of perchlorate. Since 2001, American scholars have analyzed the isotopic composition of various perchlorate reagents (used in laboratories, industry, and military) and products (used in road blasting, fireworks, pesticides, bleaching agents, and propellants). According to reported data [14, 31, 33, 34, 42], the synthetic perchlorate $\delta^{37}\text{Cl}$ value is -3.1% to $+2.3\%$; the $\delta^{18}\text{O}$ value is -24.8% to -12.5% ; the $\Delta^{17}\text{O}$ value is $0.0 \pm 0.1\%$; the ratio of $^{36}\text{Cl}/\text{Cl}$ is $\leq 2.5 \times 10^{-15} - 40 \times 10^{-15}$; and the average value of $\delta^{37}\text{Cl}$ of synthetic perchlorate is about $+0.6\%$, which is similar to the $\delta^{37}\text{Cl}$ value of raw material, NaCl (0.0 ± 10 – 15) 0.9% [43]. A similar value indicates that there is almost no fractionation of chlorine isotopes during the process of synthesizing perchlorate by electrolytic oxidation. The $\delta^{18}\text{O}$ value has a larger range of variation, which may be related to the isotope composition of the water source used in the perchlorate production process and oxygen isotope fractionation [32]. Preliminary studies have shown that ClO_4^- produced by the disproportionation reaction of commercial bleach (NaOCl) solution has an abnormally high $\delta^{37}\text{Cl}$ value ($+14.0\%$) [42]. Therefore, the isotopic composition of perchlorate is not only related to the isotopic composition of its raw materials but may also be affected by its production process.

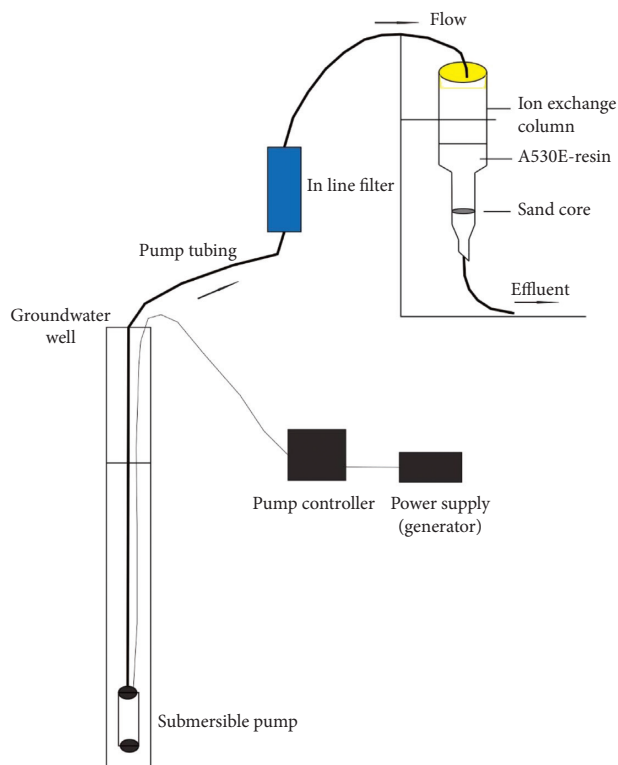


FIGURE 1: Sample collection device [41] (the left picture is the device used in the lab by authors).

4.1.2. Perchlorate of Natural Origin. It has been reported that perchlorate of natural origin is mainly distributed in the Atacama Desert in northern Chile and in the arid region of the southwestern United States. However, there are regions (such as the southern high plains and eastern New Mexico) where there is no clear historical or current evidence of the presence of rocket fuel or Chilean fertilizer sources. In these regions, perchlorate has been attributed to meteoric ClO_4^- that accumulated in the unsaturated zone, with subsequent flushing to groundwater by the advent of the irrigation [44, 45]. They have distinctly different isotopic compositions from synthetic perchlorates, and the isotopic compositions in the two regions have their own characteristics.

The Chilean saltpeter in the Atacama Desert is the most typical naturally occurring mineral that is rich in ClO_4^- . However, owing to the differences in sampling locations and detection methods, the mass content of ClO_4^- reported in the literature is not the same, ranging from 0.03% to 3.6% [46–48]. Chilean saltpeter is an important raw material for fertilizers, and the total amount of Chilean saltpeter

(imported by the United States and widely used in agriculture decades ago) has reached millions of tons [49]. It was an important potential source of ClO_4^- in groundwater (but now with the development of processing the percentage of perchlorate in Chilean fertilizers has been reduced). Bao and Gu first reported the oxygen isotopic composition of ClO_4^- in Chilean saltpeter; that is, the $\delta^{18}\text{O}$ value ranged from -24.8‰ to -4.5‰ , and the $\Delta^{17}\text{O}$ value ranged from $+4.2\text{‰}$ to $+9.6\text{‰}$ [47]. Furthermore, some scholars have successively expanded their oxygen isotope data [31, 32, 34], where the $\delta^{18}\text{O}$ value ranged from -9.3‰ to -2.2‰ , and the $\Delta^{17}\text{O}$ value ranged $+7.9\text{‰}$ to $+18.4\text{‰}$. The large positive ^{17}O anomaly of ClO_4^- in Chilean saltpeter may be the result of the photochemical interaction of atmospheric Cl and O_3 , indicating that ClO_4^- in natural minerals originated from the atmosphere, and was deposited and preserved in an arid climate with strong evaporation. The $\delta^{37}\text{Cl}$ value of ClO_4^- in Chilean saltpeter ranges from -14.5‰ to -11.8‰ [31, 32, 34], and the ratio of $^{36}\text{Cl}/\text{Cl}$ is $22 \times 10^{-15} - 590 \times 10^{-15}$ [42].

Natural perchlorate is widely distributed throughout the arid and semiarid regions of the world, such as the southwestern United States, the southern high plains of United States, and Chile [48, 50]. Perchlorate is widely distributed on the earth, but the deep research has regional limitations. The scientists have collected samples for stable isotope analysis in several regions. The $\delta^{18}\text{O}$, $\Delta^{17}\text{O}$, and $\delta^{37}\text{Cl}$ values of ClO_4^- in groundwater in the southern plateau area range from +0.55‰ to +4.8‰, +0.3‰ to +1.3‰, and +3.4‰ to +5.1‰, respectively; meanwhile, the DV area is an unsaturated zone. The $\delta^{18}\text{O}$, $\Delta^{17}\text{O}$, and $\delta^{37}\text{Cl}$ values of ClO_4^- in the sodium nitrate deposit in ore deposits ranges from +2.9‰ to +26.1‰, +8.6‰ to +18.4‰, and -3.1‰ to -0.8‰, respectively. The $^{36}\text{Cl}/\text{Cl}$ ratio of ClO_4^- in arid southwestern United States is $3,130 \times 10^{-15} - 28,800 \times 10^{-15}$ [42].

4.1.3. Comparison of Isotopic Composition of Perchlorate from Different Sources. Based on the known isotope data of perchlorate, the relation chart of $\delta^{37}\text{Cl}$ versus $\delta^{18}\text{O}$, $\Delta^{17}\text{O}$ versus $\delta^{18}\text{O}$, and $^{36}\text{Cl}/\text{Cl}$ versus $\delta^{37}\text{Cl}$ were plotted (Figure 2). Figure 1 shows that the $\delta^{37}\text{Cl}$ value (-3‰ to +2‰) of synthetic ClO_4^- partially overlaps the $\delta^{37}\text{Cl}$ value (-3‰ to +6‰) of naturally originated ClO_4^- in the arid area of the southwestern United States. ClO_4^- in saltpeter has a significantly negative $\delta^{37}\text{Cl}$ value (-15‰ to -19‰). The reason why natural ClO_4^- has an extensive range of $\delta^{37}\text{Cl}$ values is not apparent; it may be related to the regional origin of atmospheric chlorine or the formation mechanism of ClO_4^- . The synthetic ClO_4^- has a significantly different oxygen isotope composition than that of natural ClO_4^- . The $\Delta^{17}\text{O}$ value of synthetic ClO_4^- is approximately 0, while natural ClO_4^- has a positive $\Delta^{17}\text{O}$ value; hence, the $\Delta^{17}\text{O}$ value is the most sensitive and accurate indicator for identifying synthetic and naturally originated ClO_4^- . However, natural ClO_4^- in different regions shows different degrees of ^{17}O anomalies, which may be due to the different formation mechanisms and pathways of atmospheric ClO_4^- and its occurrence in environment. Estrada et al. have summarized some reactions possibly leading to the formation of ClO_4^- via O_3 and UV oxidation of ClO_x species [51]. Generally, ClO_4^- formed by atmospheric O_3 oxidation has a larger $\Delta^{17}\text{O}$ value, while ClO_4^- formed by photochemical reactions or lightning effects has a smaller $\Delta^{17}\text{O}$ value. The ^{17}O abnormal signal can be preserved for thousands or even millions of years in arid environments. ^{36}Cl is mainly produced by cosmic rays in the stratosphere; thus, atmospheric-derived ClO_4^- has a higher $^{36}\text{Cl}/\text{Cl}$ ratio, while synthetic ClO_4^- has a lower $^{36}\text{Cl}/\text{Cl}$ ratio.

4.2. Fractionation Characteristics of Isotopes during the Biodegradation of Perchlorate. The biodegradation of ClO_4^- is a multi-stage reaction catalyzed by reductase [52, 53], which can be divided into three steps: $\text{ClO}_4^- \rightarrow \text{ClO}_3^- \rightarrow \text{ClO}_2^- \rightarrow \text{Cl}^- + \text{O}_2$. The biodegradation of ClO_4^- is often accompanied by the fractionation of stable chlorine and oxygen isotopes. Previous laboratory and field studies have conducted experiments for preliminary research on the degree and characteristics of fractionation. Coleman et al. [54] and Sturchio et al. [30] used *Azospira*

suillum bacteria to conduct liquid culture medium experiments, to determine the dynamic fractionation effect of Cl isotopes, wherein acetate was the electron donor and ClO_4^- was the only electron acceptor. By conducting two separate culture fluid experiments (ClO_4^- complete degradation time is about 90 min), Coleman et al. obtained $\epsilon^{37}\text{Cl}$ values of $-15.8 \pm 0.4\%$ and $-14.8 \pm 1.3\%$ at 37°C. By performing the culture solution experiment, which has different degradation rates (ClO_4^- complete degradation time is 18 days and 5.5 h). Sturchio et al. obtained $\epsilon^{37}\text{Cl}$ values at 22°C of -16.6‰ and -12.9‰, respectively. Ader et al. [55] obtained a more accurate $\epsilon^{37}\text{Cl}$ value ($-14.98 \pm 0.15\%$) based on the statistical analysis of experimental data (reported by Coleman et al.). Additionally, Sturchio et al. [53] performed further experiments using two different strains (*A. suillum* JPLRND and *Dechlorospirillum* sp. FBR2) to degrade ClO_4^- in liquid culture at 22°C and 10°C, respectively, and simultaneously determined the fractionation effect of Cl and O. The values of $\epsilon^{37}\text{Cl}$ and $\epsilon^{18}\text{O}$ were $-13.2 \pm 0.5\%$ and $-33.1 \pm 1.2\%$, respectively, and the value of $\epsilon^{18}\text{O}/\epsilon^{37}\text{Cl}$ of the remaining proportion of ClO_4^- is always constant (2.50 ± 0.04). Sturchio et al. also used ^{18}O -rich heavy oxygen water to test whether oxygen isotope exchange occurred between ClO_4^- and H_2O during the biodegradation process. The experimental results did not show the occurrence of an oxygen isotope exchange reaction [53]. This indicated that biodegradation did not change the $\Delta^{17}\text{O}$ value of ClO_4^- . The push-pull field experiment of in situ aquifers conducted by Hatzinger et al. [36] showed that the $\epsilon^{37}\text{Cl}$ and $\epsilon^{18}\text{O}$ values are only 0.3–0.4 times that of the indoor experiment, whereas the $\epsilon^{18}\text{O}/\epsilon^{37}\text{Cl}$ ratio (2.63) is consistent with the measured value of the indoor experiment. Therefore, the consistency of the $\epsilon^{18}\text{O}/\epsilon^{37}\text{Cl}$ ratio between the indoor and in situ experiments in the field provides a possibility for stable chlorine and oxygen isotopes being able to indicate the biodegradation of perchlorate without concealing its source information. In Figure 3, the set of parallel dashed lines with arrows indicates the changing trend of the $\delta^{37}\text{Cl}$ and $\delta^{18}\text{O}$ values of ClO_4^- during the biodegradation of ClO_4^- . The concentration of ClO_4^- (remaining fraction F) can be used to inversely calculate the isotope composition before biodegradation.

4.3. Application Examples of Isotope Tracer of ClO_4^- in Groundwater. Investigating and determining the isotopic composition of different sources of ClO_4^- provide necessary data support for establishing the end-member model of the isotope characteristic value of different sources of ClO_4^- . The isotope kinetic fractionation characteristics of ClO_4^- biodegradation provide a theoretical basis for tracing the source of ClO_4^- in environmental media. The Chino Basin in California, Long Island in New York, and San Bernardino Basin in California are three typical ClO_4^- -contaminated aquifers. The isotopic composition of ClO_4^- ($\delta^{37}\text{Cl}$, $\delta^{18}\text{O}$, and $\Delta^{17}\text{O}$) in groundwater in the three regions was plotted on the end-member model diagram of the isotopic composition of ClO_4^- from different sources (as shown in Figure 4). The comprehensive characteristics of Cl and poly-oxygen

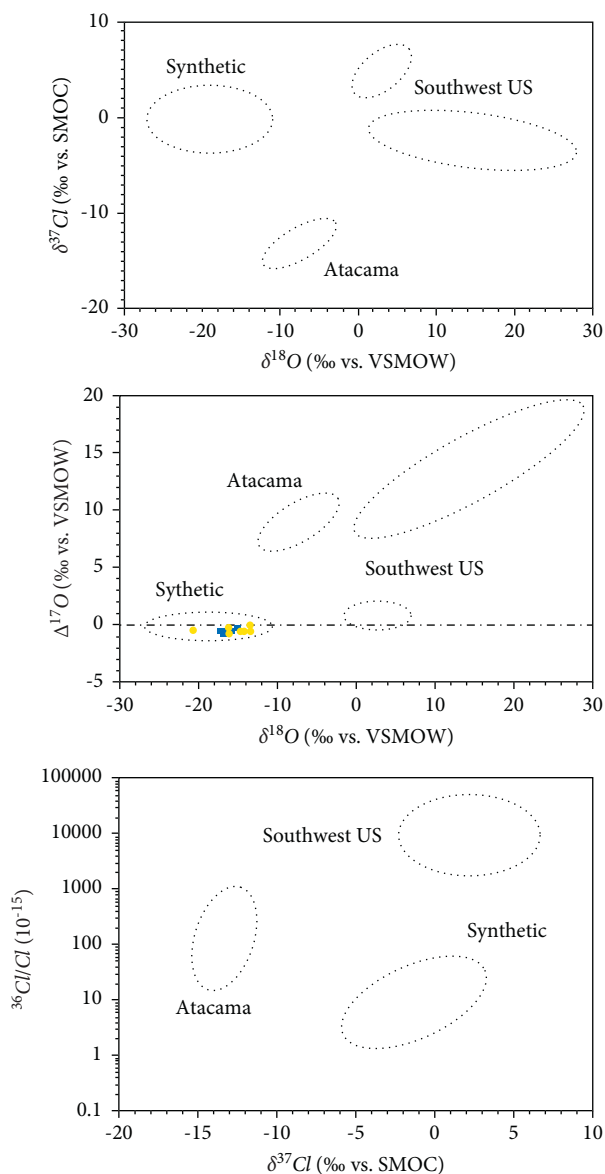


FIGURE 2: $\delta^{37}\text{Cl}$ (‰) versus $\delta^{18}\text{O}$ (‰) values (upper diagram) and $\Delta^{17}\text{O}$ (‰) versus $\delta^{18}\text{O}$ (‰) values (middle diagram) for samples of synthetic ClO_4^- , Atacama ClO_4^- , and southwest ClO_4^- . Southwest ClO_4^- is subdivided into southern SHP and DV [31, 32, 34]. $^{36}\text{Cl}/\text{Cl}$ versus $\delta^{37}\text{Cl}$ (‰) values (bottom diagram) for samples of synthetic ClO_4^- , Atacama ClO_4^- , and Southwest ClO_4^- [42]. The colored points represent the isotope value of some analytical reagents and firework samples measured by the authors (purple points: KClO_4 , CsClO_4 , NaClO_4 , RbClO_4 , and $\text{Mg}(\text{ClO}_4)_2$ and blue points: firework samples).

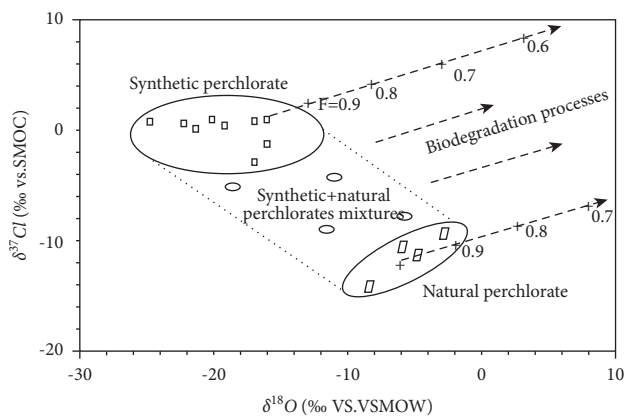


FIGURE 3: Schematic relation between characteristic $\delta^{37}\text{Cl}$ and $\delta^{18}\text{O}$ values (per mil) of synthetic and natural perchlorate samples during biodegradation processes [53].

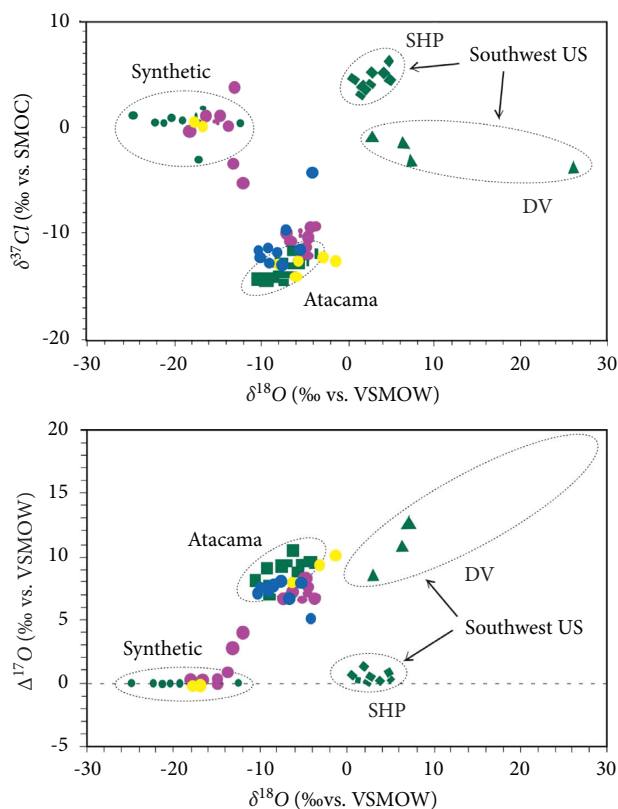


FIGURE 4: $\delta^{37}\text{Cl}$ (‰) versus $\delta^{18}\text{O}$ (‰) values and $\Delta^{17}\text{O}$ (‰) versus $\delta^{18}\text{O}$ (‰) values show stable isotope data for ClO_4^- in groundwater samples from the Chino Basin, California (blue symbols) [56], Long Island, New York (yellow symbols) [57], and southeastern San Bernardino Basin, California (red symbols) [58] in comparison to the principal known source types in the region, which is shown in Figure 1.

isotopes in the groundwater of the three regions indicated that the main source of ClO_4^- in the groundwater of the Chino Basin in California was Chilean saltpeter from the Atacama Desert, which is used as agricultural fertilizer [56]. The source of ClO_4^- in the groundwater of Long Island in New York was Chilean saltpeter from the Atacama Desert and synthetic ClO_4^- [57]. The source of ClO_4^- in the groundwater in the San Bernardino Basin of California is Chilean saltpeter from the Atacama Desert and synthetic ClO_4^- from the rocket test site; some areas are a mix of the two pollution plumes [58].

5. Conclusion and Outlook

Perchlorates from different sources have different isotopic characteristic values ($\delta^{18}\text{O}$, $\Delta^{17}\text{O}$, $\delta^{37}\text{Cl}$, and $^{36}\text{Cl}/\text{Cl}$) and are related to their formation mechanisms. The ^{17}O abnormal signal can be preserved for thousands or even millions of years in arid environments. Even if the biodegradation of perchlorate occurs under some specific conditions, along with the kinetic fractionation of chlorine and oxygen isotopes, its $\Delta^{17}\text{O}$ value or $^{36}\text{Cl}/\text{Cl}$ ratio will not change. Moreover, $\epsilon^{18}\text{O}/\epsilon^{37}\text{Cl}$ (the fractionation coefficient of

oxygen and chlorine isotopes) is constant, potentially revealing the biodegradation of perchlorate without disguising its source information. Therefore, the comprehensive characteristics of stable chlorine and poly-oxygen isotopes are expected to provide direct evidence for identifying the source of perchlorate in groundwater. However, further studies are needed to qualitatively identify and quantitatively evaluate perchlorate pollution sources.

- (1) The key problem in applying multi-isotope technology to identify the source of perchlorate in groundwater is to effectively distinguish the characteristic values of the end-member isotopes of different sources of perchlorate. Current research achievements are mainly limited to the United States and Chile and have apparent geographic limitations. The effective analysis of the source of perchlorate in polluted aquifers in different regions needs to be enriched by the isotope characteristic values and end-member model.
- (2) Nonmass fractionation of oxygen isotopes ($\Delta^{17}\text{O} > 0$) is a unique feature of natural perchlorate, which can effectively distinguish between natural sources of perchlorate and synthetic pollution sources. The isotopic composition characteristics of natural perchlorate show apparent differences in different regions and environments. To characterize its isotopic composition characteristics on a global scale and reveal the formation mechanism, it is necessary to analyze and study more representative samples from different regions.
- (3) Perchlorate pollution in groundwater is mostly caused by natural sources, and some are caused by human activities [59]. Natural and synthetic perchlorates have significantly different isotope characteristic values. Natural perchlorate isotope characteristic values have apparent geographic limitations (limited to the United States and Chile), so the more important research is to supplement the isotope signatures from other regions. At this stage, there is still considerable uncertainty in the distinction between synthetic perchlorate pollution sources. The perchlorate products produced by the same production process have similar chlorine isotope compositions; however, oxygen isotope compositions are quite different, which may be related to the water source used in the production process. Research on the isotope composition of synthetic perchlorate, its production process, and other influencing factors can provide a theoretical basis for effectively distinguishing the synthetic pollution sources of perchlorate.

Data Availability

The data used to support this study are from previous studies and experiments.

Conflicts of Interest

The authors declare that they have no conflicts of interest.

Acknowledgments

The study involved in this paper was supported by the projects Hydrogeological Survey of Weihe River Basin (DD20190333); Hydrogeological Survey of Sanjiang Plain (DD20190339); Stable Chlorine and Multi-Oxygen Isotopic Tracing of Perchlorate in Groundwater (41202169); and New Measurement Technique for Stable Chlorine and Oxygen Isotopic Compositions of Perchlorate in Groundwater (2012M511702).

References

- [1] Z. Gao, Z. Wang, S. Wang et al., "Factors that influence the chemical composition and evolution of shallow groundwater in an arid region: a case study from the middle reaches of the Heihe River, China," *Environmental Earth Sciences*, vol. 78, no. 14, p. 390, 2019.
- [2] J. Liu, Y. Peng, C. Li, Z. Gao, and S. Chen, "Characterization of the hydrochemistry of water resources of the Weibei plain, Northern China, as well as an assessment of the risk of high groundwater nitrate levels to human health," *Environmental Pollution*, vol. 268, Article ID 115947, 2021.
- [3] J. Liu, Y. Peng, C. Li, Z. Gao, and S. Chen, "An investigation into the hydrochemistry, quality and risk to human health of groundwater in the central region of Shandong Province, North China," *Journal of Cleaner Production*, vol. 282, Article ID 125416, 2021.
- [4] Z. Wen, W. Zheng, H. Shen, and M. Hu, "Research progress on the hazards, water pollution status and removal technique of perchlorate," *Environmental Chemistry*, January, vol. 38, 2019.
- [5] E. Stokstad, "Perchlorate study suggests lower risk," *Science*, vol. 307, no. 5707, p. 191b, 2005.
- [6] E. Stokstad, "Environmental health: debate continues over safety of water spiked with rocket fuel," *Science*, vol. 307, no. 5709, p. 507, 2005.
- [7] Y. Jia, X. Tang, and L. Jiaren, "Research advance in effect of perchlorate on human health," *Environmental Health*, vol. 25, 2008.
- [8] Z. Liao, D. Cao, Z. Gao, and S. Zhang, "Occurrence of perchlorate in processed foods manufactured in China," *Food Control*, vol. 107, Article ID 106813, 2020.
- [9] K. Kosaka, M. Asami, Y. Matsuoka, M. Kamoshita, and S. Kunikane, "Occurrence of perchlorate in drinking water sources of metropolitan area in Japan," *Water Research*, vol. 41, no. 15, pp. 3474–3482, 2007.
- [10] O. Quiñones, J.-E. Oh, B. Vanderford, J. H. Kim, J. Cho, and S. A. Snyder, "Perchlorate assessment of the Nakdong and Yeongsan watersheds, Republic of Korea," *Environmental Toxicology & Chemistry*, vol. 26, no. 7, pp. 1349–1354, 2007.
- [11] Y. Shi, J. Gao, and L. Xin, "The investigation of perchlorate pollution level in Liuyang River water, sediment and its nearby soil," *Environmental Chemistry*, vol. 29, no. 3, pp. 388–391, 2010.
- [12] C. A. Sanchez, B. C. Blount, L. Valentin-Blasini, S. M. Lesch, and R. I. Krieger, "Perchlorate in the feed–dairy continuum of the southwestern United States," *Journal of Agricultural and Food Chemistry*, vol. 56, no. 13, pp. 5443–5450, 2008.
- [13] S. A. Snyder, R. C. Pleus, B. J. Vanderford, and J. C. Holady, "Perchlorate and chlorate in dietary supplements and flavor enhancing ingredients," *Analytica Chimica Acta*, vol. 567, no. 1, pp. 26–32, 2006.
- [14] M. Ader, M. L. Coleman, S. P. Doyle, M. Stroud, and D. Wakelin, "Methods for the stable isotopic analysis of chlorine in chlorate and perchlorate compounds," *Analytical Chemistry*, vol. 73, no. 20, pp. 4946–4950, 2001.
- [15] T. Zhang, Q. Wu, H. W. Sun, J. Rao, and K. Kannan, "Perchlorate and iodide in whole blood samples from infants, children, and adults in Nanchang, China," *Environmental Science & Technology*, vol. 44, no. 18, pp. 6947–6953, 2010.
- [16] L. Valentin-Blasini, J. P. Mauldin, D. Maple, and B. C. Blount, "Analysis of perchlorate in human urine using ion chromatography and electrospray tandem mass spectrometry," *Analytical Chemistry*, vol. 77, no. 8, pp. 2475–2481, 2005.
- [17] Q. Wu, T. Zhang, H. Sun, and K. Kannan, "Perchlorate in tap water, groundwater, surface waters, and bottled water from China and its association with other inorganic anions and with disinfection byproducts," *Archives of Environmental Contamination and Toxicology*, vol. 58, no. 3, pp. 543–550, 2010.
- [18] S. Jiang, Y. Li, and H. Ma, "Source, pollution status and analytical methods of perchlorate in the environment," *Advances in Earth Science*, vol. 6, pp. 617–624, 2010.
- [19] National Service Center for Environmental Publications, *Interim Drinking Water Health Advisory For Perchlorate*, p. 12, National Service Center for Environmental Publications, Cincinnati, OH, USA, 2008.
- [20] USEPA (United States Environmental Protection Agency), *Interim Drinking Water Health Advisory for Perchlorate*, US Environmental Protection Agency, Washington, DC, USA, 2008, <http://www.epa.gov/safewater/contaminants/unregulated/perchlorate.html>.
- [21] B. van Aken and J. L. Schnoor, "Evidence of perchlorate (ClO₄⁻) reduction in plant tissues (poplar tree) using radiolabeled ³⁶ClO₄⁻," *Environmental Science & Technology*, vol. 36, no. 12, pp. 2783–2788, 2002.
- [22] K. Kannan, M. L. Praamsma, J. F. Oldi, T. Kunisue, and R. K. Sinha, "Occurrence of perchlorate in drinking water, groundwater, surface water and human saliva from India," *Chemosphere*, vol. 76, no. 1, pp. 22–26, 2009.
- [23] N. Her, H. Jeong, J. Kim, and Y. Yoon, "Occurrence of perchlorate in drinking water and seawater in South Korea," *Archives of Environmental Contamination and Toxicology*, vol. 61, no. 2, pp. 166–172, 2011.
- [24] T. J. Scheytt, J. Freywald, and C. J. Ptacek, "Study of selected soil, ground, and surface water samples on perchlorate in Germany: first results," *Grundwasser*, vol. 16, no. 1, pp. 37–43, 2011.
- [25] Y. Liu, S. Mou, and A. Lin, "Investigation of bromate, haloacetic acids and perchlorate in Beijing's drinking water," *Environmental Science*, vol. 25, no. 2, pp. 51–55, 2004.
- [26] Y. Liu, S. Mou, and S. Heberling, "Determination of trace level bromate and perchlorate in drinking water by ion chromatography with an evaporative preconcentration technique," *Journal of Chromatography A*, vol. 956, no. 1-2, pp. 85–91, 2002.
- [27] Y. Liu and S. Mou, "Determination of trace levels of haloacetic acids and perchlorate in drinking water by ion chromatography with direct injection," *Journal of Chromatography A*, vol. 997, no. 1-2, pp. 225–235, 2003.
- [28] USGS (U.S. Geological Survey), *Resources on Isotopes: Periodic Table-Chlorine*, 2006, http://www.rcamnl.wr.usgs.gov/isoig/period/cl_iig.html.
- [29] N. C. Sturchio, J. K. Böhlke, B. Gu, P. B. Hatzinger, and W. A. Jackson, "Isotopic tracing of perchlorate in the

- environment,” in *Handbook of Environmental Isotope Geochemistry*, pp. 437–452, Springer, Berlin Heidelberg, 2011.
- [30] N. C. Sturchio, P. B. Hatzinger, M. D. Arkins, C. Suh, and L. J. Heraty, “Chlorine isotope fractionation during microbial reduction of perchlorate,” *Environmental Science & Technology*, vol. 37, no. 17, pp. 3859–3863, 2003.
- [31] J. K. Böhlke, N. C. Sturchio, B. Gu et al., “Perchlorate isotope forensics,” *Analytical Chemistry*, vol. 77, no. 23, pp. 7838–7842, 2005.
- [32] N. C. Sturchio, J. K. Böhlke, B. Gu et al., “Stable isotopic composition of chlorine and oxygen in synthetic and natural perchlorate,” in *Perchlorate Environmental Occurrences, Interactions, and Treatment*, J. D. Coates, Ed., Springer, New York, NY, USA, 2006.
- [33] H. Bao and B. Gu, “Natural perchlorate has a unique oxygen isotope signature,” *Environmental Science & Technology*, vol. 38, no. 19, pp. 5073–5077, 2004.
- [34] W. A. Jackson, J. K. Böhlke, B. Gu, P. B. Hatzinger, and N. C. Sturchio, “Isotopic composition and origin of indigenous natural perchlorate and Co-occurring nitrate in the southwestern United States,” *Environmental Science & Technology*, vol. 44, no. 13, pp. 4869–4876, 2010.
- [35] N. C. Sturchio, J. K. Böhlke, and A. D. Beloso, “Oxygen and chlorine isotopic fractionation during perchlorate biodegradation: laboratory results and implications for forensics and natural attenuation studies,” *Environmental Science and Technology*, vol. 41, pp. 2796–2802, 2007.
- [36] P. B. Hatzinger, J. K. Böhlke, N. C. Sturchio, B. Gu, L. J. Heraty, and R. C. Borden, “Fractionation of stable isotopes in perchlorate and nitrate during in situ biodegradation in a sandy aquifer,” *Environmental Chemistry*, vol. 6, no. 1, pp. 44–52, 2009.
- [37] J. K. Böhlke, S. J. Mroczkowski, N. C. Sturchio et al., “Stable isotope analyses of oxygen ($^{18}\text{O}:^{17}\text{O}:^{16}\text{O}$) and chlorine ($^{37}\text{Cl}:^{35}\text{Cl}$) in perchlorate: reference materials, calibrations, and interferences,” *Rapid Communications in Mass Spectrometry*, vol. 31, pp. 85–110, 2017.
- [38] B. Gu, J. K. Böhlke, and N. C. Sturchio, “Removal, recovery and fingerprinting of perchlorate by ion exchange processes,” *Ion Exchange and Solvent Extraction: A Series of Advances*, CRC, Boca Raton, FL, USA, 2011.
- [39] J. Sun, S. Sun, and M. Fan, “Pollution control technologies of perchlorate in water,” *Chinese Journal of Environmental Engineering*, vol. 2, no. 4, pp. 461–465, 2008.
- [40] B. Gu, G. M. Brown, L. Maya, M. J. Lance, and B. A. Moyer, “Regeneration of perchlorate (ClO_4^-)-Loaded anion exchange resins by a novel tetrachloroferrate (FeCl_4^-) displacement technique,” *Environmental Science & Technology*, vol. 35, no. 16, pp. 3363–3368, 2001.
- [41] Guidance Document, “Validation of chlorine and oxygen isotope ratio analysis to differentiate perchlorate sources and to document perchlorate biodegradation,” <https://citeseerx.ist.psu.edu/viewdoc/download?doi=10.1.1.362.8431&rep=rep1&type=pdf>.
- [42] N. C. Sturchio, M. Caffee, A. D. Beloso Jr et al., “Chlorine-36 as a tracer of perchlorate origin,” *Environmental Science & Technology*, vol. 43, no. 18, pp. 6934–6938, 2009.
- [43] C. J. Eastoe, T. M. Peryt, O. Y. Petrychenko, and D. Geisler-Cussey, “Stable chlorine isotopes in Phanerozoic evaporites,” *Applied Geochemistry*, vol. 22, no. 3, pp. 575–588, 2007.
- [44] K. Purnendu, P. Dasgupta, M. Kalyani, and W. Andrew Jackson, “The origin of naturally occurring perchlorate: the role of atmospheric processes,” *Environmental Science & Technology*, vol. 39, pp. 1569–1575, 2005.
- [45] B. Rao, T. A. Anderson, G. J. Orris et al., “Widespread natural perchlorate in unsaturated zones of the southwest United States,” *Environmental Science & Technology*, vol. 41, no. 13, pp. 4522–4528, 2007.
- [46] E. T. Urbansky, S. K. Brown, M. L. Magnuson, and C. A. Kelty, “Perchlorate levels in samples of sodium nitrate fertilizer derived from Chilean caliche,” *Environmental Pollution*, vol. 112, no. 3, pp. 299–302, 2001.
- [47] G. Michalski, J. K. Böhlke, and M. Thiemens, “Long term atmospheric deposition as the source of nitrate and other salts in the Atacama Desert, Chile: New evidence from mass-independent oxygen isotopic compositions,” *Geochimica et Cosmochimica Acta*, vol. 68, no. 20, pp. 4023–4038, 2004.
- [48] G. E. Ericksen, “The Chilean nitrate deposits,” *American Scientist*, vol. 71, no. 4, pp. 366–374, 1983.
- [49] P. K. DasGupta, J. V. Dyke, A. B. Kirk, and W. A. Jackson, “Perchlorate in the United States. Analysis of relative source contributions to the food chain,” *Environmental Science & Technology*, vol. 40, no. 21, pp. 6608–6614, 2006.
- [50] S. Susarla, T. W. Collette, A. W. Garrison, N. L. Wolfe, and S. C. McCutcheon, “Perchlorate identification in fertilizers,” *Environmental Science & Technology*, vol. 33, no. 19, pp. 3469–3472, 1999.
- [51] N. Estrada, T. A. Anderson, J. K. Böhlke et al., “Origin of the isotopic composition of natural perchlorate: experimental results for the impact of reaction pathway and initial ClO_x reactant,” *Geochimica et Cosmochimica Acta*, vol. 311, 2021.
- [52] A. L. Seyfferth, N. C. Sturchio, and D. R. Parker, “Is perchlorate metabolized or Re-translocated within lettuce leaves? A stable-isotope approach,” *Environmental Science & Technology*, vol. 42, no. 24, pp. 9437–9442, 2008.
- [53] N. C. Sturchio, J. K. Böhlke, A. D. Beloso Jr, S. H. Streger, L. J. Heraty, and P. B. Hatzinger, “Oxygen and chlorine isotopic fractionation during perchlorate biodegradation: Laboratory results and implications for forensics and natural attenuation studies,” *Environmental Science & Technology*, vol. 41, no. 8, pp. 2796–2802, 2007.
- [54] M. L. Coleman, M. Ader, S. Chaudhuri, and J. D. Coates, “Microbial isotopic fractionation of perchlorate chlorine,” *Applied and Environmental Microbiology*, vol. 69, no. 8, pp. 4997–5000, 2003.
- [55] M. Ader, S. Chaudhuri, and J. D. Coates, “Microbial perchlorate reduction: a precise laboratory determination of the chlorine isotope fractionation and its possible biochemical basis,” *Earth and Planetary Science Letters*, vol. 269, pp. 604–612, 2008.
- [56] N. C. Sturchio, A. D. Beloso Jr, and L. J. Heraty, “Isotopic evidence for agricultural perchlorate in groundwater of the western chino basin,” in *Proceedings of the Sixth International Conference On Remediation Of Chlorinated And Recalcitrant Compounds*, pp. 18–22, Monterey, CA, USA, May 2008.
- [57] J. K. Böhlke, P. B. Hatzinger, and N. C. Sturchio, “Atacama perchlorate as an agricultural contaminant in groundwater: isotopic and chronologic evidence from Long Island, New York [J],” *Environmental Science and Technology*, vol. 43, pp. 5619–5625, 2009.
- [58] N. C. Sturchio, J. R. Hoaglund III, R. J. Marroquin et al., “Isotopic mapping of groundwater perchlorate plumes,” *Ground Water*, vol. 50, no. 1, pp. 94–102, 2011.
- [59] K. Purnendu, V. D. Y. K. E. Dasgupta Jason, and B. Andrea, “Perchlorate in the United States. Analysis of relative source contributions to the food chain,” *Environmental Science and Technology*, vol. 40, pp. 6608–6614, 2006.

Research Article

Natural Background Level and Contamination of Shallow Groundwater Salinity in Various Aquifers in a Coastal Urbanized Area, South China

Pan Bi,^{1,2} Dongya Han ,³ Chunyan Liu,³ Liquan Xiao,⁴ Heqiu Wu,⁵ and Meng Zhang¹

¹School of Water Resources and Environment, Hebei GEO University, Shijiazhuang, China

²Key Laboratory of Sustained Development and Utilization of Water Resources, Shijiazhuang, China

³Institute of Hydrogeology and Environmental Geology, Chinese Academy of Geological Sciences, Shijiazhuang, China

⁴416 Geological Team of Hunan Bureau of Geology and Mineral Exploration and Development, Zhuzhou, China

⁵Zhejiang Engineering Geophysical Survey and Design Institute Co.,Ltd., Hangzhou, China

Correspondence should be addressed to Dongya Han; handongyaycn@126.com

Received 30 May 2021; Accepted 27 July 2021; Published 9 August 2021

Academic Editor: Chengcheng Li

Copyright © 2021 Pan Bi et al. This is an open access article distributed under the Creative Commons Attribution License, which permits unrestricted use, distribution, and reproduction in any medium, provided the original work is properly cited.

Assessing natural background levels (NBLs) of chemical components in groundwater is useful for the evaluation of groundwater contamination in urbanized areas. The present study assessed the NBL of total dissolved solids (TDS) in various groundwater units in the Pearl River Delta (PRD) where urbanization is a large scale and discussed factors controlling groundwater salinity contamination in the PRD. Results showed that the NBL of TDS in groundwater in the coastal-alluvial plain was more than 1.5 times that in other groundwater units because of the seawater intrusion in this groundwater unit. By contrast, interactions of water and soils/rocks were the main factors controlling the NBLs of TDS in other groundwater units. Groundwater salinity contamination in the PRD was positively correlated with the urbanization level. Wastewater from township-village enterprises and industrial wastewater were likely to be the main sources for groundwater salinity contamination in the PRD. Moreover, the wastewater leakage from sewer systems was one of the main pathways for groundwater salinity contamination in urbanized areas, because the proportion of groundwater salinity contamination in urbanized areas formed in 1988–1998 was more than 1.5 times that in urbanized areas formed in 1998–2006 regardless of groundwater units. Besides, sewage irrigation and leakage of landfill leachate were also important sources for groundwater salinity contamination in the PRD.

1. Introduction

Groundwater plays a crucial role in our livelihoods by making itself available for drinking. For example, more than half of drinking water is sourced from groundwater globally [1]. However, groundwater is often contaminated due to the large-scale urbanization and industrialization in urbanized areas [2, 3]; thereby, its quality in these areas is often deteriorated [4]. For instance, the Pearl River Delta (PRD) is a rapidly urbanized and industrialized area in China, and groundwater in this area is often contaminated by the salinity because of various anthropogenic sources such as high levels of salinity in wastewaters [3, 5]. In addition, several studies reported that geogenic sources are mainly

responsible for the origin of groundwater salinity in Quaternary aquifers in the PRD by using isotopic, hydrochemical, and microbial evidence [6–8]. However, the origins of groundwater salinity in fissured and karst aquifers as well as the spatial distribution of groundwater salinity contamination in the PRD are unclear. Thus, in order to improve the management and protection of groundwater resources, it is necessary to evaluate the status of groundwater salinity contamination and investigate the factors controlling groundwater salinity in the PRD.

To date, the evaluation of groundwater contamination is often based on the maximum admissible concentrations of chemical components which are harmless to human beings [9–11]. In this case, the impacts of natural factors on the

concentrations of chemical components in groundwater are neglected. However, high levels of chemical components in groundwater may derive from not only anthropogenic contamination but also natural processes [12–15]. Therefore, it is more reasonable to evaluate the groundwater contamination based on natural background levels (NBLs) of chemical components in groundwater. Here, NBLs are defined as concentrations present in groundwater as controlled by natural geogenic, biological, and chemical processes [16]. Preselection is the most common method for the assessment of NBL in groundwater [17]. For example, the method of oxidation capacity (OXC), as one of the preselection methods, was often used to assess the groundwater NBL in coastal areas [16, 18].

Therefore, the objectives of this study are to assess the NBL of salinity (total dissolved solids, TDS) in the PRD by using the OXC method with Grubbs' test, to depict the spatial distribution of groundwater salinity contamination with a Kriging method and to discuss factors controlling groundwater salinity contamination in the PRD. The conclusions would be helpful for improving the management and protection of groundwater resources in the PRD.

2. Study Area

The PRD occupies a total area of $4.17 \times 10^4 \text{ km}^2$ in the southern part of Guangdong province, China. It includes nine cities, such as Guangzhou, Shenzhen, Foshan, Dongguan, Zhongshan, Zhuhai, Huizhou, Jiangmen, and Zhaoqing, in the district. It is bounded by hills in the east, west, and north and by the South China Sea in the south; thereby, its topography inclines from the east, west, and north to the south. Three major rivers, such as East River, West River, and North River, merge in the south and form the Pearl River, which finally discharges into the South China Sea. The PRD can be divided into three areas with different urbanization levels, such as urbanized area (UA), periurban area (PUA), and nonurbanized area (NUA) [13]. Besides, the UA in the PRD formed before 1988, from 1988 to 1998, and from 1998 to 2006 are denoted by UA^{1st}, UA^{2nd}, and UA^{3rd}, respectively. UA^{1st} is characterized by a lower proportion of factories in comparison with UA^{2nd} and UA^{3rd}, while UA^{3rd} shows a relatively well-constructed sewer system in comparison with UA^{1st} and UA^{2nd} [5].

The PRD was formed as a result of the Tibetan Plateau uplift during the Tertiary and Quaternary Periods. It can be divided into four groundwater units (Figure 1). Unit A is related to a coastal-alluvial plain, which is located in the central and southern parts of the PRD and consists of two marine layers and two terrestrial layers [2]. The younger marine layer (M1) has an elevation of above -20 m , and the older marine layer (M2) is located between -15 and -40 m (Figure 1). The younger terrestrial layer (T1) can be sandy fluvial deposits or clayey silt. The older terrestrial layer (T2) is dominated by sand and gravel [19]. Groundwater in this unit is recharged primarily by atmospheric precipitation, agricultural irrigation, and seawater intrusion [20, 21]. Unit B (alluvial-proluvial aquifer) is outside of unit A, which is related to the valley and interhill plains where marine layers

are absent but terrestrial layers are common. Unit C (fractured aquifer) is related to hilly areas where bedrocks are fractured. Unit D is related to karst aquifers and accounts for less than 10% of the total area [22].

3. Materials and Methods

3.1. Sampling and Analytical Techniques. Approximately 400 groundwater samples were collected from the PRD. Specifically, 124 samples, 134 samples, 132 samples, and 9 samples were collected from units A to D, respectively. All the samples were stored at 4°C until the laboratory procedures could be performed. Redox potential (Eh), pH, and dissolved oxygen (DO) were measured on site using a multiparameter instrument (WTW Multi 340i/SET, Germany). Metals (K, Na, Ca, and Mg) were measured by inductively coupled plasma mass spectrometry (Agilent 7500ce ICP-MS, Tokyo, Japan). HCO_3^- and TDS were measured using acid-base titration and gravimetric methods, respectively. NH_4^+ and other anions (NO_3^- , SO_4^{2-} , and Cl^-) were analyzed by ion chromatography (Shimadzu LC-10ADvp, Japan). To ensure data quality, each sample was analyzed in triplicate, and sample batches were regularly interspersed with standards and blanks. The relative errors of inorganic parameters were $< \pm 5\%$.

3.2. NBL Assessment. Griffioen et al. reported that oxidation capacity is calculated as $7[\text{SO}_4] + 5[\text{NO}_3]$ with the concentration of the species in $[\text{mmol/L}]$ [16]. The oxidation capacity will be useless to identify groundwater with anthropogenic influence under the condition of a strongly reductive environment because groundwater SO_4 and NO_3 are at low levels. In this case, high levels of NH_4 will be a useful indicator for the identification of contaminated groundwater, because high levels of NH_4 in shallow groundwater in the PRD originated from human activities [23]. Therefore, a preselection method, consisting of two indicators such as the oxidation capacity and NH_4 concentration, was used for the assessment of NBL in groundwater in this study. Specifically, groundwater samples with oxidation capacity $> 3 \text{ meq/L}$ or $\text{NH}_4\text{-N}$ concentrations $> 0.5 \text{ mg/L}$ in original datasets were deleted, and the remaining datasets were denoted as PS datasets. Note that a higher value of 3 meq/L was selected as the threshold value for oxidation capacity in comparison with previous studies because geogenic sources are sometimes responsible for high levels of SO_4 in groundwater in the PRD [24]. Then, TDS concentrations in PS datasets in various groundwater units were tested by Grubbs' test ($\alpha = 0.01$) until normal distributions were obtained, and the outliers in various groundwater units were deleted (Supplementary material, Section 3.2) [25]. The remaining datasets were denoted as residual datasets. The maximum concentrations of TDS in residual datasets in various groundwater units were extracted as NBLs.

3.3. Evaluation of Contamination Levels. In this study, the contamination level of salinity in groundwater was quantified by the ratios of groundwater TDS concentrations to the

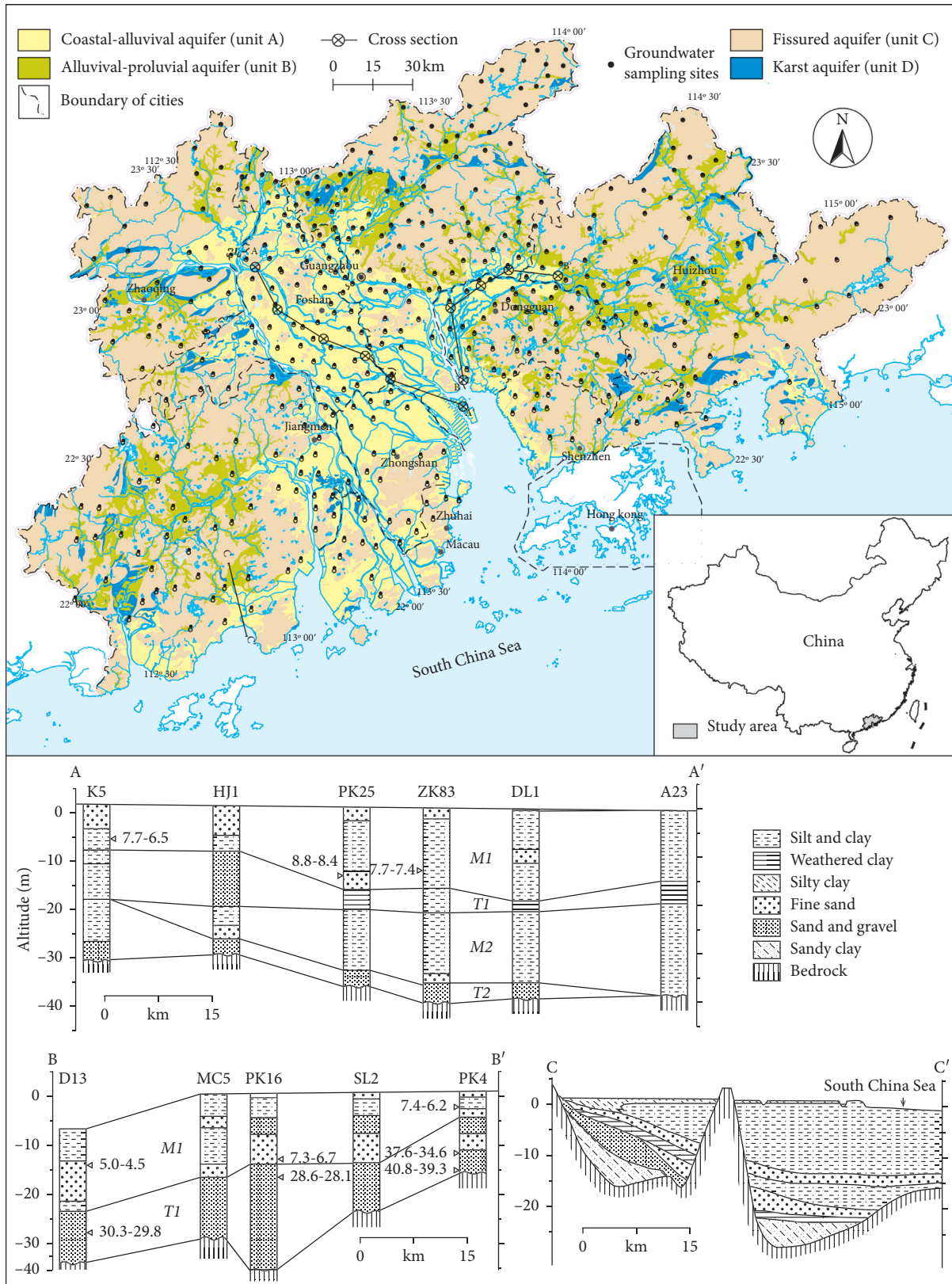


FIGURE 1: Groundwater units and sampling sites in the Pearl River Delta.

NBLs of TDS in various groundwater units. Thus, groundwater samples with different contamination levels are divided into four categories as follows: uncontaminated

(contamination level ≤ 1), low ($1 < \text{contamination level} \leq 2$), moderate ($2 < \text{contamination level} \leq 4$), and high (contamination level > 4). The spatial distribution of groundwater

salinity contamination in the PRD is depicted by a geostatistical analysis (MapGIS 10.2, China University of Geosciences, China). The universal kriging method and the estimation of empirical semivariogram models are used in MapGIS 10.2 software [26, 27]. The details are in the supplementary material (Section 3.2).

3.4. Socioeconomic Data. Socioeconomic data related to nine major cities in the PRD were compiled and used in this study. Relevant data were taken from the Statistical Yearbook of Guangdong Province and are compiled in Table S1 [28]; they include population density (PD, number of people/km²), gross domestic product (GDP, millions of Chinese yuan/km²), domestic sewage discharge (DSD, ton/km²), industrial wastewater discharge (IWD, ton/km²), ratio of urbanized areas (RUA, %), industrial enterprises above a specified size (IE, number/km²), township-village enterprises (TVEs, number/km²), agricultural output (AO, millions of Chinese yuan/km²), livestock output (LO, millions of Chinese yuan/km²), and livestock density (LD, number/km²).

3.5. Principal Components Analysis (PCA). The PCA is a useful technique for reducing a large number of variables to a small number of principal components (i.e., PCs) by linearly combining measurements made on the original variables [13]. In this study, the PCA was used to identify the relationships between the contamination level of groundwater salinity and the relevant socioeconomic data. In the PCA, only PCs with eigenvalues greater than one were retained for analyses, and the Varimax method was adopted. The terms “strong,” “moderate,” and “weak,” as applied to PC loadings, referred to absolute loading values of >0.75, 0.75–0.5, and 0.5–0.3, respectively [2].

4. Results

4.1. NBL Assessment for Groundwater Salinity. Using oxidation capacity >3 meq/L and NH₄-N concentrations >0.5 mg/L to identify groundwater samples with anthropogenic influence in this study, nearly 60% of groundwater samples with anthropogenic influence in original datasets were removed out (Figure 2), and the remaining datasets were denoted as PS datasets. Then, TDS concentrations in PS datasets in various groundwater units were tested by Grubbs’ test ($\alpha = 0.01$), and outliers in PS datasets were eliminated (Figure 3). The remaining datasets were denoted as residual datasets. The maximum concentrations of TDS in residual datasets in various groundwater units are extracted as NBLs; thereby, NBLs of TDS in units A to D were 688 mg/L, 432 mg/L, 321 mg/L, and 99 mg/L, respectively.

4.2. Distribution of Groundwater Salinity Contamination in the PRD

4.2.1. Salinity Contamination in Various Groundwater Units. As shown in Table 1, 21.1% of groundwater samples in the PRD were contaminated by salinity. Among them, low to high contamination levels of groundwater samples

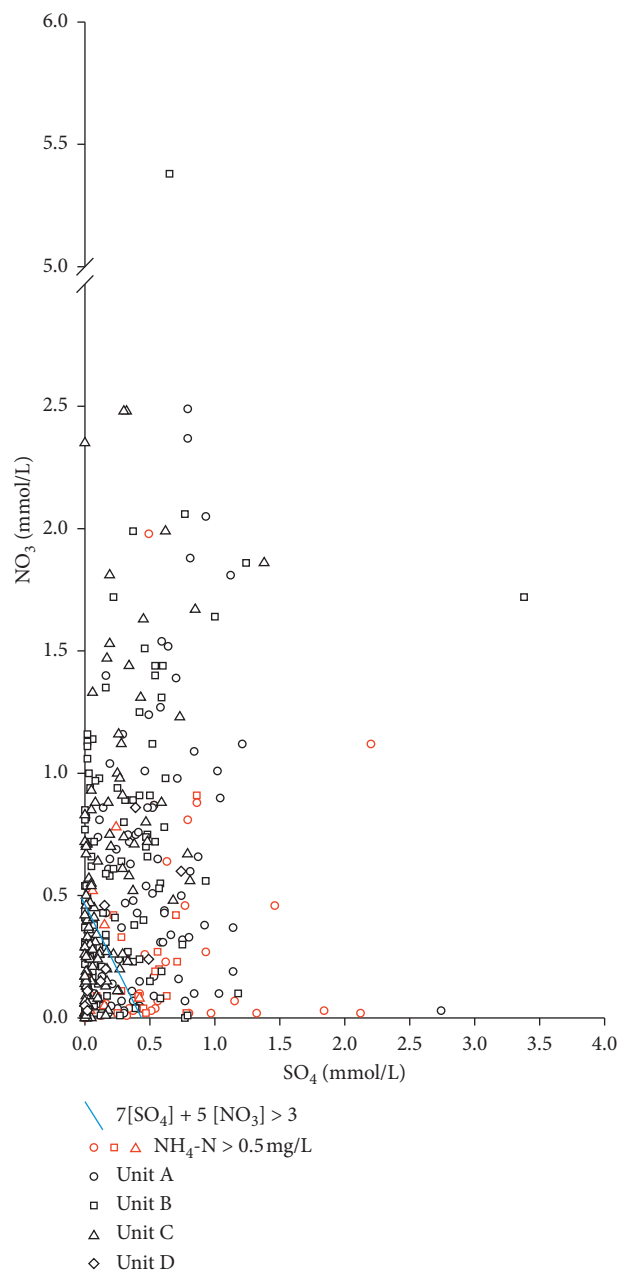


FIGURE 2: High levels of NH₄ as well as oxidation capacity in various groundwater units in the Pearl River Delta.

accounted for 16.5%, 3.8%, and 0.8%, respectively. Salinity contamination in various groundwater units in the PRD was significantly different. High levels of salinity contamination occurred in groundwater units A and B, but not in units C and D. By contrast, moderate levels of salinity contamination in groundwater unit D accounted for 44.4%, which was 10 times that in unit C and 20 times that in units A and B. Meanwhile, a low level of salinity contamination in groundwater unit A accounted for 26.6% and was more than 2 times that in other groundwater units. As far as the proportion of salinity contamination is concerned, groundwater unit D was the highest, which was 1.8 times that in unit A and 3.6 times that in units B and C.

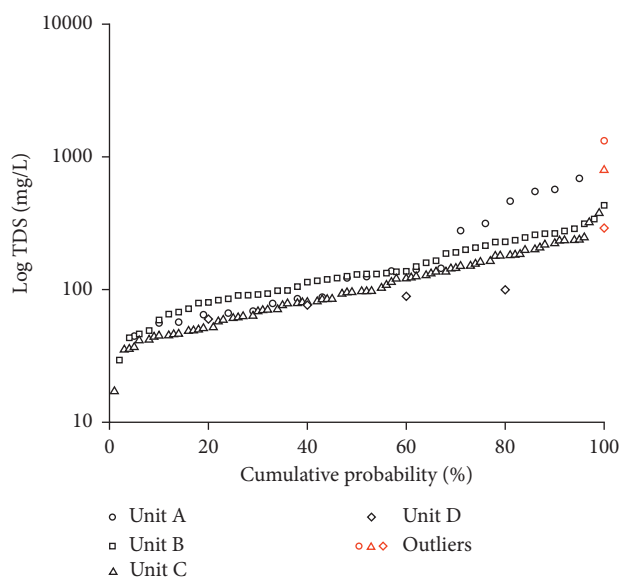


FIGURE 3: Outliers in PS datasets in various groundwater units tested by Grubbs' test.

TABLE 1: Groundwater salinity contamination in various groundwater units in the Pearl River Delta.

Contamination levels	PRD	Unit A	Unit B	Unit C	Unit D
Uncontaminated (%)	78.9	69.4	84.7	84.8	44.5
Low (%)	16.5	26.6	12.4	11.4	11.1
Moderate (%)	3.8	2.4	2.2	3.8	44.4
High (%)	0.8	1.6	0.7	0	0

4.2.2. Groundwater Salinity Contamination in Areas with Different Urbanization Levels. As seen in Table 2, the proportion of groundwater salinity contamination in UA was 29.7%, which was 1.2 times and 3.3 times that in PUA and NUA, respectively. This indicates that groundwater salinity contamination in the PRD was positively correlated with the urbanization level. Similarly, in groundwater unit A, the proportion of salinity contamination in UA was 1.8 times and 2.3 times that in PUA and NUA, respectively. Likewise, in groundwater unit B, the proportion of salinity contamination in UA was 1.2 times and 9.1 times that in PUA and NUA, respectively. By contrast, in groundwater unit C, the proportion of salinity contamination in PUA was the highest, which was 1.6 times and 3.9 times that in UA and NUA, respectively. This indicates that the correlation between the salinity contamination and the urbanization level in groundwater unit C was insignificant. Note that the salinity contamination in areas with different urbanization levels in groundwater unit D was not investigated because of too few samples. In addition, groundwater salinity contamination in UA formed in different periods in the PRD was also investigated. In groundwater unit A, proportions of salinity contamination in UA^{1st} and UA^{2nd} were close to each other and were approximately 1.5 times that in UA^{3rd} (Table S2). By contrast, the proportion of salinity contamination in groundwater unit B in UA^{2nd} was the highest and

was more than 5 times and 2 times that in UA^{1st} and UA^{3rd}, respectively (Table S2). Similarly, the proportion of salinity contamination in groundwater unit C in UA^{2nd} was also much higher than that in UA^{1st} and UA^{3rd} (Table S2).

4.2.3. Spatial Distribution of Groundwater Salinity Contamination in Various Cities. As shown in Table 3, the high level of groundwater salinity contamination occurred in Dongguan and Guangzhou cities only, which accounted for less than 1% of the total area (Figure 4). The moderate level of groundwater salinity contamination occurred in six cities except for Shenzhen, Zhuhai, and Zhaoqing, which accounted for approximately 5% of the total area (Figure 4). Among them, the occurrence of a moderate level of groundwater salinity contamination was mainly distributed in Dongguan and Zhongshan cities (Table 3). By contrast, the low level of groundwater salinity contamination occurred in all of the nine cities, which accounted for approximately 16% of the total area (Figure 4). As far as the proportion of groundwater salinity contamination is concerned, Zhongshan was the highest, which was followed by the order of Dongguan, Foshan, Guangzhou, Jiangmen, Huizhou, Shenzhen, Zhuhai, and Zhaoqing, respectively (Table 3).

4.3. Relationship between Contamination Levels of Groundwater Salinity and Socioeconomic Parameters. In this study, the relationship between the proportions of groundwater salinity contamination and socioeconomic parameters in various cities in the PRD was investigated by the PCA. Note that differences in the socioeconomic parameters of the cities resulting from differences in size were eliminated by using the values of the socioeconomic parameters per square kilometer [3, 5]. PC2 shows strong positive loadings with the proportion of groundwater salinity contamination, TVE, and IWD (Table 4).

5. Discussions

5.1. Natural Factors Controlling Salinity in Various Groundwater Units. Generally, after the exclusion of the influence of anthropogenic activities, TDS in groundwater originates from the seawater intrusion, the soil-water interaction, and the rock-water interaction [7, 29]. In this study, NBL-TDS in groundwater unit A was much higher than that in other groundwater units (Figure 3). This probably ascribes to seawater intrusion, because the intrusion of seawater with extremely high levels of TDS often occurs in groundwater unit A [21]. NBL-TDS in groundwater unit B was lower than that in groundwater unit A but much higher than that in the other two groundwater units (Figure 3). This may be attributed to the more strong interactions of water and soils/rocks in groundwater unit B in comparison with that in groundwater units C and D because the groundwater flow rate in unit B is slower in comparison with that in units C and D [22]. This is also likely to be the main reason for the much higher NBL-TDS in groundwater unit C than that in groundwater unit D.

TABLE 2: Groundwater salinity contamination in areas with different urbanization levels in the Pearl River Delta.

Contamination levels	PRD			Unit A			Unit B			Unit C		
	UA	PUA	NUA	UA	PUA	NUA	UA	PUA	NUA	UA	PUA	NUA
Uncontaminated (%)	70.3	75	90.9	57.4	76.8	81.5	77.3	80.5	97.5	80	68.4	91.8
Low (%)	24.3	18.5	7.0	40.7	18.6	11.1	17	17.1	2.5	12.5	21.1	8.2
Moderate (%)	4.7	5.6	1.4	1.9	2.3	3.7	3.8	2.4	0	7.5	10.5	0
High (%)	0.7	0.9	0.7	0	2.3	3.7	1.9	0	0	0	0	0

TABLE 3: Groundwater salinity contamination in various cities in the Pearl River Delta.

Contamination levels	Guangzhou	Shenzhen	Foshan	Dongguan	Huizhou	Zhaoqing	Jiangmen	Zhuhai	Zhongshan
Uncontaminated (%)	79.3	86.7	75.8	65	84.4	96.2	80.9	92.3	52.7
Low (%)	16.5	13.3	21	20	12.5	3.8	15.9	7.7	36.8
Moderate (%)	2.1	0	3.2	12.5	3.1	0	3.2	0	10.5
High (%)	2.1	0	0	2.5	0	0	0	0	0

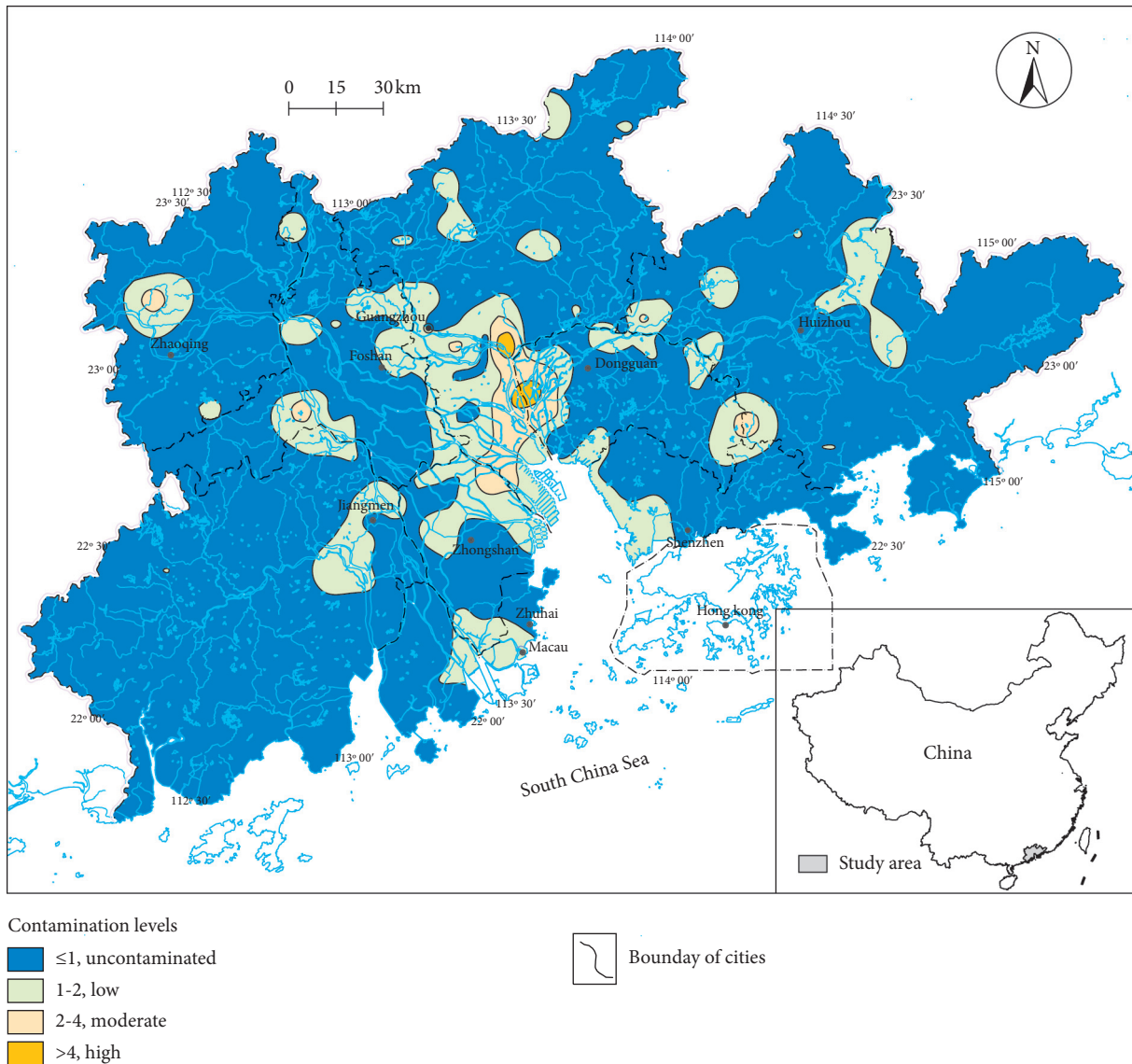


FIGURE 4: Spatial distribution of groundwater salinity contamination in the Pearl River Delta.

TABLE 4: Principal component (PC) loadings for proportions of groundwater salinity contamination and socioeconomic parameters in various cities in the Pearl River Delta

Items	PCs			
	PC1	PC2	PC3	PC4
GDP	0.990	-0.06	-0.051	-0.057
DSD	0.975	0.07	0.055	-0.188
PD	0.966	0.16	-0.136	-0.109
RUA	0.940	0.062	-0.243	0.019
IE	0.833	0.482	-0.159	0.13
PGSC ^a	0.095	0.956	0.104	0.136
TVE	-0.075	0.943	0.111	-0.276
IWD	0.386	0.819	-0.247	0.081
LO	-0.051	-0.113	0.976	-0.098
AO	-0.207	0.153	0.949	-0.008
LD	-0.142	-0.017	-0.083	0.985
Eigenvalue	4.7	2.8	2.1	1.1
Explained variance (%)	42.4	25.3	18.7	10.5
Cumulative % of variance	42.4	67.7	86.4	96.8

^a PGSC: proportion of groundwater salinity contamination. Bold numbers represent maximum absolute PC loading of one parameter.

The proportions of salinity contamination in various groundwater units were significantly different (Table 1), indicating that groundwater salinity contamination in the PRD is affected by natural factors. A much higher proportion of salinity contamination in groundwater unit D than that in other groundwater units indicates that groundwater unit D has a higher risk of groundwater salinity contamination in comparison with other groundwater units in the PRD (Table 1) because the vadose zone in groundwater unit D is commonly characterized by more coarse-grained media in comparison with other groundwater units [22]. In addition, the proportion of salinity contamination in groundwater unit A was approximately 2 times that in groundwater units B and C (Table 1). This may not ascribe to natural factors but anthropogenic factors. In theory, the proportion of salinity contamination in groundwater unit A should be lower than that in groundwater units B and C if groundwater salinity contamination in various units is controlled by the property of media of vadose zone, because vadose zone in groundwater unit A is characterized by more fine-grained media in comparison with groundwater units B and C [22], which will result in the lower groundwater vulnerability of groundwater unit A in comparison with groundwater units B and C in the PRD. On the other hand, the ratio of UA in groundwater unit A was much higher than that in groundwater units B and C (Figures 1 and S1), and UA was commonly accompanied by more factories and industrial wastewater in comparison with other areas [5]. Thus, it can be concluded that a higher ratio of UA in groundwater unit A than that in groundwater units B and C is likely to be responsible for the higher proportion of salinity contamination in groundwater unit A in comparison with that in groundwater units B and C.

5.2. Anthropogenic Factors Controlling Groundwater Salinity Contamination in the PRD. A much higher proportion of groundwater salinity contamination in UA than that in PUA

and NUA indicates that human activities during urbanization should be the main factors (Table 2). Groundwater contamination such as nitrate and phosphorus contaminations in urbanized areas resulting from human activities was often identified by various socioeconomic parameters [3, 5]. Therefore, the relationship between the proportions of groundwater salinity contamination and socioeconomic parameters in various cities in the PRD was investigated by the PCA, to identify which human activities mainly result in groundwater salinity contamination in the PRD. As shown in Table 4, the proportion of groundwater salinity contamination is accompanied by TVE and IWD in the same PC. This indicates that wastewater from TVE and industrial wastewater is probably the main sources of groundwater salinity contamination in the PRD on a regional scale because industrial wastewater and wastewater from TVE with high levels of TDS were sometimes illegally discharged into rivers or ground surface without treatment [20]. For instance, the amounts of TVE in Zhongshan and Dongguan were more than 3 times that in other cities (Table S1), and the industrial wastewater discharges in Zhongshan and Dongguan were also significantly higher than those in other cities (except for Foshan) (Table S1). Correspondingly, the proportions of groundwater salinity contamination in both Zhongshan and Dongguan were more than 1.4 times that in other cities (Table 3). By contrast, the amount of industrial wastewater discharge in Zhaoqing was markedly lower than that in other cities (Table S1). Correspondingly, the proportion of groundwater salinity contamination in Zhaoqing was significantly lower than that in other cities (Table 3). This is also supported by the evidence that the proportions of groundwater salinity contamination in UA^{1st} were much lower than those in UA^{2nd} and UA^{3rd} in some groundwater units such as B and C (Table S2) because UA^{1st} has a lower proportion of factories as well as a lower discharge of industrial wastewater in comparison with UA^{2nd} and UA^{3rd} [5]. In addition, the proportions of groundwater salinity contamination in various units in UA^{2nd} were more than 1.5 times those in UA^{3rd} (Table S2), indicating that the wastewater leakage from sewer systems may be one of the main pathways for groundwater salinity contamination in UA in the PRD because UA^{3rd} shows a relatively well-constructed sewer system in comparison with UA^{2nd} [5].

The proportions of groundwater salinity contamination in PUA were significantly higher than those in NUA in various groundwater units (Table 2). This is probably attributed to the infiltration of industrial wastewater and domestic sewage. On one hand, illegal discharge of industrial wastewater with high levels of TDS from factories into the nearby ground surface sometimes occurred in PUA but none in NUA because some factories such as TVE were distributed in PUA but none in NUA [12, 13]. On the other hand, domestic sewage with high levels of TDS was also often discharged into the nearby ground surface in PUA in the PRD because a large number of people lived in the PUA where the sewer system was sometimes missing [2, 5]. Therefore, the infiltration of industrial wastewater and domestic sewage is likely to be the main source of groundwater salinity contamination in PUA in the PRD.

Though the proportion of groundwater salinity contamination in NUA was much lower than that in UA and PUA, it was still considerable, especially in groundwater unit A (Table 2). As shown in Figures 4 and S1, NUA contaminated by groundwater salinity was mainly located at a river network area adjacent to the Pearl River Estuary. This indicates that sewage irrigation may be mainly responsible for groundwater salinity contamination in NUA in the PRD. On one hand, most rivers in this river network area were contaminated by industrial and domestic sewage due to urbanization and industrialization, thereby resulting in high levels of TDS occurring in these polluted river waters [30]. On the other hand, agricultural lands within NUA near rivers were often irrigated by river waters [4, 20]. Besides, a few groundwater samples characterized by relatively high levels of TDS within NUA were near landfills such as Datianshan landfill and Hongmei town landfill [5, 31], and these groundwater samples in the west boundary of Dongguan city and southeast of Guangzhou city showed low to high levels of salinity contamination (Figure 4). This indicates that the leakage of landfill leachate should also be an important source for groundwater salinity contamination in NUA in the PRD because these landfills often lacked antiseepage measure and landfill leachate showed extremely high levels of TDS [13, 31].

6. Conclusions

Results showed that NBLs of TDS in groundwater units A to D were 688 mg/L, 432 mg/L, 321 mg/L, and 99 mg/L, respectively. The seawater intrusion was likely to be responsible for the much higher NBL-TDS in groundwater unit A than that in other groundwater units. By contrast, higher NBL-TDS in groundwater unit B than that in groundwater units C and D was probably attributed to the more strong interactions of water and soils/rocks in groundwater unit B in comparison with that in groundwater units C and D. This was also likely to be the main reason for the much higher NBL-TDS in groundwater unit C than that in groundwater unit D.

The proportion of salinity contamination in groundwater unit D was much higher than that in other groundwater units. This may be attributed to the more coarse-grained media of vadose zone in groundwater unit D in comparison with other groundwater units. By contrast, a higher ratio of UA in groundwater unit A than that in groundwater units B and C was probably responsible for the higher proportion of salinity contamination in groundwater unit A in comparison with that in groundwater units B and C.

Groundwater salinity contamination in the PRD was positively correlated with the urbanization level. Furthermore, proportions of salinity contamination in UA^{2nd} were much higher than that in UA^{3rd} regardless of groundwater units. By contrast, the proportion of salinity contamination in UA^{3rd} was also much higher than that in UA^{1st} in both groundwater units B and C but contrary in groundwater unit A. Wastewater from TVE and industrial wastewater were likely to be the main sources for groundwater salinity contamination in the PRD, and the wastewater leakage from

sewer systems was one of the main pathways for groundwater salinity contamination in UA. Besides, sewage irrigation and leakage of landfill leachate were also important sources for groundwater salinity contamination in the PRD.

Data Availability

The data used to support the findings of this study are included within the article.

Conflicts of Interest

The authors declare that there are no conflicts of interest regarding the publication of this paper.

Acknowledgments

This research was supported by the Graduate Students Teaching Case of Hebei Province (KCJSZ2019092), the Postgraduate Innovation Funding Project of Hebei Province (CXZZSS2020115), the Fundamental Research Funds for Hunan Academy of Geology (no. 201904), and the China Geological Survey Grant (DD20160309).

Supplementary Materials

Table S1: socioeconomic data for the nine major cities of the PRD in 2006. Table S2: groundwater salinity contamination in UA formed in different periods in the Pearl River Delta. Figure S1: the expansion of urbanization in the PRD. (*Supplementary Materials*)

References

- [1] A. Mukherjee, B. Scanlon, A. Aureli, S. Langan, H. Guo, and A. McKenzie, *Global Groundwater: Source, Scarcity, Sustainability, Security and Solutions*, Elsevier, Amsterdam, Netherlands, first edition, 2020.
- [2] G. Huang, C. Liu, J. Sun, M. Zhang, J. Jing, and L. Li, "A regional scale investigation on factors controlling the groundwater chemistry of various aquifers in a rapidly urbanized area: a case study of the Pearl River Delta," *Science of the Total Environment*, vol. 625, pp. 510–518, 2018.
- [3] G. Huang, C. Liu, Y. Zhang, and Z. Chen, "Groundwater is important for the geochemical cycling of phosphorus in rapidly urbanized areas: a case study in the Pearl River Delta," *Environmental Pollution (Barking, Essex: 1987)*, vol. 260, Article ID 114079, 2020.
- [4] F. Zhang, G. Huang, Q. Hou, C. Liu, Y. Zhang, and Q. Zhang, "Groundwater quality in the Pearl River Delta after the rapid expansion of industrialization and urbanization: distributions, main impact indicators, and driving forces," *Journal of Hydrology*, vol. 577, Article ID 124004, 2019.
- [5] M. Zhang, G. Huang, C. Liu, Y. Zhang, Z. Chen, and J. Wang, "Distributions and origins of nitrate, nitrite, and ammonium in various aquifers in an urbanized coastal area, south China," *Journal of Hydrology*, vol. 582, Article ID 124528, 2020.
- [6] X. Wu, L. Zhang, B. X. Hu, Y. Wang, and Z. Xu, "Isotopic and hydrochemical evidence for the salinity origin in the coastal aquifers of the Pearl River Delta, Guangzhou, China," *Journal of Contaminant Hydrology*, vol. 235, Article ID 103732, 2020.

- [7] Y. Wang and J. J. Jiao, "Origin of groundwater salinity and hydrogeochemical processes in the confined Quaternary aquifer of the Pearl River Delta, China," *Journal of Hydrology*, vol. 438-439, pp. 112-124, 2012.
- [8] S. Sang, X. Zhang, H. Dai, B. X. Hu, H. Ou, and L. Sun, "Diversity and predictive metabolic pathways of the prokaryotic microbial community along a groundwater salinity gradient of the Pearl River Delta, China," *Scientific Reports*, vol. 8, Article ID 17317, 2018.
- [9] B. Backman, D. Bodiš, P. Lahermo, S. Rapant, and T. Tarvainen, "Application of a groundwater contamination index in Finland and Slovakia," *Environmental Geology*, vol. 36, no. 1-2, pp. 55-64, 1998.
- [10] Z. Jia, J. Bian, and Y. Wang, "Impacts of urban land use on the spatial distribution of groundwater pollution, Harbin City, Northeast China," *Journal of Contaminant Hydrology*, vol. 215, pp. 29-38, 2018.
- [11] N. S. Rao and M. Chaudhary, "Hydrogeochemical processes regulating the spatial distribution of groundwater contamination, using pollution index of groundwater (PIG) and hierarchical cluster analysis (HCA): a case study," *Groundwater for Sustainable Development*, vol. 9, Article ID 100238, 2019.
- [12] Q. Hou, Q. Zhang, G. Huang, C. Liu, and Y. Zhang, "Elevated manganese concentrations in shallow groundwater of various aquifers in a rapidly urbanized delta, south China," *The Science of the Total Environment*, vol. 701, Article ID 134777, 2020.
- [13] G. Huang, C. Liu, L. Li, F. Zhang, and Z. Chen, "Spatial distribution and origin of shallow groundwater iodide in a rapidly urbanized delta: a case study of the Pearl River Delta," *Journal of Hydrology*, vol. 585, Article ID 124860, 2020.
- [14] C. Li, X. Gao, Y. Liu, and Y. Wang, "Impact of anthropogenic activities on the enrichment of fluoride and salinity in groundwater in the Yuncheng Basin constrained by Cl/Br ratio, $\delta^{18}\text{O}$, $\delta^2\text{H}$, $\delta^{13}\text{C}$ and $\delta^7\text{Li}$ isotopes," *Journal of Hydrology*, vol. 579, Article ID 124211, 2019.
- [15] C. Li, X. Gao, S. Li, and J. Bundschuh, "A review of the distribution, sources, genesis, and environmental concerns of salinity in groundwater," *Environmental Science and Pollution Research*, vol. 27, no. 33, pp. 41157-41174, 2020.
- [16] J. Griffioen, H. F. Passier, and J. Klein, "Comparison of selection methods to deduce natural background levels for groundwater units," *Environmental Science & Technology*, vol. 42, no. 13, pp. 4863-4869, 2008.
- [17] K. Hinsby, M. T. Condesso de Melo, and M. Dahl, "European case studies supporting the derivation of natural background levels and groundwater threshold values for the protection of dependent ecosystems and human health," *Science of the Total Environment*, vol. 401, no. 1-3, pp. 1-20, 2008.
- [18] D. Ducci, M. T. C. de Melo, E. Preziosi, M. Sellerino, D. Parrone, and L. Ribeiro, "Combining natural background levels (NBLs) assessment with indicator kriging analysis to improve groundwater quality data interpretation and management," *Science of the Total Environment*, vol. 569-570, pp. 569-584, 2016.
- [19] Y. Zong, W. W.-S. Yim, F. Yu, and G. Huang, "Late Quaternary environmental changes in the Pearl River mouth region, China," *Quaternary International*, vol. 206, no. 1-2, pp. 35-45, 2009.
- [20] G. Huang, J. Sun, Y. Zhang, Z. Chen, and F. Liu, "Impact of anthropogenic and natural processes on the evolution of groundwater chemistry in a rapidly urbanized coastal area, South China," *Science of the Total Environment*, vol. 463-464, pp. 209-221, 2013.
- [21] G. Huang, M. Zhang, C. Liu, L. Li, and Z. Chen, "Heavy metal(loid)s and organic contaminants in groundwater in the Pearl River Delta that has undergone three decades of urbanization and industrialization: distributions, sources, and driving forces," *Science of the Total Environment*, vol. 635, pp. 913-925, 2018.
- [22] Guangdong Hydrogeological Second Team, *Regional Hydrogeological Survey Report*, Guangdong Hydrogeological Second Team, Guangzhou, China, 1981, in Chinese.
- [23] X. Li, C. Tang, Y. Cao, and X. Li, "Carbon, nitrogen and sulfur isotopic features and the associated geochemical processes in a coastal aquifer system of the Pearl River Delta, China," *Journal of Hydrology*, vol. 575, pp. 986-998, 2019.
- [24] Y. Wang, J. J. Jiao, and J. A. Cherry, "Occurrence and geochemical behavior of arsenic in a coastal aquifer-aquitard system of the Pearl River Delta, China," *Science of the Total Environment*, vol. 427-428, pp. 286-297, 2012.
- [25] A. N. Analytical Methods Committee, "Using the Grubbs and Cochran tests to identify outliers," *Analytical Methods*, vol. 7, no. 19, pp. 7948-7950, 2015.
- [26] K. S. Gundogdu and I. Guney, "Spatial analyses of groundwater levels using universal Kriging," *Journal of Earth System Science*, vol. 116, no. 1, pp. 49-55, 2007.
- [27] Y. Wu, Y. Wang, and X. Xie, "Spatial occurrence and geochemistry of soil salinity in Datong basin, northern China," *Journal of Soils and Sediments*, vol. 14, no. 8, pp. 1445-1455, 2014.
- [28] Guangdong Province Statistical Bureau, *2006 Statistical Yearbook of Guangdong Province*, China Statistical Publisher House, Beijing, China, 2007.
- [29] F. Larsen, L. V. Tran, H. Van Hoang, L. T. Tran, A. V. Christiansen, and N. Q. Pham, "Groundwater salinity influenced by Holocene seawater trapped in incised valleys in the Red River delta plain," *Nature Geoscience*, vol. 10, no. 5, pp. 376-381, 2017.
- [30] Water Resources Department of Guangdong Province, *Guangdong Water Resources Bulletin in 2006*, Water Resources Department of Guangdong Province, Guangzhou, China, Chinese, 2007.
- [31] G. Huang, Z. Chen, F. Liu, J. Sun, and J. Wang, "Impact of human activity and natural processes on groundwater arsenic in an urbanized area (South China) using multivariate statistical techniques," *Environmental Science and Pollution Research*, vol. 21, no. 22, pp. 13043-13054, 2014.

Research Article

Survey and Risk Assessment of Contaminants in Soil from a Nitrogenous Fertilizer Plant Located in North China

Xizhao Tian ¹, Cunliang Fan,¹ Zhiqiang Gong,¹ Ziting Yuan,¹ Zhiyuan Ma,¹ Xiaosen Xing,² Wei He,¹ and Pengfei Jin ¹

¹Hebei Key Laboratory of Environment Monitoring and Protection of Geological Resources, Hebei Geological Environment Monitoring Institute, Shijiazhuang 050000, China

²Land Resources Exploration Center, Bureau of Geology and Mineral Exploration and Development of Hebei Province, Wuhan, China

Correspondence should be addressed to Pengfei Jin; 676704360@qq.com

Received 11 March 2021; Accepted 21 June 2021; Published 2 August 2021

Academic Editor: Xubo Gao

Copyright © 2021 Xizhao Tian et al. This is an open access article distributed under the Creative Commons Attribution License, which permits unrestricted use, distribution, and reproduction in any medium, provided the original work is properly cited.

China is the world's largest consumer of fertilizer, with fertilizer plants widely distributed throughout the country. With the removal and closing of fertilizer factories in recent years, pollutant surveys and risk assessments (human health risks) for these sites have become increasingly necessary. However, there has been little research on contaminated fertilizer factory sites. This study aimed to characterize the distribution of pollutants, assess the health risk of the site, and calculate the remediation area and volume in a typical fertilizer plant site in North China. A total of 443 samples were collected in 2019; they indicated that the study site had high concentrations of copper (Cu), ammonia-nitrogen (NH₃-N), total petroleum hydrocarbons (TPH), and fluoride at maximum ratios (the ratio of the highest value of all test data for a particular pollutant to the standard value of the pollutant) of 3.30, 2.55, 19.69, and 1.10, respectively. The health risk assessment results suggested that some hazard quotients exceeded the threshold safe level (>1 established by environmental regulations). The risk control values of soil were 2000 mg/g (Cu), 826 mg/g (TPH), and 1549 mg/g (NH₃-N), and the total remediation soil volume was 72860.71 m³. The results provided basic information on soil pollution control and environmental management in a contaminated fertilizer plant site.

1. Introduction

Nitrogen is the first element in soil for plant growth. The nitrogenous fertilizer has been intensively used in agricultural systems to achieve higher yields in China. China is the largest consumer of fertilizer and has the biggest nitrogen production in the world [1–3]. Fertilizer plants are widely distributed throughout China. A large amount of chemicals have been released from these plants into soil and groundwater during their production. In recent years, with the change of fertilizer demand from chemical fertilizer to organic fertilizer, lots of nitrogen fertilizer plants have been closed. The land of these plants had been planned to be used for residential or recreational purposes [4]. Investigation and assessment of contaminants left in these sites is necessary for their safe redevelopment. A large number of studies have

focused on the investigation and assessment of contaminants on petroleum [5], coking [6], and chemical-contaminated sites [7]. However, there has been little concern about the fertilizer-contaminated sites, but in fact, this kind of site could have serious environmental impacts and human health risks.

Ammonia-nitrogen (NH₃-N) is the most typical pollutant found at fertilizer-contaminated sites [8]. As a major element determining plant growth and productivity, inorganic and organic forms of NH₃-N in the soil can be absorbed by plants through their roots [9, 10]. However, high levels of NH₃-N have become an increasingly significant environmental problem [11], along with the acidification and eutrophication of ecosystems and climate change [12]. Although NH₃-N is not considered a carcinogenic pollutant when assessing human health risks, the exposure

to $\text{NH}_3\text{-N}$ at high concentrations could be harmful to the respiratory tract, eyes, and skin [13, 14]. Compared with $\text{NH}_3\text{-N}$, other typical pollutants, such as copper (Cu), total petroleum hydrocarbons (TPH), and fluoride, are at relatively low concentrations in fertilizer-contaminated sites. Even so, they cannot be neglected because of potential bioaccumulation and carcinogenicity.

Understanding the fate and transport of the contaminants present on fertilizer plant sites and identifying their environmental exposure risks are not only the preconditions for soil pollution prevention and control but also to provide important information for making decisions on polluted site remediation. The specific objectives of this study were to (1) characterize the distribution of pollutants in the fertilizer-contaminated site, (2) assess the health risk of pollutants in the study site and identify health risk exposure pathways, and (3) calculate the remediation soil area and volume.

2. Materials and Methods

2.1. Contaminated Site Characterization. The fertilizer plant in this study is located in Linzhang County in the southern part of Hebei Province, belonging to Taihang Mountain's foreland and flood plain. Construction waste and miscellaneous fill (0.1–2.8 m) are distributed on the surface of the study area, and below them are silt (8.8–11.4 m), silty clay (0.6–2.3 m), and silt (0.4–7.0 m) formed in alluvial and diluvial sediments of quaternary. The site began operating in 1975 and shut down completely in 1999; it covers an area of $53 \times 10^3 \text{ m}^2$ (Figure 1). The plant received anthracite, water, electrolytic copper, and catalyst as the raw material. The main product of the plant was ammonia ($30 \times 10^3 \text{ t/a}$), and the byproduct was ammonium bicarbonate ($100 \times 10^3 \text{ t/a}$). However, poor pollution controls and production technology during the operational period caused serious environmental pollution. Many hazardous substances were released into the soil, resulting in potential damage to the surrounding environment and the plant site. A detailed survey of the contaminants present along with a risk assessment is essential if the site is to be redeveloped, in particular as residential land.

2.2. Soil Sampling. A total of 55 soil sampling sites were planned in the plant (Figure 2). The depths of soil sampling from a soil-drilling core were decided by soil lithology and the transport character of contaminants. The soil cores were collected by a drilling rig (SH-30, drilling rig manufacturer). The sampling standard is that one sample is taken from 0.5 m on the surface, and the vertical sampling interval is less than 2 m between 0.5 m and 6 m; if the sampling distance is less than 6 m, one sample is taken every 3 m until no obvious pollution odor is found on the spot. The specific locations of the sampling points this time are 0–0.5 m, 1–1.5 m, 3–3.5 m, 5–5.5 m, 8–8.5 m, 11–11.5 m, 14–14.5 m, 17–17.5 m, and 20–20.5 m. The vertical sampling interval was less than 2 m in 0.5–6 m, and the sampling interval was 3 m at most when the depth exceeded 6 m. To avoid cross-contamination, the sampling personnel replaced their disposable gloves after

retrieving each sample. The samples to be analyzed for TPH and $\text{NH}_3\text{-N}$ were transferred to 250 mL brown glass bottles as soon as possible, and the samples to be analyzed for copper and fluoride were transferred to valve bags. All the samples were stored at 4°C and transported to the laboratory for analysis immediately. In total, 443 samples were collected in April and August of 2019.

2.3. Sample Analyses. All analyses were completed by the Pony Testing International Group. Table 1 provides the selected analytical methods employed to measure copper, TPH, fluoride, and $\text{NH}_3\text{-N}$. To corroborate the results and determine the accuracy of each method, 82 duplicate samples were analyzed by Hebei Shipu Testing Technology Service Co., Ltd. The relative deviation and relative standard deviation can meet the national standard (technical code for soil environmental monitoring HJ/T 166-2004).

2.4. Assessment Standard. TPH and copper concentrations were converted using the risk screening and risk intervention values in accordance with the soil environmental quality risk control standard for soil contamination of development land (GB36600-2018) [18]. However, fluoride and $\text{NH}_3\text{-N}$, which could not be found in GB36600-2018, were calculated using the technical guidelines for the assessment of contaminated sites (HJ25.3-2014) [19].

The risk assessment of soil contaminants was carried out according to HJ 25.3-2014 [19]. To simplify calculations, the soil was divided into 6 layers as given in Table 2. It is worth mentioning that because the pollutants did not exceed the standard in the 20–25 m depth layer, the layer was ignored.

According to the plan for land utilization of Linzhang County, the future land use pattern of the fertilizer site was residential. Therefore, both adults and children were considered the sensitive human receptors under the residential scenario. The soil exposure of the local population was estimated by considering six different routes: oral ingestion, dermal contact, inhalation of soil particles by mouth, inhalation of gaseous pollutants from the surface soil in the outdoor air, and inhalation of gaseous pollutants from the underlying soil in outdoor and indoor air. The hazard quotient (HQ) of exposure pathways was estimated using the equations given in Table 3.

2.5. Contaminated Soil Remediation. According to the health risk assessment guidelines, human health might be harmed when the hazard quotient exceeds 1, and soil remediation is necessary. The risk control values of soil (RCVS) were calculated using the equations given in Tables 4 and 5. Furthermore, to avoid excessive remediation, RCVS was compared with the screening value of GB36600-2018 [18].

3. Results and Discussion

3.1. Contaminant Characteristics and Sources. The soil sample results are given in Table 6. Cu concentrations

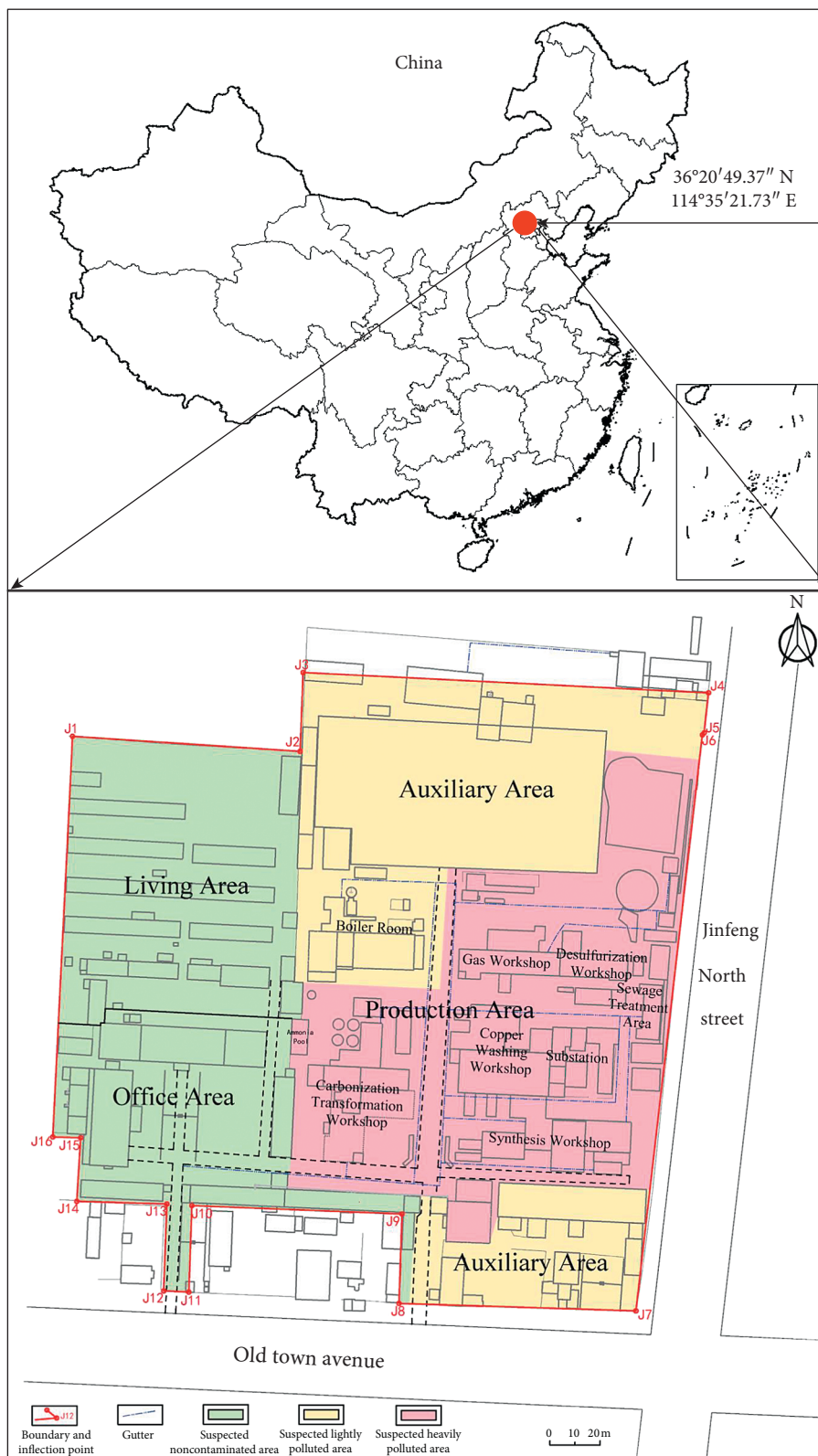


FIGURE 1: Overview of the study area.

ranged from 5.94 mg/kg to 6590 mg/kg, with an average of 107.82 mg/kg and a maximum ratio of 3.3. As shown in Figures 3(a) and 4, samples with higher concentrations were

mainly distributed among the copper washing workshop and production area entrance, where copper ammonia acetate solution was received as a raw material for the

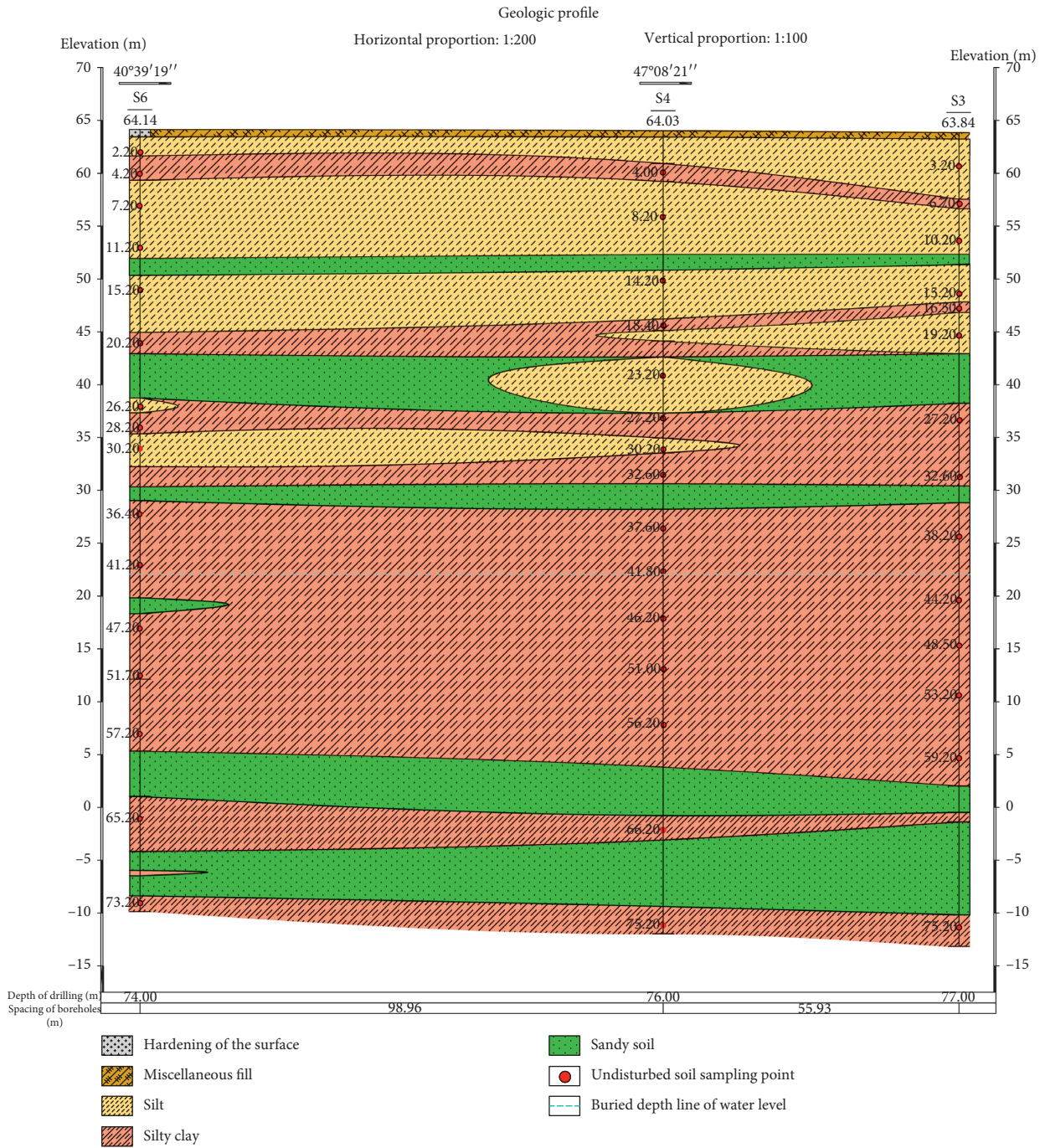


FIGURE 2: Stratigraphic profile of the study area.

TABLE 1: Target pollutants and analytical methods.

Target pollutants	Test method	Reference
Cu	Atomic adsorption spectrometry	[14]
TPH	Gas chromatography	[15]
Fluoride	Ion selective electrode method	[16]
NH ₃ -N	UV-visible scenery photometry	[17]

NH₃-N, ammonia-nitrogen; TPH, total petroleum hydrocarbons.

TABLE 2: Soil layers and depth.

Layer	Soil	Depth (m)
1	Silt	0–4.5
2	Clay	4.5–6.5
3	Silt	6.5–10
4	Silt	10–15
5	Silt	15–20
6	Silt	25–30

TABLE 3: Calculating models of hazard quotient.

Exposure pathway	Explanation	Calculation model	Equation number
Oral ingestion	6 ways receptors are exposed to pollutants	$HQ_{ois} = OISER_{nc} \times C_{sur}/RfD_o \times SAF$	(1)
Dermal contact		$HQ_{dcs} = DCSE_{nc} \times C_{sur}/RfD_d \times SAF$	(2)
Inhalation of soil particles by mouth		$HQ_{pis} = PISER_{nc} \times C_{sur}/RfD_i \times SAF$	(3)
Inhalation of gaseous pollutants from the surface soil in outdoor air		$HQ_{io1} = C_{sur} \times IOVER_{nc1}/RfD_i \times SAF$	(4)
Inhalation of gaseous pollutants from the underlying soil in outdoor air		$HQ_{io2} = C_{sub} \times IOVER_{nc2}/RfD_i \times SAF$	(5)
Inhalation of gaseous pollutants from the underlying soil in indoor air		$HQ_{iiv1} = C_{sub} \times IIVER_{nc1}/RfD_i \times SAF$	(6)

TABLE 4: Major parameters in the calculation models of hazard quotient.

Parameter	Explanation	Value	Unit
SAF	Reference dose distribution ratio for exposure to soil	0.5	/
C_{sur}	Concentration of contaminants in soil	434	mg/kg
C_{sub}	Concentration of contaminants in underlying soil	434	mg/kg
RfD_i	Reference dose for inhalation	$7E-02$	/
$IOVER_{nc1}$	Exposure dose by inhaling gaseous pollutants from the surface soil in outdoor air	$9.88E-06$	/
$IOVER_{nc2}$	Exposure dose by inhaling gaseous pollutants from the underlying soil in outdoor air	$1.14E-06$	/
$IIVER_{nc1}$	Exposure dose by inhaling gaseous pollutants from the underlying soil in indoor air	$1.60E-04$	/

TABLE 5: Calculation models of risk control values of soil (RCVS).

Exposure pathway	Explanation	Calculation model	Equation number
Oral ingestion	Formulas for calculating the amount of contaminants ingested orally	$RCVS_{ois} = ACR/OISER_{ca} \times SF_o$	(7)
Dermal contact	Formula for calculating the amount of contaminants ingested by skin contact	$RCVS_{dcs} = ACR/DCSE_{ca} \times SF_d$	(8)
Inhalation of soil particles	Inhaled soil particle pollutant quantity calculation formula	$RCVS_{pis} = ACR/PISER_{ca} \times SF_i$	(9)

TABLE 6: Sample analysis results.

Variable	Pollutant concentration (mg/kg)			Screening value (mg/kg)	Control value (mg/kg)	Detection rate (%)	Overstandard rate (%)	Maximum ratio
	Max	Mean	Min					
Cu	6590.00	107.82	5.94	2000	8000	100	1.81	3.30
NH ₃ -N	3951.00	445.19	0.14	1549	—	100	10.16	2.55
TPH	16263.00	129.19	<3.00	826	5000	30.70	1.81	19.69
Fluoride	1150	424.94	127.00	1050	—	100	0.23	1.10

NH₃-N, ammonia-nitrogen; TPH, total petroleum hydrocarbons.

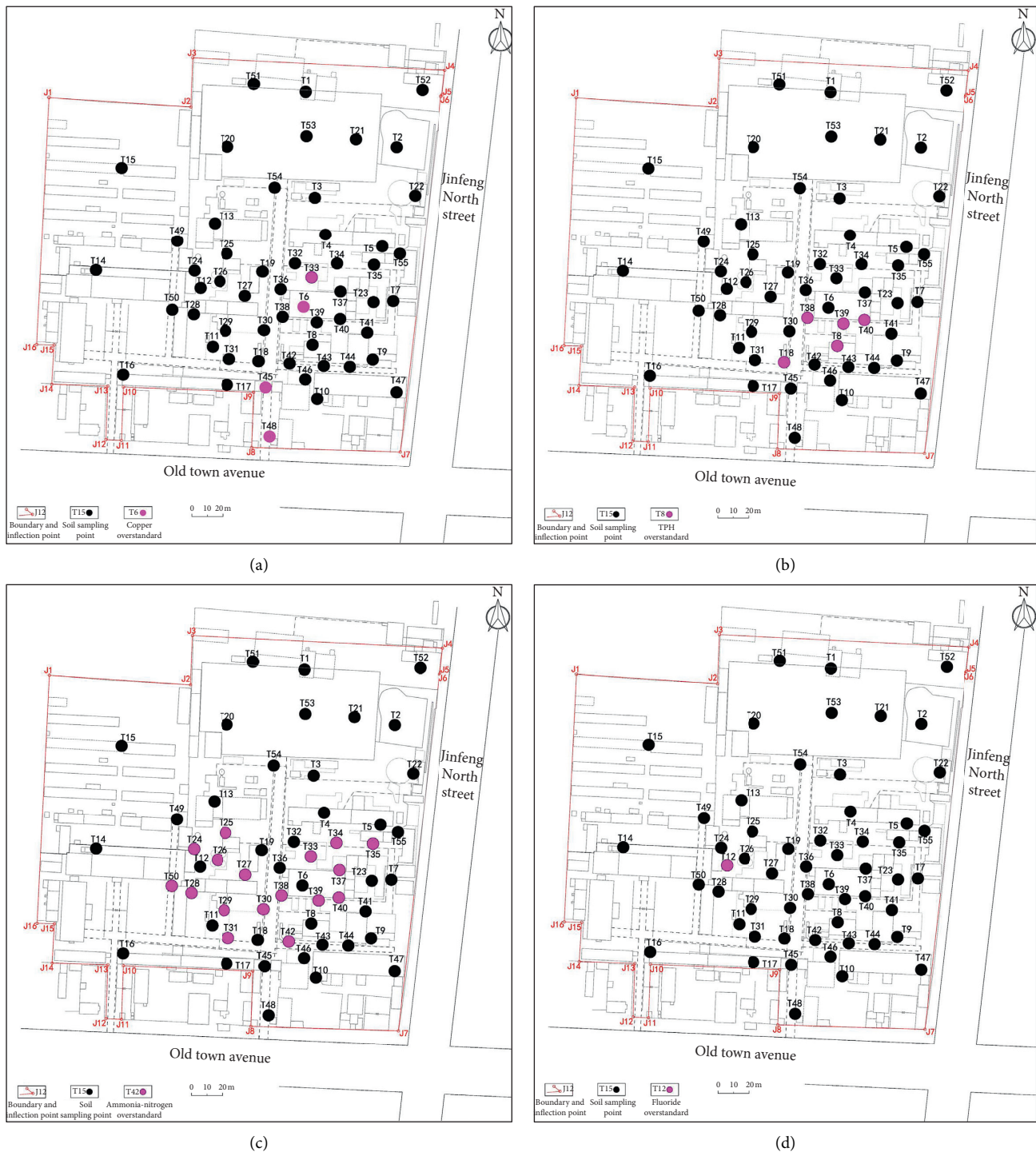


FIGURE 3: Overstandard points of the study area. (a) Cu, (b) TPH, (c) NH₃-N, (d) fluoride. NH₃-N, ammonia-nitrogen; TPH, total petroleum hydrocarbons.

adsorption of CO, CO₂, O₂, and H₂S. Thus, it can be concluded that the main reason for high Cu concentrations was the corrosion and aging of the machine that accelerated the release of wastewater [20, 21].

TPH ranged from <3 mg/kg to 16263 mg/kg with an average concentration of 129.19 mg/g. The maximum ratio

was 19.69, and the distribution of TPH was relatively concentrated (Figure 4). However, TPH was not a raw material used in the fertilizer plant. It could be concluded that TPH was from the lubricating oil leakage of machines in the process of operation or migration (Figure 3(b)). The pollution level decreased with increasing depth due to

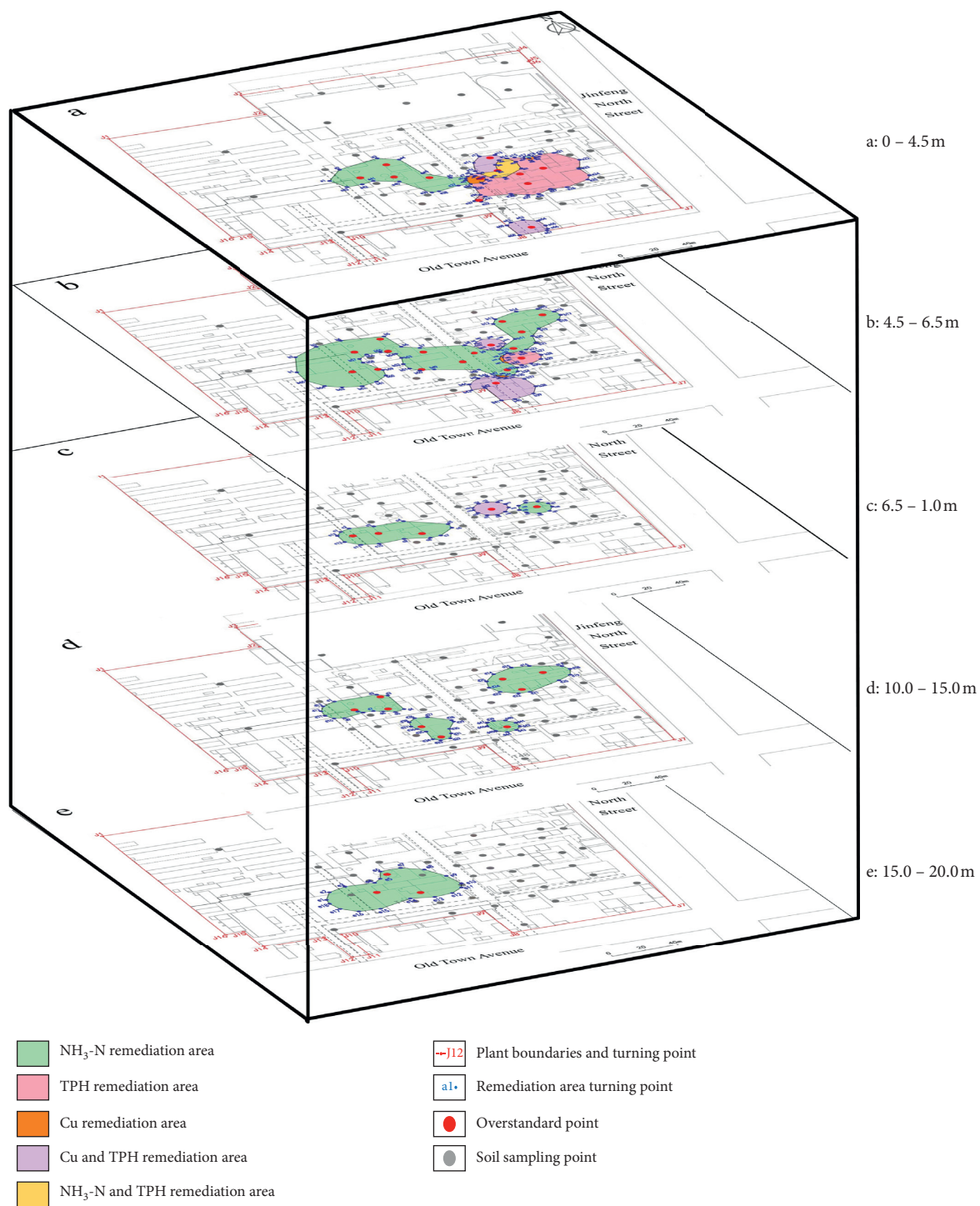


FIGURE 4: Polluted areas from different soil layers. (a) The first layer, (b) the second layer, (c) the third layer, (d) the fourth layer, (e) the fifth layer, (f) the sixth layer.

TABLE 7: Pollutant levels from different layers and locations.

Pollutant	Layer	Polluted area (m ²)	Maximum pollutant concentration (mg/kg)	Maximum ratio	Distribution region
Cu	1	908.09	6590	3.30	Copper washing compression workshop (T6)
	2	1038.06	6162	3.08	Production area entrance (T45)
	3	253.45	5050	2.53	Copper washing compression workshop (T6)
TPH	1	2730.22	16263	19.69	Compression workshop (T40)
	2	318.48	2130	2.58	Compression workshop (T8)
NH ₃ -N	1	1829.33	3951	3.30	Carbonization transformation workshop (T24)
	2	5739.5	3316	2.14	Carbonization transformation workshop (T50)
	3	1516.05	2799	1.81	Copper washing compression workshop (T40)
	4	2844.85	3713	2.40	Copper washing compression workshop (T35)
	5	2484.11	3785	2.44	Carbonization transformation workshop (T28)
	6	150.97	1747	1.13	Copper washing compression workshop (T33)
Fluoride	1	7	1150	1.10	Carbonization transformation workshop (T12)

NH₃-N, ammonia-nitrogen; TPH, total petroleum hydrocarbons.

interception by the soil (Table 7). The low volatility, low solubility, and high hydrophobicity and sorption capacity of TPH made remediation difficult [22, 23].

As the main product of the fertilizer plant, NH₃-N concentrations ranged from 0.14 mg/kg to 3951 mg/kg, with a mean concentration of 445.1 mg/kg and a maximum ratio of 2.55. The main layers of the plant site were silt and silty clay with low water permeability. With the migration of rainfall and wastewater, NH₃-N could permeate down to a high depth. The deepest depth that the sample drill could reach was 27 m, and NH₃-N was present in those samples. As shown in Figures 5(c) and 3, NH₃-N was distributed near the copper washing and carbonization transformation workshops. The pollution level was not typically consistent with the depth, which suggests that the area had been polluted with NH₃-N for many years (Table 7). This could be attributed to the leakage of wastewater and the leaching of solid waste. Furthermore, poor pollution control and environmental protection awareness during the operational period could have been key factors affecting the contamination of the site.

Fluoride ranged from 127 mg/kg to 1150 mg/kg with a mean concentration of 424.94 mg/kg and a maximum ratio of 1.10. The overstandard point was at the ammonia pool of the carbonation transformation workshop. The fluoride-polluted area was relatively small compared with the other contaminants, and fluoride was only present in the surface soil (first layer) (Table 7). The presence of fluoride may be attributed to the atmospheric deposition of coal burn or the high background value [24, 25].

The polluted areas were 2199.6 m², 3048.7 m², 14564.81 m², and 7 m² for Cu, TPH, NH₃-N, and fluoride, respectively. These areas could be potentially harmful for

human health. Therefore, it was necessary to conduct a health risk assessment as per HJ25.3-2014 [26]. It should be mentioned that the total polluted area of the last 4 layers was not consistent with the increasing depth. The reason for this requires further investigation and analysis.

3.2. Health Risk Assessment. The hazard quotients in soils of the study area were calculated from Table 3 and are given in Table 8. Based on the values obtained, the main potential exposure pathway of Cu, fluoride, and TPH could be from oral ingestion. Inhalation of soil particles and dermal contact were the second most likely pathways for fluoride and TPH, respectively. However, the values with different exposure pathways of NH₃-N varied significantly in the following order: inhalation of gaseous pollutants from the surface soil in outdoor air > inhalation of soil particles. The contribution of inhalation of gaseous pollutants from the underlying soil in the outdoor and indoor air for NH₃-N was insignificant and may be ignored.

In general, the contribution rates of oral ingestion, dermal contact, and inhalation of gaseous pollutants from the surface soil in the outdoor air were 43.3%, 30.6%, and 25.9%, respectively. These results suggested that wearing safety masks would be an effective measure to reduce the negative health effects for workers and residents in the study site.

As given in Table 8, as the soil depth increased, the concentration of most of the pollutants tested decreased gradually. In the first two layers (0–6.5 m), the hazard quotients of Cu, NH₃-N, and TPH were greater than 1. In the third layer (6.5 m–10 m), Cu and NH₃-N were higher than the standard HQ. Until the fourth (10 m–15 m) and fifth

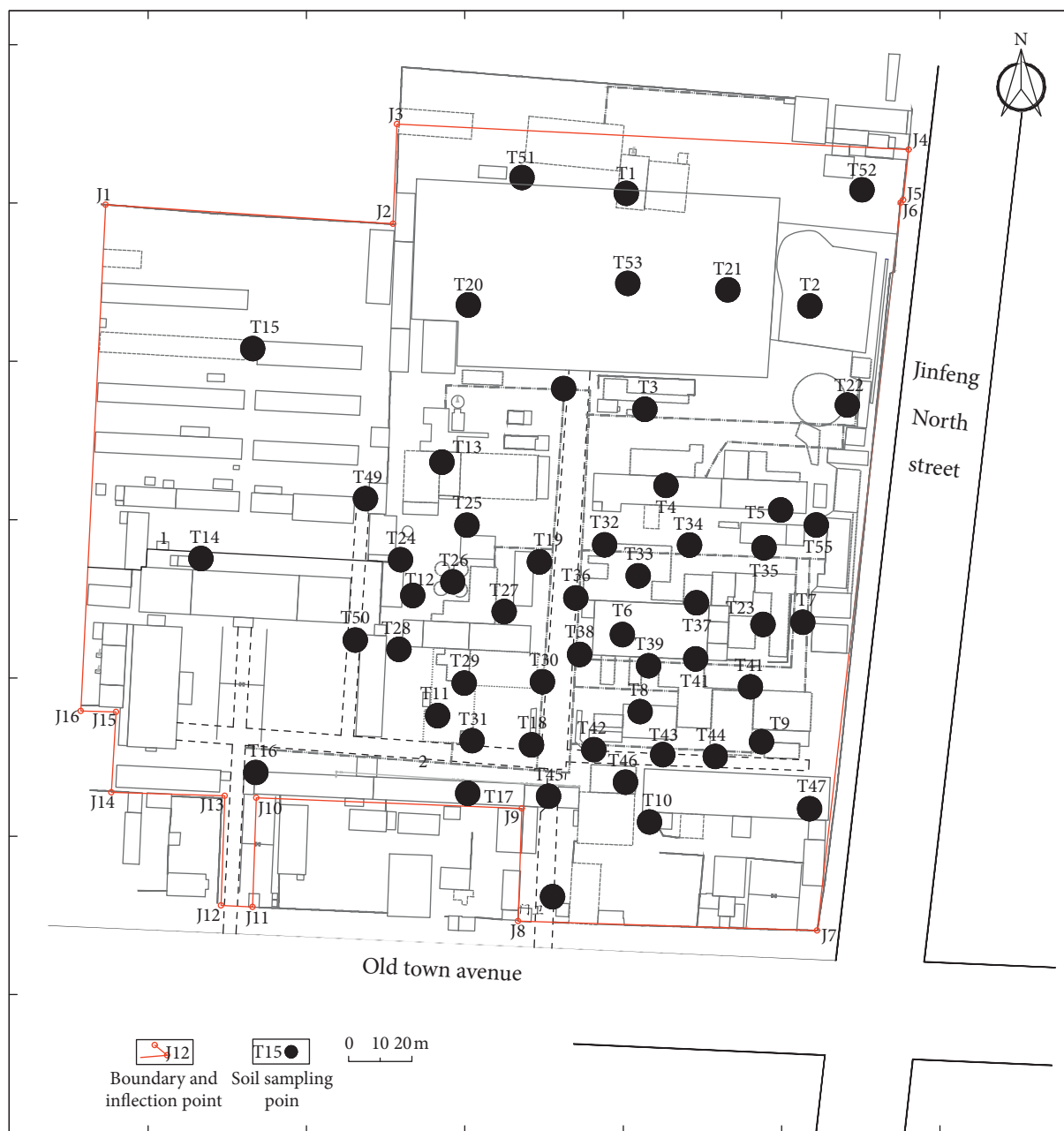


FIGURE 5: Sampling points in the study area.

layer (15 m–20 m), the HQs of $\text{NH}_3\text{-N}$ were 2.32 and 2.34, respectively. Li et al. also found that the surface soil was more vulnerable to contamination by pollutants compared with deeper soil. Those results indicated that the comprehensive HQs of the study site were relatively high and the soil should be remediated [27, 28].

3.3. The Target Value of Contaminated Soil Remediation and the Amount of Pollution. The RSVs of Cu, TPH, and $\text{NH}_3\text{-N}$ were calculated and are presented in Table 9, except for fluoride, which had an $\text{HQ} < 1$. The calculated RSVs of Cu and TPH were lower than GB36600-2018 [22]; thus, the final RSVs was based on GB36600-2018.

TABLE 8: HQs of pollutants in different layers.

Contaminants	Layer	HQ						Total
		HQ _{ois}	HQ _{dcs}	HQ _{pis}	HQ _{iov1}	HQ _{iov2}	HQ _{iiv1}	
Cu	1	3.29E+00						3.29
	2	3.08E+00						3.08E+00
	3	2.52E+00						2.52E+00
Fluoride	1	3.83E-01		1.83E-02				4.04E-01
NH ₃ -N	1			2.10E-02	2.40E+00	1.18E-06	1.63E-08	2.42E+00
	2			1.76E-02	2.01E+00	9.92E-07	1.37E-08	2.02E+00
	3			1.48E-02	1.70E+00	8.37E-07	1.16E-08	1.72E+00
	4			2.01E-02	2.30E+00	1.13E-06	1.57E-08	2.32E+00
	5			2.01E-02	2.32E+00	1.13E-06	1.57E-08	2.34E+00
	6			2.00E-03	3.21E-01	1.23E-06	2.57E-08	3.23E-01
TPH	1	8.12E+00	1.16E+01					1.97E+01
	2	1.06E+00	1.51E+00					2.57E+00
Total		1.85E+01	1.31E+01	1.14E-01	1.11E+01	6.5E-06	9.87E-08	4.27E+01
Total (%)		43.3	30.6	0.2	25.9	0	0	100

HQ, hazard quotient; NH₃-N, ammonia-nitrogen; TPH, total petroleum hydrocarbons.

TABLE 9: RSVS of contaminants of concern.

Contaminant	RSVS (mg/kg)		
	Calculated	GB36600-2018	Final
Cu	1890	2000	2000
TPH	820	826	826
NH ₃ -N	1549	--	1549

NH₃-N, ammonia-nitrogen; TPH, total petroleum hydrocarbons.

TABLE 10: Study site remediation statistics.

Layer	Targeted pollutants	Remediation area (m ²)	Remediation volume (m ³)
1	Cu, TPH, NH ₃ -N	5259.41	23667.35
2	Cu, TPH, NH ₃ -N	7307.12	14614.24
3	Cu, NH ₃ -N	1874.79	6561.77
4	NH ₃ -N	2965.5	14827.5
5	NH ₃ -N	2637.97	13189.85
Total			72860.71

NH₃-N, ammonia-nitrogen; TPH, total petroleum hydrocarbons.

The remediation area and volume for the targeted pollutants for each different layer were determined by interpolation and manual correction; results are given in Table 10. The spatial distribution of the remediation area for Cu, TPH, and NH₃-N is shown in Figure 6. Cu and TPH need to be remediated only in the first three layers. The Cu and TPH remediation areas overlapped almost completely in

the second and third layers. In contrast, the area that requires remediation of NH₃-N comprises almost five layers. The total remediation volume was 72860.71 m³ after superposition. These results show that a risk assessment is necessary where fertilization plants have been operational, and they can be used to compare, develop, and select remediation options.

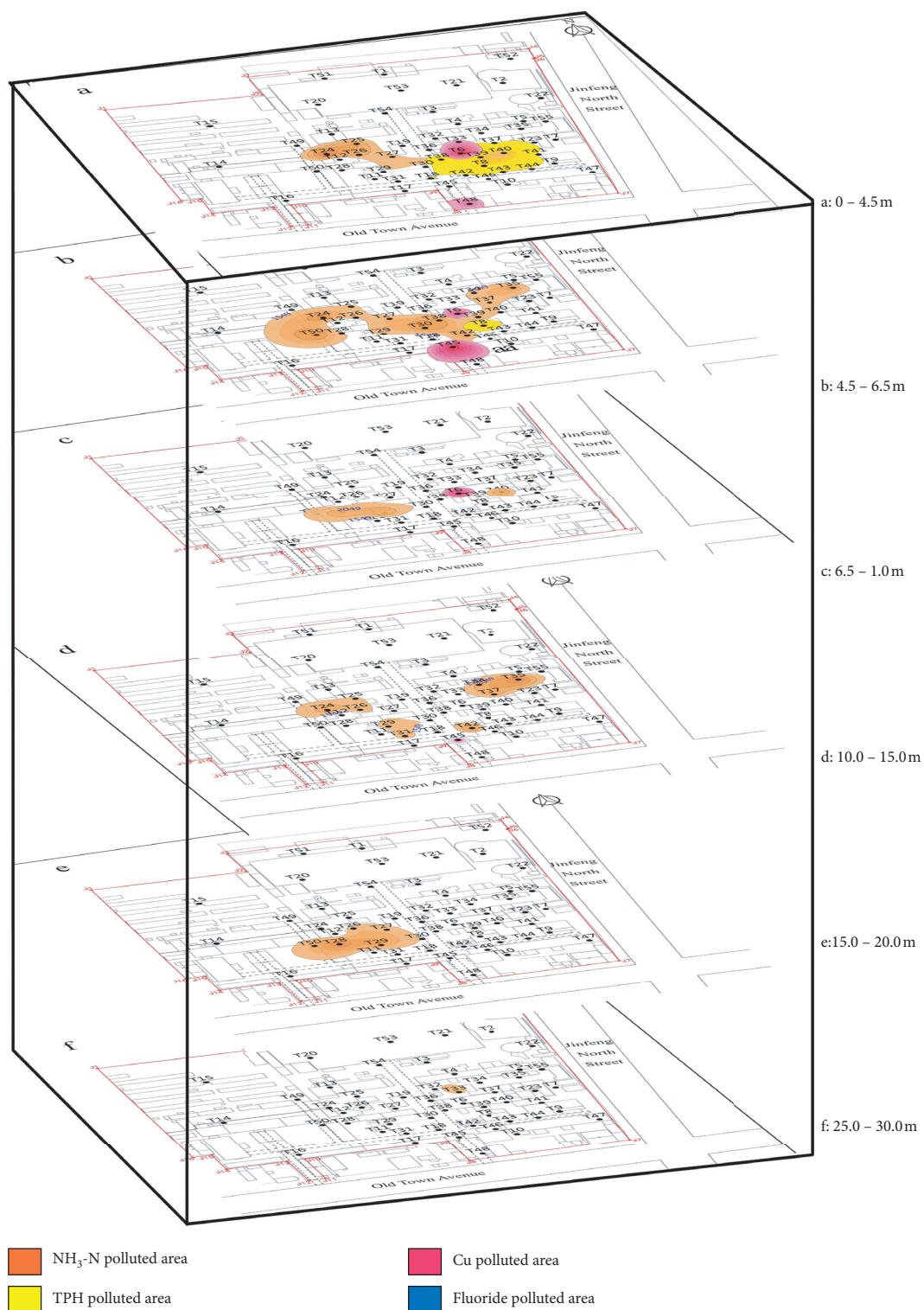


FIGURE 6: Remediation areas from different soil layers: (a) the first layer; (b) the second layer; (c) the third layer; (d) the fourth layer; (e) the fifth layer.

4. Conclusion

In this study, a pollutant survey and risk assessment of soils were carried out in a fertilizer plant in Linzhang County, North China. The results indicated that the site was polluted by four main contaminants: fluoride, copper, TPH, and $\text{NH}_3\text{-N}$. These contaminants were mainly attributed to coal burning, the leakage of wastewater, and lubricating oil. Their presence also reflected the poor pollution controls and environmental protection awareness during the operation period. The total areas polluted by fluoride, Cu, TPH, and $\text{NH}_3\text{-N}$ were 7 m^2 , 2199.6 m^2 , 3048.7 m^2 , and 14564.81 m^2 , respectively. The hazard quotients found were relatively high and indicate that oral ingestion, inhalation of soil particles, and inhalation of gaseous pollutants from the surface soil in the outdoor air could be the main exposure pathways of this site without any remediation steps. RSVS was calculated and compared with GB36600-2018, and the final total remediation soil volume was 72860.71 m^3 after superposition. To solve the problem of soil pollution and protect public health in the study area, the enterprise and local government should make more efforts to remediate the soil pollution. This study provides useful information and reference for environmental management in fertilizer plant sites.

Data Availability

The data used to support the findings of this study are included within the article, and any data in the full-text can be quoted and does not involve the situation of leakage.

Conflicts of Interest

The authors declare that they have no conflicts of interest.

Acknowledgments

The authors thank LetPub (<http://www.letpub.com>) for its linguistic assistance and scientific consultation during the preparation of this manuscript. The fund of this study mainly comes from the national financial project—the Soil Pollution Status Investigation Project of Key Industry Enterprises in Hebei Province.

References

- [1] W.-F. Zhang, Z.-X. Dou, P. He et al., "New technologies reduce greenhouse gas emissions from nitrogenous fertilizer in China," *Proceedings of the National Academy of Sciences*, vol. 110, no. 21, pp. 8375–8380, 2013.
- [2] Y. Du, B. Cui, Q. Zhang et al., "Effects of manure fertilizer on crop yield and soil properties in China: a meta-analysis," *Catena*, vol. 193, Article ID 104617, 2020.
- [3] X. Ju, B. Gu, Y. Wu, and J. N. Galloway, "Reducing China's fertilizer use by increasing farm size," *Global Environmental Change*, vol. 41, pp. 26–32, 2016.
- [4] Y. C. Chien, "Field study of in situ remediation of petroleum hydrocarbon contaminated soil on site using microwave energy," *Journal of Hazardous Materials*, vol. 199–200, pp. 457–461, 2012.
- [5] I. S. Park and J. W. Park, "Determination of a risk management primer at petroleum-contaminated sites: developing new human health risk assessment strategy," *Journal of Hazardous Materials*, vol. 185, no. 2-3, pp. 1374–1380, 2011.
- [6] W. Hou, L. Zhang, Y. Li et al., "Distribution and health risk assessment of polycyclic aromatic hydrocarbons in soil from a typical contaminated urban coking sites in Shenyang city," *Bulletin of Environmental Contamination and Toxicology*, vol. 95, no. 6, pp. 815–821, 2015.
- [7] G. Liu, J. Niu, C. Zhang, and G. Guo, "Characterization and assessment of contaminated soil and groundwater at an organic chemical plant site in Chongqing, Southwest China," *Environmental Geochemistry and Health*, vol. 38, no. 2, pp. 607–618, 2016.
- [8] T. Kiba and A. Krapp, "Plant nitrogen acquisition under low availability: regulation of uptake and root architecture," *Plant and Cell Physiology*, vol. 57, no. 4, pp. 707–714, 2016.
- [9] T. Zakharova, F. Tatàno, and V. Menshikov, "Health cancer risk assessment for arsenic exposure in potentially contaminated areas by fertilizer plants: a possible regulatory approach applied to a case study in Moscow region-Russia," *Regulatory Toxicology and Pharmacology*, vol. 36, no. 1, pp. 22–33, 2002.
- [10] R. Zuo, X. Chen, X. Li et al., "Distribution, genesis, and pollution risk of ammonium nitrogen in groundwater in an arid loess plain, northwestern China," *Environmental Earth Sciences*, vol. 76, no. 17, Article ID 629, 2017.
- [11] M. Van Damme, L. Clarisse, S. Whitburn et al., "Industrial and agricultural ammonia point sources exposed," *Nature*, vol. 564, no. 7734, pp. 99–103, 2018.
- [12] J. Wu and Z. Sun, "Evaluation of shallow groundwater contamination and associated human health risk in an alluvial plain impacted by agricultural and industrial activities, mid-west China," *Exposure and Health*, vol. 8, no. 3, pp. 311–329, 2016.
- [13] M. E. Davidson, J. Schaeffer, M. L. Clark et al., "Personal exposure of dairy workers to dust, endotoxin, muramic acid, ergosterol, and ammonia on large-scale dairies in the high plains Western United States," *Journal of Occupational and Environmental Hygiene*, vol. 15, no. 3, pp. 182–193, 2018.
- [14] Ministry of Ecology and Environment of China (MEEC), *Soil and Sediment-Determination of Copper, Zinc, Lead, Nickel and Chromium-Flame Atomic Absorption Spectrophotometry (HJ 491-2019)*, MEEC, Beijing, China, 2019, In Chinese.
- [15] European Committee for Standardization (ECS), *Soil Quality-Determination of Content of Hydrocarbon in the Range C10 to C40 by Gas Chromatography*, ECS, Brussels, Belgium, ISO 16703:2004, 2011.
- [16] General Administration of Quality Supervision, *Inspection and Quarantine of China (GAQSIQC), Soil Quality-Analysis of Fluoride-Iron Selective Electrometry (GB/T 22104-2008)*, GAQSIQC, Beijing, China, 2008, In Chinese.
- [17] Ministry of Environmental Protection of China (MEPC), *Soil-Determination of Ammonium, Nitrite and Nitrate by Extraction with Potassium Chloride Solution-Spectrophotometric Methods (HJ 634-2012)*, MEPC, Beijing, China, 2012, In Chinese.
- [18] Ministry of Ecology and Environment of China (MEEC), *Soil Environment Quality Risk Control Standard for Soil Contamination of Development Land (GB 36600-2018)*, MEEC, Beijing, China, 2018, In Chinese.

- [19] Ministry of Environmental Protection of China (MEPC), *Technical Guidelines for Risk Assessment of Contaminated Sites (HJ 25.3-2014)*, MEPC, Beijing, China, 2014, In Chinese.
- [20] Z. Ma, K. Chen, Z. Li, J. Bi, and L. Huang, "Heavy metals in soils and road dusts in the mining areas of Western Suzhou, China: a preliminary identification of contaminated sites," *Journal of Soils and Sediments*, vol. 16, no. 1, pp. 204–214, 2016.
- [21] E. Wcislo, J. Bronder, A. Bubak, E. Rodriguez-Valdes, and J. L. R. Gallego, "Human health risk assessment in restoring safe and productive use of abandoned contaminated sites," *Environment International*, vol. 94, pp. 436–448, 2016.
- [22] S.-H. Do, J.-H. Jo, Y.-H. Jo, H.-K. Lee, and S.-H. Kong, "Application of a peroxymonosulfate/cobalt (PMS/Co(II)) system to treat diesel-contaminated soil," *Chemosphere*, vol. 77, no. 8, pp. 1127–1131, 2009.
- [23] C. H. Yen, K. F. Chen, C. M. Kao, S. H. Liang, and T. Y. Chen, "Application of persulfate to remediate petroleum hydrocarbon-contaminated soil: feasibility and comparison with common oxidants," *Journal of Hazardous Materials*, vol. 186, no. 2-3, pp. 2097–2102, 2011.
- [24] H. G. Mikkonen, R. van de Graaff, A. T. Mikkonen et al., "Environmental and anthropogenic influences on ambient background concentrations of fluoride in soil," *Environmental Pollution*, vol. 242, pp. 1838–1849, 2018.
- [25] J. Chen, G. Liu, Y. Kang et al., "Atmospheric emissions of F, As, Se, Hg, and Sb from coal-fired power and heat generation in China," *Chemosphere*, vol. 90, no. 6, pp. 1925–1932, 2013.
- [26] J. Li, J. Fan, J. Jiang et al., "Human health risk assessment of soil in an abandoned arsenic plant site: implications for contaminated site remediation," *Environmental Earth Sciences*, vol. 78, no. 24, Article ID 673, 2019.
- [27] Y. Zou, Y. Li, L. Hu et al., "Health risk assessment of arsenic in soils from three thermal power plants in Southwest China," *Human and Ecological Risk Assessment: An International Journal*, vol. 26, no. 5, pp. 1221–1233, 2020.
- [28] L. Hu, L. Bai, J. Kang, and J. Jia, "Contamination level and potential health risk assessment of hexavalent chromium in soils from a coal chemical industrial area in Northwest China," *Human and Ecological Risk Assessment: An International Journal*, vol. 26, no. 5, pp. 1300–1312, 2020.

Research Article

Hydrogeochemical Characteristics and Formation of Low-Temperature Geothermal Waters in Mangbang-Longling Area of Western Yunnan, China

Xing-Wang Chang,^{1,2} Mo Xu ,¹ Liang-Wen Jiang,² Xiao Li ,¹ and Yun-Hui Zhang ³

¹State Key Laboratory of Geohazard Prevention and Geoenvironment Protection, Chengdu University of Technology, Chengdu 610059, China

²China Railway Eryuan Engineering Group Co. Ltd., Chengdu, Sichuan 610031, China

³Faculty of Geosciences and Environmental Engineering, Southwest Jiaotong University, Chengdu 611756, China

Correspondence should be addressed to Mo Xu; xm@cdu.edu.cn

Received 15 January 2021; Accepted 14 July 2021; Published 28 July 2021

Academic Editor: Kaustubha Mohanty

Copyright © 2021 Xing-Wang Chang et al. This is an open access article distributed under the Creative Commons Attribution License, which permits unrestricted use, distribution, and reproduction in any medium, provided the original work is properly cited.

Numerous low-temperature geothermal waters are distributed extensively in Mangbang-Longling of western Yunnan in China, whose formation mechanism has not been completely investigated yet. This study focused on the hydrogeochemical evolution, reservoir temperature, and recharge origin of geothermal waters using hydrogeochemical and deuterium-oxygen (D-O) isotopic studies. The low-temperature geothermal waters were characterized by HCO₃-Na type, while shallow cold spring was of the hydrochemical type of HCO₃-Ca. The hydrogeochemical characteristics of low-temperature geothermal waters were mainly determined by the dissolution of silicate minerals based on the geological condition and correlations of major and minor ions. The reservoir temperatures of low-temperature geothermal waters ranged from 111°C to 126°C estimated by silica geothermometry and the silicon-enthalpy graphic method. Low-temperature geothermal waters circulated at the largest depth of 1794–2077 m where deep high-temperature geothermal waters were involved. The data points of δD and $\delta^{18}O$ of the hot spring water samples in the study area show a linear right-up trend, indicating the $\delta^{18}O$ reaction between the water and rock and a possible mixture of magmatic water from below. The low-temperature thermal waters were recharged by meteoric water at the elevation of 2362–3653 m calculated by δD values. Upwelling by heating energy, low-temperature geothermal waters were exposed as geothermal springs in the fault and fracture intersection and mixed by up to 72% shallow cold waters at surface. Based on acquired data, a conceptual model of the low-temperature geothermal waters in the Mangbang-Longling area was proposed for future exploitation.

1. Introduction

Energy shortage has been the serious problem for human beings globally due to explosive population growth, accelerated industrialization, and developed living standards [1]. Nowadays, the energy supplied for the whole world consists of fossil fuels and renewable energy. It is noted fossil fuels will be consumed in decades, and thus, renewable energy is expected to be the predominate energy in future. Among renewable energy sources, geothermal energy presents large exploring potential and is welcome all over the

world [2–4]. The geothermal system with reservoir temperature lower than 150°C at 1000 m depth is clarified as low-temperature geothermal resource [5]. Due to the advantages of universal distribution and general application, low-temperature geothermal resource has been becoming the research hotspot globally [6–12].

Due to the intensive tectono-magmatic evolution, the Himalaya geothermal belt in China is the famous geothermal area for massive geothermal energy, including southern Tibet, western Yunnan, and western Sichuan [13, 14]. Among them, western Yunnan possesses numerous and

widespread high- and low-temperature geothermal waters, representing an outstanding natural laboratory for investigating the genetic mechanism for the geothermal system [15]. Although a wealth of studies concerns the geothermal waters in western Yunnan, the majority was concentrated on the high-temperature geothermal waters in the Rehai and Banglazhang regions [16–24]. In comparison, low-temperature geothermal waters in adjacent Mangbang-Longling areas have been scarcely analyzed. As a result, it is generally suggested that the high-temperature geothermal waters were heated by the underlying magma chamber and were characterized by the involvement of magmatic contents [25]. In contrast, the genetic mechanism of low-temperature geothermal waters remains controversial and has yet to be further investigated. In addition, the relationship between high-temperature and low-temperature geothermal waters is enigmatic. The imbalanced research for the low-temperature geothermal system seriously hampers the comprehensive exploitation of geothermal resource in western Yunnan.

Therefore, we present hydrogeochemical and isotopic analyses (including major and trace elements, as well as deuterium and oxygen isotopes) for fourteen geothermal waters and one cold spring collected from the Mangbang-Longling area in western Yunnan. This study is aimed to the hydrogeochemical characteristic of geothermal and cold spring waters, clarify water-rock interaction, estimate reservoir temperature, and trace recharge source. Our new findings are expected to construct the genetic mechanism of the low-temperature geothermal system, providing the reference for future management and sustainable exploitation of geothermal resource in the Mangbang-Longling area of western Yunnan.

2. Study Area

The Mangbang-Longling area is situated in western Yunnan, southwestern China (Figure 1). It is typical of subtropical monsoon climate with average annual air temperature of 14.8°C and mean annual rainfall of 1470 mm. The geomorphology is typical of medium-high mountain with the elevations of 900–3800 m. The Longchuan and Daying rivers traverse southwestwardly through the Mangbang-Longling area, fed by several streams.

Tectonically, the Mangbang-Longling area is bordered by the Longling-Ruili fault to the east and the Dayingjiang fault to the west [26]. Due to the subduction of the Neo-Tethyan Ocean and subsequent continental collision, widespread magmatic and hydrothermal activities were developed in the western Yunnan [27–30]. In the study area, the Gaoligong Group metamorphic rocks and Yanshanian granitic rocks are exposed instead of sedimentary strata [31]. Neogene volcanic rocks and Pliocene basaltic rocks are formed as overlying cap rocks. Numerous NNW-NW and NS-trending secondary faults and fractures were developed extensively by continuous India-Asia collision [32]. Abundant secondary faults and fractures provide the permeable way for groundwater circulation. In the study area, groundwater is mainly recharged by precipitation and local runoff. The aquifers consist of carbonate and silicate rocks.

As a considerable segment of Himalaya geothermal belt, western Yunnan reserves abundant geothermal resource [33]. Geothermal waters are mostly exposed in the faults or their intersections (Figures 1 and 2). The temperatures of geothermal waters vary greatly with the range of 20–96°C. High-temperature geothermal waters (hydrochemical type: Cl-HCO₃-Na) are mostly assembled in the Rehai and Balazhang area, while low-medium temperature geothermal waters (hydrochemical type: HCO₃-Na) are distributed dispersedly in the Mangbang-Longling area.

3. Sampling and Methodology

Fourteen geothermal springs and one cold spring were sampled in the Mangbang-Longling area. Physicochemical parameters of geothermal waters (e.g., temperature, pH, alkalinity, and total dissolved solids (TDS)) were measured in situ using WTW. The concentration of HCO₃⁻ was measured using Gran titration. The experiments were conducted in the State Key Laboratory of Geohazard Prevention and Geoenvironment Protection, Chengdu University of Technology, within one week after sampling. Major cations (e.g., K⁺, Na⁺, Ca²⁺, and Mg²⁺) were analyzed by inductively coupled plasma-optical emission spectrometry (ICP-OES) (Thermo Fisher ICAP-6300), while major anions (Cl⁻ and SO₄²⁻) were determined by ion chromatography (Dionex ICS-1100). Charge balances between major anions and cations were within the error range of ±10%.

The δD and δ¹⁸O values were reported in delta (δ) relative to VSMOW (Vienna Standard Mean Ocean Water) using conventional δ (‰) notation. The analytical precision for δD and δ¹⁸O was ±0.6‰ and ±0.2‰, respectively.

4. Analytical Results

4.1. Hydrogeochemical Characteristics. The physical properties and chemical compositions of geothermal waters and cold waters in the Mangbang-Longling area are given in Table 1. The exposed temperature and pH values of geothermal waters had a range of 24–57°C and 6.5–7.3, respectively. Na and HCO₃ were the primary cation and anion, indicative of the HCO₃-Na hydrochemical type (Figure 3). The contents of SiO₂, Sr, Li, As, and F were relatively low and constant. In comparison, high-temperature geothermal waters displayed Cl-HCO₃-Na hydrochemical type and higher contents of SiO₂, Sr, Li, As, and F, indicating involvements of deep magmatic compositions [23].

One cold water sample was analyzed for comparison. Cold water sample was characterized as HCO₃-Ca type, according to the hydrogeochemical compositions (Figure 3). The minor contents of SiO₂, Sr, Li, As, and F were very low and constant as well.

4.2. Environmental Isotopes. The δ¹⁸O and δD compositions (vs. Vienna Standard Mean Ocean Water (VSMOW)) of the geothermal water samples varied from -9.2‰ to -11.1‰ and from -57.8‰ to -78.9‰, respectively. Cold water

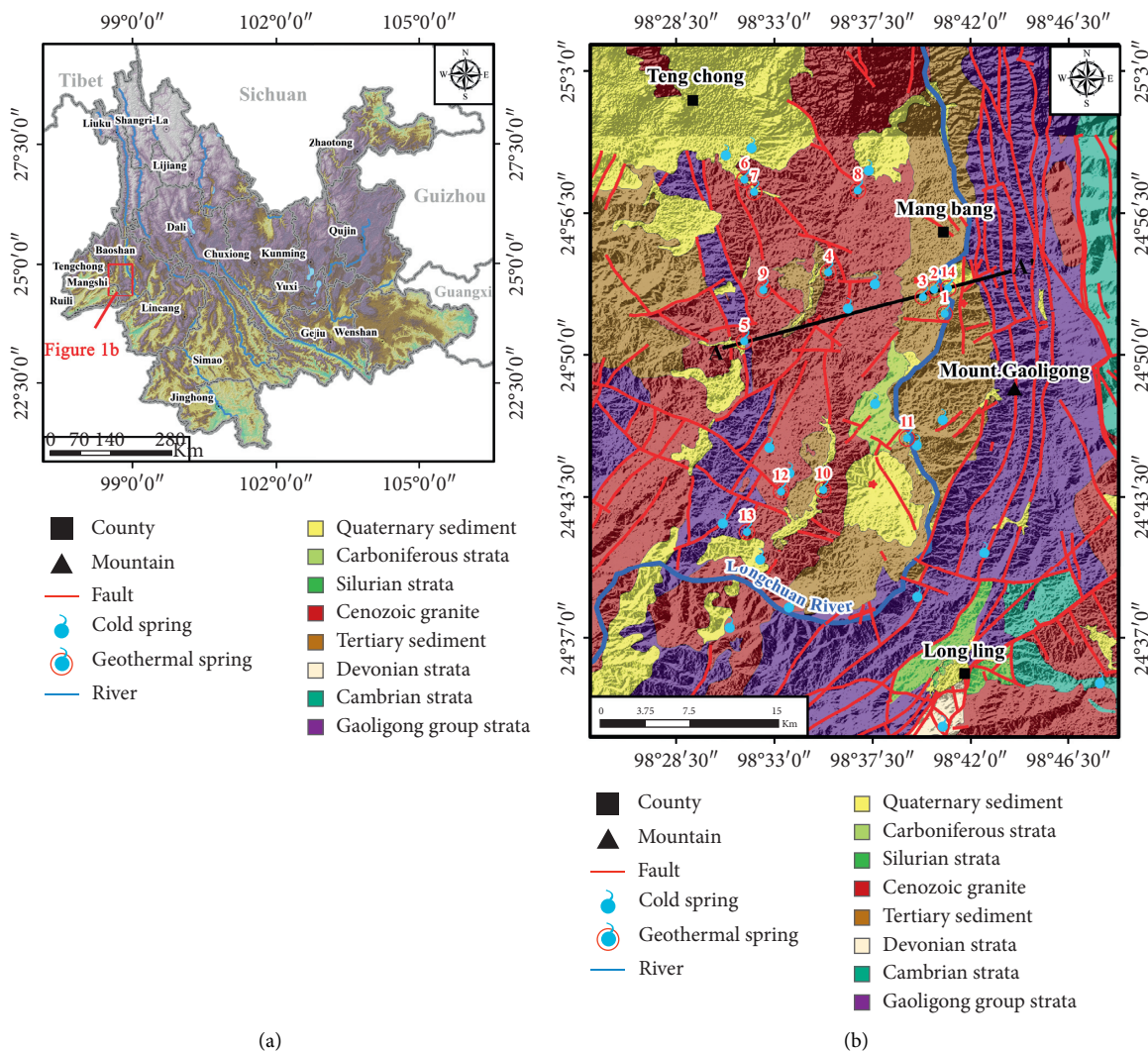


FIGURE 1: Geological map of the Mangbang-Longling area in western Yunnan within the distribution of geothermal waters.

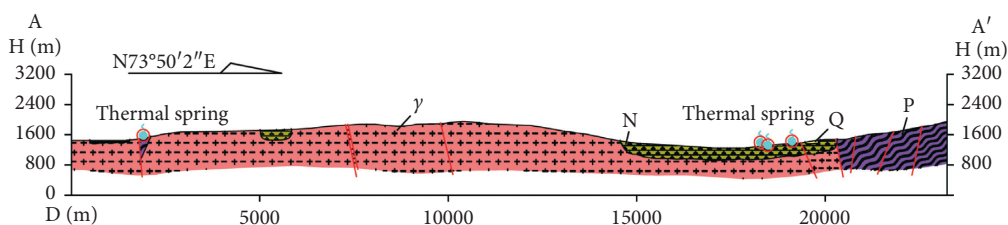


FIGURE 2: Schematic geological cross-sections of A-A' reported in Figure 1.

sample showed relatively enriched $\delta^{18}\text{O}$ (-8.5‰) and δD (-56.6‰) compositions than those of geothermal waters.

4.3. Multiminerall Saturation Indices. The thermodynamic process of the groundwater system can be clarified by mineral equilibrium calculation, which is helpful to reflect the process of water-rock interaction [14]. Mineral saturation indices (SI) of geothermal waters were calculated for evaluating mineral equilibrium based on discharge temperature and pH. The PHREEQC 3.0 software was carried

out to calculate multiminerall SI values [35]. In this study, calculated SI values of most selected minerals (excepted chalcedony and quartz) were lower than zero, indicating geothermal water occurs in undersaturated condition. Detailed results are given in Table 2.

5. Discussion

5.1. Processes Controlling the Hydrogeochemical Compositions. Cl is characterized as the conservative affinity and hardly altered by water-rock interactions and adsorption

TABLE 1: Chemical and isotopic analyses of geothermal water and cold spring samples.

Sample no.	GS1	GS2	GS3	GS4	GS5	GS6	GS7	GS8	GS9	GS10	GS11	GS12	GS13	GS14	CS1
X	17467700	17466890	17466025	17458696	17452200	17452250	17453000	17461020	17453690	17458250	17464774	17455000	17452350	17467957	17466957
Y	2751100	2753164	2752528	2754645	2748820	2762500	2761450	2761550	2753164	2736240	2740586	2736100	2732700	2753276	2760757
Local elevation	1200	1200	1270	1780	1507	1670	1690	1820	1720	1335	1150	1390	1240	1300	1200
T	28.5	24	30	45.5	57	35	36	42	39	51	30	51	53	24	10
pH	6.7	6.9	7.1	7.2	7.1	7	7.2	7.3	7.1	7.2	6.5	6.8	6.5	6.5	6.5
TDS	770	530	388	156	196	124	244	138	118	208	868	132	230	97	76
Flow	1.2	1.2	18.9	0.9	2.1	3.1	0.3	2.0	5.0	3.0	0.0	2.9	0.8	0.8	5.5
K	11.7	8.8	5.5	0.6	0.7	0.8	0.5	0.6	0.7	1.5	10.2	1.1	11.9	2.0	0.2
Na	206.0	130.0	70.3	41.9	54.9	31.7	44.4	34.6	28.4	57.9	258.0	40.3	157.6	32.0	1.8
Ca	27.6	29.0	39.0	0.8	1.1	2.5	0.8	0.9	1.4	0.6	68.6	1.7	1.1	20.0	28.056
Mg	28.0	15.4	21.1	0.0	0.0	0.1	0.0	0.0	0.1	0.0	9.8	0.1	0.0	2.9	2.432
Cl	3.9	2.4	2.1	0.9	1.7	0.9	1.3	0.6	0.5	1.5	4.5	1.8	3.8	1.7	0.5
SO ₄	1.9	0.4	5.4	10.2	8.9	4.8	5.8	6.8	6.3	10.1	0.1	10.2	16.3	3.8	9.61
HCO ₃	692.0	490.0	379.0	100.8	118.5	98.2	103.1	102.7	72.4	148.2	917.0	85.4	354.9	167.6	91.02
Sr	0.440	0.290	0.370	0.028	0.034	0.048	0.022	0.025	0.026	0.026	0.590	0.048	0.031	0.172	0.02305
SiO ₂	62	78	66	70	76	57	63	51	59	78	62	62	82	50	15.2
Li	0.170	0.020	0.001	0.022	0.090	0.014	0.029	0.008	0.010	0.049	0.210	0.050	0.199	0.006	0.0076
As	0.005	0.002	0.001	0.002	0.002	0.002	0.003	0.001	0.001	0.005	0.003	0.001	0.001	0.004	0.0032
F	1.6	1.7	0.3	2.5	6.8	3.4	6.5	1.4	1.8	3.0	5.8	0.8	2.2	0.1	0.03
Hydrochemical type	HCO3-Na	HCO3-Na	HCO3-Na	HCO3-Na	HCO3-Na	HCO3-Na	HCO3-Na	HCO3-Na	HCO3-Na	HCO3-Na	HCO3-Na	HCO3-Na	HCO3-Na	HCO3-Ca-Na	HCO3-Ca
Charge balance (%)	6.0	3.0	3.9	-0.3	6.2	-6.2	3.5	-8.1	0.0	-1.8	1.8	6.0	7.0	-3.5	-0.5
δD	-72.6	-67.2	-63.3	-78.9	-72.1	-69.6	-70.9	-74.0	-72.9	-71.5	-70.9	-68.2	-70.6	-57.8	-69.1
$\delta^{18}O$	-10.9	-9.6	-9.2	-11.1	-10.8	-10.6	-10.7	-11.1	-10.9	-9.9	-10.7	-10.0	-10.3	-9.6	-9.18
Elevation difference	1631	1423	1273	1873	1612	1515	1565	1685	1642	1588	1565	1462	1554	1062	1015.384615
Recharge elevation	2831	2623	2543	3653	3119	3185	3255	3505	3362	2923	2715	2852	2794	2362	2215

Note: GS, geothermal spring; CS, cold spring; cations, anions, SiO₂, and TDS, trace elements in mg/L; isotopic ratio in ‰ relative to the VSMOW standard; elevation in m.

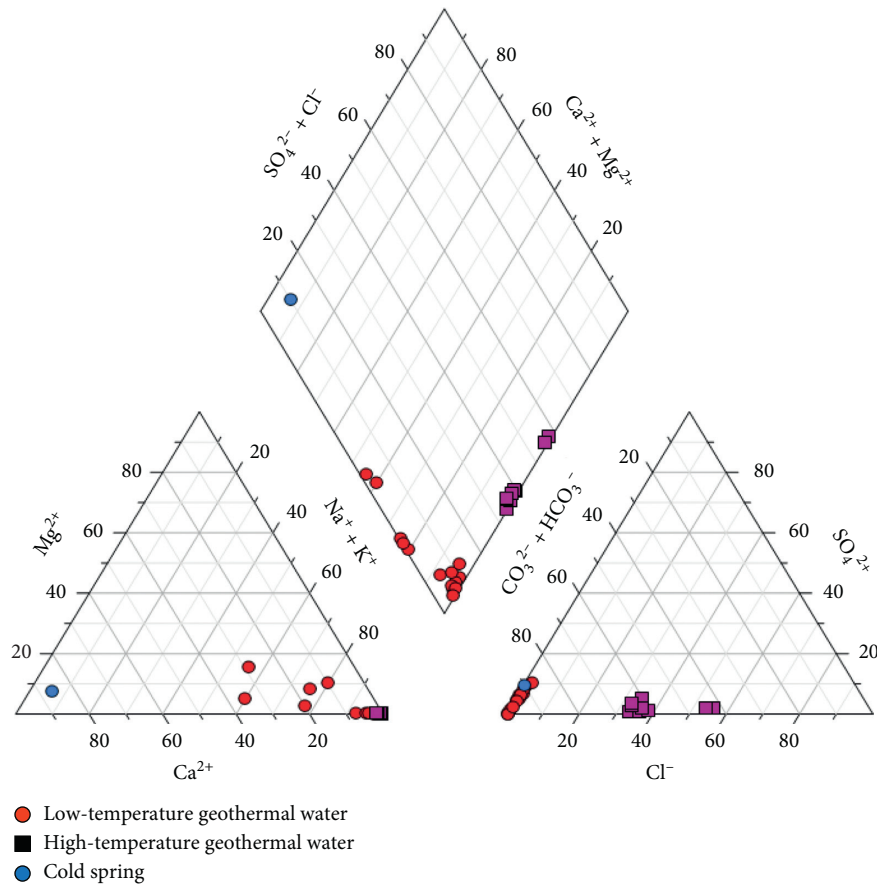


FIGURE 3: Piper plot of water samples [34]. Low-temperature geothermal waters and cold spring are from this study. High-temperature geothermal waters are from [23].

TABLE 2: Saturation indices of different minerals in geothermal waters.

Sample	GS1	GS2	GS3	GS4	GS5	GS6	GS7	GS8	GS9	GS10	GS11	GS12	GS13	GS14
Anhydrite	-4.07	-4.66	-3.37	-4.52	-4.48	-4.36	-4.8	-4.65	-4.47	-4.69	-4.92	-4.21	-4.36	-3.64
Aragonite	-0.26	-0.34	-0.3	-2.43	-2.24	-1.95	-2.45	-2.38	-2.32	-2.41	0.22	-2.18	-1.86	-0.86
Calcite	-0.12	-0.19	-0.16	-2.29	-2.1	-1.81	-2.31	-2.24	-2.18	-2.27	0.36	-2.04	-1.72	-0.72
Chalcedony	0.18	0.28	0.2	0.23	0.26	0.14	0.18	0.09	0.15	0.28	0.18	0.18	0.3	0.08
Chrysotile	-5.78	-6.25	-5.94	-15.59	-14.3	-12.51	-15.68	-15	-12.57	-15.55	-7.23	-12.69	-15.7	-8.58
CO ₂	-1.07	-1.21	-1.32	-1.87	-1.8	-1.88	-1.86	-1.86	-2.01	-1.7	-0.95	-1.94	-1.34	-1.65
Dolomite	0.19	-0.26	-0.18	-6.09	-5.43	-4.53	-6.1	-6.02	-5.07	-5.93	0.3	-4.91	-5.08	-1.87
Gypsum	-3.82	-4.41	-3.12	-4.27	-4.23	-4.11	-4.55	-4.4	-4.22	-4.44	-4.67	-3.96	-4.11	-3.39
Halite	-7.69	-8.08	-8.4	-8.95	-8.57	-9.08	-8.77	-9.24	-9.35	-8.6	-7.54	-8.67	-7.79	-8.81
Quartz	0.59	0.69	0.62	0.64	0.68	0.55	0.6	0.5	0.57	0.69	0.59	0.59	0.71	0.5
Sepiolite	-3.95	-4.1	-4.01	-10.41	-9.49	-8.5	-10.54	-10.82	-8.51	-10.3	-4.92	-8.56	-10.36	-5.97
SiO ₂ (a)	-0.64	-0.55	-0.62	-0.59	-0.56	-0.68	-0.64	-0.74	-0.67	-0.55	-0.64	-0.65	-0.52	-0.74
Talc	-1.66	-1.93	-1.76	11.37	-10.01	-8.46	-11.54	-11.92	-8.49	-11.23	-3.11	-8.57	-11.34	-4.65

of rock-forming. For this reason, the relationship between the Cl and other major ions is efficient to trace the hydro-geochemical processes during the formation of geothermal waters. In this study, the relationship between the Cl content and other ion concentrations is shown in Figure 4. It is noteworthy that Cl contents had an obvious liner relationship with K (squared regression coefficient = 0.9336), Na (squared regression coefficient = 0.8362), and SiO₂ (squared regression coefficient = 0.7019). Low-temperature geothermal waters in the Mangbang-Longling area were believed to be the results by

mixture between surface cold water and a deep geothermal fluid. Notably, the squared regression coefficient of K vs. Cl was higher than squared regression coefficients of Na vs. Cl and SiO₂ vs. Cl. Considering widespread exposure of silicate rocks (granitic and metamorphic rocks) in the Mangbang-Longling area, the concentrations of Na and SiO₂ were probably influenced by water-rock reaction (dissolution of silicates) and ion exchange.

However, the plots in the Ca, Mg, HCO₃, SO₄, and F vs. Cl diagrams represented scattered distributions, suggesting

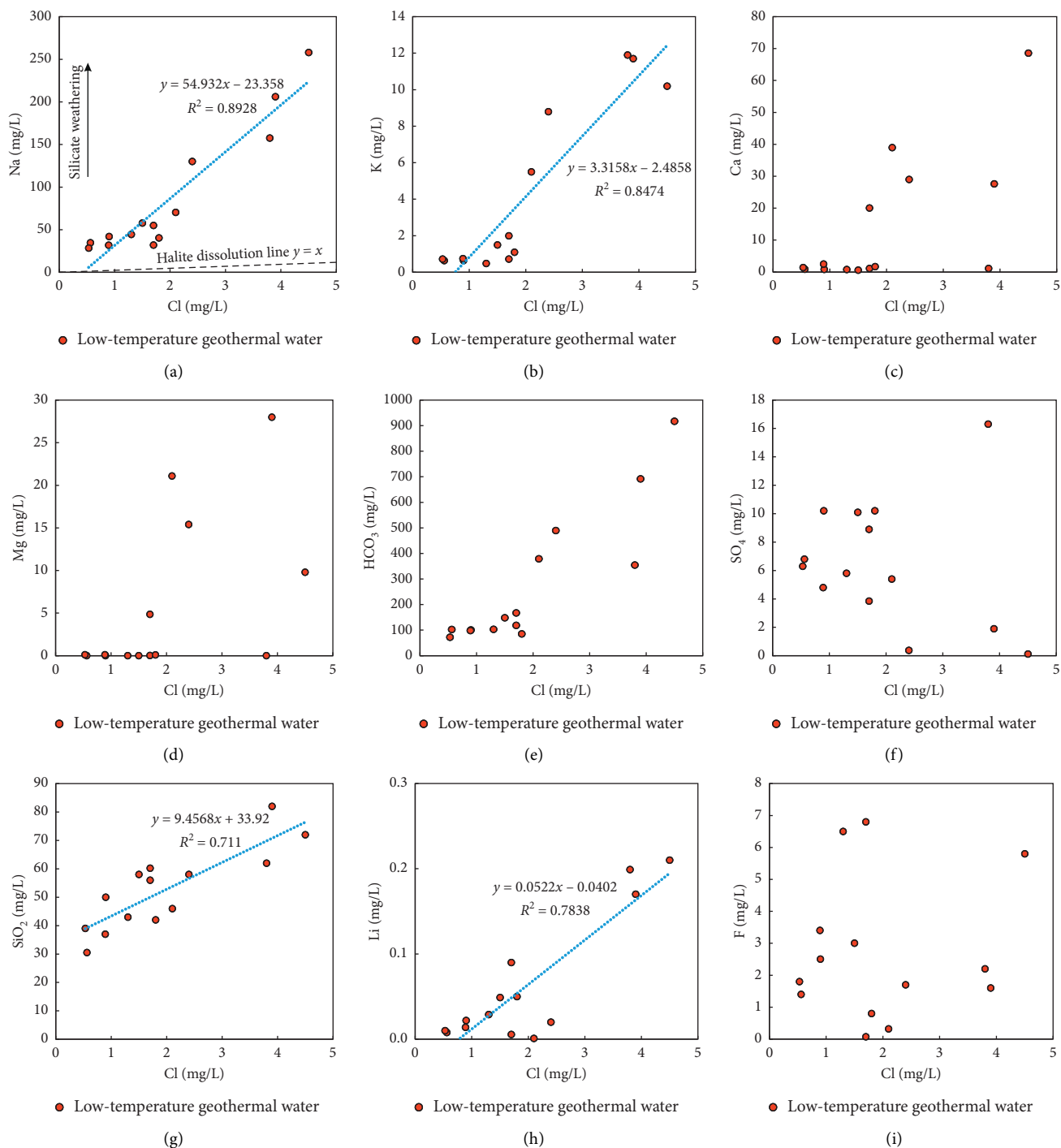


FIGURE 4: The plots of Cl against (a) Na, (b) K, (c) Ca, (d) Mg, (e) HCO_3^- , (f) SO_4^{2-} , (g) SiO_2 , (h) Li, and (i) F.

that these ions are derived from multiple sources (Figures 4(e)–4(i)). Ca, Mg, and HCO_3^- were originated from the dissolution of calcite and dolomite, in the case of the Ca/HCO_3^- and $(\text{Ca} + \text{Mg})/\text{HCO}_3^-$ ratios of 1. In this study, the Ca/HCO_3^- and $(\text{Ca} + \text{Mg})/\text{HCO}_3^-$ ratios were lower than 1 (Figures 5(a) and 5(b)). Meanwhile, the saturation indices of carbonate minerals (calcite and dolomite) were lower than zero, excluding the possibility of carbonate reservoir. The depletion of Ca and Mg were attributed to ion exchange

from silicates dissolution, while enrichment of HCO_3^- in the silicate reservoir was probably derived from escaped geothermal gases dominated by CO_2 . The concentrations of Ca and SO_4^{2-} did not yield a 1:1 line in Figure 5(c), implying hydrogeochemical concentrations of geothermal waters is unlikely determined by dissolution of gypsum.

Large number of the samples were plotted along the 1:1 line in the $(\text{Na} + \text{K})\text{--Cl}$ and $(\text{Ca} + \text{Mg})\text{--}(\text{SO}_4^{2-} + \text{HCO}_3^-)$ diagram. Hence, the hydrogeochemical composition of the

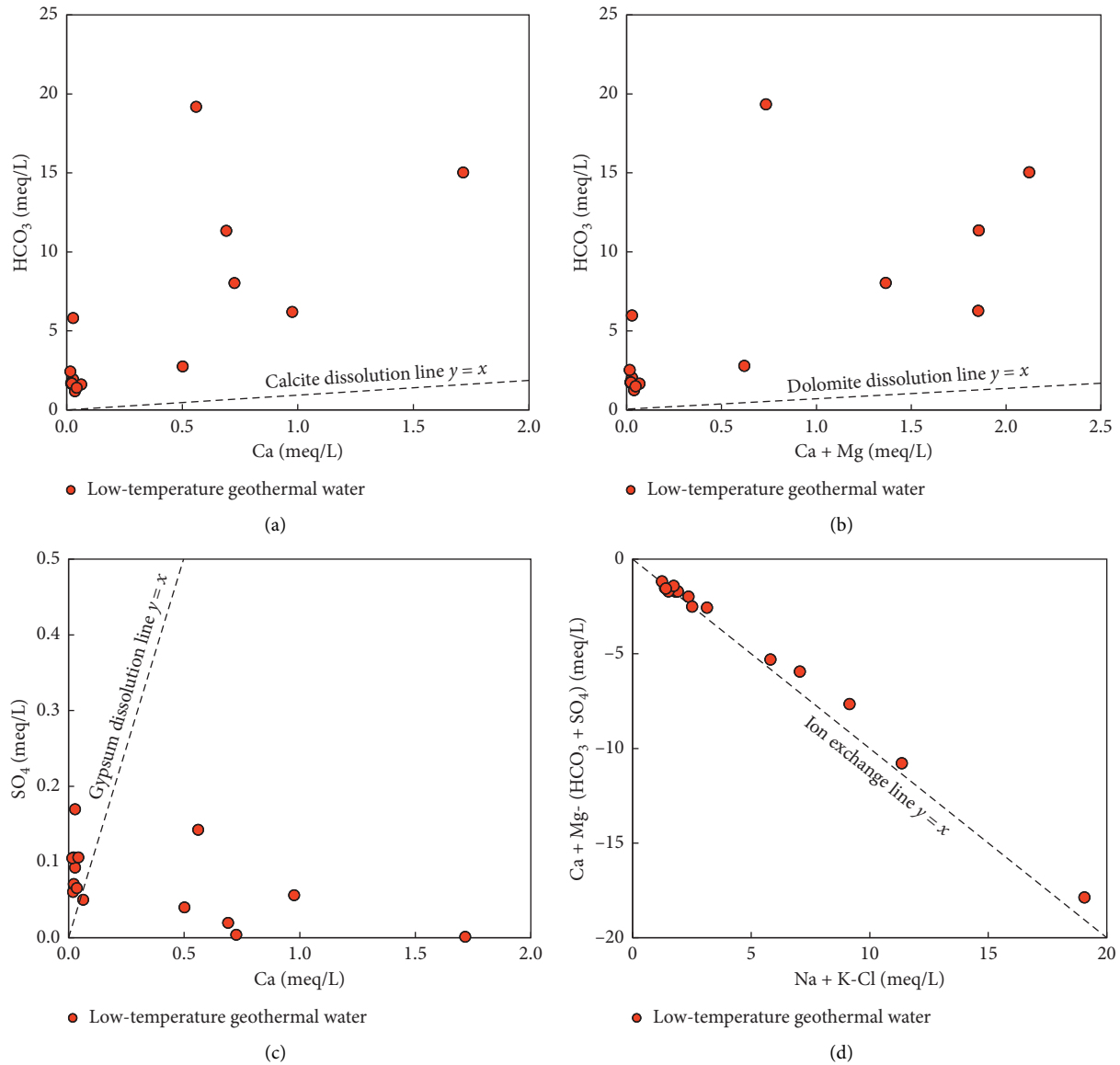


FIGURE 5: Diagrams used to identify hydrogeochemical processes based on the concentrations of major constituents in water. (a) Ca vs. HCO_3^- , (b) Ca + Mg vs. $\text{HCO}_3^- + \text{SO}_4^-$, (c) Ca vs. SO_4^- , and (d) Na + K - Cl vs. Ca + Mg - ($\text{HCO}_3^- + \text{SO}_4^-$).

samples was mainly attributed to a cation-exchange process which is the result of silicate dissolution (Figure 5(d)).

5.2. Reservoir Temperature and Circulation Depth.

Geothermometers determining reservoir temperature are based on the equilibrium of temperature-dependent reactions that occur in the reservoir [36].

5.2.1. Classical Geothermometry. The classical chemical geothermometers (e.g., cation and silica) are applicable for the estimation of the equilibrium temperature in geothermal reservoirs [37–39]. Considering this, cation and silica geothermometers were used to calculate the equilibrium temperatures, whose results are listed in Table 3. However, the results from the cation geothermometers had a great range and variation with wellhead temperatures. In

the Na-K-Mg ternary diagram, all plots of geothermal waters were largely deviated from the full equilibrium line and plot in the area of immature waters (Figure 6). Saturation indices of most minerals (except quartz and chalcedony) lower than zero were also typical of immature affinity. Hence, none of the low-temperature geothermal waters in the Mangbang-Longling area had reached full equilibrium with the host rock. In this study, silica geothermometers were more applicable to the geothermal waters than cation geothermometers in this study. Additionally, the oversaturated condition of silicate minerals (quartz and chalcedony) also supported the feasibility of silica geothermometers.

Silica geothermometry, including quartz and chalcedony geothermometers, is the approach to estimate reservoir temperature considering the soluble concentrations of silica minerals. Various silica geothermometers

TABLE 3: Geothermometer calculations of the geothermal waters (unit: °C).

Sample no.	GS1	GS2	GS3	GS4	GS5	GS6	GS7	GS8	GS9	GS10	GS11	GS12	GS13	GS14
Quartz [40]	144	151	146	148	151	141	144	137	142	151	144	144	153	137
Quartz (maximum steam loss) [40]	138	145	140	141	144	136	139	133	137	145	138	138	146	133
Chalcedony [41]	118	126	120	122	125	115	118	111	116	126	118	118	128	111
Na-K [38]	191	203	213	117	110	139	101	126	142	143	168	146	211	197
Na-K-Ca [36]	152	153	148	100	96	106	88	104	111	127	132	117	190	131
K-Mg [38]	58	58	45	83	74	58	76	83	58	105	67	68	175	45

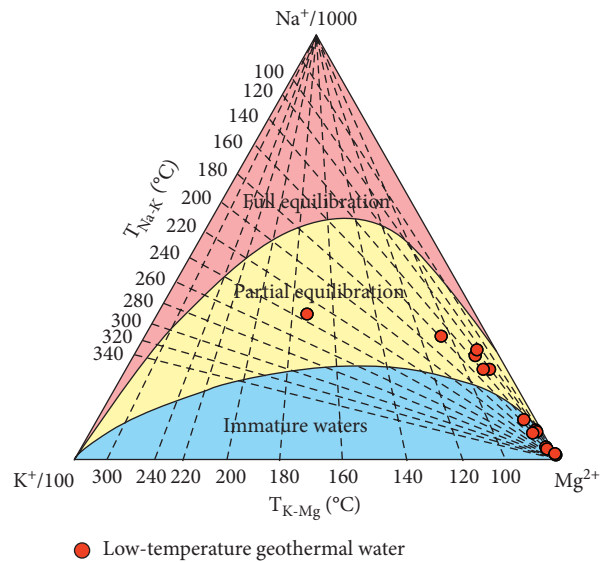


FIGURE 6: Graphical evaluation of water-rock equilibration temperatures for geothermal waters using Na-K-Mg concentrations in “mg/L” [38].

were applied in this study (Table 3). Of note, the chalcedony geothermometer was chosen on the basis of the distribution of samples in the $\log(K^2/Mg)$ versus the $\log(SiO_2)$ diagram (Figure 7).

Quartz geothermometer is applied for the reservoir with high temperatures at 150°C and above, while chalcedony geothermometer yields more accurate results when geothermal waters reach equilibrium below 180°C [45]. In the Mangbang-Longling area, the estimated reservoir temperatures calculated by silica geothermometers were lower than 150°C. As such, it is believable that the estimate reservoir temperatures of geothermal waters in the Mangbang-Longling area ranged 111–126°C calculated by the chalcedony geothermometer.

5.2.2. Silicon-Enthalpy Graphic Method. Cold water is believed to be involved in the formation of low-temperature geothermal water due to the immature affinity. In this study, the silica-enthalpy mixing model with the plots of cold and geothermal water was used to estimate the reservoir temperature and mixing ratio (Figure 8) [39]. In the silica-enthalpy mixing model, the average value of cold water samples was chosen as end member point “a” and geothermal water samples were noted as end member point “b.” A red line linking end member points “a” and “b” intersected with the vertical line of the boiling point

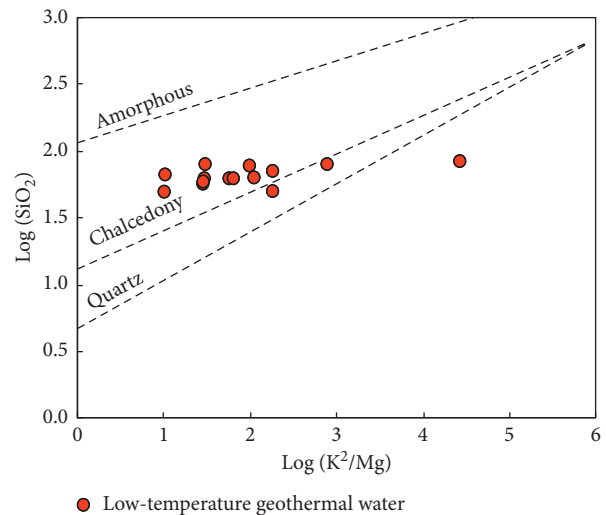


FIGURE 7: Cross-plot of $\log(K^2/Mg)$ vs. $\log(SiO_2)$, unit: mg/L [42]. The lines are drawn using $\log(SiO_2) = 4.52 - (731/(t^\circ C + 273.15))$ for amorphous silica, $\log(SiO_2) = 4.69 - (1032/(t^\circ C + 273.15))$ for chalcedony, and $\log(SiO_2) = 5.19 - (1309/(t^\circ C + 273.15))$ for quartz from [43] and $\log(K^2/Mg) = 14 - (4410/(t^\circ C + 273.15))$ from [44].

(96°C) at point “c” and Quartz solubility line at the point “d.” The horizontal axis of point “d” (151°C) suggested the reservoir temperature when no steam separated before

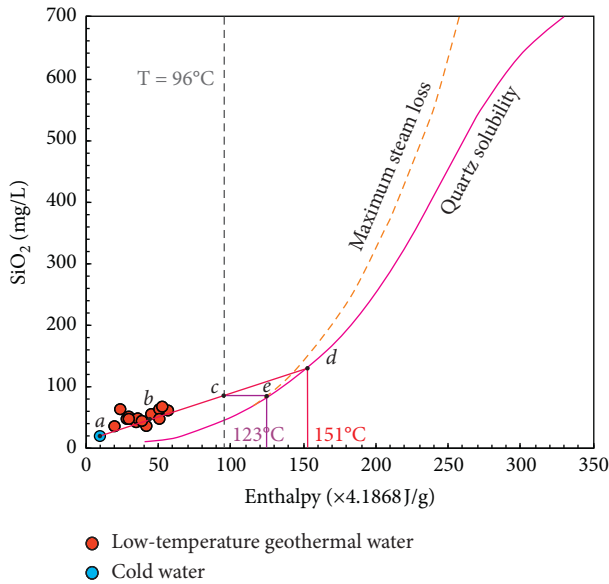


FIGURE 8: The silica-enthalpy plot of the geothermal waters and cold water (Truesdell and [40]).

mixing. Point “c” was intersected horizontally with the maximum steam loss line at point “e.” The horizontal axis of point “e” (123°C) was the reservoir temperature in the condition of steam separation occurs before mixing. Therefore, the reservoir temperature of 123°C obtained by point “e” was more comparable to the results calculated by the chalcedony geothermometer (111–126°C). The mixing ratio of shallow cold water can be approximately obtained by the length ratio between line ab and line ad, that is to say, 72%.

Fournier [46] raised the silica-enthalpy equations to estimate the mixing ratios of cold waters and the temperatures of initial geothermal waters. The silica-enthalpy equations are given as follows:

$$H_c X + H_h (1 - X) = H_s, \quad (1)$$

$$Si_c X + Si_h (1 - X) = Si_s. \quad (2)$$

In equations (1) and (2), H_h is the enthalpy of initial geothermal water, H_c signifies the enthalpy of cold water, H_s represents the enthalpy of geothermal water, X is the mixing ratio of cold water, Si_h defines the SiO_2 contents of initial geothermal water, and Si_c shows the SiO_2 contents of cold water. The results of silica-enthalpy equations indicated the mixing ratios of cold waters, and the temperatures of initial geothermal waters are 69–74% and 180–270°C.

5.2.3. Circulation Depth. When geothermal water is heated by heat flow from below, the circulation depth of geothermal water in the studied area is estimated using the following equation:

$$Z = \frac{(T_z - T_0)}{G} + Z_0, \quad (3)$$

where Z is the circulation depth (m), T_z is the geothermal reservoir temperature obtained by a reasonable geothermometer (°C), T_0 is the annual average temperature of recharge area (°C), G is thermal gradient (°C/m), and Z_0 is the thickness of the constant temperature zone (m). In this study case, the annual average temperature of recharge area is 17.5°C, and therefore, $T_0 = 17.5^\circ\text{C}$, $Z_0 = 30$ m, and $G = 5.3^\circ\text{C}/100$ m [47, 48]. Based on the above calculated reservoir temperatures (111–126°C), the largest circulation depth of geothermal water was inferred as 1794–2077 m in the Mangbang-Longling area.

5.3. Recharge Origin. H and O stable isotopes (δD and $\delta^{18}O$) have been proved to be a robust way for tracing recharge origin of geothermal water. In this study, the geothermal waters present the δD values of -57.8‰ to -78.9‰ (average = -70.0‰) and $\delta^{18}O$ values of -9.2‰ to -11.1‰ (average = -10.4‰), respectively. The plots of geothermal waters were close around the local meteoric water line (LMWL) in the δD – $\delta^{18}O$ graph (Figure 9), indicative of a meteoric origin. Geothermal water plots were slightly deviated from the LMWL and further link with high-temperature geothermal water and magmatic water in a straight line. Hence, weak water-rock interaction and involvements of high-temperature geothermal water occurred in the formation of low-temperature geothermal water.

δD and $\delta^{18}O$ values have been extensively employed to calculate the recharge elevation because of their altitude effect. Considering the existence of oxygen drifting, the δD values of the geothermal waters are more reliable to estimate the recharge elevation in this study. The recharge elevation difference (ΔH) of geothermal water are calculated based on the following equation: $\delta D = -0.026 \cdot \Delta H - 30.2$ [49, 50]. Accordingly, the recharge elevation differences of the low-temperature geothermal waters in the Mangbang-Longling area were calculated as 1062–1873 m, indicating the elevations of recharge area range from 2362 m to 3653 m. The recharge elevation well coincided with the elevation range of 900–3800 m in the study area.

5.4. Conceptual Model of Low-Temperature Geothermal Waters in the Mangbang-Longling Area. According to the geological condition and hydrogeochemical and isotopic results above, a conceptual model of low-temperature geothermal water in the Mangbang-Longling area was built as schematically depicted in Figure 10, which is a qualitative, schematic representation of (or part of) reality. Geothermal water was recharged by common meteoric water at the elevation of 2362–3653 m. Afterward, meteoric water is driven by topographical conditions, flows along fault and fractures, and finally transfers to geothermal water by heating by heat flow from below. Assuming a geothermal gradient of $5.3^\circ\text{C}/100$ m, geothermal water infiltrates into the subsurface at the reservoir with the largest circulation depth of 1794–2077 m and temperature of 111–126°C. During the circulation, the hydrogeochemical characteristics of geothermal water (HCO_3 -Na type) were mainly determined by the water-rock interaction with a widespread silicate aquifer

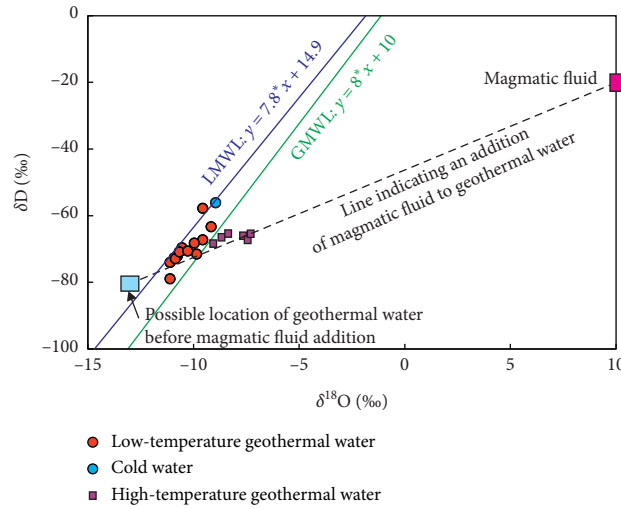


FIGURE 9: Plots of $\delta^{18}O$ vs. δD for the geothermal water and cold water samples, modified after [17]. GMWL, global meteoric water line; LMWL, local meteoric water line. Low-temperature geothermal water and cold water samples are from this study. High-temperature geothermal water samples are cited from [17].

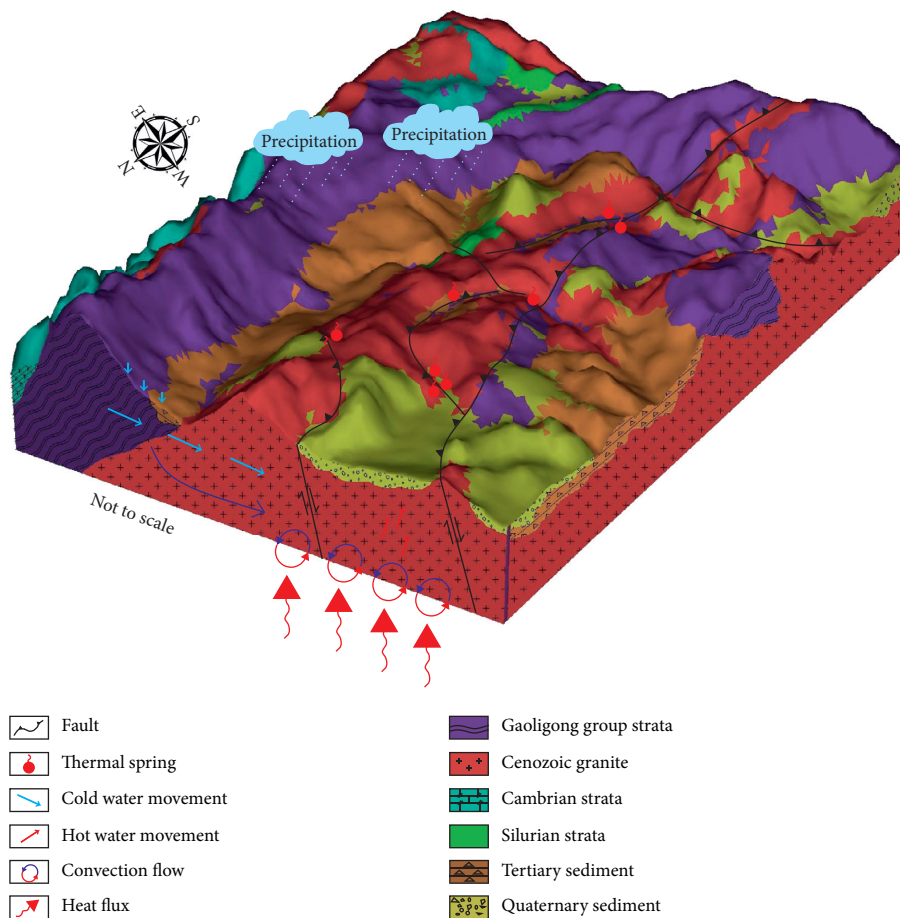


FIGURE 10: Conceptual model of low-temperature geothermal water in the Mangbang-Longling area.

(e.g., granite and metamorphic rocks). It is noteworthy that the involvement of high-temperature geothermal water had been verified during the formation of low-temperature geothermal water. Finally, low-temperature geothermal

water was mixed with up to 72% shallow cold water of HCO_3 -Ca type and exposed as geothermal spring in the high permeability areas, such as fault and fracture intersection.

6. Conclusion

This study was the first to present the hydrogeochemistry and geothermometry of the low-temperature thermal waters in the Mangbang-Longling area of western Yunnan. In this context, the results obtained from geochemical and isotopic studies are listed as follows.

- (1) The low-temperature geothermal waters were characterized by $\text{HCO}_3\text{-Na}$ type, while shallow cold spring is of the hydrochemical type of $\text{HCO}_3\text{-Ca}$
- (2) Hydrogeochemical characteristics of low-temperature geothermal waters were mainly affected by the water-rock interaction with silicate minerals
- (3) Low-temperature geothermal waters possessed reservoir temperature of 111–126°C and largest circulation depth of 1794–2077 m and were mixed with up to 72% shallow cold waters
- (4) δD and $\delta^{18}\text{O}$ evidence showed the low-temperature thermal waters were recharged by meteoric water at the elevation of 2362 m to 3653 m. The data points of δD and $\delta^{18}\text{O}$ of the hot spring water samples in the study area show a linear right-up trend, indicating the $\delta^{18}\text{O}$ reaction between the water and rock and a possible mixture of magmatic water from below. Deep high-temperature geothermal waters were involved in the formation of low-temperature thermal waters.

Data Availability

The data used to support the findings of the study are available from the corresponding author upon request.

Conflicts of Interest

The authors declare that they have no conflicts of interest.

Acknowledgments

The authors thank Qiang Zhang and Xun Huang at the State Key Laboratory of Geohazard Prevention and Geoenvironment Protection, Chengdu University of Technology, for their assistance and helpful discussion. This research was supported by the Fundamental Research Funds for the Central Universities (2682020CX10 and 2682021ZTPY063).

References

- [1] H. Zhang and Y. Xie, "Alleviating freshwater shortages with combined desert-based large-scale renewable energy and coastal desalination plants supported by Global Energy Interconnection," *Global Energy Interconnection*, vol. 2, no. 3, pp. 205–213, 2019.
- [2] S.-M. Lu, "A global review of enhanced geothermal system (EGS)," *Renewable and Sustainable Energy Reviews*, vol. 81, pp. 2902–2921, 2018.
- [3] P. Olasolo, M. C. Juárez, M. P. Morales, S. D'Amico, and I. A. Liarte, "Enhanced geothermal systems (EGS): a review," *Renewable and Sustainable Energy Reviews*, vol. 56, pp. 133–144, 2016.
- [4] X. Zhang and Q. Hu, "Development of geothermal resources in China: a review," *Journal of Earth Science*, vol. 29, no. 2, pp. 452–467, 2018.
- [5] A. Stefánsson, S. Arnórsson, Á. E. Sveinbjörnsdóttir, J. Heinemaier, and H. Kristmannsdóttir, "Isotope (δD , $\delta^{18}\text{O}$, 3H , $\delta^{13}\text{C}$, ^{14}C) and chemical (B, Cl) Constrains on water origin, mixing, water-rock interaction and age of low-temperature geothermal water," *Applied Geochemistry*, vol. 108, Article ID 104380, 2019.
- [6] M. Blasco, L. F. Auqué, M. J. Gimeno, P. Acero, J. Gómez, and M. P. Asta, "Mineral equilibria and thermodynamic uncertainties in the geothermometrical characterisation of carbonate geothermal systems of low temperature. The case of the Alhama-Jaraba system (Spain)," *Geothermics*, vol. 78, pp. 170–182, 2019.
- [7] M. Blasco, M. J. Gimeno, and L. F. Auqué, "Low temperature geothermal systems in carbonate-evaporitic rocks: mineral equilibria assumptions and geothermometrical calculations. Insights from the arnedillo thermal waters (Spain)," *Science of The Total Environment*, vol. 615, pp. 526–539, 2018.
- [8] A. Gökğöz and H. Akdağoğlu, "Hydrogeology and hydrogeochemistry of a coastal low-temperature geothermal field: a case study from the Datça Peninsula (SW Turkey)," *Environmental Earth Sciences*, vol. 75, no. 15, p. 1143, 2016.
- [9] J. I. Morales-Arredondo, M. V. Esteller-Alberich, M. A. Armienta Hernández, and T. A. K. Martínez-Florintino, "Characterizing the hydrogeochemistry of two low-temperature thermal systems in central Mexico," *Journal of Geochemical Exploration*, vol. 185, pp. 93–104, 2018.
- [10] S. Pasvanoğlu and M. Çelik, "Hydrogeochemical characteristics and conceptual model of Çamlidere low temperature geothermal prospect, northern Central Anatolia," *Geothermics*, vol. 79, pp. 82–104, 2019.
- [11] E. Pekkan and S. Kahraman, "Evaluation of the conceptual model of low-temperature thermal water of Kızılınler Region, Eskişehir, Turkey," *Geothermics*, vol. 84, Article ID 101739, 2020.
- [12] J. Pepin, M. Person, F. Phillips et al., "Deep fluid circulation within crystalline basement rocks and the role of hydrologic windows in the formation of the Truth or Consequences, New Mexico low-temperature geothermal system," *Geofluids*, vol. 15, no. 1-2, pp. 139–160, 2015.
- [13] Q. Guo, "Hydrogeochemistry of high-temperature geothermal systems in China: a review," *Applied Geochemistry*, vol. 27, no. 10, pp. 1887–1898, 2012.
- [14] X. Li, X. Huang, X. Liao, and Y. Zhang, "Hydrogeochemical characteristics and conceptual model of the geothermal waters in the xianshuihe fault zone, southwestern China," *International Journal of Environmental Research and Public Health*, vol. 17, no. 2, p. 500, 2020.
- [15] Z. J. Liao, W. Tong, S. B. Liu, and F. S. Zhao, "High-temperature hydrothermal systems in west yunnan province, China," *Geothermics*, vol. 15, pp. 627–631, 1986.
- [16] J. Du, C. Liu, B. Fu et al., "Variations of geothermometry and chemical-isotopic compositions of hot spring fluids in the rehai geothermal field, southwestern China," *Journal of Volcanology and Geothermal Research*, vol. 142, no. 3-4, pp. 243–261, 2005.
- [17] Q. Guo, M. Liu, J. Li, X. Zhang, W. Guo, and Y. Wang, "Fluid geochemical constraints on the heat source and reservoir temperature of the Banglazhang hydrothermal system,


- Yunnan-Tibet Geothermal Province, China,” *Journal of Geochemical Exploration*, vol. 172, pp. 109–119, 2017.
- [18] Q. Guo, B. Planer-Friedrich, M. Liu, J. Li, C. Zhou, and Y. Wang, “Arsenic and thioarsenic species in the hot springs of the Rehai magmatic geothermal system, Tengchong volcanic region, China,” *Chemical Geology*, vol. 453, pp. 12–20, 2017.
- [19] Q. Guo and Y. Wang, “Geochemistry of hot springs in the Tengchong hydrothermal areas, Southwestern China,” *Journal of Volcanology and Geothermal Research*, vol. 215, pp. 61–73, 2012.
- [20] B. P. Hedlund, J. K. Cole, A. J. Williams et al., “A review of the microbiology of the Rehai geothermal field in Tengchong, Yunnan Province, China,” *Geoscience Frontiers*, vol. 3, no. 3, pp. 273–288, 2012.
- [21] M. Liu, Q. Guo, X. Zhang, and Y. Wang, “Characteristic solutes in geothermal water from the Rehai hydrothermal system, Southwestern China,” *Journal of Earth Science*, vol. 26, no. 1, pp. 140–148, 2015.
- [22] Z. Shanguan, C. Zhao, H. Li, Q. Gao, and M. Sun, “Evolution of hydrothermal explosions at Rehai geothermal field, Tengchong volcanic region, China,” *Geothermics*, vol. 34, no. 4, pp. 518–526, 2005.
- [23] M. Wang, X. Zhou, Y. Liu, H. Xu, Y. Wu, and L. Zhuo, “Major, trace and rare earth elements geochemistry of geothermal waters from the Rehai high-temperature geothermal field in Tengchong of China,” *Applied Geochemistry*, vol. 119, Article ID 104639, 2020.
- [24] G. Zhang, C.-Q. Liu, H. Liu, Z. Jin, G. Han, and L. Li, “Geochemistry of the Rehai and ruidian geothermal waters, yunnan province, China,” *Geothermics*, vol. 37, no. 1, pp. 73–83, 2008.
- [25] Y. Zhang, H. Tan, W. Zhang, H. Wei, and T. Dong, “Geochemical constraint on origin and evolution of solutes in geothermal springs in western Yunnan, China,” *Geochemistry*, vol. 76, no. 1, pp. 63–75, 2016.
- [26] H. Zou, H.-W. Cao, L. Bagas et al., “Origin of the Mo-bearing xiaoshuijing syenogranite in the tengchong terrane, SW China,” *Ore Geology Reviews*, vol. 105, pp. 258–272, 2019.
- [27] H.-W. Cao, Y.-H. Zhang, L. Tang et al., “Geochemistry, zircon U–Pb geochronology and Hf isotopes of jurassic-cretaceous granites in the Tengchong terrane, SW China: implications for the mesozoic tectono-magmatic evolution of the eastern tethyan tectonic domain,” *International Geology Review*, vol. 61, no. 3, pp. 257–279, 2019.
- [28] H.-W. Cao, Y.-H. Zhang, M. Santosh et al., “Mineralogy, zircon U-Pb-Hf isotopes, and whole-rock geochemistry of late cretaceous-eocene granites from the Tengchong terrane, western Yunnan, China: record of the closure of the Neo-Tethyan Ocean,” *Geological Journal*, vol. 53, no. 4, pp. 1423–1441, 2018.
- [29] H.-W. Cao, Y.-H. Zhang, Q.-M. Pei et al., “U-Pb dating of zircon and cassiterite from the Early Cretaceous Jiaojiguan iron-tin polymetallic deposit, implications for magmatism and metallogeny of the Tengchong area, western Yunnan, China,” *International Geology Review*, vol. 59, no. 2, pp. 234–258, 2017.
- [30] Y.-H. Zhang, Y.-S. Wang, W.-S. Wang, J. Liu, L.-L. Yuan et al., “Zircon U-Pb-Hf isotopes and mineral chemistry of early cretaceous granodiorite in the lunggar iron deposit in central Lhasa, Tibet Y, China,” *Journal of Central South University*, vol. 26, no. 12, pp. 3457–3469, 2019.
- [31] Y. Fang, Y.-H. Zhang, S.-T. Zhang, H.-W. Cao, H. Zou, and J.-H. Dong, “Early Cretaceous I-type granites in the Tengchong terrane: new constraints on the late Mesozoic tectonic evolution of southwestern China,” *Geoscience Frontiers*, vol. 9, no. 2, pp. 459–470, 2018.
- [32] S. Mohadjer, T. A. Ehlers, R. Bendick, and S. G. Mutz, “Review of GPS and Quaternary fault slip rates in the Himalaya-Tibet orogen,” *Earth-Science Reviews*, vol. 174, no. 1, pp. 39–52, 2017.
- [33] Z. Liao, “Hot Springs in Southwestern China,” *Springer Hydrogeology*, pp. 79–163, Berlin, Germany, 2018.
- [34] A. M. Piper, “A graphic procedure in the geochemical interpretation of water-analyses,” *Transactions, American Geophysical Union*, vol. 25, no. 6, pp. 914–928, 1944.
- [35] D. L. Parkhurst and C. Appelo, “Description of input and examples for PHREEQC version 3: a computer program for speciation, batch-reaction, one-dimensional transport, and inverse geochemical calculations,” *US Geological Survey*, 2013.
- [36] R. O. Fournier and A. H. Truesdell, “An empirical Na-K-Ca geothermometer for natural waters,” *Geochimica et Cosmochimica Acta*, vol. 37, no. 5, pp. 1255–1275, 1973.
- [37] R. O. Fournier, “Geochemical and hydrologic considerations and the use of enthalpy-chloride diagrams in the prediction of underground conditions in hot-spring systems,” *Journal of Volcanology and Geothermal Research*, vol. 5, no. 1-2, pp. 1–16, 1979.
- [38] W. F. Giggenbach, “Geothermal solute equilibria. derivation of Na-K-Mg-Ca ge indicators,” *Geochimica et cosmochimica acta*, vol. 52, no. 12, pp. 2749–2765, 1988.
- [39] A. Truesdell and R. Fournier, “Procedure for estimating the temperature of a hot-water component in a mixed water by using a plot of dissolved silica versus enthalpy,” *Journal of Research of the U. S. Geological Survey*, vol. 5, pp. 49–52, 1977.
- [40] R. Fournier, “Chemical geothermometers and mixing models for geothermal systems,” *Geothermics*, vol. 5, no. 1-4, pp. 41–50, 1977.
- [41] S. Arnórsson, E. Gunnlaugsson, and H. Svavarsson, “The chemistry of geothermal waters in Iceland. III. Chemical geothermometry in geothermal investigations,” *Geochimica et Cosmochimica Acta*, vol. 47, no. 3, pp. 567–577, 1983.
- [42] W. F. Giggenbach and R. B. Glover, “Tectonic regime and major processes governing the chemistry of water and gas discharges from the rotorua geothermal field, New Zealand,” *Geothermics*, vol. 21, no. 1-2, pp. 121–140, 1992.
- [43] R. W. Henley, “Chemical equilibrium; hydrothermal deposits; geochemistry; water chemistry,” *Geothermal Resources*, 1984.
- [44] F. D’amore and C. Panichi, “Geochemistry in geothermal exploration,” *International Journal of Energy Research*, vol. 9, no. 3, pp. 277–298, 1985.
- [45] R. O. Fournier, “The behavior of silica in hydrothermal solutions,” in *Geology and Geochemistry of Epithermal Systems*, B. R. Berger and P. M. Bethke, Eds., Society of Economic Geologists, Littleton, CO, USA, 1985.
- [46] R. Fournier, “Geochemical indicators of subsurface temperature- part 2 estimation and fraction of hot water mixed with cold water,” *Journal of Research of the U. S. Geological Survey*, vol. 2, 1974.
- [47] Y. Liu, X. Zhou, Z. Deng et al., “Hydrochemical characteristics and genesis analysis of the Jifei hot spring in Yunnan, southwestern China,” *Geothermics*, vol. 53, pp. 38–45, 2015.
- [48] Z. H. Zhou, C. Y. Xiang, and J. M. Zhao, “Characteristics of geothermal field in West yunnan,” *Journal of Seismological Research*, vol. 18, no. 1, pp. 41–48, 1995.
- [49] J. Yu, H. Zhang, F. Yu, and D. Liu, “Oxygen and hydrogen isotopic compositions of meteoric waters in the eastern part of

Xizang,” *Chinese Journal of Geochemistry*, vol. 3, no. 2, pp. 93–101, 1984.

- [50] Y. Zhang, M. Xu, X. Li et al., “Hydrochemical characteristics and multivariate statistical analysis of natural water system: a case study in kangding county, southwestern China,” *Water*, vol. 10, no. 1, p. 80, 2018.

Research Article

Hydrogeochemistry of Fluorine in Groundwater in Humid Mountainous Areas: A Case Study at Xingguo County, Southern China

Jinhui Liu,¹ Xinfeng Wang¹ ,^{2,3} Weidong Xu,¹ Mian Song,² Lei Gong,² Mengnan Zhang,² Linbo Li,¹ and Lishan He¹

¹State Key Laboratory of Nuclear Resources and Environment, East China University of Technology, Nanchang 330013, China

²Center for Hydrogeology and Environmental Geology Survey, China Geological Survey, Baoding 071051, China

³Hebei Center for Ecological and Environmental Geology Research, Hebei GEO University, 136 Huaian Road, Shijiazhuang 050031, China

Correspondence should be addressed to Xinfeng Wang; wangxinfeng@mail.cgs.gov.cn

Received 1 March 2021; Accepted 6 July 2021; Published 15 July 2021

Academic Editor: Chengcheng Li

Copyright © 2021 Jinhui Liu et al. This is an open access article distributed under the Creative Commons Attribution License, which permits unrestricted use, distribution, and reproduction in any medium, provided the original work is properly cited.

The understanding of F^- concentration in groundwater in humid areas is limited although there are lots of research on high-fluoride groundwater in arid areas. In this paper, with controlling factors of F^- concentrations in humid areas as the focus, 130 groundwater samples, obtained from four subsystems in Northwest Xingguo County, Jiangxi Province, China, were investigated to demonstrate the controlling factors of F^- concentrations in humid areas. According to analytical results, the following hydrogeochemical characteristics of the fluorine in humid mountainous areas were determined: (1) F^- concentration is positively correlated with total dissolved solids (TDS), Ca^{2+} , HCO_3^- , and pH; (2) the groundwater features a high flow rate and low TDS; (3) the equilibrium constant of CaF_2 is less than its solubility product constant, and the fluorine-bearing minerals in rocks are in a dissolved state; and (4) the dissolved fluoride-bearing minerals constitute the main sources of F^- in the groundwater. Fluorine mainly comes from groundwater fluorine-bearing minerals in metamorphic rocks. Moreover, the low F^- concentration in the groundwater mainly results from the fast flow rate of groundwater. Fluoride in groundwater has great potential hazards in humid areas.

1. Introduction

Fluorine is an indispensable trace element in the human body. It is an essential component to maintain the normal development of human bones. However, excessive fluoride in the human body can lead to endemic fluorosis [1]. It is stipulated in Standards for Drinking Water Quality (GB 5749-2006) and Quality Standard for Groundwater (GB/T 14848-2017) that F^- concentration in drinking water should be less than 1.0 mg/L. Water with F^- concentration greater than 1.0 mg/L is defined as high-fluoride water [2].

In recent years, fluorine hydrogeochemical study indicates that dissolved fluorine in groundwater mainly originates from fluorine-bearing minerals [3–8]. Climate, topography, hydrogeological conditions, and hydrochemical

environment take the major control of the migration and enrichment of fluorine [9–15]. At the same mineralization level, the higher the hardness of water is, the higher the Ca^{2+} concentration is and the lower the F^- content is in arid areas [10]. In semiarid areas of China (e.g., North China Plain), F^- concentration in groundwater is positively correlated with Na^+ concentration and pH, while negatively correlating with Ca^{2+} contents [16–22]. Meanwhile, Ca^{2+} is the main hydrochemical factor that controls the formation of high-fluoride water in deep groundwater [11]. In shallow groundwater in the North China Plain, Ca^{2+} concentration exerts the greatest influence on the F^- content, which is significantly positively correlated with pH [23]. Fluorine is more liable to be enriched in the weakly alkaline groundwater environment (pH = 7–9) [6, 20–29]. There is a

remarkable positive correlation between Na^+ and F^- , and the enrichment of Ca^{2+} and Mg^{2+} will inhibit the enrichment of F^- [30]. With respect to groundwater chemistry, the fluoride concentration is usually high in Na-HCO_3 type groundwater and low in Ca-HCO_3 type groundwater [6, 20, 31–35]. The deficiency of calcium ion concentration in the groundwater from calcite precipitation favors fluorite dissolution leading to excess fluoride concentration. The groundwater is oversaturated with respect to calcite and undersaturated with respect to fluorite [36–41]. Evapotranspiration leads to precipitation of calcite, lowering of Ca activity, and increase in Na/Ca ratios, and this allows an increase in F⁻ levels in the arid area [39, 42–44].

In a previous study on fluorine dissolved in groundwater, most scholars focused on the source, migration, and enrichment of fluorine in arid and semiarid areas and alkaline and weak alkaline environment, and they achieved many good results. The research results of this paper have important theoretical and practical significance for people to understand the migration and enrichment characteristics of fluorine in weak acidic and acidic groundwater in humid areas. The groundwater is widely distributed and the flow rate is fast; the F^- in groundwater will migrate to any areas where the groundwater flows. Therefore, fluorine in groundwater has great potential harm in humid areas. The hydrogeochemistry of fluorine in humid mountainous areas is still important. In this paper, the hydrogeochemistry of groundwater and factors controlling the distribution of fluoride in groundwater of Northwest Xingguo County, southern China, have been evaluated. The main objectives of this paper are as follows: hydrogeochemical characteristics of fluorine in groundwater in humid areas, including the source of fluorine and its influencing factors.

2. Geology and Hydrogeology

2.1. Geographical Setting. The study area, Northwest Xingguo County, Jiangxi Province (also referred to as the area) lies in $\text{E}115^{\circ}00' - \text{E}115^{\circ}15'$ and $\text{N}26^{\circ}20' - \text{N}26^{\circ}30'$, with an area of about 460 km^2 . It features a humid subtropical monsoon climate, with an average annual temperature of 18.8°C and an average annual rainfall of 1560 mm. The surface water is composed of Suishui River, Jianshui River, Shuicha River, and Wushu River. In the low-middle mountains, it mainly develops metamorphic rocks and granite. Hilly terrain of granite is distributed in the southeastern. It is a low mountainous area in general with an altitude less than 1000 m. The terrain is steep, V-shaped valleys are commonly developed, and the elevation of the highest peak is 1176 m in the area.

2.2. Geology. The area is mainly comprised of strata of Sinian, Cambrian, Devonian, Carboniferous, and Quaternary with an outcrop area of 402 km^2 , accounting for 87.3% of the total survey area. The strata of Sinian and Cambrian are well developed and fully exposed. Magmatic rocks, mainly including plutonic intrusion and vein rocks, are

generally distributed in the southeastern part of the area. Granite is common in the area, with an outcrop area of 58.67 km^2 . The vein rocks are mainly composed of quartz veins, granite veins, lamprophyre veins, and diabase veins (Figure 1).

2.3. Hydrogeology

2.3.1. Characteristics of Water-Bearing Formations. According to the geological and hydrogeological characteristics, the water-bearing formations in the area can be divided into three types: (1) porous water-bearing formation of loose rocks, (2) porous-fissured water-bearing formation of clastic rocks, and (3) fissured water-bearing formation of magmatic rocks and metamorphic rocks. The distribution areas of these three types are 20.78 km^2 , 86.56 km^2 , and 352.66 km^2 , accounting for 4.52%, 18.82%, and 76.66% of the total area, respectively.

The porous water-bearing formations of loose rocks are mainly distributed along river banks, and the lithology of the aquifer is mainly characterized by sand, gravel, and pebble. The burial depth of the water table is 0.5–2.5 m, the TDS of groundwater samples is 0.029–0.145 g/L, and the hydrochemical type is $\text{HCO}_3^- \text{Ca}$.

The porous-fissured water-bearing formations of clastic rocks are distributed in the northeast, northwest, and southwest of the area, with a spring flow of 0.014–9.328 L/s and a single well water yield greater than $100 \text{ m}^3/\text{d}$. Hydrochemical types are mainly $\text{HCO}_3^- \text{Ca}$ or $\text{HCO}_3^- \text{Ca-Mg}$, and TDS is 0.090–0.284 g/L for this type.

As for the granite bearing weathering-fissure water, the single well water yield is $4.73 - 12.66 \text{ m}^3/\text{d}$ and the hydrochemical type is $\text{HCO}_3^- \text{Na}$. However, regarding the fissured water-bearing formations of metamorphic rocks of Cambrian and Sinian, single well water yields are $0.92 - 60.93 \text{ m}^3/\text{d}$ and $2.65 - 3.82 \text{ m}^3/\text{d}$ and share a common hydrochemical type of $\text{HCO}_3^- \text{Ca}$.

2.3.2. Groundwater System. The area is located in the upper reaches of the Ganjiang River, the third-scale (III) groundwater subsystem in the Yangtze River basin. There are fourth-scale groundwater subsystems in the area, precisely including Pingjiang River (III_{2-1}), Liangkou River (III_{3-1}), Yuntingshui River (III_{4-1}), and Wushu River (III_{5-1}). According to the Groundwater System Division Guideline (GWI-A5) issued by the China Geological Survey, the area is divided into four fifth-scale groundwater subsystems (Table 1).

2.3.3. Recharge, Runoff, and Discharge. According to the distribution characteristics of the topography, geomorphology, and surface water in the area, the groundwater is replenished through atmospheric precipitation. The groundwater flows from west to east in the Suishui groundwater system and from north to south in the Jianshui River and Wushu river groundwater systems. The groundwater discharges into rivers, springs, and wells.

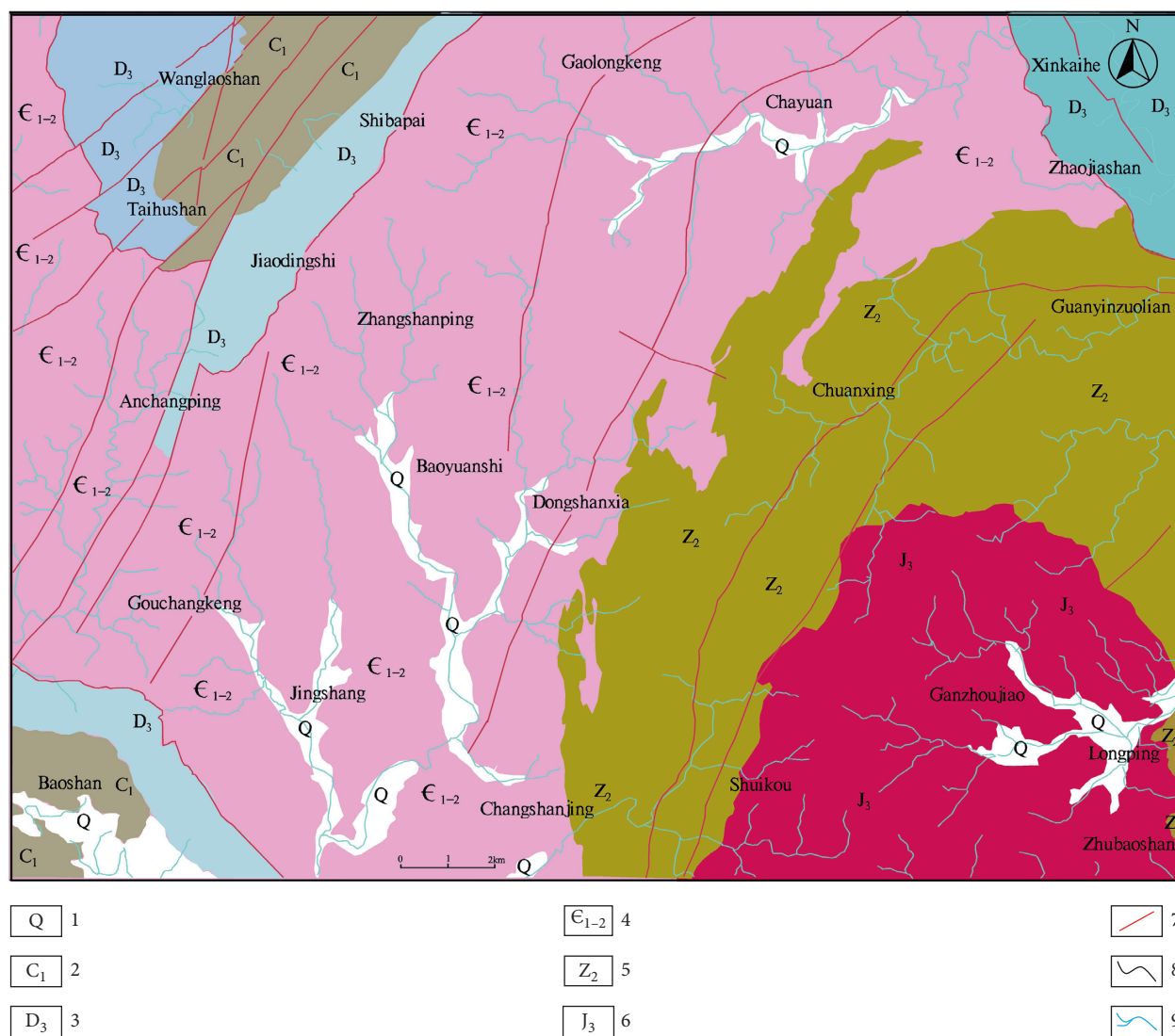


FIGURE 1: Geological map of Northwest Xingguo County. 1: quaternary; 2: early carboniferous; 3: late Devonian; 4: early and middle-late Cambrian; 5: middle Sinian; 6: granite in late Jurassic; 7: fault; 8: stratigraphic boundary; 9: river.

TABLE 1: Groundwater system division in Northwest Xingguo County.

Name and code of third-scale subsystem	Name and code of fourth-scale subsystem	Name and code of fifth-scale subsystem	Area (km ²)
Upper reaches of Ganjiang III ₁			
Gongshui III ₂	Pingjiang River III ₂₋₁	Suishui River III ₂₋₁₋₂	213
Gan III ₃	Liangkou River III ₃₋₁	Jianshui River III ₃₋₁₋₁	152
Gan III ₄	Yuntingshui River III ₄₋₁	Shuicha River III ₄₋₁₋₁	33
Gan III ₅	Wushu River III ₅₋₁	Wushu River III ₅₋₁₋₁	62

3. Methods and Materials

A total of 130 groundwater samples were collected from the outcrops of the four groundwater subsystems: Suishui River III₂₋₁₋₂, Jianshui River III₃₋₁₋₁, Shuicha River III₄₋₁₋₁, and Wushu River III₅₋₁₋₁, from June 23 to August 23, 2017 (Figure 2). Major hydrochemical parameters (e.g., F⁻, Ca²⁺, HCO₃⁻, pH, and TDS) in these water samples were analyzed in the field. Hash DR2800 spectrophotometer was employed for F⁻ testing, reagent titration method was adopted for Ca²⁺

and HCO₃⁻ testing, and acidimeter and test pen were used for pH and TDS testing, respectively. The results are shown in Table 2.

4. Results and Discussion

4.1. *Hydrogeochemistry of Groundwater.* The chemical composition of 15 representative groundwater outcrops (springs, wells) was tested in order to further determine the hydrogeochemical characteristics of groundwater in the

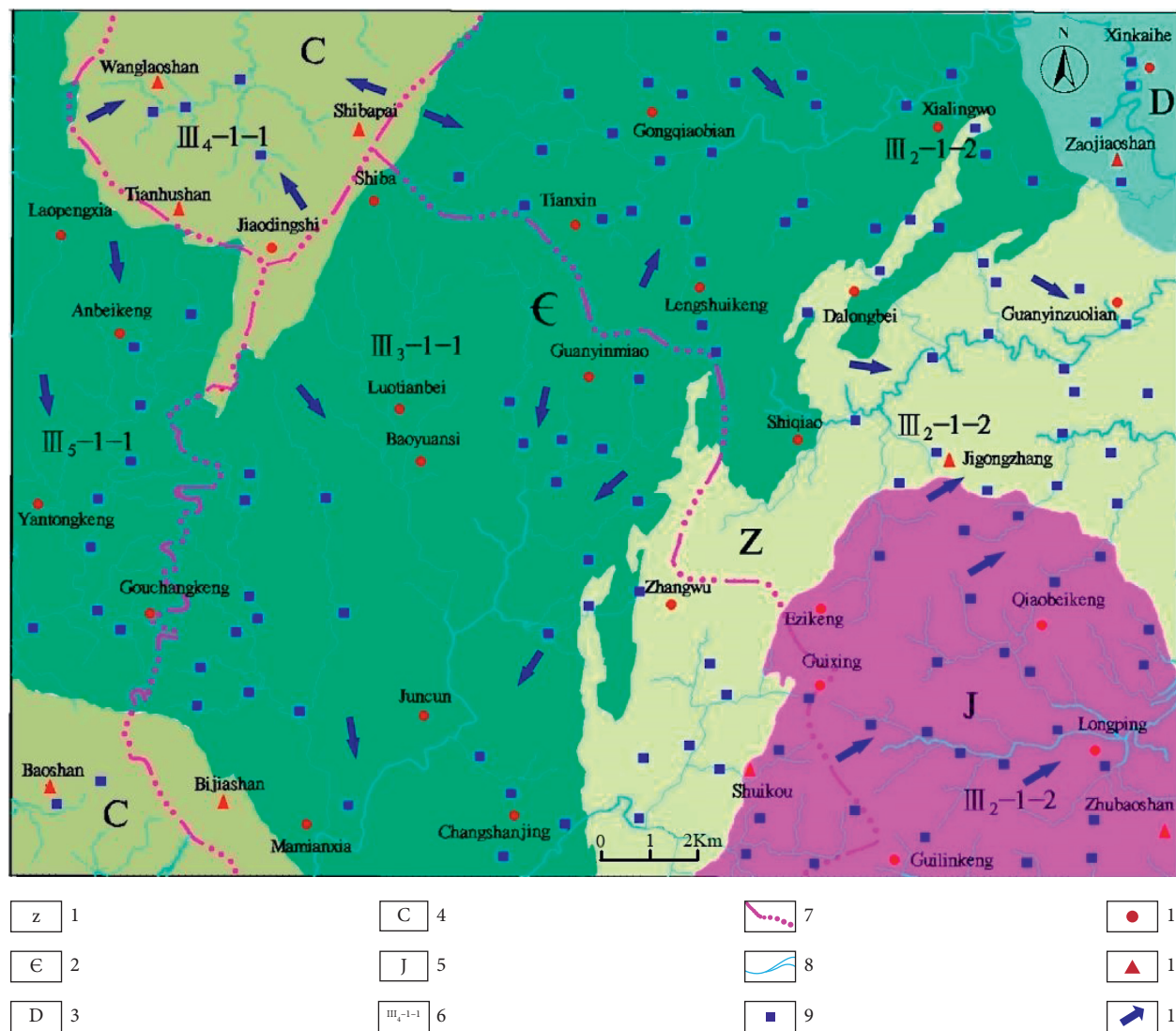


FIGURE 2: Sampling locations of groundwater in Northwest Xingguo County. 1: Sinian fissured water-bearing formation of metamorphic rock; 2: Cambrian fissured water-bearing formation of metamorphic rock; 3: Devonian porous-fissured water-bearing formation of clastic rock; 4: carboniferous porous-fissured water-bearing formation of clastic rock; 5: Jurassic fissured water-bearing formation of granite; 6: code of groundwater system; 7: boundary of fifth-scale groundwater subsystem; 8: surface water system; 9: sampling location; 10: village; 11: peak; and 12: groundwater flow direction.

TABLE 2: Summary of Ca^{2+} , HCO_3^- , pH, TDS, and F^- in groundwater of different groundwater subsystems.

Groundwater subsystem	Number of samples	Ca^{2+} (mg/L)		HCO_3^- (mg/L)		pH		TDS (mg/L)		F^- (mg/L)	
		Range	Average	Range	Average	Range	Average	Range	Average	Range	Average
Suishui River III ₂₋₁₋₂	79	1-32	9.2	3.05-73.22	24.6	5.19-8.48	6.3	5-125	41.7	0.02-1.32	0.19
Jianshui River III ₃₋₁₋₁	36	3-46	15.4	6.10-67.12	26.1	5.60-7.32	6.5	15-155	59.5	0.02-0.51	0.15
Shuicha River III ₄₋₁₋₁	4	1-5	2.5	6.10-12.20	8.4	5.37-6.83	6.2	8-19	14.3	0.02-0.09	0.06
Wushu River III ₅₋₁₋₁	11	2-54	15.2	6.10-140.35	34.4	5.85-7.42	6.7	16-194	64.7	0.01-0.28	0.08

study area. The groundwater chemical components were tested in various groundwater systems in this survey, and the test results show that the main ion components in

groundwater under natural conditions are Ca^{2+} , Na^+ , and HCO_3^- . The chemical type of groundwater is mainly HCO_3^- Ca-Na, and the second is HCO_3^- Ca-Mg (Table 3). According

to the Piper triple-variation diagram, all groundwater in the study area is located in the bicarbonate type water area and is mainly located in the Ca type water area with low TDS hydrogeochemical characteristics (Figure 3).

4.2. Factors Affecting the Distribution of Fluoride in Groundwater

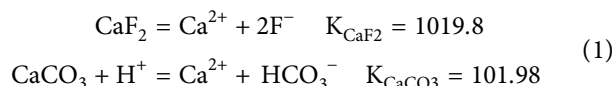
4.2.1. pH Condition. The fluoride contents are in positive correlation with pH [18, 19, 26, 45]. Previous studies show that pH value varies from 7.3 to 9.0 in high-fluoride water [46, 47]. Fluorine-bearing minerals in carbonate areas of weakly alkali environments are more liable to dissolve, resulting in high fluorine concentration in water [48]. The pH in groundwater is generally 6.3–6.7. The F^- concentration is positively correlated with pH in the groundwater of the three subsystems (Suishui River III₂₋₁₋₂, Jianshui River III₅₋₁₋₁, and Wushu River III₅₋₁₋₁) (Figure 4). It is not conducive to the dissolution of fluorine-bearing minerals owing to its low pH, and thus the F^- concentration in it is low.

4.2.2. The Impact of TDS. High fluoride groundwater generally has high TDS and high HCO_3^- in the weak alkaline environment [29]. The relationship between F^- and TDS in the groundwater samples collected from different groundwater subsystems in the studied area is shown in Figure 5. It is indicated that the F^- concentration is positively correlated with TDS in each groundwater subsystem. The reason is that ions in groundwater cannot be saturated owing to the fast water cycle rate in bedrock mountainous areas.

4.2.3. F^- and Ca^{2+} Balance. The relationship between F^- and Ca^{2+} in the groundwater is shown in Figure 6. It is indicated that F^- concentrations are positively correlated with Ca^{2+} concentrations in the groundwater subsystems of Suishui River III₂₋₁₋₂, Jianshui River III₅₋₁₋₁, and Wushu River III₅₋₁₋₁. The groundwater features the temperature of 16–25°C, low TDS (14.3–64.7 mg/L), and low Ca^{2+} concentration (2.5–15.4 mg/L). Therefore, the Ca^{2+} and F^- concentrations can be considered as their activity values.

The equilibrium constant of CaF_2 ($K = [Ca^{2+}][F^-]^2$) in the samples was calculated and compared to its solubility product constant (K_{sp}) (Table 4). The result indicates that, under natural conditions, the solubility product constants are higher than the equilibrium constants, whereas the saturation indexes (SI) of CaF_2 are negative. This further confirms that the fluorine-bearing minerals in rocks are in a dissolving state and the increase of Ca^{2+} will not lead to the precipitation of CaF_2 . However, the F^- concentration tends to be negatively correlated with Ca^{2+} concentration in arid areas [2, 12, 14]. This is because Ca^{2+} and F^- are saturated in high-fluorine groundwater in arid areas and, therefore, the increase of Ca^{2+} concentration will lead to CaF_2 precipitation and the decrease of F^- concentration accordingly.

4.2.4. The Dissolution of Minerals. As mentioned above, high F^- groundwater mostly locates in Na- HCO_3 type. F^- concentrations in the groundwater are also positively correlated with HCO_3^- concentrations (Figure 7), indicating HCO_3^- concentration is another important factor affecting F^- concentration in the study area. The anions in the groundwater are mainly HCO_3^- (8.4–34.4 mg/L), and CaF_2 is in a dissolved state as mentioned above. The dissolution-precipitation equilibrium relationship between CaF_2 and $CaCO_3$ is expressed as follows:



The number of F^- and HCO_3^- increases with the dissolution of $CaCO_3$ and CaF_2 in the groundwater subsystems. In other words, the dissolution will lead to a positive correlation between F^- and HCO_3^- . This is another hydrochemical characteristic of F^- in bedrock mountainous areas in a humid climate.

4.2.5. The Dissolution of Biotite. Fluorine concentration in granite ranges from 0.044% to 0.216%. The biotite $[K(Mg, Fe^{2+})_3(Al, Fe^{3+})Si_3O_{10}(OH, F)_2]$, which accounts for 15%–30% in metamorphic rocks, constitutes the main fluorine-bearing minerals. Firstly, the fluorine-bearing minerals in these rocks dissolve and thus F^- is released into the groundwater. Secondly, a faster flow rate of groundwater occurs in the area since it is located in the low–middle mountainous area. This probably leads to low F^- concentration in the groundwater. Thirdly, the groundwater in the area shows weakly acidic characteristics, which may promote the dissolution of fluorine-bearing minerals. According to the results obtained from the hydrogeological survey in the area, it can be concluded that fluorine in the groundwater mainly comes from the interaction between the groundwater and the fluorine-bearing minerals in metamorphic rocks.

4.2.6. Gibbs Diagram. Gibbs diagram built a simple and effective diagram that can be used to compare $TDS \sim (Na^+ / (Na^+ + Ca^{2+}))$ or $TDS \sim (Cl^- / (Cl^- + HCO_3^-))$; this can be used to identify the influencing factors of the groundwater hydrochemistry. For example, the chemical composition is primarily affected by rock weathering, evaporation, and crystallization of soluble salts [50, 51].

According to the chemical composition data of groundwater, the Gibbs diagram of the study area is shown in Figure 8. The TDS of groundwater in the study area is located in 47.7–172.3 mg/L, and the ratio of $Na / (Na + Ca)$ and $Cl / (Cl + HCO_3)$ is between 0.056–0.554 and 0.010–0.114, respectively. It shows that the groundwater is characterized by high Na^+ and Ca^{2+} and suggests a geochemical source of granite and metamorphic rocks. Therefore, it can be considered that fluorine in groundwater comes from the dissolution of fluorine-containing minerals in these rocks. The Gibbs analysis of groundwater also indicates that the formation of groundwater chemical

TABLE 3: Chemical composition of various groundwater systems in the study area.

Groundwater system	Sample number	Water chemical composition (mg/L)										Chemical type of groundwater
		K ⁺	Na ⁺	Ca ²⁺	Mg ²⁺	HCO ₃ ⁻	CO ₃ ²⁻	SO ₄ ²⁻	Cl ⁻	NO ₃ ⁻	TDS	
Suishui River (III ₂₋₁₋₂)	SJ051	3.10	8.84	7.13	0.30	43.01	0.00	2.23	3.54	20.55	88.7	HCO ₃ ⁻ Na·Ca
	SJ014	1.21	4.49	5.01	0.11	37.63	0.00	2.06	0.57	0.12	51.2	HCO ₃ ⁻ Ca·Na
	GJ002	1.09	6.99	10.34	0.38	53.76	0.00	3.98	1.74	0.17	78.5	HCO ₃ ⁻ Ca·Na
	SJ070	0.56	2.48	4.06	1.30	37.63	0.00	2.60	0.61	0.90	50.1	HCO ₃ ⁻ Ca·Na
	GJ003	0.78	2.48	15.42	2.61	69.89	0.00	3.69	1.12	0.10	96.1	HCO ₃ ⁻ Ca
	SJ104	0.77	2.03	6.58	2.08	37.63	0.00	2.50	1.03	0.11	52.7	HCO ₃ ⁻ Ca·Mg·Na
	SJ058	1.27	1.37	5.03	0.45	26.88	0.00	1.80	3.47	7.45	47.7	HCO ₃ ⁻ Ca·Na
	SJ036	6.43	3.77	21.01	3.54	83.33	2.64	6.62	1.80	1.52	130.7	HCO ₃ ⁻ Ca·Na
	SJ154	1.69	3.54	7.35	2.66	48.38	5.29	3.77	1.11	0.11	73.9	HCO ₃ ⁻ Ca·Na·Mg
Jianshui River (III ₃₋₁₋₁)	GJ001	0.89	3.92	8.26	2.93	59.13	0.00	5.43	0.61	1.12	82.3	HCO ₃ ⁻ Ca·Mg
	SJ113	7.64	4.59	18.45	4.96	86.01	0.00	8.23	8.19	7.91	146.0	HCO ₃ ⁻ Ca·Na
	SJ184	1.38	11.52	18.32	4.07	94.08	2.64	7.24	1.35	0.10	140.7	HCO ₃ ⁻ Ca·Na
	SQ049	0.56	2.40	5.04	2.01	43.01	0.00	1.61	0.55	0.10	55.3	HCO ₃ ⁻ Ca·Mg
	SJ029	10.80	5.17	23.86	3.26	102.14	0.00	8.65	4.71	13.68	172.3	HCO ₃ ⁻ Ca·Na
Wushu River (III ₅₋₁₋₁)	SQ052	0.91	0.77	12.97	2.11	56.45	2.64	7.88	0.91	1.32	86	HCO ₃ ⁻ Ca

Note: the data in the table is tested by the Nanchang Supervision Center of Mineral Resources, Ministry of Land and Resources, 2017.

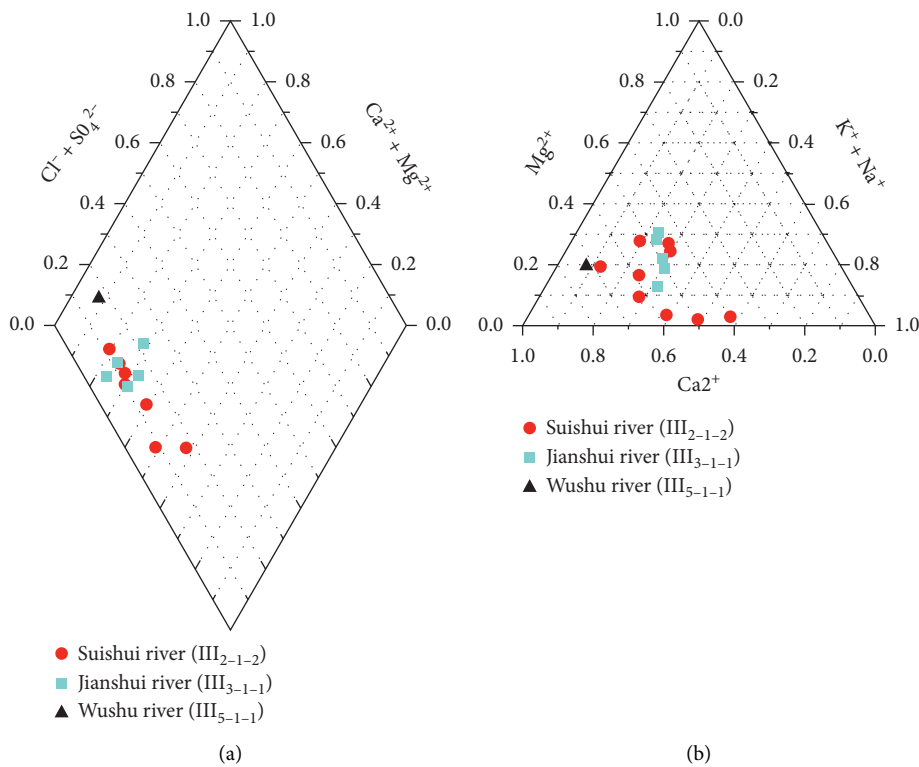


FIGURE 3: Continued.

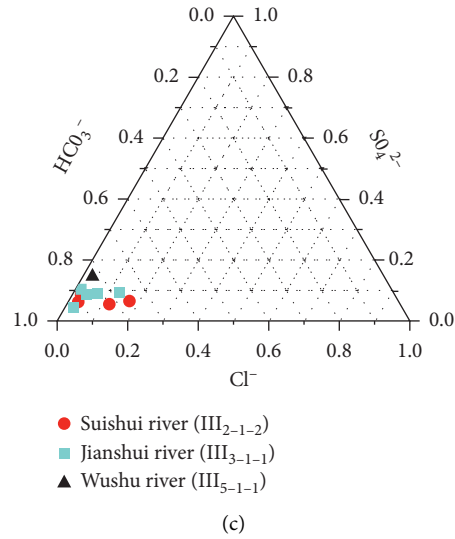


FIGURE 3: The water chemical pipe triple-variation figure of Northwest Xingguo County.

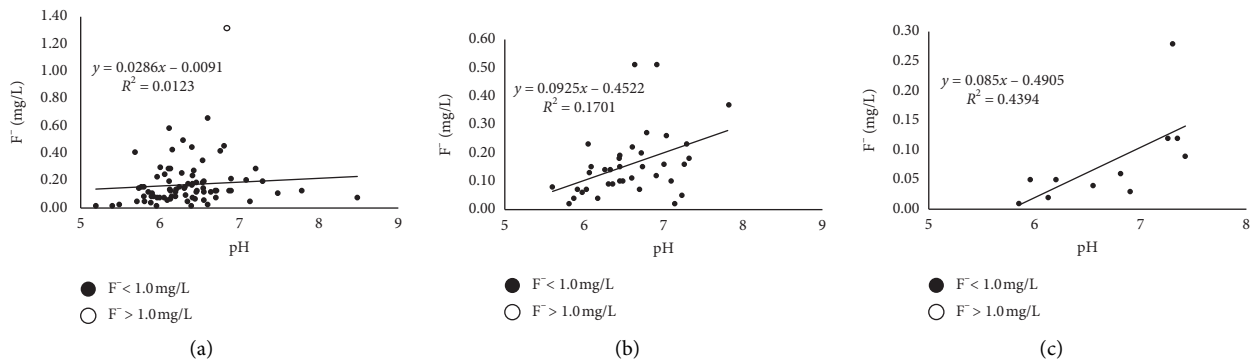


FIGURE 4: Relationship between F^- and pH in the groundwater of different subsystems. (a) Groundwater subsystem of Suishui River. (b) Groundwater subsystem of Jianshui River. (c) Groundwater subsystem of Wushu River.

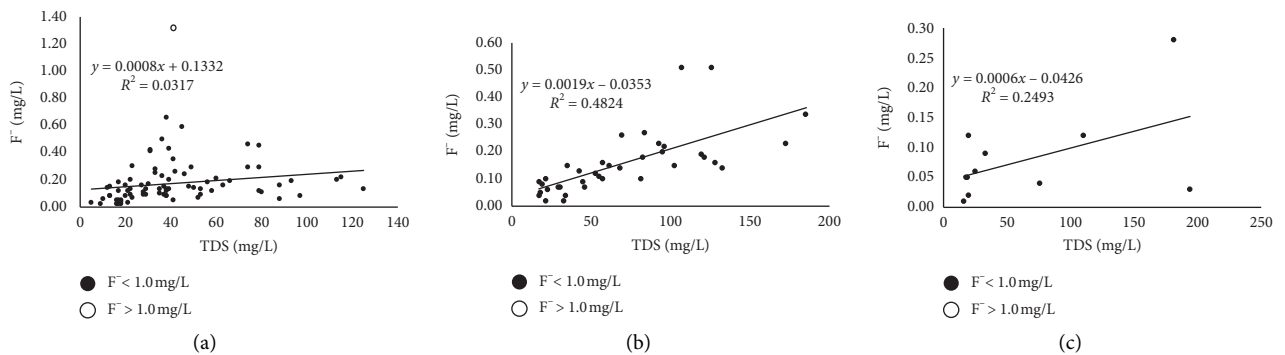


FIGURE 5: Relationship between F^- and TDS in groundwater of different subsystems. (a) Groundwater subsystem of Suishui River. (b) Groundwater subsystem of Jianshui River. (c) Groundwater subsystem of Wushu River.

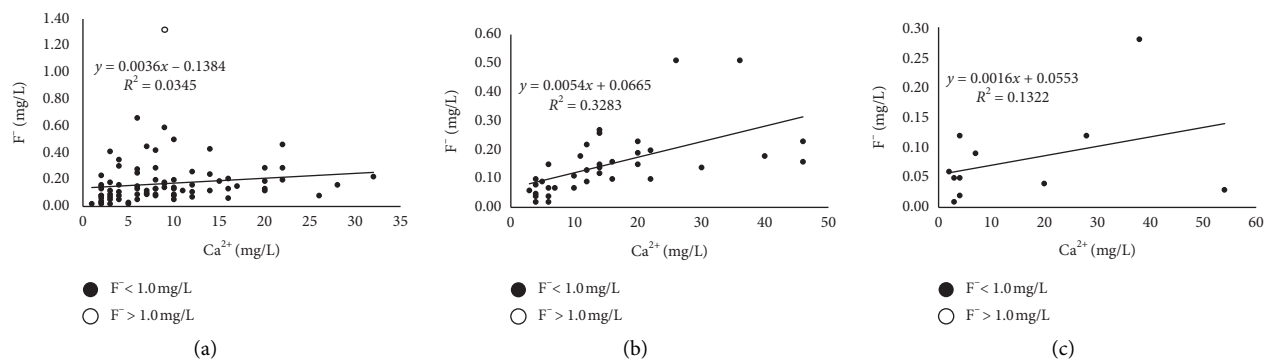


FIGURE 6: Relationship between F^- and Ca^{2+} in groundwater of different subsystems. (a) Groundwater subsystem of Suishui River. (b) Groundwater subsystem of Jianshui River. (c) Groundwater subsystem of Wushu River.

TABLE 4: Equilibrium constant (K), solubility product constant (K_{sp}), and SI of CaF_2 in groundwater.

Sample no.	F^- (mg/L)	Ca^{2+} (mg/L)	K	K_{SP} ($t = 18^\circ C$)	K_{SP} ($t = 25^\circ C$)	SI ($t = 18^\circ C$)
SJ157	0.09	2	1.122×10^{-15}			-4.482
SQ066	0.02	5	1.385×10^{-16}			-5.390
SJ148	0.62	24	6.389×10^{-13}			-1.726
SJ156	0.03	54	3.366×10^{-15}	3.40×10^{-11}	3.95×10^{-11}	-4.004
SJ097	0.76	20	8.000×10^{-13}			-1.628
SJ138	0.2	60	1.662×10^{-13}			-2.311
SJ103	1.18	89	8.582×10^{-12}			-0.598
SJ184	0.32	130	9.219×10^{-13}			-1.567

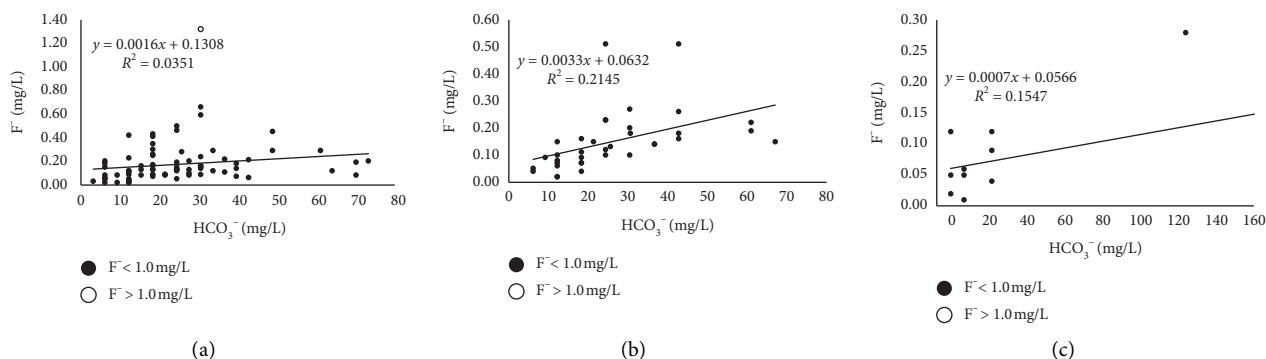


FIGURE 7: Relationship between F^- and HCO_3^- in groundwater of different subsystems. (a) Groundwater subsystem of Suishui River. (b) Groundwater subsystem of Jianshui River. (c) Groundwater subsystem of Wushu River.

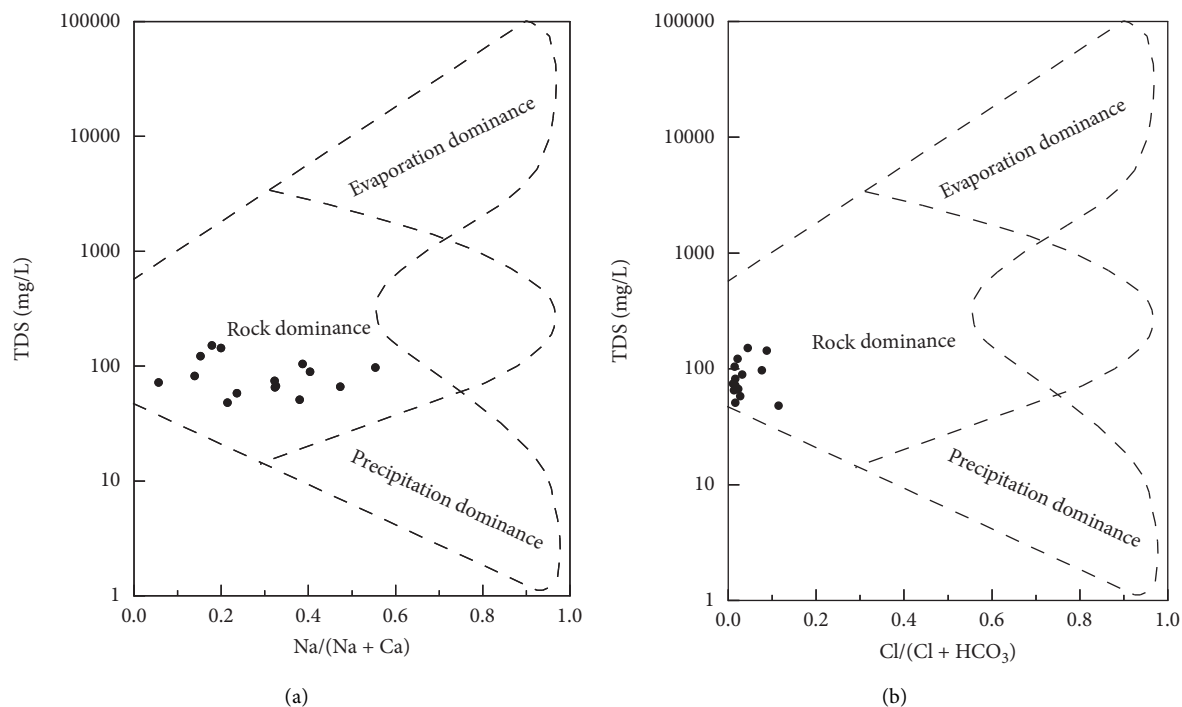


FIGURE 8: Gibbs diagram for groundwater samples.

components in Xingguo County is dominated by rock weathering reactions; that is, water-rock interaction plays an important role in the migration and enrichment of fluoride in groundwater.

5. Conclusion

In this paper, the migration, enrichment characteristics, and influencing factors of fluorine in weak acidic and acidic groundwater in humid mountainous areas are described. The F^- concentration is positively correlated with the contents of TDS, Ca^{2+} , and HCO_3^- and pH value in the groundwater subsystems in the area owing to the intensive exchange of groundwater with aquifer minerals. In the study area, TDS of groundwater is low and the fluorine-bearing minerals (mainly CaF_2) in the rocks are in a dissolved state, with solubility product constant less than its equilibrium constant. Fluoride mainly originates from the interaction between the groundwater and fluorine-bearing minerals. Moreover, the F^- concentration is low in the area due to the fast flow rate of groundwater. Fluoride in groundwater has great potential hazards in humid areas. This study has important theoretical and practical significance for understanding the hydrogeochemical characteristics of fluorine in humid areas.

Data Availability

The data have been published in the Geological Cloud.

Conflicts of Interest

The authors declare that they have no conflicts of interest.

Acknowledgments

The study involved in this paper was supported by the project of China Geological Survey titled Environmental Geological Survey on a Scale of 1:50,000 along Xianning–Yueyang and Nanchang–Huaihua Highways in Middle Reaches of the Yangtze River (DD20179262).

References

- [1] H. X. Xing, L. Li, W. Y. Ge et al., "Spatial distribution characteristics and genesis of fluorine in Huaibei groundwater in Anhui Province," *Geochemistry*, vol. 126, no. 2, pp. 163–168, 2014.
- [2] S. J. Li, X. J. Wang, J. Zhou, X. M. Tang, and Z. P. Wang, "Study on the distribution regularity of high fluorine groundwater in the fourth system of Beijing area," *Modern Geology*, vol. 135, no. 2, pp. 407–414, 2012.
- [3] T. Lu, X. B. Gao, X. B. Zhang, and C. C. Li, "Distribution and assessment of hydrogeochemical processes of rich groundwater using PCA model: a case study in the Yuncheng Basin, China," *Acta Geochimica*, vol. 39, no. 2, pp. 216–225, 2020.
- [4] D. Li, X. Gao, Y. Wang, and W. Luo, "Diverse mechanisms drive fluoride enrichment in groundwater in two neighboring sites in northern China," *Environmental Pollution*, vol. 237, pp. 430–441, 2018.
- [5] M. P. C. Marimon, A. Roisenberg, A. V. Suhogusoff, and A. P. Viero, "Hydrogeochemistry and statistical analysis applied to understand fluoride provenance in the Guarani Aquifer System, Southern Brazil," *Environmental Geochemistry and Health*, vol. 35, no. 3, pp. 391–403, 2013.
- [6] L. G. Liang, M. Z. Zhu, S. M. Zhu, L. P. Zhang, and X. J. Xie, "Spatial distribution and enrichment of fluoride in geothermal water from eastern Guangxi, China," *Safety and Environmental Engineering*, vol. 22, no. 1, pp. 1–6, 2015.

- [7] X. Gao, W. Luo, X. Luo, C. Li, X. Zhang, and Y. Wang, "Indigenous microbes induced fluoride release from aquifer sediments," *Environmental Pollution*, vol. 252, pp. 580–590, 2019.
- [8] X. Q. Li, L. R. Zhu, X. W. Hou, and L. Zhang, "Distribution and evolutionary mechanism of shallow high fluoride groundwater in taiyuan basin," *Acta Geoscientica Sinica*, vol. 28, no. 1, pp. 55–61, 2007.
- [9] F. J. Luan, J. L. Zhou, Y. Y. Zeng, Y. X. Gao, and J. T. Liu, "Distribution characteristics and enrichment factors of fluorine in groundwater in typical areas of southern Xinjiang," *Environmental Chemistry*, vol. 35, no. 6, pp. 1203–1211, 2016.
- [10] J. Y. Guo, "Characteristics of groundwater environment and control of drinking water safety risk in high fluoride area in the desert basin of kelantan," Doctoral dissertation, Changan University, Xi'an, China, 2014.
- [11] B. Zhang, "Distribution regularity and genesis of high fluorine groundwater in the northwest plain of Shandong," Master's thesis, China University of Geosciences (Beijing), Beijing, China, 2014.
- [12] L. R. Xu, Z. H. Xu, and J. Chang, "Analysis of the distribution characteristics of fluorine and its influencing factors in the groundwater of Pingdu," *China Rural Water Conservancy and Hydropower*, vol. 35, no. 7, pp. 42–44, 2012.
- [13] G. Xu, J. Liu, Q. S. Zhu, W. N. Wang, and X. W. He, "Distribution characteristics and influencing factors of fluorine in shallow groundwater in Huaibei plain, Anhui Province," *Journal of Water Resources and Water Engineering*, vol. 20, no. 5, pp. 9–13, 2009.
- [14] H. Shen, "Study on the source and enrichment regularity of fluorine in groundwater in Yanchi district," Master's thesis, Chinese Academy of Geosciences, Beijing, China, 2005.
- [15] J. T. Wan, Q. C. Hao, G. R. Gong, C. Su, Y. L. Cui, and Q. Liu, "Distribution and genesis of high-fluorine groundwater in southwestern Shandong Province," *Geoscience*, vol. 27, no. 2, pp. 448–453, 2013.
- [16] A. Rashid, A. Farooqi, X. B. Gao, S. Zahir, S. Noor, and J. A. Khattak, "Geochemical modeling, source apportionment, health risk exposure and control of higher fluoride in groundwater of sub-district Dargai, Pakistan," *Chemosphere*, vol. 243, pp. 1–11, 2020.
- [17] C. Li, X. Gao, and Y. Wang, "Hydrogeochemistry of high-fluoride groundwater at Yuncheng Basin, northern China," *Science of the Total Environment*, vol. 508, pp. 155–165, 2015.
- [18] M. S. Abu Jabal, I. Abustan, M. R. Rozaimy, and H. Al-Najar, "Fluoride enrichment in groundwater of semi-arid urban area: khan Younis City, southern Gaza Strip (Palestine)," *Journal of African Earth Sciences*, vol. 100, no. 3, pp. 259–266, 2014.
- [19] H. Guo, Y. Zhang, L. Xing, and Y. Jia, "Spatial variation in arsenic and fluoride concentrations of shallow groundwater from the town of Shahai in the Hetao basin, Inner Mongolia," *Applied Geochemistry*, vol. 27, no. 11, pp. 2187–2196, 2012.
- [20] H. Ou, G. P. Lu, X. N. Hu et al., "Fluoride enrichment in geothermal waters in Xinyi-Lianjiang region, Guangdong," *Environmental Chemistry*, vol. 38, no. 5, pp. 1128–1138, 2019.
- [21] R. Y. Mao, H. M. Guo, Y. F. Jia et al., "Distribution characteristics and genesis of fluoride groundwater in the Hetao basin, Inner Mongolia," *Earth Science Frontiers*, vol. 23, no. 2, pp. 260–268, 2016.
- [22] C. Y. Yi, "Study on the migration and transformation of fluorine in the water-soil system of the typical region of North China Plain," Master's thesis, China University of Geology, Wuhan, China, 2013.
- [23] R. P. Liu, H. Zhu, M. Z. Kang et al., "Hydrogeochemistry of the fluoride in groundwater in the dali area of the guanzhong basin," *Hydrogeology and Engineering Geology*, vol. 36, no. 5, pp. 84–88, 2009.
- [24] L. N. Xing, H. M. Guo, L. Wei et al., "Evolution feature and genesis of fluoride groundwater in shallow aquifer from north China plain," *Journal of Earth Sciences and Environment*, vol. 34, no. 4, pp. 57–67, 2012.
- [25] Q. Y. Hao, X. T. Xu, X. B. Zhang, and L. Zhou, "Hydrochemical characteristics and genesis of high-fluorine shallow groundwater in yanggu area of the northwestern shandong, China," *Journal of Earth Sciences and Environment*, vol. 42, no. 5, pp. 668–677, 2020.
- [26] D. L. Lei, X. G. Fu, H. F. Geng, and X. L. Dong, "Distribution rules of high fluoride water and its environmental impacts in Cangzhou City," *Water Resources Protection*, vol. 23, no. 2, pp. 43–46, 2007.
- [27] N. Yang, J. F. Liu, A. M. Liao et al., "Distribution and formation factors of high fluoride deep groundwater in typical area of north Anhui Province," *Hydrogeology and Engineering Geology*, vol. 44, no. 3, pp. 33–41, 2017.
- [28] R. Zuo, P. Gu, Y. G. Teng, Q. Wang, J. S. Wang, and B. Wang, "Spatial distribution and genesis of the high-fluorine groundwater in the lower liaohe river plain," *Hydrogeology and Engineering Geology*, vol. 42, no. 3, pp. 135–141, 2015.
- [29] J. Zhang, J. L. Zhou, W. H. Nai, and Y. Y. Zeng, "Characteristics of high fluoride groundwater in plain of Yarkant river basin in Xinjiang," *Journal of Arid Land Resources and Environment*, vol. 34, no. 4, pp. 100–106, 2020.
- [30] L. H. Wu, "Chemical characteristics and genesis of high fluorine groundwater in Hengshui area," Master's thesis, China University of Geology (Beijing), Beijing, China, 2015.
- [31] G.-T. Chae, S.-T. Yun, B. Mayer et al., "Fluorine geochemistry in bedrock groundwater of South Korea," *Science of The Total Environment*, vol. 385, no. 1, pp. 272–283, 2007.
- [32] D. Mondal and S. Gupta, "Fluoride hydrogeochemistry in alluvial aquifer: an implication to chemical weathering and ion-exchange phenomena," *Environmental Earth Sciences*, vol. 73, no. 7, pp. 3537–3554, 2015.
- [33] C. Calvi, D. Martinez, C. Dapeña, and F. Gutheim, "Abundance and distribution of fluoride concentrations in groundwater: la ballenera catchment, southeast of Buenos Aires Province, Argentina," *Environmental Earth Sciences*, vol. 75, no. 6, p. 534, 2016.
- [34] X. He, T. Ma, Y. Wang, H. Shan, and Y. Deng, "Hydrogeochemistry of high fluoride groundwater in shallow aquifers, Hangjinhouqi, Hetao Plain," *Journal of Geochemical Exploration*, vol. 135, pp. 63–70, 2013.
- [35] O. Sracek, H. Wanke, N. N. Ndakunda, M. Mihaljevič, and F. Buzek, "Geochemistry and fluoride levels of geothermal springs in Namibia," *Journal of Geochemical Exploration*, vol. 148, no. 1, pp. 96–104, 2015.
- [36] P. Mamatha and S. M. Rao, "Geochemistry of fluoride rich groundwater in kolar and tumkur districts of Karnataka," *Environmental Earth Sciences*, vol. 61, no. 1, pp. 131–142, 2010.
- [37] J. Li, H. Zhou, K. Qian et al., "Fluoride and iodine enrichment in groundwater of North China Plain: evidences from speciation analysis and geochemical modeling," *Science of The Total Environment*, vol. 598, no. 2, pp. 239–248, 2017.
- [38] D. Mondal, G. Dutta, and S. Gupta, "Inferring the fluoride hydrogeochemistry and effect of consuming fluoride-contaminated drinking water on human health in some endemic areas of Birbhum district, West Bengal," *Environmental Geochemistry and Health*, vol. 38, no. 2, pp. 557–576, 2016.

- [39] G. Jacks, P. Bhattacharya, V. Chaudhary, and K. P. Singh, "Controls on the genesis of some high-fluoride groundwaters in India," *Applied Geochemistry*, vol. 20, no. 2, pp. 221–228, 2005.
- [40] C. Liang, Y. Wu, and S. J. Li, "Distribution and geochemical processes for the formation of high fluoride groundwater in datong basin," *Geological Science and Technology Information*, vol. 33, no. 2, pp. 154–159, 2014.
- [41] C. Wu, X. Wu, Y. S. Zhang, Y. Y. Dong, and P. C. Zhu, "Distribution characteristics and genesis of high fluoride groundwater in the niuxin mountain, Qinhuangdao," *Earth Science Frontiers*, vol. 25, no. 4, pp. 307–315, 2018.
- [42] D. V. Reddy, P. Nagabhushanam, B. S. Sukhija, A. G. S. Reddy, and P. L. Smedley, "Fluoride dynamics in the granitic aquifer of the wailapally watershed, Nalgonda district, India," *Chemical Geology: Isotope Geoscience Section*, vol. 269, no. 3, pp. 278–289, 2010.
- [43] L. L. Shao, S. K. Yang, W. K. Wang, and X. F. Feng, "Distribution regularity of fluorine in shallow groundwater in unsaturated soils of kuitun river basin, Xinjiang," *Journal of Earth Sciences and Environment*, vol. 28, no. 4, pp. 64–68, 2006.
- [44] Z. T. Han, F. W. Zhang, J. Y. Gui, H. Shen, L. Chen, and X. L. Lv, "Research on the genesis of high-fluoride groundwater in Yanchi area and direction for low-fluoride groundwater prospect," *Journal of Arid Land Resources and Environment*, vol. 23, no. 12, pp. 151–156, 2009.
- [45] W. Zhang, X. D. Fu, and F. R. Zhang, "The relationship between the high fluorine content of groundwater and the pH value, water temperature and the ratio of $(Na^+ + K^+)/Ca$: a case study of yongcheng mine area," *Geology and Resources*, vol. 13, no. 2, pp. 109–111, 2004.
- [46] Y. B. Sun, W. K. Wang, C. C. Zhang, L. Duan, Y. H. Wang, and H. Li, "Formation and evolution mechanism of shallow-layer high fluorine water in Guanzhong Basin," *Hydrogeology and Engineering Geology*, vol. 40, no. 6, pp. 117–122, 2013.
- [47] C. C. Zhang, W. K. Wang, Y. B. Sun, H. Li, and Z. Wei, "Formation and evolution mechanism of shallow-layer high fluorine water in Guanzhong Basin," *Journal of Water Resources and Water Engineering*, vol. 24, no. 3, pp. 76–80, 2013.
- [48] V. K. Saxena and A. Shakeel, "Inferring the chemical parameters for the dissolution of fluoride in groundwater," *Environmental Geology*, vol. 43, no. 4, pp. 731–736, 2003.
- [49] Z. J. Gao, J. T. Liu, J. G. Feng, M. Wang, and G. W. Wu, "Hydrogeochemical characteristics and the suitability of groundwater in the alluvial-diluvial plain of southwest Shandong Province, China," *Water*, vol. 11, p. 5177, 2019.
- [50] Z. Gao, Z. Wang, S. Wang et al., "Factors that influence the chemical composition and evolution of shallow groundwater in an arid region: a case study from the middle reaches of the Heihe River, China," *Environmental Earth Sciences*, vol. 78, no. 14, p. 390, 2019.
- [51] A. Naaz and Anshumali, "Hydrogeochemistry of fluoride-rich groundwaters in semiarid region of Central India," *Arabian Journal of Geosciences*, vol. 8, no. 12, pp. 10585–10596, 2015.

Research Article

Hydrochemistry and Entropy-Based Groundwater Quality Assessment in the Suining Area, Southwestern China

Yunhui Zhang ^{1,2}, Xiao Li ³, Ming Luo,⁴ Changli Wei,⁴ Xun Huang,¹ Yong Xiao ^{1,2},
Limao Qin,¹ and Qiuming Pei ¹

¹Faculty of Geosciences and Environmental Engineering, Southwest Jiaotong University, Chengdu 611756, China

²Yibin Research Institute, Southwest Jiaotong University, Yibin 644000, China

³State Key Laboratory of Geohazard Prevention and Geoenvironment Protection, College of Environment and Civil Engineering, Chengdu University of Technology, Chengdu 610059, China

⁴Sichuan Institute of Geological Survey, Chengdu 610081, China

Correspondence should be addressed to Xiao Li; lixiao@cdut.edu.cn

Received 10 February 2021; Accepted 27 May 2021; Published 8 June 2021

Academic Editor: Xubo Gao

Copyright © 2021 Yunhui Zhang et al. This is an open access article distributed under the Creative Commons Attribution License, which permits unrestricted use, distribution, and reproduction in any medium, provided the original work is properly cited.

Groundwater is an essential resource for sustainable development, whose quality is significant for human health. In the present study, twenty-eight groundwater samples were collected from domestic tube wells and public water supply wells in the Suining area, southwestern China. The integration of statistical analysis, correlations of ions, geomodelling, and entropy-weighted water quality index (EWQI) was carried out to clarify the hydrochemistry and groundwater quality in the study area. By the statistical analysis, the cations followed the concentration order as $\text{Ca}^{2+} > \text{Na}^+ > \text{Mg}^{2+} > \text{K}^+$, while anions' concentrations were $\text{HCO}_3^- > \text{SO}_4^{2-} > \text{Cl}^- > \text{NO}_3^- > \text{F}^-$. Piper trilinear diagram showed the hydrochemical type was characterized as Ca-HCO₃. Correlations of ions and geomodelling revealed the concentrations of major ions were mainly determined by carbonate dissolution and ion exchange process, and NO_3^- concentrations were controlled by agriculture activities. EWQI computation demonstrated that most of the groundwater samples possessed EWQI values higher than 100. Therefore, groundwater quality is lower than the permissible limit of the World Health Organization (WHO), suitable for drinking purposes in the Suining area. Our study provides vital knowledge for groundwater management in the Suining and other similar areas.

1. Introduction

Groundwater is the basic and vital resource for humans living around the world. However, groundwater quality is deteriorating due to the rapid development of industrialization and urbanization, great growth of population, and excessive use of fertilizers [1–3]. So far, groundwater has been contaminated by nitrate, fluoride, arsenic, heavy metal elements, etc., seriously threatening to human health [4–8]. Comprehensive investigations of groundwater chemistry, mechanism analysis, and quality evolution can provide robust information for groundwater protection, which have been carried out globally [9–11].

Understanding groundwater chemistry is the critical fundament for mechanism analysis and quality evolution

[12–14]. For numerous hydrochemical data, a statistical approach is used to analyse the general scope, which is shown in the Box-Whisker diagram [15]. The Piper trilinear diagram can present the water type clearly [16]. The mechanism for groundwater chemistry is mainly determined by natural processes and anthropogenic activities [17–19]. Natural processes generally consist of water-rock interaction, precipitation, and evaporation. Gibbs plots are regarded as the classic approach to distinguish the natural governing factors affecting groundwater chemistry [20]. Correlations of different ions and geomodelling can further constrain the rock type involving water [21]. Assessment of groundwater quality is a hot topic for numerous researchers. In the previous study, the traditional water quality index (WQI) was introduced to evaluate groundwater quality

firstly [22–24]. Considering the various hydrochemical parameters, the WQI approach is not efficient to reveal the groundwater quality. The methodology for evaluating groundwater quality has experienced several stages from the traditional water quality index (WQI) to entropy water quality index (EWQI). The EWQI with entropy values involving various hydrochemical parameters has been believed to be a more robust approach due to its more comprehensive computation [19, 25–29]. In addition, the Geography Information System software (GIS) is helpful to reveal the spatial distribution of EWQI values. Therefore, the EWQI analysis has been extensively conducted for groundwater quality evaluation.

The Chengdu Plain is the area where industrialization and urbanization are rapidly increasing since the national developing strategy of the Chengdu-Chongqing economic circle was generated in the year 2020. The Suining area is an important city in the Chengdu Plain with a population of 3.6 million. The agriculture industry is active in the Suining area where the lands of 389 thousand hectares are exploited for extensive agricultural activity. However, scarce research has so far been conducted to understand the comprehensive evaluation of groundwater chemistry and quality from the Suining area. Therefore, the objectives of our study are as follows: (1) investigating the preliminary characteristics of groundwater chemistry, (2) identifying the factors controlling groundwater chemistry, and (3) evaluating groundwater quality using EWQI. The achievements of our study are hopeful to provide references for effective groundwater protection and management in future.

2. Materials and Methods

2.1. Study Area. The Suining area is located in the eastern part of the Sichuan Province, southwestern China, within the scope of E105°03'26"-106°59'49" and N30°10'50"-31°10'50" (Figure 1). The study area belongs to a subtropical humid monsoon climate with an annual temperature of 17°C and annual precipitation of 900 mm. The geomorphology is characterized as hilly and low mountain areas, with an elevation of 300–600 m. Rivers are developed in the Suining area where the Fu River is the dominant river (Figure 1).

The study area is situated in the Central Sichuan fold belt [30]. The strata are composed of the Quaternary sediments, Jurassic-Cretaceous calcareous mudstones and sandstones, and Triassic limestones (Figure 2) [31]. The Quaternary sediments contain sands, gravels, silty clay, and clay. The Jurassic-Cretaceous calcareous mudstones and sandstones consist of clay minerals (hydromica, kaolinite, and montmorillonite), detrital minerals (quartz, feldspar, and mica), and calcite. The Triassic limestones are dominated by calcite with less dolomite. Structures are not developed in the Suining area except for some E-W-trending wide folds. Groundwater mainly includes pore fissure water and fissure water and is recharged by infiltration of precipitation and local runoff. The Jurassic-Cretaceous calcareous sandstones are the main aquifers, while the mudstones are identified as confining beds [12]. The depth of groundwater is shallow

and lower than 20 m. So far, groundwater has been exploited by local residents for domestic and irrigation goals.

2.2. Field Sampling and Laboratory Measurements. In this study, a total of twenty-eight groundwater samples were collected within the Suining area from groundwater wells during June 2016. Sampling sites were equally distributed in the study area. Prior to sampling, at least ten minutes were taken to pump stagnant water in the wells. Every sample bottle was rinsed three times by the sample water. All of the groundwater samples were analysed for hydrochemical compositions in the Laboratory of the Sichuan Provincial Bureau of Geology and Mineral Resources. Total dissolved solids (TDS) and major cations (e.g., K⁺, Na⁺, Ca²⁺, and Mg²⁺) were analysed by an atomic absorption spectrophotometer (AA6100; Techcomp, China). Cl⁻, SO₄²⁻, NO₃⁻, and F⁻ were measured using ion chromatography (IC6100; Wayee, China). Chemical oxygen demand (COD) and total hardness (TH) and HCO₃⁻ were determined by titration. The charge balance error (CBE) ranged from -4.14% to +0.43% (calculated based on Equation (1)), validating the accuracy of experimental analyses:

$$\text{CBE} = \frac{\sum \text{cations} - \sum \text{anions}}{\sum \text{cations} + \sum \text{anions}} \times 100\%. \quad (1)$$

2.3. Data Processing and Analysis. The statistical analysis for hydrochemical parameters was compiled based on SPSS 25. Piper diagram was drawn by AquaChem software version 3.0, showing the hydrochemical type.

The Materials and Methods section should contain sufficient detail so that all procedures can be repeated. It may be divided into headed subsections if several methods are described. The saturation index (SI) of specific minerals was computed using PHREEQC 3.0, based on the following equation:

$$\text{SI} = \log\left(\frac{\text{IAP}}{K}\right), \quad (2)$$

where IAP represents ion activity in groundwater and K is the solubility constant under specific temperature.

The entropy-weighted water quality index (EWQI) is the approach for evaluating water quality by entropy value involving various hydrochemical parameters. In general, the EWQI values were computed by four steps as follows:

Step 1: the eigenvalue matrix X is obtained as follows:

$$X = \begin{bmatrix} x_{11} & x_{12} & \cdots & x_{1n} \\ x_{21} & x_{22} & \cdots & x_{2n} \\ \vdots & \vdots & \ddots & \vdots \\ x_{m1} & x_{m2} & \cdots & x_{mn} \end{bmatrix}, \quad (3)$$

where m is the total number of water samples and n signifies the number of hydrochemical parameters.

Step 2: the standard evaluation matrix “ Y ” is calculated as follows:

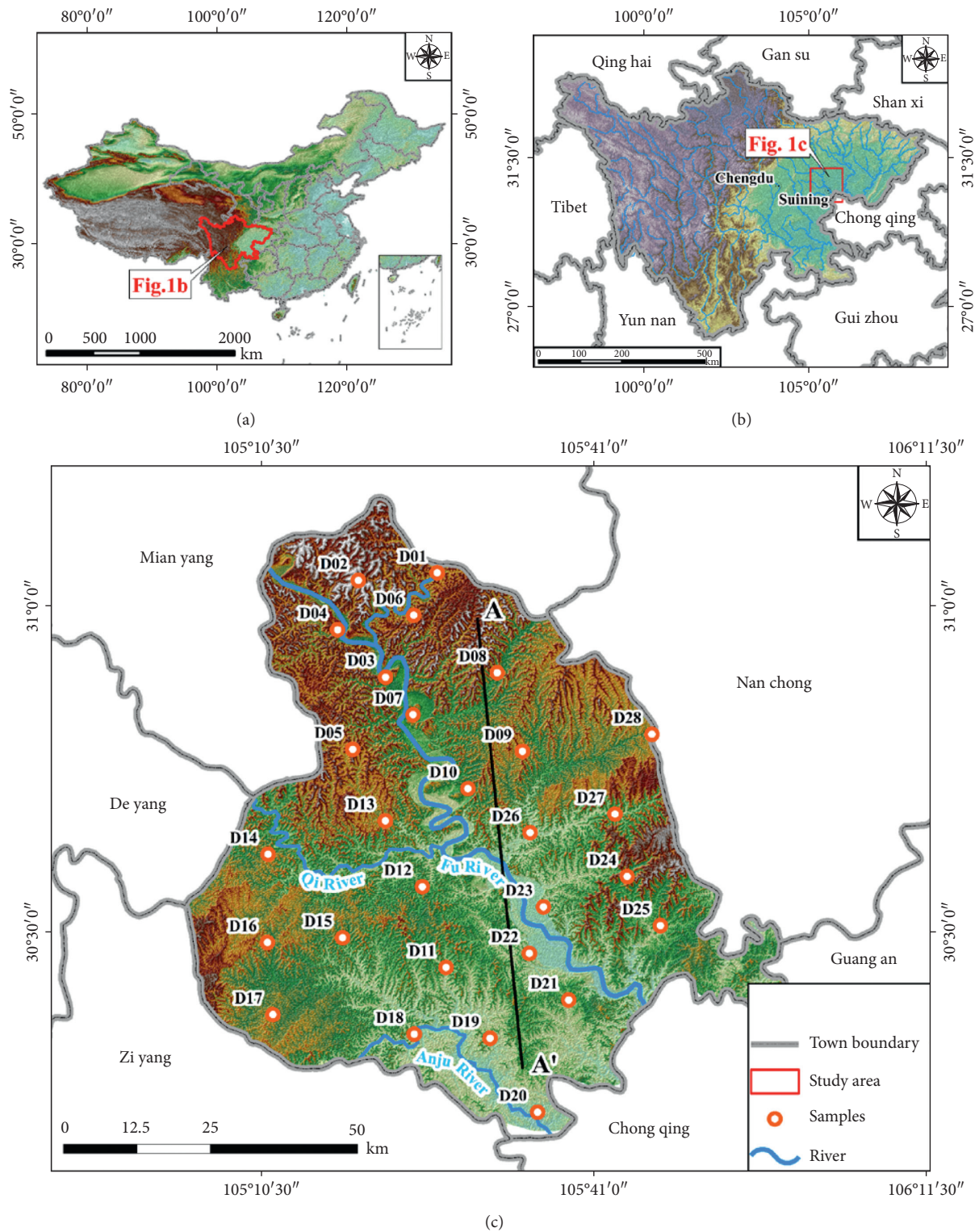


FIGURE 1: Study area location and sampling point distribution.

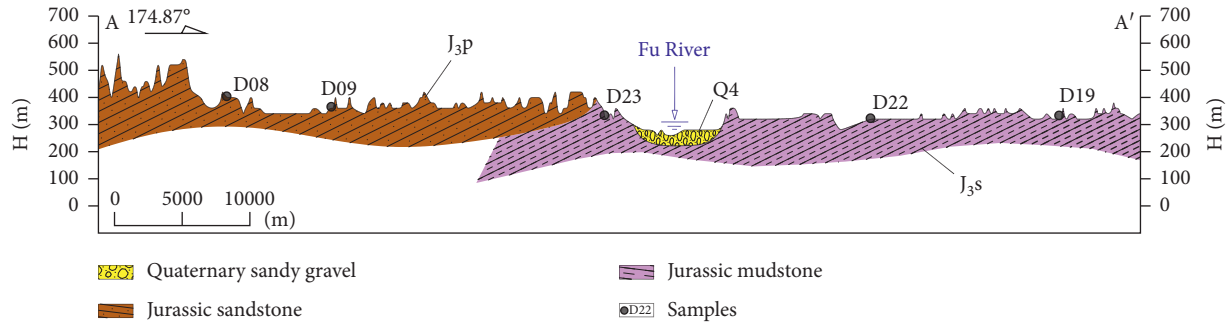


FIGURE 2: Geological section A-A' of the study area.

$$y_{ij} = \begin{cases} \frac{x_{ij} - (x_{ij})_{\min}}{(x_{ij})_{\max} - (x_{ij})_{\min}}, & \text{benefit type,} \\ \frac{(x_{ij})_{\max} - x_{ij}}{(x_{ij})_{\max} - (x_{ij})_{\min}}, & \text{cost type,} \end{cases} \quad (4)$$

$$Y = \begin{bmatrix} y_{11} & y_{12} & \cdots & y_{1n} \\ y_{21} & y_{22} & \cdots & y_{2n} \\ \vdots & \vdots & \ddots & \vdots \\ y_{m1} & y_{m2} & \cdots & y_{mn} \end{bmatrix}, \quad (5)$$

where $(x_{ij})_{\max}$ and $(x_{ij})_{\min}$ are the maximum and minimum values of the hydrochemical parameters of the water samples, respectively, and “ y_{ij} ” is the standardization process.

Step 3: the information entropy “ e_j ” is acquired as follows:

$$e_j = -\frac{1}{\ln m} \sum_{i=1}^m (P_{ij} \times \ln P_{ij}), \quad (6)$$

where P_{ij} is the parameter value ratio of parameter j for sample i , achieved based on Equation (6):

$$P_{ij} = \frac{y_{ij}}{\sum_i^m y_{ij}}. \quad (7)$$

Afterwards, the entropy weight “ w_j ” can be obtained as follows:

$$w_j = \frac{1 - e_j}{\sum_{i=1}^n (1 - e_j)}. \quad (8)$$

Step 4: the quality rating scale “ q_j ” of each parameter could be computed by the following equation:

$$q_j = \frac{C_j}{S_j} \times 100, \quad (9)$$

where C_j is the concentration of each hydrochemical parameter j and S_j represents the permissible limit of the World Health Organization standards for specific hydrochemical parameter j .

Finally, the EWQI value can be computed using the following equation:

$$EWQI = \sum_{j=1}^m (w_j \times q_j). \quad (10)$$

The classification of water quality based on EWQI is shown in Table 1.

3. Results and Discussion

3.1. General Characteristics of Groundwater Chemistry.

The statistical results of hydrochemical parameters are presented in Table 2 and Figure 3, which were compared with the standard limits of the World Health Organization (WHO). The pH values varied from 7.1 to 8.4 (mean = 7.6), indicating neutral to slightly alkaline character and permissible for drinking purpose. Total dissolved solids (TDS) had concentrations of 20–830 mg/L, within the permissible drinking standard. The total hardness (TH) values ranged from 160.14 mg/L to 550.50 mg/L (mean = 389.99 mg/L). 17.86% of groundwater samples exceeding the permissible limit of 450.00 mg/L displayed the hard to very hard affinity (Figure 4(a)) and were unsuitable for drinking. Based on the statistical results, the major cations and anions followed the order of concentrations as follows: Ca^{2+} (46.10–184.40 mg/L) > Na^+ (8.70–78.00 mg/L) > Mg^{2+} (6.10–42.60 mg/L) > K^+ (0.90–25.00 mg/L), and HCO_3^- (140.30–530.90 mg/L) > SO_4^{2-} (45.90–207.00 mg/L) > Cl^- (7.20–90.50 mg/L). Ca^{2+} and HCO_3^- were the dominated cation and anion, respectively, characterized as the hydrochemical type of Ca-HCO₃ (Figure 4(b)). Most of the major ions (except Ca^{2+}) possessed concentrations less than the permissible limit for drinking purpose (Table 2). Of note, the NO_3^- , NO_2^- , and NH_4^+ concentrations of groundwater samples were found beyond the permissible limit. Among them, NO_3^- had the highest concentrations of 0.20–244.00 mg/L, with 50% of groundwater samples exceeding the maximum allowable limit of 50 mg/L. NO_2^- and NH_4^+ concentrations varied from 0.01 to 6.05 mg/L and 0.03 to 1.53 mg/L, within 18.57% and 11.43% of groundwater samples exceeding the permissible limit, respectively. Hence, nitrate contamination was identified in the Suining area. The F^- concentrations (0.2–0.6 mg/L) were obviously lower than the recommended level of drinking water standard.

TABLE 1: Classification criteria of water quality based on EWQI, according to reference [25].

Rank	EWQI	Water quality
1	<50	Excellent
2	50–100	Good
3	100–150	Medium
4	150–200	Poor
5	>200	Extremely poor

TABLE 2: Statistical results of hydrochemical parameters and drinking water standards.

Parameters	Max	Min	Mean	SD	CV (%)	Guideline	% of SEL
pH	8.4	7.10	7.6	0.25	3.37	6.5–8.5*	0.00
TDS	830	201	563	140	24.90	1000*	0.00
TH	550.50	160.14	389.99	89.04	22.83	450.00*	17.86
K ⁺	25.00	0.90	3.75	4.77	126.98	—	—
Na ⁺	78.00	8.70	31.66	14.81	46.76	200**	0.00
Ca ²⁺	184.40	46.10	118.68	30.67	25.85	75**	92.86
Mg ²⁺	42.60	6.10	22.75	8.68	38.14	50**	0.00
Cl ⁻	90.50	7.20	30.62	22.98	75.06	250*	0.00
SO ₄ ²⁻	207.00	45.90	93.60	42.20	45.09	250*	0.00
HCO ₃ ⁻	530.90	140.30	348.31	89.41	25.67	—	—
NO ₃ ⁻	244.00	0.20	68.12	61.42	90.17	50**	50.00
NO ₂ ⁻	6.05	0.01	0.43	1.41	327.39	0.02*	18.57
NH ₄ ⁺	1.53	0.03	0.23	0.30	129.05	0.2*	11.43
F ⁻	0.6	0.2	0.4	0.10	27.16	1.0*	0.00

SD, standard deviation; CV (%), coefficient of variation; *Chinese Guidelines [32]; **WHO Guidelines [33]; % of SEL, % of samples exceeding the acceptable limit.

3.2. Factors Controlling Groundwater Chemistry. The natural sources controlling ion concentrations generally include evaporation, rock weathering, and precipitation. Gibbs raised the classified diagram for distinguishing the different natural sources [34]. In the Gibbs diagram, all groundwater samples are plotted in the area of rock dominance (Figure 5), indicating that water-rock interaction is the natural process determining the ion concentrations of groundwater.

3.3. Sources of Major Ions

3.3.1. Correlation of Major Ions for Mineral Dissolution. The correlation of major ions has been extensively used to clarify the mineral types involving the water-rock interaction (Figure 6). When the dissolution of halite is the main process, the mole ratio between Cl⁻ and Na⁺ is equal to one. Most of the groundwater samples plotted below the $y = x$ line, against the possibility of halite dissolution. The excess Na⁺ concentration was probably derived from silicate dissolution or ion exchange. The dissolution of gypsum would lead to the molar ratio between SO₄²⁻ and Ca²⁺ equal to one. All of the groundwater samples drifted under the $y = x$ line. The dissolution of gypsum was unlikely to be the main natural process, implying there are possibilities that some processes contribute Ca²⁺. In the Ca²⁺ vs. HCO₃⁻, groundwater samples followed the $y = x$ line, implying the occurrence of calcite dissolution. Molar concentrations of Ca²⁺, Mg²⁺, Na⁺, and HCO₃⁻ constructed by Gaillardet et al. (1999) have been considered as the efficient approach to

evaluate the effects of carbonate rocks, silicate rocks, and evaporite rocks on the hydrochemical compositions [35]. In this study, groundwater samples fell in the zone between the carbonate rocks and silicate rocks. Hence, silicates and carbonates rather than evaporites had a contribution to groundwater chemistry. Accordingly, groundwater samples were distributed in the areas of silicate weathering and calcite dissolution.

Ion exchange has been reported as the natural process universally occurring in the groundwater system [36–38]. The relationship between $(Ca^{2+} + Mg^{2+}) - (SO_4^{2-} + HCO_3^-)$ and $(Na^+ + K^+ - Cl^-)$ can be employed to identify the ion exchange. The plots of groundwater samples displayed a negative correlation, revealing the ion exchange existed between Ca²⁺ and Na⁺. Moreover, the chloroalkaline indices (CAI-I and CAI-II) are feasible to constrain the type of ion exchange. When the CAI-I and CAI-II values are higher than zero, reverse ion exchange occurs. In contrast, ion exchange is supported by the CAI-I and CAI-II values lower than zero. In this study, most of the groundwater samples possessed the CAI-I and CAI-II values lower than zero. Hence, ion exchange between Ca²⁺ and Na⁺ was proposed in the study area.

3.3.2. Saturation Index for Estimating Possible Mineral Phases. Saturation index (SI) is viable to reflect the mineral equilibrium state in the groundwater system. In this study, saturation indices of calcite, dolomite, gypsum, and halite were computed by Phreeqc 3.0, as shown in Figure 6(i). The

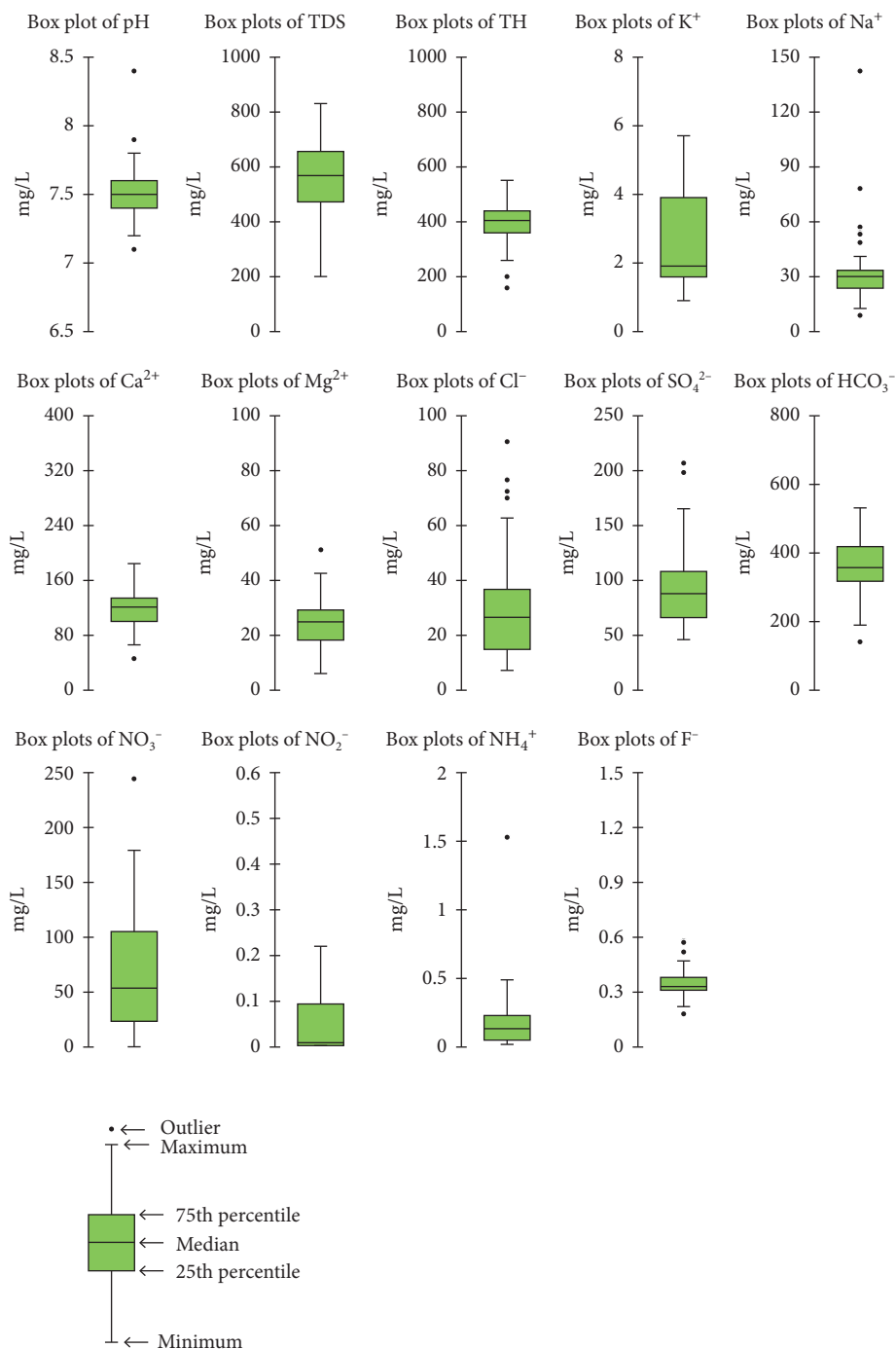


FIGURE 3: Box and Whisker plot of hydrochemical parameters of groundwater samples.

saturation indices of gypsum and halite were obviously lower than zero, implying the unsaturated state. Dolomite and calcite represented the oversaturated state by the saturation indices greater than zero. Hence, the hydrochemical compositions were mainly attributed to the dissolution of carbonate minerals.

3.3.3. Groundwater Quality Assessment Based on EWQI. The EWQI approach has been extensively used to evaluate the comprehensive effects of hydrochemical parameters on

overall water quality [25, 26, 39]. The EWQI values lower than 100 imply that the water quality reaches the permissible limit for drinking purpose. In the present study, the concentrations of Ca^{2+} , Mg^{2+} , Na^+ , K^+ , Cl^- , SO_4^{2-} , HCO_3^- , F^- , NO_3^- , and TDS were involved in the computation of the EWQI. Herein, the EWQI values had a range of 95–235 (average value = 175) and were evaluated from rank 2 to rank 5 (Figure 7(a)). The majority of groundwater samples displayed the levels of Rank: 4 poor, lower than permissible drinking standard of the WHO.

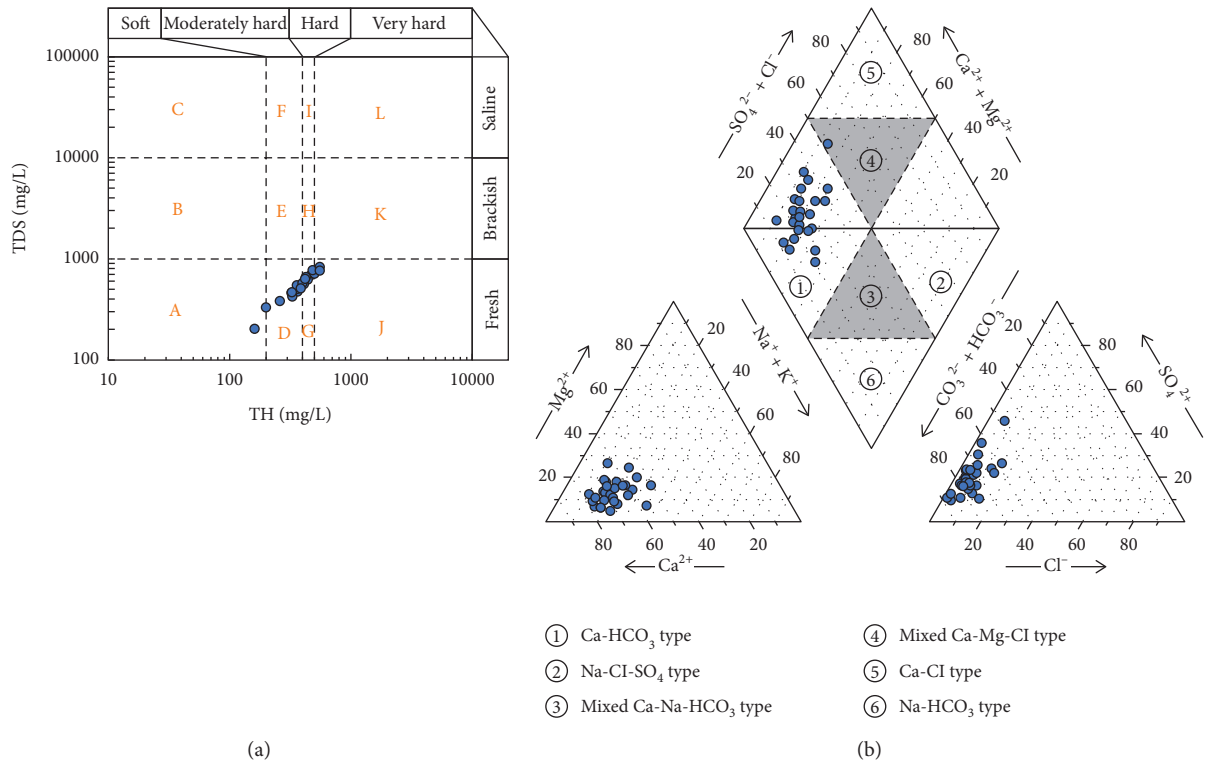


FIGURE 4: Scatter plots of (a) TH versus TDS demonstrating groundwater quality and (b) Piper trilinear diagram for groundwater samples.

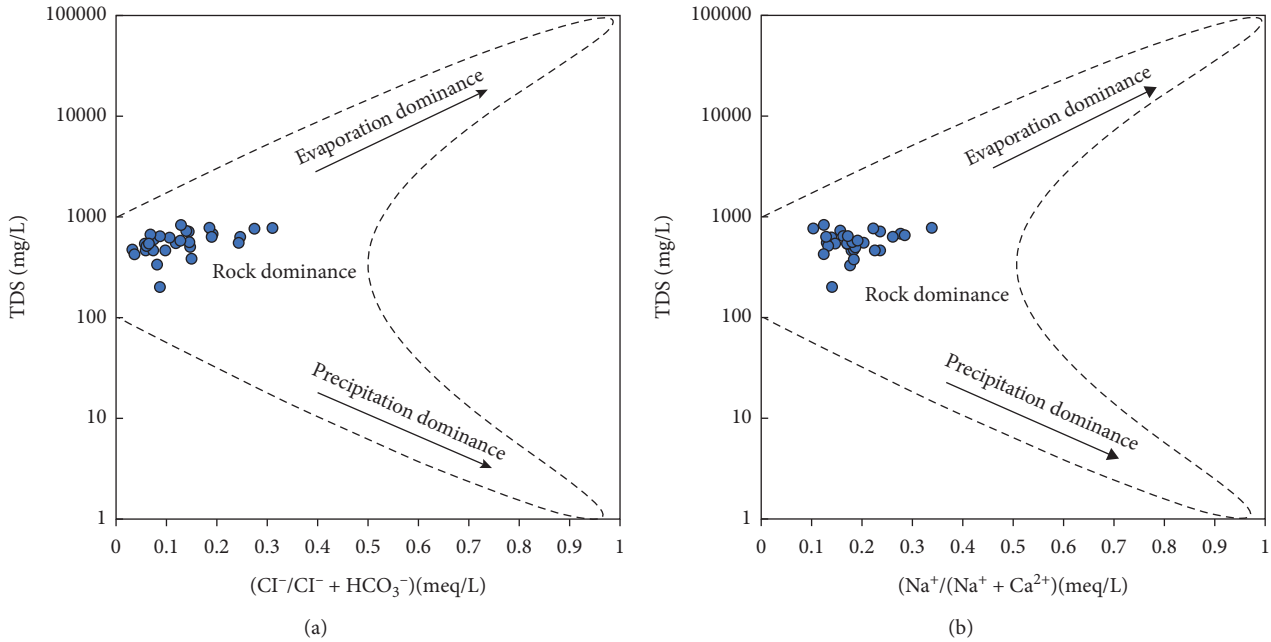


FIGURE 5: Gibbs diagrams demonstrating the mechanisms governing groundwater chemistry. (a) TDS vs. $Cl^-/(Cl^-+HCO_3^-)$; (b) TDS vs. $Na^+/(Na^++Ca^{2+})$.

The spatial distribution of the EWQI rank was visualized by the normal Kriging interpolation approach in the Geography Information System software (GIS) (Figure 7(b)). In Figure 7(b), the groundwater samples in the vast majority of the study area were not allowable for drinking purpose.

Some local places in the western and middle parts of the study area had groundwater whose EWQI values largely exceeded the permissible limit for safe drinking. Therefore, the western and middle parts of the study area should be paid more attention for groundwater protection in future.

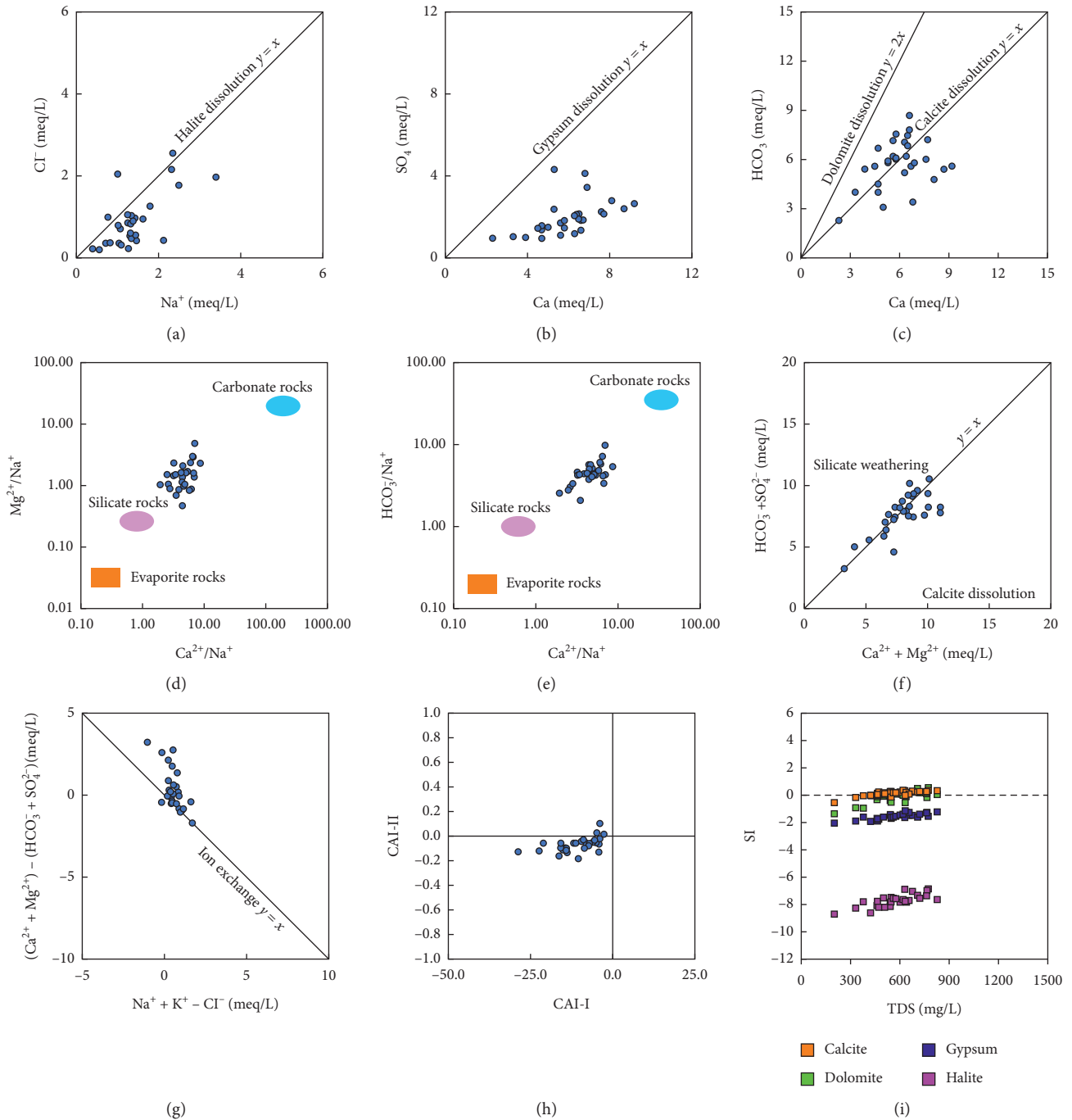


FIGURE 6: Correlation diagrams of (a) Cl^- vs. Na^+ , (b) SO_4^{2-} vs. Ca^{2+} , (c) HCO_3^- vs. Ca^{2+} , (d) $(\text{Mg}^{2+}/\text{Na}^+)$ vs. $(\text{Ca}^{2+}/\text{Na}^+)$, (e) $(\text{HCO}_3^-/\text{Na}^+)$ vs. $(\text{Ca}^{2+}/\text{Na}^+)$, (f) $\text{HCO}_3^- + \text{SO}_4^{2-}$ vs. $\text{Ca}^{2+} + \text{Mg}^{2+}$, (g) $(\text{Ca}^{2+} + \text{Mg}^{2+}) - (\text{HCO}_3^- + \text{SO}_4^{2-})$ vs. $\text{Na}^+ + \text{K}^+ - \text{Cl}^-$, (h) chloroalkaline indices CAI-I vs. CAI-II, and (i) SI vs. TDS.

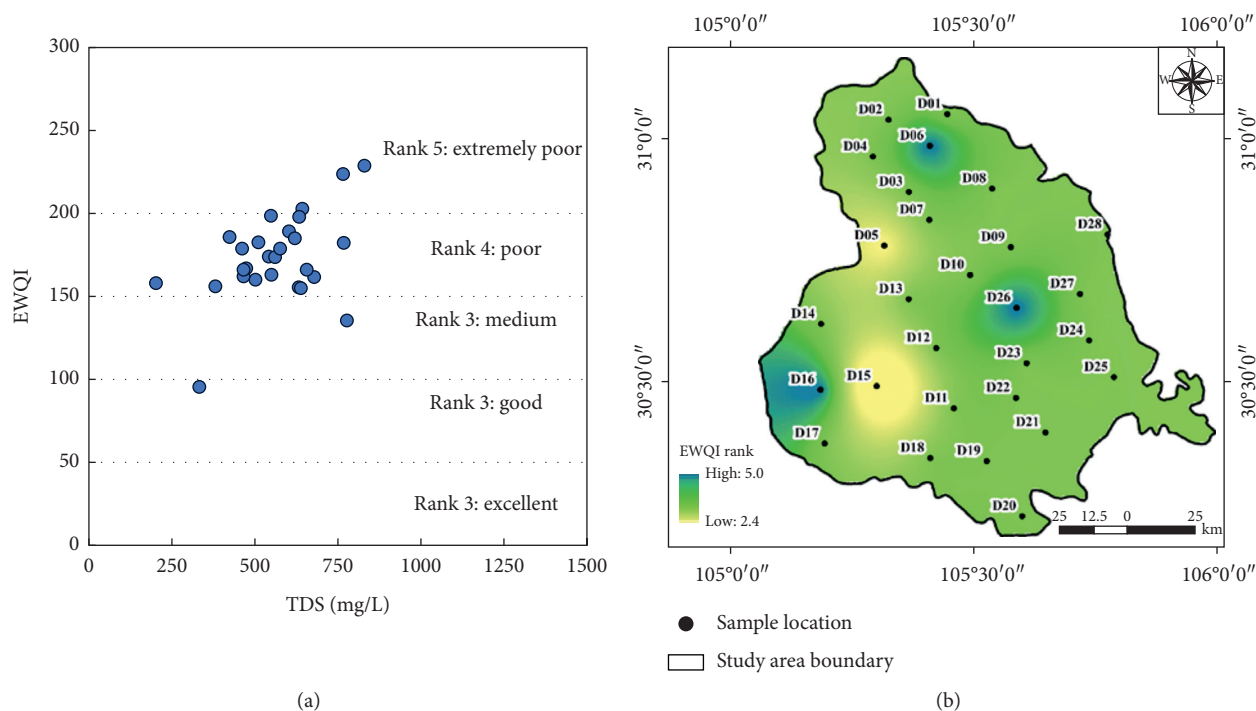


FIGURE 7: (a) The relationship between the entropy-weighted water quality index (EWQI) and TDS and (b) spatial distribution of groundwater quality based on the EWQI rank.

4. Conclusions

In this study, twenty-eight groundwater samples were collected from the Suining area for hydrogeochemical analysis and quality assessment in order to better exploit and utilize groundwater resources. The main conclusions were drawn as follows:

- (1) Groundwater samples represented alkaline affinity and high TDS values with Ca-HCO₃ type. The average cation and anion concentrations followed the order of Ca²⁺ > Na⁺ > Mg²⁺ > K⁺ and HCO₃⁻ > SO₄²⁻ > Cl⁻ > NO₃⁻ > F⁻. Nitrate contamination was identified by the NO₃⁻ concentrations of 0.20–244.00 mg/L.
- (2) Ratios of major ions and geochemical modelling collectively revealed that hydrogeochemical compositions were dominated by carbonate dissolution and ion exchange.
- (3) Entropy-weighted water quality index (EWQI) indicated that most of the total samples were unsuitable for drinking. The western and middle parts of the study area with higher EWQI values should be paid more attention for groundwater protection in future.

Data Availability

The data used to support the findings of the present study are available from the corresponding author upon request.

Conflicts of Interest

The authors declare that they have no conflicts of interest.

Acknowledgments

This research was funded by the Natural Science Foundation of China (42072313), the Fundamental Research Funds for the Central Universities (2682020CX10), and the Student Research Training Program of Southwest Jiaotong University (202010613072 and 201019).

References

- [1] J. Wu, J. Bian, H. Wan, Y. Ma, and X. Sun, "Health risk assessment of groundwater nitrogen pollution in Songnen Plain," *Ecotoxicology and Environmental Safety*, vol. 207, Article ID 111245, 2021.
- [2] S. Chen, Z. Tang, J. Wang et al., "Multivariate analysis and geochemical signatures of shallow groundwater in the main urban area of chongqing, southwestern China," *Water*, vol. 12, no. 10, p. 2833, 2020.
- [3] N. Adimalla, H. Qian, and M. J. Nandan, "Groundwater chemistry integrating the pollution index of groundwater and evaluation of potential human health risk: a case study from hard rock terrain of south India," *Ecotoxicology and Environmental Safety*, vol. 206, Article ID 111217, 2020.
- [4] G. Zhu, X. Wu, J. Ge, F. Liu, W. Zhao, and C. Wu, "Influence of mining activities on groundwater hydrochemistry and heavy metal migration using a self-organizing map (SOM)," *Journal of Cleaner Production*, vol. 257, Article ID 120664, 2020.
- [5] M. Hossain and P. K. Patra, "Hydrogeochemical characterisation and health hazards of fluoride enriched groundwater in diverse aquifer types," *Environmental Pollution*, vol. 258, Article ID 113646, 2020.
- [6] A. Banning, "Geogenic arsenic and uranium in Germany: large-scale distribution control in sediments and

- groundwater," *Journal of Hazardous Materials*, vol. 405, Article ID 124186, 2020.
- [7] Y. Teng, R. Zuo, Y. Xiong, J. Wu, Y. Zhai, and J. Su, "Risk assessment framework for nitrate contamination in groundwater for regional management," *Science of The Total Environment*, vol. 697, Article ID 134102, 2019.
- [8] J. Qiao, Y. Zhu, X. Jia, M. a. Shao, X. Niu, and J. Liu, "Distributions of arsenic and other heavy metals, and health risk assessments for groundwater in the Guanzhong Plain region of China," *Environmental Research*, vol. 181, Article ID 108957, 2020.
- [9] P. Li and H. Qian, "Water resources research to support a sustainable China," *International Journal of Water Resources Development*, vol. 34, no. 3, pp. 327–336, 2018.
- [10] X. Gao, X. Li, W. Wang, and C. Li, "Human activity and hydrogeochemical processes relating to groundwater quality degradation in the yuncheng basin, northern China," *International Journal of Environmental Research and Public Health*, vol. 17, no. 3, p. 867, 2020.
- [11] J. Li, "Evaluating spatiotemporal variations of groundwater quality in northeast beijing by self-organizing map," *Water*, vol. 12, no. 5, 2020.
- [12] Y. Zhang, Y. Dai, Y. Wang, X. Huang, Y. Xiao, and Q. Pei, "Hydrochemistry, quality and potential health risk appraisal of nitrate enriched groundwater in the Nanchong area, southwestern China," *Science of The Total Environment*, vol. 784, Article ID 147186, 2021.
- [13] C. Li, X. Gao, S. Li, and J. Bundschuh, "A review of the distribution, sources, genesis, and environmental concerns of salinity in groundwater," *Environmental Science and Pollution Research*, vol. 27, no. 33, pp. 41157–41174, 2020.
- [14] C. Li, X. Gao, Y. Liu, and Y. Wang, "Impact of anthropogenic activities on the enrichment of fluoride and salinity in groundwater in the Yuncheng Basin constrained by Cl/Br ratio, $\delta^{18}\text{O}$, $\delta^2\text{H}$, $\delta^{13}\text{C}$ and $\delta^7\text{Li}$ isotopes," *Journal of Hydrology*, vol. 579, Article ID 124211, 2019.
- [15] Y. Xiao, "Hydrogeochemical features and genesis of confined groundwater and health perspectives for sustainable development in urban hengshui, north China plain," *Journal of Chemistry*, vol. 2021, Article ID 5578192, 15 pages, 2021.
- [16] Y. Luo, "Groundwater geochemical signatures and implication for sustainable development in a typical endorheic watershed on Tibetan plateau," *Environmental Science and Pollution Research*, 2021.
- [17] Y. Zhou, P. Li, L. Xue, Z. Dong, and D. Li, "Solute geochemistry and groundwater quality for drinking and irrigation purposes: a case study in Xinle City, North China," *Geochemistry*, vol. 80, no. 4, Article ID 125609, 2020.
- [18] S. He, P. Li, J. Wu, V. Elumalai, and N. Adimalla, "Groundwater quality under land use/land cover changes: a temporal study from 2005 to 2015 in Xi'an, Northwest China," *Human and Ecological Risk Assessment: An International Journal*, vol. 26, no. 10, pp. 2771–2797, 2020.
- [19] P. Li, X. He, and W. Guo, "Spatial groundwater quality and potential health risks due to nitrate ingestion through drinking water: a case study in Yan'an City on the Loess Plateau of northwest China," *Human and Ecological Risk Assessment: An International Journal*, vol. 25, no. 2, pp. 11–31, 2019.
- [20] J. Li, Z. Shi, M. Liu, G. Wang, F. Liu, and Y. Wang, "Identifying anthropogenic sources of groundwater contamination by natural background levels and stable isotope application in Pinggu basin, China," *Journal of Hydrology*, vol. 596, Article ID 126092, 2021.
- [21] S. Qu, Z. Shi, X. Liang, G. Wang, and J. Han, "Multiple factors control groundwater chemistry and quality of multi-layer groundwater system in Northwest China coalfield - using self-organizing maps (SOM)," *Journal of Geochemical Exploration*, vol. 227, Article ID 106795, 2021.
- [22] N. Adimalla and H. Qian, "Groundwater quality evaluation using water quality index (WQI) for drinking purposes and human health risk (HHR) assessment in an agricultural region of Nanganur, south India," *Ecotoxicology and Environmental Safety*, vol. 176, pp. 153–161, 2019.
- [23] M. Dhanasekarapandian, S. Chandran, D. S. Devi, and V. Kumar, "Spatial and temporal variation of groundwater quality and its suitability for irrigation and drinking purpose using GIS and WQI in an urban fringe," *Journal of African Earth Sciences*, vol. 124, pp. 270–288, 2016.
- [24] S. Krishna Kumar, R. Bharani, N. S. Magesh, P. S. Godson, and N. Chandrasekar, "Hydrogeochemistry and groundwater quality appraisal of part of south Chennai coastal aquifers, Tamil Nadu, India using WQI and fuzzy logic method," *Applied Water Science*, vol. 4, no. 4, pp. 341–350, 2014.
- [25] N. Adimalla, *Application of the Entropy Weighted Water Quality Index (EWQI) and the Pollution Index of Groundwater (PIG) to Assess Groundwater Quality for Drinking Purposes: A Case Study in a Rural Area of Telangana State*, Archives of Environmental Contamination and Toxicology, India, 2021.
- [26] M. S. U. Hasan and A. K. Rai, "Groundwater quality assessment in the Lower Ganga Basin using entropy information theory and GIS," *Journal of Cleaner Production*, vol. 274, Article ID 123077, 2020.
- [27] N. Adimalla, H. Qian, and P. Li, "Entropy water quality index and probabilistic health risk assessment from geochemistry of groundwaters in hard rock terrain of Nanganur County, South India," *Geochemistry*, vol. 80, no. 4, Article ID 125544, 2020.
- [28] J. Liu, Y. Peng, C. Li, Z. Gao, and S. Chen, "Characterization of the hydrochemistry of water resources of the Weibei Plain, Northern China, as well as an assessment of the risk of high groundwater nitrate levels to human health," *Environmental Pollution*, vol. 268, Article ID 115947, 2021.
- [29] C. Wu, X. Wu, C. Qian, and G. Zhu, "Hydrogeochemistry and groundwater quality assessment of high fluoride levels in the Yanchi endorheic region, northwest China," *Applied Geochemistry*, vol. 98, pp. 404–417, 2018.
- [30] H.-W. Cao, G.-M. Li, R.-Q. Zhang et al., "Genesis of the Cuonadong tin polymetallic deposit in the Tethyan Himalaya: evidence from geology, geochronology, fluid inclusions and multiple isotopes," *Gondwana Research*, vol. 92, pp. 72–101, 2021.
- [31] S. Liu, Y. Yang, B. Deng et al., "Tectonic evolution of the sichuan basin, southwest China," *Earth-Science Reviews*, vol. 213, Article ID 103470, 2021.
- [32] M. Dietmar, *Standards for Groundwater Quality*, Standards Press of China, Beijing, China, 2017.
- [33] World Health Organization, *Guidelines for Drinking-Water Quality*, World Health Organization, Geneva, Switzerland, 4th edition, 2011.
- [34] R. J. Gibbs, "Mechanisms controlling world water chemistry," *Science*, vol. 170, no. 3962, pp. 1088–1090, 1970.
- [35] J. Gaillardet, "Global silicate weathering and CO₂ consumption rates deduced from the chemistry of large rivers," *Chemical Geology*, vol. 159, no. 1, pp. 3–30, 1999.
- [36] Y. Xiao, X. Gu, S. Yin, X. Pan, J. Shao, and Y. Cui, "Investigation of geochemical characteristics and controlling

- processes of groundwater in a typical long-term reclaimed water use area,” *Water*, vol. 9, no. 10, 800 pages, 2017.
- [37] E. P. Tziritis, P. S. Datta, and R. Barzegar, “Characterization and assessment of groundwater resources in a complex hydrological basin of Central Greece (kopaida basin) with the joint use of hydrogeochemical analysis, multivariate statistics and stable isotopes,” *Aquatic Geochemistry*, vol. 23, 2017.
- [38] M. Sudheer Kumar, “Principal component and multivariate statistical approach for evaluation of hydrochemical characterization of fluoride-rich groundwater of Shaslar Vagu watershed, Nalgonda District, India,” *Arabian Journal of Geosciences*, vol. 10, no. 4, 2017.
- [39] N. Adimalla, H. Qian, and P. Li, “Entropy Water Quality Index and Probabilistic Health Risk Assessment from Geochemistry of Groundwaters in Hard Rock Terrain of Nanganur County, South India,” *Geochemistry*, vol. 80, Article ID 125544, 2019.

Research Article

Degradation of High-Concentration Nitrate Nitrogen in Groundwater: A Laboratory Study

Manxi Liu,¹ Lu Xia,¹ Ruinan Liu,¹ Zongjun Gao ,¹ Cong Han,¹ Jianguo Feng,¹ Jing Wang,¹ Wanlong Qu,^{2,3} and Tongju Xing^{2,3}

¹College of Earth Science and Engineering, Shandong University of Science and Technology, Qingdao, China

²Qingdao Geo-Engineering Surveying Institute (Qingdao Geological Exploration and Development Bureau), Qingdao, China

³Key Laboratory of Urban Geology and Underground Space Resources, Shandong Provincial Bureau of Geology and Mineral Resources, Qingdao, China

Correspondence should be addressed to Zongjun Gao; zongjungao1964@163.com

Received 12 April 2021; Revised 13 May 2021; Accepted 22 May 2021; Published 29 May 2021

Academic Editor: Junbing Pu

Copyright © 2021 Manxi Liu et al. This is an open access article distributed under the Creative Commons Attribution License, which permits unrestricted use, distribution, and reproduction in any medium, provided the original work is properly cited.

To investigate effective and reasonable methods for the remediation of nitrate nitrogen pollution in groundwater, two groups of laboratory denitrification experiments were conducted: one on the effect of native denitrifying microbes in groundwater and another on the effect of artificially added denitrifying microbes. The water used in the experiment was typical groundwater with a high concentration of nitrate nitrogen. The temperature was controlled at 15°C. Both groups of experiments established four types of culture environments: anaerobic, anaerobic with an added carbon source (glucose), aerobic, and aerobic with an added carbon source (glucose). The results indicated that native denitrifying microbes in the groundwater have almost no ability to remove high concentrations of nitrate nitrogen. However, artificially added denitrifying microbes can effectively promote denitrification. Artificially added denitrifying microbes had the highest activity in an anaerobic environment in which a carbon source had been added, and the rate removal of a high concentration of nitrate nitrogen in groundwater was the highest and reached as high as 89.52%.

1. Introduction

Groundwater is an important part of water resources, with a stable quantity of high-quality water. It is one of the important water sources for agricultural irrigation, industry, mining, and urban life. However, with the development of society and economy and the influence of human activities, increasing amounts of environmental pollution problems have gradually been exposed, particularly the pollution of groundwater, whose scope has expanded from point to surface and from shallow to deep. In addition, the number of types of pollutants has been increasing. The degree of pollution is becoming increasingly serious [1–4]. Owing to the discharge and leakage of domestic sewage and substandard industrial wastewater, an unreasonable recharge of sewage, the leaching of fecal and solid waste, the application of a large number of chemical fertilizers and pesticides in rural areas, dry and wet deposition of nitrogen oxides in the

atmosphere, and excessive exploitation of groundwater, the concentration of nitrate nitrogen in groundwater has been increasing, thus, resulting in serious pollution to the environment [5–8]. Groundwater with a high concentration of nitrate nitrogen poses a major threat to human beings and other organisms, since the excessive intake of nitrate results in its reduction to toxic nitrite in the human body [9–11], which can be further transformed into nitrosamines. Nitrosamine is a “three-cause” substance, which easily causes digestive system diseases, methemoglobinemia (blue baby disease), and other problems [12–15].

The problem of nitrate pollution of groundwater has aroused widespread concern in academic circles. The effective remediation of nitrate pollution of groundwater has become the focus of widespread concern. The conventional processes (flocculation sedimentation-filtration-chlorine disinfection) applied for water potability do not eliminate nitrate from the groundwater [16], and special treatment

processes are required to lower the concentration of nitrate to acceptable levels. Currently, the main remediation methods of nitrate pollution in groundwater are physical, chemical, and biological methods. Although there are many methods, each has its own limitations in practical application [17–20]. In terms of eliminating nitrate pollution in groundwater and reducing the cost of denitrification, the biological method is the most effective method that is currently used [21, 22]. This method is characterized by high efficiency and low consumption, so it has been extensively studied. Bioremediation methods primarily rely on the denitrification of microorganisms to remove pollutants from groundwater [23, 24]. Most of the denitrifying microbes involved in the denitrification process are heterotrophic facultative anaerobes, which cannot synthesize organic matter themselves and need to consume additional carbon sources to produce energy and conduct cell synthesis and deoxidation [25]. Currently, the research on bioremediation methods is primarily focused on the selection of denitrifying microbes and carbon sources.

Trudell et al. [26] conducted a large number of experiments that proved that solid organic carbon can also be used as a substrate for denitrification. Schipper et al. [27], Robinson-Lora et al. [28], and Moorman et al. [29] selected solid carbon sources for denitrification experiments and achieved good denitrification results. However, solid carbon sources are mostly natural materials, such as sawdust, rice straw, and bark, and their carbon release is uncontrollable, which easily causes secondary pollution, aquifer blockage, and other problems [30, 31]. Compared with solid carbon sources, liquid carbon sources have a fast dissolution rate and highly efficient reactions. Studies have shown [32–39] that common carbon sources, such as methanol, ethanol, acetic acid, sucrose, and glucose can promote denitrification. In addition, different carbon sources have varying effects on denitrification. There are also many studies on denitrifying microbes [40–43]. Wang et al. [44] successfully isolated denitrifying microbes from groundwater in intensive vegetable growing areas. Zhang et al. [45] isolated denitrifying microbes from soil and verified their ability to perform denitrification. Using a shaking flask experiment, Wang [46] revealed that the groundwater polluted by nitrate contains a large number of indigenous microorganisms, which can degrade the nitrate in the presence of an additional carbon source. Li et al. [47] showed that the sludge of the anaerobic section of a sewage treatment plant contains denitrifying microbes, which are highly active after enrichment and culture. Zhang et al. [37] and Zhang et al. [38, 39] proved that the combination of optimized artificial denitrification agents and common carbon sources such as ethanol can clearly remove nitrate pollution from groundwater. Previous studies have made substantial progress in verifying that both liquid and solid carbon sources can promote denitrification. There is denitrification by indigenous microorganisms in groundwater, which can be enhanced by adding carbon sources to degrade nitrate pollution. Biological bacteria and fungi are beneficial for removing nitrate nitrogen in groundwater. However, research mostly adopts groundwater and synthetic water with low concentrations of nitrate

nitrogen. There are few research results on the comparison of effects of native denitrifying microbes in groundwater with those that have been artificially added on the remediation of groundwater with a high concentration of nitrate nitrogen. In view of these considerations, this study selected glucose as the carbon source and attempted to investigate the effect of the denitrification of native denitrifying microbes in groundwater and artificially added denitrifying microbes under different combinations of oxygen and carbon sources.

2. Materials and Methods

2.1. Sampling. Studies have shown that, owing to the long-term application of nitrogen fertilizer in vegetable growing areas, the content of nitrate nitrogen in groundwater is very high. The water used in the experiments was taken from the groundwater in a vegetable growing area (36.71565°N, 120.31963°E), and the sampling depth was 5 m. After sampling on the spot, the water was placed into a polyethylene bottle that was washed twice with water samples and sealed with sealing film. The samples were transported to the laboratory in an incubator at 4°C with a built-in ice bag and processed within 24 hours.

2.2. Enrichment and Cultivation of Sludge. To investigate the effect of artificial addition of denitrifying microbes on denitrification, the sludge containing denitrifying microbes was collected from the aeration tank of a sewage treatment plant (35.94553°N, 120.21454°E), placed in a polyethylene bottle, transported to the laboratory at 25°C, and treated and cultured within 24 hours.

The nutrient solution was prepared with distilled water, and the main components were KNO₃ (0.37 g/L), C₆H₁₂O₆ (0.1562 g/L), CH₃OH (320 uL/L), and KH₂PO₄ (0.044 g/L).

The collected sludge was statically placed, and the supernatant was removed. The sedimentation of the lower layer of the sludge was packed into six 1 L conical bottles, which each contained 700 mL. A total of 350 mL of the nutrient solution was added to each conical bottle and sparged with high-purity nitrogen for 5 minutes. They were then sealed with film designed to maintain freshness and film to seal to maintain the anaerobic environment and cultured at 25°C for 14 days. During the period of cultivation, the nutrient solution was changed every 48 hours. The supernatant in the conical bottle was removed, and then, 350 mL of the newly configured nutrient solution was added and sparged with high-purity nitrogen for 5 minutes. The bottles were sealed with both types of film and cultured at 25°C. A volume of 350 mL of supernatant was discarded from the enriched sludge in each conical bottle, and all the excess sludge in the conical bottle was poured into a 5 L beaker and shaken well for inoculation. The settling ratio (SV%) of the mixed sludge was 90%. The concentration of the mixed sludge was 9838 mg/L. The C/N ratio of the mixed sludge was 16.3.

2.3. Experimental Design. In this study, two groups of experiments were designed to investigate the efficiency of denitrification of native denitrifying microbes in

groundwater and artificially added denitrifying microbes. Four conditions were established in each group, which were anaerobic, anaerobic with an added carbon source, aerobic, and aerobic with an added carbon source conditions. The anaerobic conditions were introduced by sparging with high-purity nitrogen for 3 minutes and sealing the bottle cap with sealing film.

Analytically pure glucose was used as the sole carbon source for microbial growth, and its concentration was controlled as 1 g/L. Each time, 100 mL of water samples was taken and placed in 150 mL volume serum bottles. The 15 mL of sludge that was cultured and enriched was inoculated to water. The serum bottle was placed in a BOD constant temperature incubator (American Hash Company, 205-2). The temperature was controlled at 15°C. The water samples were collected, and the indices were determined every 24 hours. The control consisted of three parallel samples. The specific experimental design is shown in Figure 1.

2.4. Test Index and Determination Method. The experimental indices include the pH, Oxidation-Reduction Potential (ORP), nitrate nitrogen (NO_3^- -N), nitrite nitrogen (NO_2^- -N), and ammonia nitrogen (NH_4^+ -N).

The supernatant of cultured water samples was tested, in which the pH and ORP were determined directly. The water samples were then filtered through a 0.45 μm filter membrane to determine the amounts of nitrate nitrogen (NO_3^- -N), nitrite nitrogen (NO_2^- -N), and ammonia nitrogen (NH_4^+ -N). All of the detection methods were conducted in accordance with the national standard method [48], and the main analytical methods are shown in Table 1.

2.5. Data Processing and Drawing Methods. The mean and standard deviation of three parallel samples were calculated under each culture condition. Origin software (OriginLab, Northampton, MA, USA) was used to draw the figures.

$$\text{the removal rate of nitrate nitrogen} = \frac{\text{reduced nitrate nitrogen}}{\text{initial nitrate nitrogen}} \cdot 100\% \quad (1)$$

3. Results and Discussion

The results of two groups of experiments were compared to determine the effects of native denitrifying microbes in groundwater and denitrifying microbes that were artificially added on denitrification in groundwater with a high concentration of nitrate nitrogen.

3.1. Removal of Nitrate Nitrogen. The changes in concentration of nitrate nitrogen in water samples under the action of native denitrifying microbes are shown in Figure 2(a). The trend of change of concentration of nitrate nitrogen in the water samples under the four culture conditions was basically the same and unstable. During the culture period, there was both an increase and a decrease in nitrate nitrogen. The

overall rate of removal increased during the first 5 days of the experiment. It reached its maximum value of 10% on day 4 under the condition of aerobic with an added carbon source. This indicated that denitrification occurred, and the degree of denitrification was the highest on day 4. The nitrate nitrogen only increased on day 3, possibly owing to ammoxidation [49]. The increase was the largest under the condition of anaerobic with an added carbon source, which changed from an initial concentration of 281.81 mg/L to 309.77 mg/L. The overall rate of removal decreased from days 6 to 12 of the experiment as the nitrate nitrogen accumulated. The rate of removal under the anaerobic condition decreased to 0.78% on day 12. In addition, from days 6 to 8, the nitrate nitrogen increased continuously under the condition of anaerobic with an added carbon source. The change in concentration was slightly different from those under the other three conditions. The concentration of nitrate nitrogen under the other three conditions increased at first and then decreased.

As seen in Figure 2(a), the rate of removal of nitrate nitrogen in the water samples was not obvious under the four conditions. The denitrification efficiency cannot be effectively promoted by adding a carbon source and creating an anaerobic condition. The final concentration of nitrate nitrogen was close to that of the initial concentration, and there was basically no removal of nitrate nitrogen. This shows that the native denitrifying microbes in water samples cannot efficiently promote denitrification when glucose is added as a carbon source and whether oxygen is provided or not, so they were unable to reduce the high concentration of nitrate nitrogen in water samples.

In contrast, as shown in Figure 2(b), the denitrification efficiency of artificially added denitrifying microbes in the four culture conditions showed obvious differences with the passage of culture time. The concentration of nitrate nitrogen in the water samples decreased to varying degrees. The efficiency of denitrification was the most effective under the condition of anaerobic with an added carbon source. The rate of removal increased gradually with the duration of the experiment. On day 7, the concentration of nitrate nitrogen decreased from an initial concentration of 266.2 mg/L to 27.9 mg/L, and the rate of removal reached 89.52%. The denitrification effect under the condition of aerobic with an added carbon source was less than that of anaerobic condition in which a carbon source was added. The concentration of nitrate nitrogen decreased gradually with the experiment, and the rate of removal gradually increased. On day 7, the concentration of nitrate nitrogen decreased from the initial concentration of 266.2 mg/L to 103.8 mg/L, and the rate of removal reached 55.16%. Denitrification was not performed effectively under anaerobic or aerobic conditions, and the concentration of nitrate remained basically the same. During the experiment, the concentration of nitrate nitrogen increased and decreased but decreased as a whole. On day 7 under the anaerobic condition, the concentration of nitrate nitrogen decreased from an initial concentration of 266.2 mg/L to 220.3 mg/L, and the rate of removal was 17.24%. The concentration of nitrate nitrogen increased slightly on days 2 and 5 of the experiment, which may be

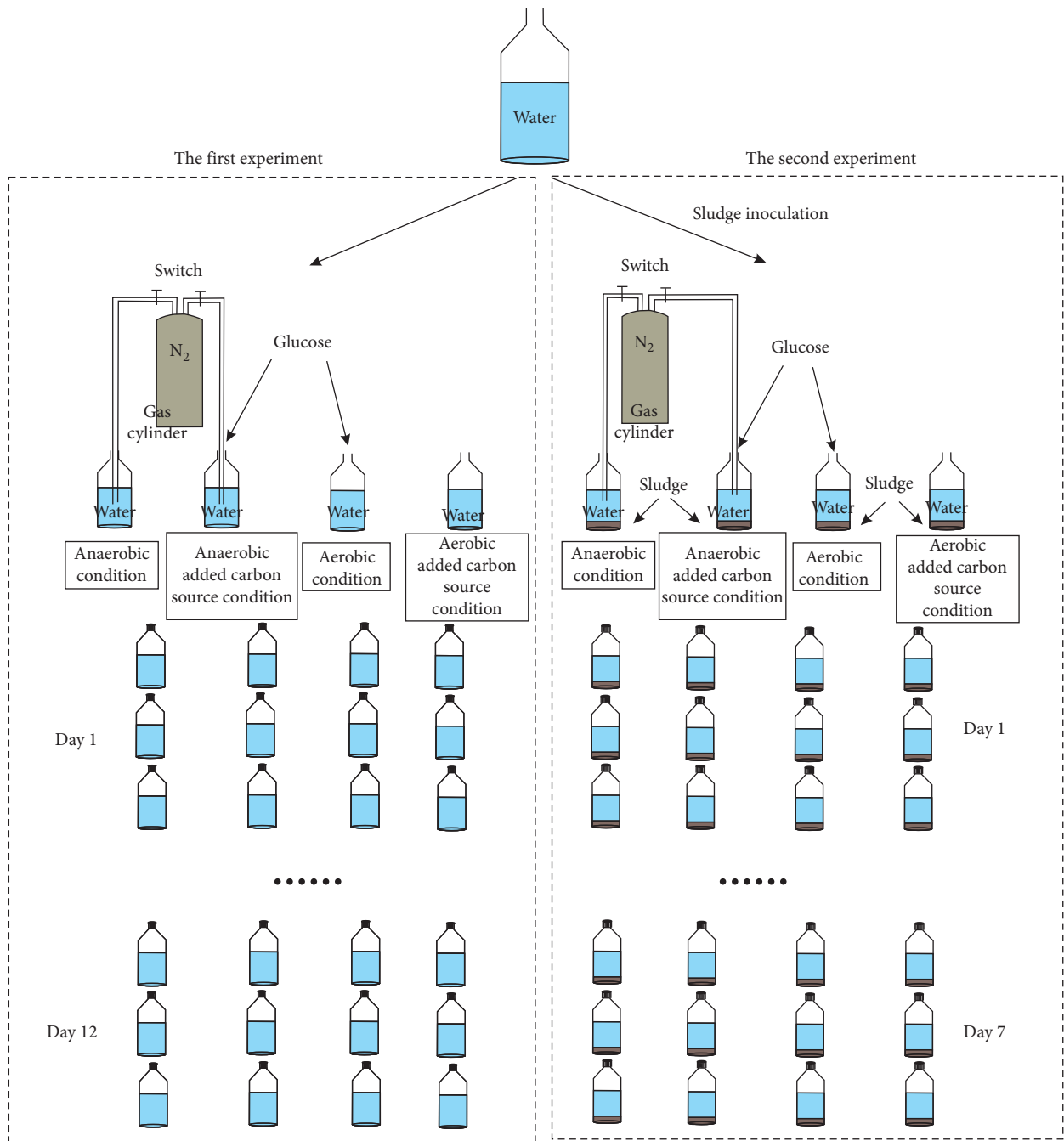


FIGURE 1: Diagram of the experimental design.

TABLE 1: Detection method of test index.

Serial number	Index	Detection method
1	pH	Hash electrode method
2	ORP	Hash electrode method
3	NO ₃ ⁻ -N	Ultraviolet spectrophotometry
4	NO ₂ ⁻ -N	N-(1-naphthyl)-ethylenediamine spectrophotometry
5	NH ₄ ⁺ -N	Nessler's reagent spectrophotometry

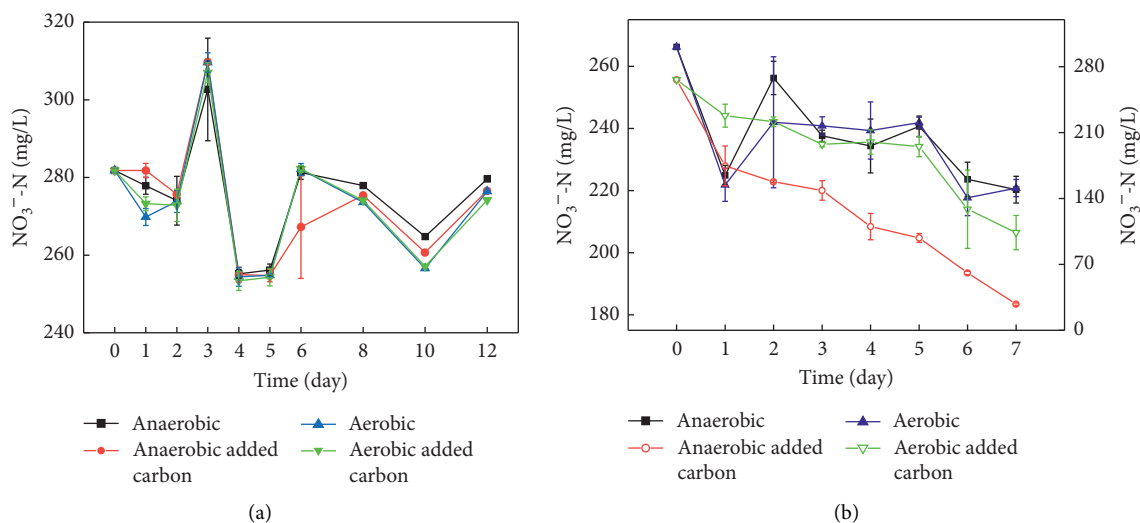


FIGURE 2: Changes in nitrate nitrogen. The solid point is based on the left longitudinal axis, and the hollow point is based on the right longitudinal axis.

owing to ammonification [49]. Under aerobic conditions, the concentration of nitrate nitrogen decreased from an initial concentration of 266.2 mg/L to 217.67 mg/L, and on day 6, the rate of removal was 18.23%. The concentration of nitrate nitrogen increased slightly on days 2, 5, and 7 of the experiment, which may be owing to ammonification [49].

Comparing the experimental results of the two groups, there was a significant difference in the rate of removal of nitrate nitrogen under the influence of the two types of microbes. The rate of removal of nitrate nitrogen in the water samples in which artificially added denitrifying microbes had been added was significantly better than that under the action of native denitrifying microbes. In addition, the maximum rate of removal of nitrate nitrogen under the action of native denitrifying microbe was only 10%. The rate of removal is not obvious, which shows that the native denitrifying microbes in groundwater are not capable of removing high concentrations of nitrate nitrogen in water samples. In addition, large amounts of denitrifying microbes are needed to promote the denitrification effect, so as to achieve the purpose of reducing high concentrations of nitrate nitrogen in groundwater.

In addition, when the changes in concentration of nitrate nitrogen of artificially added denitrifying microbe water samples under four culture conditions were compared, it can be seen that artificially added denitrifying microbes produced the strongest activity under anaerobic condition in which glucose was provided as a carbon source. It was highly effective at denitrifying a high concentration of nitrate nitrogen in groundwater with a rate of removal rate as high as 89.25%. The experimental results showed that for the groundwater with a high concentration of nitrate nitrogen, the introduction of denitrifying microbes and the provision of an anaerobic environment while using glucose as a carbon source could significantly reduce the concentration of nitrate nitrogen in the groundwater. However, the lowest concentration of nitrate nitrogen in the water samples was 27.9 mg/L, which still does not meet the quality standard of

class III groundwater (≤ 20 mg/L). The experimental culture time was too short and did not provide adequate time for the complete denitrification of the nitrate nitrogen.

3.2. Accumulation of Nitrite Nitrogen. It can be seen in Figure 3(a) that under the action of native denitrifying microbes, the accumulation of nitrite nitrogen in the water samples under the four culture conditions was not obvious. The concentration of nitrite nitrogen increased at first and then decreased during the experiment. The change in concentration of nitrite nitrogen under the condition of anaerobic with an added carbon source was more obvious than that under the other three conditions. The concentration was the highest on day 12 of the experiment, which increased from an initial concentration of 0.004 mg/L to 0.6 mg/L. The concentration of nitrite nitrogen under the condition of aerobic with an added carbon source changed more gradually than that under the condition of anaerobic with an added carbon source. Additionally, the concentration was highest on day 8, representing an increase from an initial concentration of 0.004 mg/L to 0.123 mg/L. With the progression of the experiment, the concentration of nitrite nitrogen decreased again, and the concentration decreased to 0.057 mg/L on day 12 of the experiment. The change in concentration of nitrite nitrogen under anaerobic and aerobic conditions tended to be consistent, and it was very small. After 12 days of culture, the concentration of nitrite nitrogen under the anaerobic condition changed from 0.004 mg/L to 0.008 mg/L. Under the aerobic condition, the concentration of nitrite nitrogen changed from 0.004 mg/L to 0.009 mg/L.

Thus, it can be seen that under the action of native denitrifying microbes, the accumulation of nitrite nitrogen in water samples under the four culture conditions was not obvious. The concentration of nitrate nitrogen was basically unchanged, which provides additional evidence that the degree of denitrification was not high enough. The native

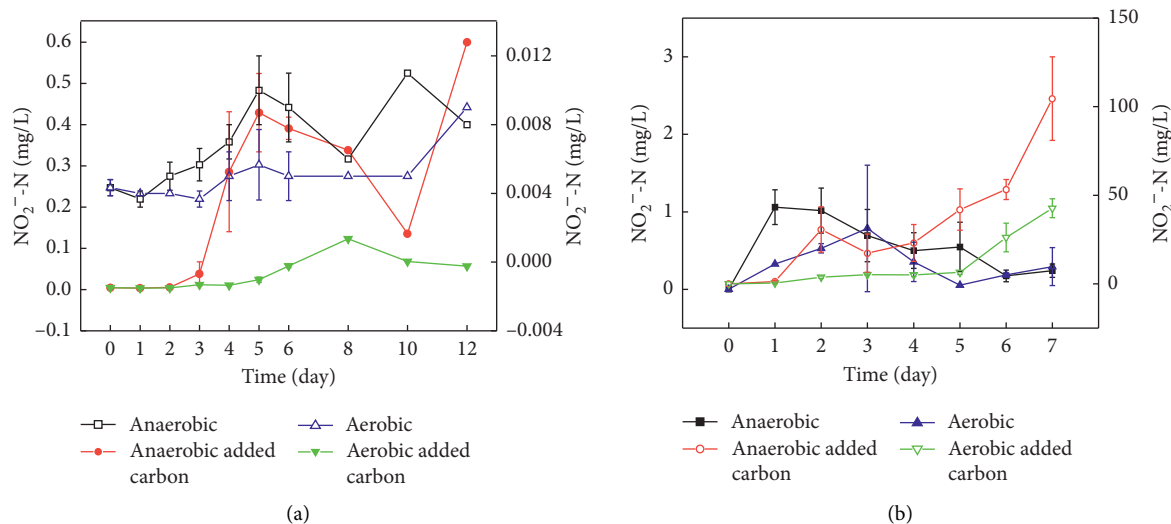


FIGURE 3: Changes in nitrite nitrogen. The solid point is based on the left longitudinal axis, and the hollow point is based on the right longitudinal axis.

denitrifying microbes in water samples failed to effectively promote denitrification under the combined conditions of whether or not glucose was added as a carbon source, and oxygen was provided.

As shown in Figure 3(b), the concentration of nitrite nitrogen in the water samples increased as a whole under anaerobic and aerobic conditions with an added carbon source, and nitrite nitrogen accumulated to greater amounts. The concentration of nitrite nitrogen in the anaerobic condition with an added carbon source increased the most significantly compared with the other three conditions, and the concentration increased from 0.003 mg/L to 104.533 mg/L on day 7 of the experiment. Under the condition of aerobic with an added carbon source, the concentration of nitrite nitrogen increased significantly, from the concentration of 0.003 mg/L to 42.667 mg/L on day 7 of the experiment. The overall change in the concentrations of nitrite nitrogen under anaerobic and aerobic conditions was almost the same, showing a trend of increasing at first and then decreasing. Compared with the original water sample, there was an accumulation of nitrite nitrogen, but it was very low. Under the anaerobic condition, the concentration of nitrite nitrogen was the highest on the first day of the experiment and increased from 0.003 mg/L to 1.061 mg/L. The concentration of nitrite nitrogen decreased again to 0.24 mg/L on day 7 of the experiment. Under the aerobic condition, the concentration of nitrite nitrogen was the highest on day 3 of the experiment, which resulted in an increase from 0.003 mg/L to 0.787 mg/L. The concentration of nitrite nitrogen decreased again to 0.293 mg/L on day 7 of the experiment.

Under the action of artificially added denitrifying microbes, nitrite nitrogen in the water accumulated to varying degrees under the four culture conditions but only slightly under anaerobic and aerobic conditions. The accumulation under the conditions of anaerobic with an added carbon source and aerobic with an added carbon source was more

obvious, particularly under the condition of anaerobic with an added carbon source. Simultaneously, the nitrate nitrogen declined the most quickly under the condition of anaerobic with an added carbon source, which showed that the denitrification effect was the strongest in the water sample under the condition of anaerobic with an added carbon source, and the artificially added denitrifying microbes played a role and effectively promoted denitrification.

Nitrite nitrogen is the intermediate product of the denitrification process, and this compound accumulated during both experiments. In addition, the faster the concentration of nitrate decreased, the more nitrite nitrogen accumulated, which is the incomplete embodiment of denitrification. The reason for this phenomenon could be that the culture time was not long enough; the reaction container was a serum bottle; the volume was fixed, and denitrification was not complete. During the process of denitrification, the rate of action of nitrate reductase is faster than that of nitrite reductase. Under the conditions suitable for denitrification, a large amount of nitrate can be rapidly reduced to nitrite, resulting in a large amount of accumulation. Only when denitrification is complete will the accumulation of nitrite gradually decrease. In addition, the culture temperature of this experiment was set at 15°C. Zhang Lin et al. [50] found that the temperature had a substantial effect on the accumulation of nitrite nitrogen during the process of denitrification, decreasing the activity of the enzyme and inhibiting the transformation of nitrite nitrogen to ammonia nitrogen at 15°C, thus, resulting in the accumulation of nitrite nitrogen. The factors that affect the rate of growth of microorganisms, such as C/N and the type of carbon source, also led to the accumulation of nitrite nitrogen [2, 51–53]. At the beginning of the experiments, the concentration of carbon source was 1 g/L, and the C/N was not well controlled. The lack of a carbon source in the latter stage of the reaction may also lead to the accumulation of nitrite nitrogen. In future experiments, we can choose a larger

reaction container to prolong the continuous culture time and change the concentration of carbon source and the type of carbon source to explore the nutrient carbon source that can enhance the effect of microbial denitrification.

3.3. Accumulation of Ammonia Nitrogen. As shown in Figure 4(a), the concentration of ammonia nitrogen in water increased at first and then decreased under the four culture conditions. Additionally, ammonia nitrogen did not obviously accumulate during the experiment. Under the anaerobic condition, the concentration of ammonia nitrogen reached its maximum on day 3 and increased from 0.037 mg/L to 0.39 mg/L. As the experiment continued, the concentration of ammonia nitrogen decreased to 0.163 mg/L on day 5 and tended to be stable. The concentration of ammonia nitrogen was 0.14 mg/L on day 12 of the experiment. Under the condition of anaerobic with an added carbon source, the change of ammonia nitrogen concentration was small, and the trend was relatively moderate. The concentration of ammonia nitrogen reached its maximum on day 2 of the experiment, increasing from 0.037 mg/L to 0.157 mg/L and gradually stabilizing with the experiment. The concentration was 0.07 mg/L on day 12 of the experiment. The concentration of ammonia nitrogen under the anaerobic condition and the condition of anaerobic with an added carbon source barely changed and was less than 0.5 mg/L, which meets the Chinese drinking water standard. Under the aerobic condition, the concentration of ammonia nitrogen increased from 0.037 mg/L to 0.27 mg/L on the first day, then decreased to 0.123 mg/L on day 3, and stabilized from days 3 to 6. With the progress of the experiment, the concentration increased rapidly from days 6 to 8, reached a maximum value of 0.56 mg/L on day 8, decreased gradually, and then decreased to 0.03 mg/L on day 12 of the experiment. Compared with the original water sample, there was no accumulation of ammonia nitrogen. Under the condition of aerobic with an added carbon source, ammonia nitrogen accumulated the most on day 5, increased from the initial concentration of 0.037 mg/L to 0.27 mg/L, decreased to 0 on day 6, and then almost no longer accumulated.

The formation of ammonium suggested that dissimilatory nitrate reduction to ammonia (DNRA) was occurring. DNRA is a side reaction of denitrification and competes with denitrification [54–56]. The balance of denitrification and DNRA depends on temperature, oxygen, nitrate availability, and organic carbon [54, 57]. Some data showed that using glucose as an organic carbon source can easily stimulate the formation of ammonia nitrogen [58]. Ammonia nitrogen is unstable and easily oxidized to nitrate. Under the aerobic condition, the concentration of ammonia nitrogen increased significantly only on the first day and from days 6 to 8. Under the aerobic condition with an added carbon source, the concentration of ammonia nitrogen only increased from days 3 to 5, which could be owing to the decrease in nitrate concentration and the occurrence of DNRA reaction. In addition, the concentration of ammonia nitrogen was less than 0.2 mg/L during the whole experiment. Anaerobic condition with an added carbon source is more conducive to denitrification, less nitrate is dissimilated

to ammonium, and the concentration of ammonia nitrogen was always less than 0.2 mg/L. Under the anaerobic condition, ammonia nitrogen is not easily oxidized, and the concentration of ammonia nitrogen increased many times over the course of the experiment.

As seen in Figure 4(b), the change of ammonia nitrogen under the conditions of anaerobic with an added carbon source and aerobic with an added carbon source was basically the same, and the trend line is relatively smooth, showing a trend of increasing at first and then decreasing. Under the anaerobic condition, the concentration of ammonia nitrogen reached its maximum on day 2 and increased from 0.08 mg/L to 0.54 mg/L. With the progression of the experiment, the concentration decreased gradually to 0.3 mg/L on day 7. Under the condition of aerobic with an added carbon source, the concentration of ammonia nitrogen reached its maximum on day 3 and increased from 0.08 mg/L to 2.4 mg/L. The concentration decreased gradually during the course of the experiment, dropping to 0.617 mg/L on day 7 of the experiment. Under the condition of anaerobic with an added carbon source, the concentration of ammonia nitrogen increased as a whole. It consistently accumulated during the first 3 days of the experiment from an initial concentration of 0.08 mg/L to the maximum concentration of 3.67 mg/L and decreased to 0.67 mg/L on day 4. It then increased gradually with the progress of the experiment, reaching 3.15 mg/L on day 7 of the experiment. Under the aerobic condition, the concentration of ammonia nitrogen increased at first and then decreased. The trend line fluctuated greatly. The accumulation of ammonia nitrogen was the highest on day 2 of the experiment, representing an increase from 0.08 mg/L to 0.92 mg/L. With the progress of the experiment, it decreased to 0 on day 6 and remained stable until the end of the experiment.

Denitrification and DNRA are two processes that exist simultaneously and compete with each other in both aerobic and anaerobic environments. Under the aerobic condition and the condition of aerobic with an added carbon source, ammonia nitrogen obviously accumulated only on day 2 owing to DNRA, but with the progress of the experiment, the ammonia nitrogen was easily oxidized; the concentration decreased gradually, and the final concentration was low. Additionally, the concentration of ammonia nitrogen gradually decreased to 0 under aerobic conditions. On the whole, the accumulation of ammonia nitrogen in the water sample under the condition of anaerobic with an added carbon source was more obvious than that under the other three conditions. Ammonia nitrogen is not easily oxidized, and the DNRA process produces ammonia nitrogen, while glucose as a carbon source readily stimulates the formation of ammonia nitrogen [58]. However, not much of this compound accumulates. Ammonia oxidation [49] may have only occurred on day 4, and the concentration of ammonia nitrogen decreased. Under anaerobic conditions, ammonia nitrogen is not easily oxidized. However, owing to the addition of denitrifying bacteria, the amount of denitrification is relatively strong. DNRA only occurs at the beginning of the experiment, and a small amount of ammonia nitrogen accumulates.

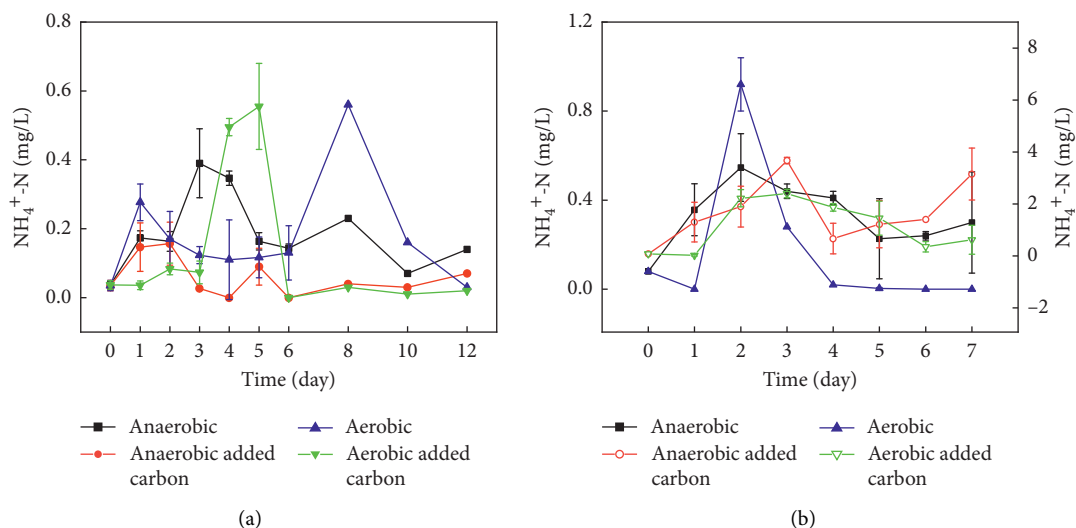


FIGURE 4: Changes in ammonia nitrogen. The solid point is based on the left longitudinal axis, and the hollow point is based on the right longitudinal axis.

At the beginning of the experiment, ammonia nitrogen accumulated to varying degrees under the four culture conditions, which may be owing to the sufficient dissolved organic matter or added carbon source in the water sample at the initial stage, and the dissimilation of nitrate nitrogen to ammonia nitrogen under the action of artificially added denitrifying microbes and native denitrifying microbes in water. In the latter stage, the denitrification effect gradually became strong, the effect of DNRA was weakened, and the difference of the four culture conditions led to a difference in the final accumulation of ammonia nitrogen.

In the two groups of experiments, the accumulation of ammonia nitrogen was not obvious as a whole, and there was only a certain accumulation of ammonia nitrogen in the water when denitrifying microbes were added artificially under the condition of anaerobic with an added carbon source. It is hypothesized that the reason for this phenomenon could be that the DNRA process and the existence of microorganisms and anaerobic conditions with an added carbon source promote the activity of microorganisms and increase the rate of release of ammonia nitrogen.

3.4. Changes in pH. The changes in pH in water under four culture conditions are shown in Figure 5(a). The change of pH under anaerobic and aerobic conditions was basically the same, and the whole trend increased at first and then decreased. On the first day, the water samples changed from weakly acidic to weakly alkaline and maintained this alkaline environment throughout the experiment. Combined with the change in nitrate nitrogen, denitrification occurred at the beginning of the experiment, the production of alkaline substances increased the pH, and the water sample was weakly alkaline [59]. There was a sudden increase in pH from day 6 to 8 of the experiment. The pH increased to 8.24 under anaerobic conditions and to 7.85 under aerobic conditions. Combined with the change in nitrate nitrogen,

this may be owing to the enhancement of denitrification and the production of alkaline substances [59]. The pH value increased. With the progress of the experiment, the pH gradually decreased. On day 12 of the experiment, the pH decreased to 7.36 under anaerobic conditions and to 7.11 under aerobic conditions. The natural denitrifying microbes in the water samples can produce organic acids [59] by biochemical reactions with the help of original organic matter, resulting in a gradual decrease in the pH. The change in pH was basically the same under the conditions of anaerobic with an added carbon source and aerobic with an added carbon source. On the first day of the experiment, the water samples changed from weakly acidic to weakly alkaline, but the trend line was relatively smooth. Additionally, the water sample was weakly alkaline all of the time. On day 12 of the experiment, the pH was 7.05 under the condition of anaerobic with an added carbon source and 7.11 under the condition of aerobic with an added carbon source. Combined with the change in nitrate nitrogen, denitrification occurred at the beginning of the experiment, and the production of alkaline substances increased the pH. The water sample was weakly alkaline [59].

As shown in Figure 5(b), the change in pH under anaerobic and aerobic conditions was basically the same. The trend line was relatively flat, and the value changed from 6.68 to 7.5. The water sample was weakly alkaline. Under the condition of anaerobic with an added carbon source, the change in pH was relatively smooth. The value always fluctuated around 6.68, but it was always less than 7, and the water sample was weakly acidic. Under the condition of aerobic with an added carbon source, the pH fluctuated greatly, and the value changed from 6.68 to 8.2. The sample fluctuated from 5 to 8.5. Owing to the alkaline substance produced by denitrification [59], the water sample changed from weakly acidic to weakly alkaline on the first day. It became acidic from day 2 to 5, which may be owing to the strong biochemical effect of microbes using external a carbon source

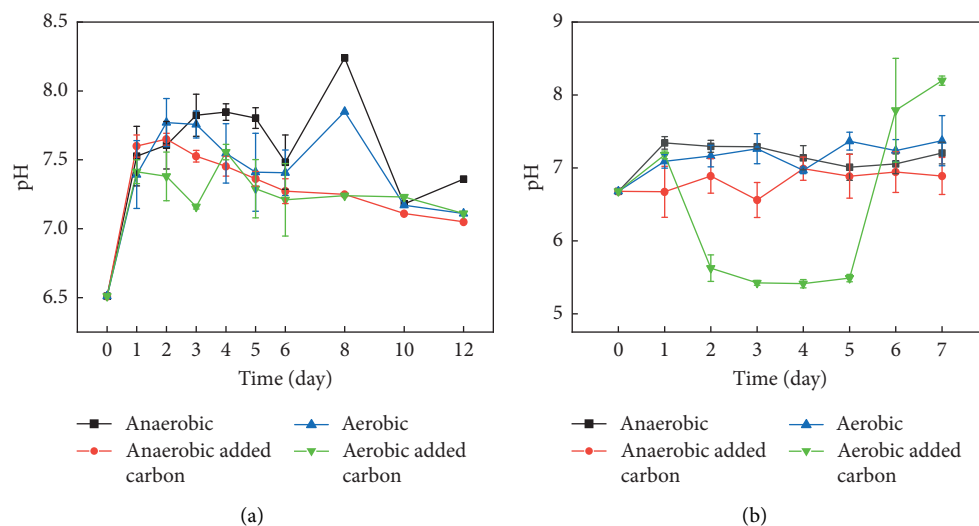


FIGURE 5: Changes in pH.

and the production of more organic acids [59]. In addition, the pH was between 5 and 6. It became weakly alkaline from day 6 to 7. Combined with the change in nitrate nitrogen, the amount of denitrification was stronger during this period, resulting in an increase in the pH.

Denitrification itself can increase the pH by releasing CO_2 and hydroxide (OH^-). Normally, these combine to yield HCO_3^- , but if the production of OH^- exceeds that of CO_2 , the pH can increase [60]. The dynamic balance of alkaline substances produced by denitrification and organic acids produced by biochemical reactions will affect the change in the pH of the system.

Under the action of artificially added denitrifying microbes, combined with the changes in nitrate nitrogen, the changes in pH in water samples as a whole were visible. Under anaerobic and aerobic conditions, the water sample was maintained in a weakly alkaline environment, which could be that more alkaline substances were produced by denitrification than organic acids produced by biochemical action [59]. And it was in a relatively stable state, so that the pH value of the water sample was more stable. Under the condition of anaerobic with an added carbon source, the water sample was maintained in the weakly acidic environment. The reaction was relatively strong, and more organic acids were produced following the addition of glucose as the carbon source. Additionally, denitrification was very strong, and the two effects were in a state of equilibrium to ensure that the water sample maintained a weakly acidic environment. The substantial change of pH value under the condition of aerobic with an added carbon source may be owing to the instability of denitrification and biochemical reactions under these culture conditions.

Too high or too low a pH value will affect the denitrification effect. Although denitrification still occurs when the pH value exceeds the optimal range, it may lead to the accumulation of intermediate toxic products (such as nitrite) [50]. When the changes of pH in the two groups of experiments were compared and connected with the changes

in nitrate nitrogen and nitrite nitrogen concentration under different conditions, a pH value between 6.5 and 7 was found to be suitable for the growth and reproduction of denitrifying microbes. It aided in denitrification.

3.5. Changes in the ORP. As shown in Figure 6(a), the change of ORP under anaerobic and aerobic conditions was basically the same and showed a downward trend as a whole. The ORP fluctuated greatly from days 4 to 10 of the experiment. On day 12 of the experiment, the ORP decreased from 211.2 mV to 132 mV under anaerobic conditions. In addition, the ORP decreased from 211.2 mV to 146.1 mV under aerobic conditions. Under the conditions of anaerobic with an added carbon source and aerobic with an added carbon source, the change in ORP was basically the same. It showed a downward trend as a whole, and the trend line in the later stage of the experiment was relatively flat. On day 12 of the experiment, the ORP decreased from 211.2 mV to 149.4 mV under the condition of anaerobic with an added carbon source, and the ORP decreased from 211.2 mV to 154.4 mV under the condition of aerobic with an added carbon source.

The ORP can characterize the relative degree of oxidation or reduction. When the ORP is positive, the solution can oxidize to some extent. When the ORP is negative, the solution shows some degree of reduction. Its numerical change reflects the relative change of oxidation and reduction. The ORP decreased on the first day of the experiment. Combined with the change in nitrate nitrogen, it showed that denitrification occurred, the ability to oxidize decreased, and reduction occurred in the system. With the progress of the experiment, the ORP fluctuated and gradually stabilized, indicating that denitrification and ammonia oxidation occurred in the system. Denitrification is a reduction and will reduce the ability to oxidize and ORP. Ammonia oxidation consists of oxidation, which will increase the ability to oxidize and ORP. The change in ORP reflected the relative degree of denitrification and

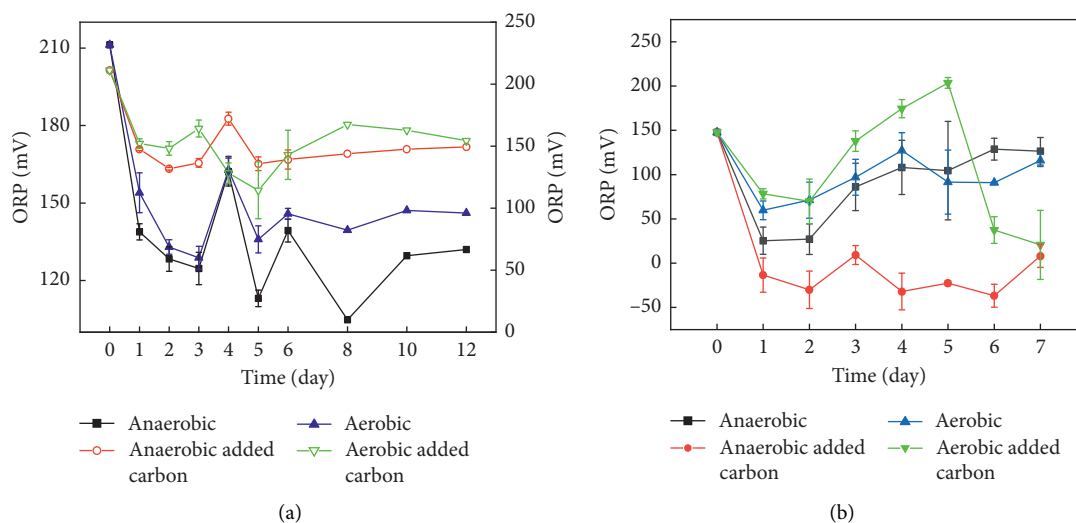


FIGURE 6: Changes in ORP. The solid point is based on the left longitudinal axis, and the hollow point is based on the right longitudinal axis.

ammoxidation. Thus, it can be seen that there was some ability to oxidize in the water under the four culture conditions. Denitrification occurred in the water, but it was not strong enough to make the water sample reductive.

As shown in Figure 6(b), the changes of ORP under anaerobic and aerobic conditions were basically the same, showing a trend of decreasing at first and then increasing. Under anaerobic conditions, the ORP decreased from 147.8 mV to 27.1 mV on the first day, and the tendency to oxidize in the water sample decreased. It then gradually increased with the progress of the experiment. The ORP increased to 126.33 mV on day 7. Under aerobic conditions, the ORP decreased from 147.8 mV to 59.7 mV on the first day, and the tendency of the water sample to oxidize decreased. It then gradually increased with the progress of the experiment. The ORP increased to 116.03 mV on day 7. Combined with the changes of nitrate nitrogen under these two conditions, denitrification was strong at the beginning of the experiment owing to the artificial addition of denitrifying microbes. The ORP decreased rapidly on the first day, and the ability of the water sample to oxidize decreased. With the progress of the experiment, ammoxidation occurred in the system to enhance the ability of the water to oxidize, and the ORP gradually increased. Simultaneously, there was no carbon source added. Because of the lack of organic carbon in water, the weakening of denitrification may also lead to an increase in ORP.

Under the condition of aerobic with an added carbon source, the ORP decreased during the first 5 days and then increased. At the beginning of the experiment, owing to the artificial addition of the denitrifying microbes and the addition of a carbon source, the process of denitrification was strong. Additionally, the ORP decreased rapidly on days 1 and 2, and the ability of the water sample to oxidize weakened. In the later stage, the aerobic environment enhanced the occurrence of ammoxidation, the ORP increased, and the ability to oxidize increased. The ORP then quickly decreased to 20.6 mV from days 6 to 7. Combined with the changes in nitrate nitrogen,

denitrification was enhanced, and the ability of water samples to oxidize decreased during this period. Under the condition of anaerobic with an added carbon source, the changes in the ORP showed a downward trend as a whole, which decreased rapidly to a negative value on the first day. The trend line changed smoothly from days 2 to 7. Most of the ORP had a negative value. In the reaction system, denitrification was the strongest, ammoxidation was relatively weak, and the water samples showed a tendency to be reduced.

The ORP value reflected the redox property to some extent. A comparison of the data of two groups of experiments indicated that the water sample with artificially added denitrifying microbes showed some degree of reducibility under the condition of anaerobic with an added carbon source, which was beneficial to denitrification.

The experimental results showed that with the effect of the artificial addition of denitrifying microbes, the denitrification effect was the most effective under the condition of anaerobic with an added carbon source, which could effectively reduce the content of nitrate nitrogen. During the course of the experiment, the amount of nitrate nitrogen continuously decreased, and the rate of removal was the highest. Both nitrite nitrogen and ammonia nitrogen accumulated. Ammonia nitrogen accumulated to a lower degree, and the accumulation of nitrite was obvious. Sludge as denitrifying microbe can effectively promote denitrification.

Future areas of research will involve how to reduce the accumulation of nitrite nitrogen at the same time as removing the nitrate nitrogen and completely promoting denitrification and how to better apply bioremediation to the actual remediation of groundwater pollution.

4. Conclusions

Through two groups of laboratory experiments, this paper explored the feasibility and effectiveness of native denitrifying and artificially added denitrifying microbe sat

removing high concentrations of nitrate nitrogen in groundwater under different combinations of oxygen and carbon source.

Under the setting of four culture conditions, the concentration of nitrate nitrogen in the water sample that was subjected to native denitrifying microbes basically changed the same amount, and the change was unstable. There were processes of both reduction and an increase in nitrate nitrogen. In addition, the highest rate of removal of nitrate nitrogen was only 10%. This percentage is inadequate for remediation effects. The native denitrifying microbes in the water lacked the ability to remove the high concentration of nitrate nitrogen in the water sample.

Under the same four culture conditions, the concentration of nitrate nitrogen in water samples to which denitrifying microbes were artificially added changed significantly, and they decreased significantly with the increase in culture time. The change in concentration of nitrate nitrogen and the changes in nitrite nitrogen, ammonia nitrogen, pH, and ORP can reflect the ability of denitrifying microbes to remove nitrate nitrogen in the water under the four culture conditions. The removal was most effective under the condition of anaerobic with an added carbon source, and the rate of removal reached as high as 89.52%. In addition, the rate of removal under the condition of aerobic with an added carbon source was more effective, and the rate of removal was 55.16%. The rate of removal under anaerobic and aerobic conditions was not very high, and both the removal rates were less than 20%. Therefore, the artificially added denitrifying microbes have higher activity and a more significant effect under anaerobic conditions with the provision of glucose as a carbon source, which can effectively promote denitrification in water and reduce the concentration of nitrate nitrogen in the water.

Compared with the changes in five indices in water treated by microbes from different sources under the same culture condition, artificially added denitrifying microbes functioned significantly better than the native denitrifying microbes in water samples, which could better promote denitrification.

Data Availability

The raw data required to reproduce these findings cannot be shared at this time as the data also form part of an ongoing study.

Conflicts of Interest

The authors declare that there are no conflicts of interest regarding the publication of this article.

Acknowledgments

This research was supported by the Scientific Research Foundation of Qingdao Geo-Engineering Surveying Institute (No. 2019-QDDZYKY01).

References

- [1] K. Ganesh, J. B. Joshi, and S. B. Sawant, "Cellulase deactivation in a stirred reactor," *Biochemical Engineering Journal*, vol. 4, no. 2, pp. 137–141, 2000.
- [2] M. Gómez, E. Hontoria, and J. González-López, "Effect of dissolved oxygen concentration on nitrate removal from groundwater using a denitrifying submerged filter," *Journal of Hazardous Materials*, vol. 90, no. 3, pp. 267–278, 2002.
- [3] M. Volokita, A. Abeliovich, and M. I. M. Soares, "Denitrification of groundwater using cotton as energy source," *Water Science and Technology*, vol. 34, no. 1-2, pp. 379–385, 1996.
- [4] M. Volokita, S. Belkin, A. Abeliovich, and M. I. M. Soares, "Biological denitrification of drinking water using newspaper," *Water Research*, vol. 30, no. 4, pp. 965–971, 1996.
- [5] K. B. Moore, B. Ekwurzel, B. K. Esser, G. B. Hudson, and J. E. Moran, "Sources of groundwater nitrate revealed using residence time and isotope methods," *Applied Geochemistry*, vol. 21, no. 6, pp. 1016–1029, 2006.
- [6] Z. Qiao, R. Sun, Y. Wu et al., "Characteristics and metabolic pathway of the bacteria for heterotrophic nitrification and aerobic denitrification in aquatic ecosystems," *Environmental Research*, vol. 191, p. 110069, 2020.
- [7] X. Liu, Y. Wu, R. Sun et al., " $\text{NH}_4^+\text{-N}/\text{NO}_3^-\text{-N}$ ratio controlling nitrogen transformation accompanied with $\text{NO}_2^-\text{-N}$ accumulation in the oxic-anoxic transition zone," *Environmental Research*, vol. 189, p. 109962, 2020.
- [8] Z. Qiao, Y. Wu, J. Qian et al., "A lab-scale study on heterotrophic nitrification-aerobic denitrification for nitrogen control in aquatic ecosystem," *Environmental Science and Pollution Research*, vol. 27, no. 9, pp. 9307–9317, 2020.
- [9] A. M. Fan, "Nitrate and nitrite in drinking water: a toxicological review," *Encyclopedia of Environmental Health*, pp. 137–145, 2011.
- [10] S. Khademikia, Z. Rafiee, M. M. Amin, P. Poursafa, M. Mansourian, and A. Modaberi, "Association of nitrate, nitrite, and total organic carbon (TOC) in drinking water and gastrointestinal disease," *Journal of Environmental and Public Health*, vol. 20134 pages, 2013.
- [11] P. M. Vitousek, J. D. Aber, R. W. Howarth et al., "Human alteration of the global nitrogen cycle: sources and consequences," *Ecological Applications*, vol. 7, no. 3, pp. 737–750, 1997.
- [12] J. N. Kostraba, E. C. Gay, M. Rewers, and R. F. Hamman, "Nitrate levels in community drinking waters and risk of IDDM: an ecological analysis," *Diabetes Care*, vol. 15, no. 11, pp. 1505–1508, 1992.
- [13] M. Qasemi, M. Farhang, H. Biglari et al., "Health risk assessments due to nitrate levels in drinking water in villages of Azadshahr, Northeastern Iran," *Environmental Earthences*, vol. 77, no. 23, p. 782, 2018.
- [14] H. Rezaei, A. Jafari, B. Kamarehie et al., "Health-risk assessment related to the fluoride, nitrate, and nitrite in the drinking water in the Sanandaj, Kurdistan County, Iran," *Human and Ecological Risk Assessment: An International Journal*, vol. 25, no. 5, pp. 1242–1250, 2019.
- [15] M. Hurtado-Martinez, B. Muñoz-Palazon, V. M. Robles-Arenas, A. Gonzalez-Martinez, and J. Gonzalez-Lopez, "Biological nitrate removal from groundwater by an aerobic granular technology to supply drinking water at pilot-scale," *Journal of Water Process Engineering*, vol. 40, p. 101786, 2021.
- [16] M. I. M. Soares, "Biological denitrification of groundwater," *Environmental Challenges*, vol. 40, pp. 183–193, 2000.

- [17] A. Abdelouas, L. Deng, E. Nuttall, W. Lutze, B. Fritz, and J.-L. Crovisier, "Réduction in situ des ions nitrate dans des eaux par les bactéries indigènes," *Comptes Rendus de l'Académie des Sciences-Series IIA-Earth and Planetary Science*, vol. 328, no. 3, pp. 161–166, 1999.
- [18] P. M. Ayyasamy, K. Shanthy, P. Lakshmanaperumalsamy, S.-J. Lee, N.-C. Choi, and D.-J. Kim, "Two-stage removal of nitrate from groundwater using biological and chemical treatments," *Journal of Bioscience and Bioengineering*, vol. 104, no. 2, pp. 129–134, 2007.
- [19] G. M. Cao, L. H. Zhang, M. Sheng, and Y. D. Liu, "Biological denitrification of groundwater by a composite membrane bioreactor," *Environmental Engineering*, vol. 864–867, pp. 2083–2089, 2014.
- [20] X. Wang and J. Wang, "Removal of nitrate from groundwater by heterotrophic denitrification using the solid carbon source," *Science in China Series B: Chemistry*, vol. 52, no. 2, pp. 236–240, 2009.
- [21] V. Matěj, S. Čížinská, J. Krejčí, and T. Janoch, "Biological water denitrification—a review," *Enzyme & Microbial Technology*, vol. 14, no. 3, pp. 170–183, 1992.
- [22] R. B. Mellor, J. Ronnenberg, W. H. Campbell, and S. Diekmann, "Reduction of nitrate and nitrite in water by immobilized enzymes," *Nature*, vol. 355, no. 6362, pp. 717–719, 1992.
- [23] N. Dineshkumar, C. Saravanakumar, M. Vasanth, M. Muralidhar, and S. V. Alavandi, "Genetic and physiological characterization of denitrifying bacteria from brackishwater shrimp culture ponds of India," *International Biodeterioration & Biodegradation*, vol. 92, pp. 49–56, 2014.
- [24] J. Smith, C. Wagner-Riddle, and K. Dunfield, "Season and management related changes in the diversity of nitrifying and denitrifying bacteria over winter and spring," *Applied Soil Ecology*, vol. 44, no. 2, pp. 138–146, 2010.
- [25] W. J. Pabich, I. Valiela, and H. F. Hemond, "Relationship between DOC concentration and vadose zone thickness and depth below water table in groundwater of Cape Cod, USA," *Biogeochemistry*, vol. 55, no. 3, pp. 247–268, 2001.
- [26] M. R. Trudell, R. W. Gillham, and J. A. Cherry, "An in-situ study of the occurrence and rate of denitrification in a shallow unconfined sand aquifer," *Journal of Hydrology*, vol. 83, no. 3–4, pp. 251–268, 1986.
- [27] L. A. Schipper and M. Vojvodić-Vuković, "Nitrate removal from groundwater and denitrification rates in a porous treatment wall amended with sawdust," *Ecological Engineering*, vol. 14, no. 3, pp. 269–278, 2000.
- [28] M. A. Robinson-Lora and R. A. Brennan, "The use of crab-shell chitin for biological denitrification: batch and column tests," *Bioresource Technology*, vol. 100, no. 2, pp. 534–541, 2009.
- [29] T. B. Moorman, T. B. Parkin, T. C. Kaspar, and D. B. Jaynes, "Denitrification activity, wood loss, and N₂O emissions over 9 years from a wood chip bioreactor," *Ecological Engineering*, vol. 36, no. 11, pp. 1567–1574, 2010.
- [30] L. A. Schipper, G. F. Barkle, J. C. Hadfield, M. Vojvodic-Vukovic, and C. P. Burgess, "Hydraulic constraints on the performance of a groundwater denitrification wall for nitrate removal from shallow groundwater," *Journal of Contaminant Hydrology*, vol. 69, no. 3–4, pp. 263–279, 2004.
- [31] C. Su and R. W. Puls, "Removal of added nitrate in cotton burr compost, mulch compost, and peat: mechanisms and potential use for groundwater nitrate remediation," *Chemosphere*, vol. 66, no. 1, pp. 91–98, 2007.
- [32] S. Aslan and A. Turkman, "Nitrate and pesticides removal from contaminated water using biodenitrification reactor," *Process Biochemistry*, vol. 41, no. 4, pp. 882–886, 2006.
- [33] M. A. Gómez, J. González-López, and E. Hontoria-García, "Influence of carbon source on nitrate removal of contaminated groundwater in a denitrifying submerged filter," *Journal of Hazardous Materials*, vol. 80, no. 1–3, pp. 69–80, 2000.
- [34] A. Mohseni-Bandpi and D. J. Elliott, "Groundwater denitrification with alternative carbon sources," *Water Science and Technology*, vol. 38, no. 6, pp. 237–243, 1998.
- [35] A. Mohseni-Bandpi, D. J. Elliott, and A. Momeny-Mazdeh, "Denitrification of groundwater using acetic acid as a carbon source," *Water Science and Technology*, vol. 40, no. 2, pp. 53–59, 1999.
- [36] N. Yan, X. Jin, and J. Zhang, "A comparison between the processes of denitrification with glucose and methanol as carbon source," *Journal of Shanghai Teachers University*, vol. 31, no. 3, pp. 41–44, 2002.
- [37] S. Zhang, Y. Zhang, F.-E. Zhang, and J. Jing, "Remediation of nitrate-contaminated groundwater in situ using a microecological techniques," *Journal of Agro-Environmental Science*, vol. 23, no. 6, pp. 1223–1227, 2004.
- [38] Y. Zhang, S. Zhang, J. H. Jing, and H. B. Hou, "An experimental study of microbial removal of nitrogen pollutant from groundwater," *Acta Geoscientica Sinica*, vol. 27, no. 3, pp. 283–288, 2006.
- [39] Y. Zhang, S. Zhang, C. L. Liu, X. Y. Wang, M. Zhang, and C. Song, "Experimental study on in-site remediation of groundwater polluted by nitrogen," *China Water & Wastewater*, vol. 23, no. 11, pp. 8–12, 2007.
- [40] S. Aslan and H. Cakici, "Biological denitrification of drinking water in a slow sand filter," *Journal of Hazardous Materials*, vol. 148, no. 1–2, pp. 253–258, 2007.
- [41] C. D. Rocca, V. Belgiorno, and S. Meriç, "Heterotrophic/autotrophic denitrification (HAD) of drinking water: prospective use for permeable reactive barrier," *Desalination*, vol. 210, no. 1–3, pp. 194–204, 2007.
- [42] Z. Shen, Y. Yin, and J. Wang, "Biological denitrification using poly(butanediol succinate) as electron donor," *Applied Microbiology and Biotechnology*, vol. 100, no. 13, pp. 6047–6053, 2016.
- [43] Z. Qiao, R. Sun, Y. Wu, S. Hu, X. Liu, and J. Chan, "Microbial heterotrophic nitrification-aerobic denitrification dominates simultaneous removal of aniline and ammonium in aquatic ecosystems," *Water, Air, & Soil Pollution*, vol. 231, no. 3, p. 112, 2020.
- [44] L. Wang, J. Li, X. Z. Song, and T. Z. Guo, "Isolation and identification of denitrifying bacteria from groundwater contaminated with nitrate of a typical intensive vegetable cultivation area," *Ecology & Environment*, vol. 17, no. 5, pp. 2078–2081, 2008.
- [45] X. L. Zhang and Y. X. Liang, "Screening of a strain denitrobacteria and its denitrification characteristic," *Freshwater Fisheries*, vol. 36, no. 5, pp. 28–32, 2006.
- [46] X. L. Wang, "Study on in-situ microbial remediation of nitrate contaminated groundwater simulator," *Hefei University of Technology*, 2010.
- [47] T. Li, W. Li, C. Feng, and W. Hu, "In-situ biological denitrification using pretreated maize stalks as carbon source for nitrate-contaminated groundwater remediation," *Water Supply*, vol. 17, no. 1, pp. 1–9, 2017.
- [48] A. D. Eaton, L. S. Clesceri, A. E. Greenberg, and M. A. H. Franson, "Standard methods for the examination of

- water and wastewater,” *American Journal of Public Health and the Nation’s Health*, vol. 56, no. 3, pp. 387-388, 1966.
- [49] R. J. Tu, W. Jin, S. F. Han et al., “Rapid enrichment and ammonia oxidation performance of ammonia-oxidizing archaea from an urban polluted river of China,” *Environmental Pollution*, vol. 255, p. 113528, 2019.
- [50] L. Zhang, L. N. Zheng, Y. N. Chen, J. N. Xiao, L. Zhang, and L. Wang, “Experimental study on removal of nitrate in groundwater with PRB,” *Journal of Tianjin University of Technology*, vol. 30, no. 6, pp. 61-64, 2014.
- [51] S. Ge, Y. Peng, S. Wang, C. Lu, X. Cao, and Y. Zhu, “Nitrite accumulation under constant temperature in anoxic denitrification process: the effects of carbon sources and COD/NO₃-N,” *Bioresource Technology*, vol. 114, pp. 137-143, 2012.
- [52] C. Glass and J. Silverstein, “Denitrification kinetics of high nitrate concentration water: pH effect on inhibition and nitrite accumulation,” *Water Research*, vol. 32, no. 3, pp. 831-839, 1998.
- [53] W. J. Hunter, “Accumulation of nitrite in denitrifying barriers when phosphate is limiting,” *Journal of Contaminant Hydrology*, vol. 66, no. 1-2, pp. 79-91, 2003.
- [54] O. Gibert, S. Pomierny, I. Rowe, and R. M. Kalin, “Selection of organic substrates as potential reactive materials for use in a denitrification permeable reactive barrier (PRB),” *Bioresource Technology*, vol. 99, no. 16, pp. 7587-7596, 2008.
- [55] C. M. Greenan, T. B. Moorman, T. C. Kaspar, T. B. Parkin, and D. B. Jaynes, “Comparing carbon substrates for denitrification of subsurface drainage water,” *Journal of Environmental Quality*, vol. 35, no. 3, pp. 824-829, 2006.
- [56] B. M. Patterson, M. E. Grassi, G. B. Davis, B. S. Robertson, and A. J. McKinley, “Use of polymer mats in series for sequential reactive barrier remediation of ammonium-contaminated groundwater: laboratory column evaluation,” *Environmental Science & Technology*, vol. 36, no. 15, pp. 3439-3445, 2002.
- [57] B. G. Ogilvie, M. Rutter, and D. B. Nedwell, “Selection by temperature of nitrate-reducing bacteria from estuarine sediments: species composition and competition for nitrate,” *FEMS Microbiology Ecology*, vol. 23, no. 1, pp. 11-22, 1997.
- [58] B. H. L. Kelso, R. V. Smith, and R. J. Laughlin, “Effects of carbon substrates on nitrite accumulation in freshwater sediments,” *Applied and Environmental Microbiology*, vol. 65, no. 1, pp. 61-66, 1999.
- [59] Z. T. Liu, Y. D. Chen, and Y. P. Jiang, “A preliminary study on removing nitrate in groundwater by using rice wine for the rural drinking water,” *Ground Water*, vol. 37, no. 4, pp. 44-47, 2015.
- [60] M. O. Rivett, S. R. Buss, P. Morgan, J. W. N. Smith, and C. D. Bemment, “Nitrate attenuation in groundwater: a review of biogeochemical controlling processes,” *Water Research*, vol. 42, no. 16, pp. 4215-4232, 2008.

Research Article

Hydrogeochemical Features and Genesis of Confined Groundwater and Health Perspectives for Sustainable Development in Urban Hengshui, North China Plain

Yong Xiao ¹, Kui Liu ¹, Qichen Hao ², Jianfeng Li ², Yunhui Zhang ¹,
Weizhe Cui ², Limao qin,¹ and Qiuming Pei ¹

¹Faculty of Geosciences and Environmental Engineering, Southwest Jiaotong University, Chengdu 611756, China

²Institute of Hydrogeology and Environmental Geology, Chinese Academy of Geological Science, Shijiazhuang 050061, China

Correspondence should be addressed to Qichen Hao; haoqichen_iheg@163.com

Received 6 February 2021; Revised 11 March 2021; Accepted 25 March 2021; Published 16 April 2021

Academic Editor: Junbing Pu

Copyright © 2021 Yong Xiao et al. This is an open access article distributed under the Creative Commons Attribution License, which permits unrestricted use, distribution, and reproduction in any medium, provided the original work is properly cited.

Groundwater in confined aquifers is the preferred water resource worldwide, and its hydrochemical quality is the premise for sustainable development. A systematic hydrogeochemical research was conducted to get insight into the hydrochemical characteristics, genesis, and potential health threats of confined groundwater, based on analytical data of 45 groundwater samples collected from the urban area of Hengshui, Central North China Plain (NCP). The results showed most groundwater had desirable hydrochemical quality with a nearly neutral to slightly alkaline nature and dominantly soft-fresh Cl-Na face. Solute chemistry was governed by rock-water interaction including minerals dissolution and ion exchange, but out of the anthropogenic influences. All nitrogen pollutants and Zn were within the desirable limit, while F⁻, Mn, and Fe were beyond the desirable limit recommended by WHO in 28.9%, 15.6%, and 68.9% of samples. Overall chronic health risk from these toxic elements was identified in terms of various populations and mainly contributed by F⁻. Infants were more prone to the health risks of aqueous pollutants. Differential water supplies based on hydrochemical quality are recommended, and water improvement measures are suggested to be conducted aiming at the harmful fluoride in confined groundwater. The present research could provide valuable references for the health sustainability of confined groundwater utilization in sedimentary plains like NCP worldwide.

1. Introduction

The available freshwater is dominantly stored underground and accounts for approximately 96% of the total liquid freshwater on Earth [1]. Groundwater is a significant water source enabling the security of water and food and the key factor lifting the rural populations out of poverty over the world [2–5], especially in arid and semiarid regions with relative scarcity of surface water [6–10]. The availability of groundwater resources for the human community is limited not only by the water quantity but also by the hydrochemical quality [11, 12]. A full understanding of the hydrochemical features, mechanisms, and quality is the premise of effective management and sustainable development of groundwater resources in any region across the world [13, 14].

Groundwater chemistry is influenced or even governed by many factors including natural and anthropogenic ones [15, 16]. Generally, the natural groundwater chemistry is determined by the hydrochemical components of recharge water, lithology of aquifers along the groundwater flow path, residence time, groundwater hydrodynamic, and evaporation [17–21]. These factors are fundamental for the natural formation and evolution of groundwater chemical components [22–25], while anthropogenic factors from all aspects of human society including domestic, agricultural, and industrial activities can dramatically modify the composition of groundwater chemistry through direct pollutants input or indirect change of the hydrogeochemical conditions of natural mechanisms [26–31]. The driving forces from the human community to the evolution of groundwater

chemistry have more significant influences on the phreatic aquifers rather than the confined aquifers due to the protection of aquitards. In addition, evaporation usually has great effects on the salinity of phreatic groundwater, which would not occur in the confined aquifers [23, 32–34]. Thus, phreatic groundwater is found with poorer hydrochemical quality than confined groundwater [16, 35–39].

Attention has been concentratedly paid to the hydrochemistry and responsibilities for the poor quality of phreatic groundwater in the past decades [40–44] due to the fragility of unconfined aquifers to the influences of external pollutions and extreme hydrological events. Great achievements have been obtained through these efforts on the understanding of hydrochemical features, evolutions, and mechanisms of shallow underground aquatic systems and effectively guided groundwater management globally [14, 44–47]. However, the confined groundwater is not lucky as the phreatic one. It is rarely concerned regarding the hydrogeochemical quality because it is regarded as the cleanest and best quality water beneath the traditional viewpoint. Although it is rare for confined groundwater affected by external factors on its hydrochemical quality, the potential poor quality as a result of the internal factors cannot be evaded [48]. Geogenic poor quality of groundwater has been one of the greatest threats to the water supply for human society and is widely reported in many regions across the world [48–54]. Thus, concerns on the hydrochemical quality and genesis are indispensable for confined groundwater if utilized for the human community.

The present research focuses on the hydrochemistry and health implication of confined water in large sedimentary plains. A subarea of the North China Plain (NCP), one of the global research hotspots of Anthropocene groundwater science, was investigated to provide references to the sustainable development of confined groundwater resources in other similar great sedimentary plains worldwide. The major aims of the present research were to (1) get insight into the hydrogeochemical features of confined groundwater, (2) reveal the mechanisms forming the hydrochemistry, (3) determine the toxic elements and their potential health threats, and (4) finally propose scientific management suggestions for the health sustainability of groundwater resources.

2. Study Area

The study area is located in the central area of the NCP (Figure 1). It lies between the latitude of 37°36′10″N–37°49′55″N and the longitude of 115°25′17″E–115°51′12″E and spreads over an area of 591 km². It represents semiarid continental monsoon conditions with an annual average temperature of 12.7°C. The average annual rainfall is approximately 500 mm where 75% occurs during the rainy season from June to September. The annual evaporation rate varies from ~1,300 mm to ~2,600 mm, approximating 3–5 times of the local rainfall. The land use type in this region is dominated by agricultural land, followed by urban land and industrial land.

Geologically, the study area belongs to the alluvial-lacustrine plain of the central NCP. The NCP is one of the largest sedimentary plains in the world and formed during the Cenozoic and Mesozoic era. This area is flat and descends slightly from the west towards the east with an elevation in the range of 22–27 m. Groundwater in this area mainly occurs in the Quaternary deposits with a thickness of more than 500 m [55]. This large Quaternary groundwater system provides the major quantity of water resource for the local development in various social-economic and ecological aspects.

The lithology of the Quaternary deposits varies from pebble to clay and silt, resulting in multiple aquifer groups vertically (Figure 2). The first continuous and stable aquitard is observed at the depth of 50–80 m below the ground surface. Generally, aquifers above this aquitard are defined as the phreatic aquifers, and those below this are identified as confined aquifers. Due to the wide distribution of saline water in phreatic aquifers [49], confined aquifers are regarded as the most potential aquifers supporting the development of the study area [33, 55]. The confined aquifers have a relatively poor water alternative ability and are mainly recharged and discharged through the lateral and vertical flow naturally.

Owing to the scarcity of surface water and high salinity of phreatic groundwater, water supply for various consumers of human society in this region mainly depends on the confined groundwater. Thus, human exploitation has become the main discharge form of the confined aquifers in the past decades [50]. In particular, agricultural irrigation, the largest water consumer, in recent decades has dominantly relied on confined groundwater [56], resulting in many groundwater depression cones in the confined aquifers as well as ground subsidence. These drastic changes of the hydraulic and geological environment also caused the evolution of the hydrogeochemical environment in confined aquifers and finally threatened the hydrochemical quality of groundwater [57], for example, the releasing of iodine into groundwater [58]. Thus, it is significantly necessary to perform targeted works to get insight into the hydrochemical quality, genesis, and potential quality issues of confined groundwater [59].

3. Material and Methods

3.1. Sampling and Analytical Techniques. In the present study, a total of 45 groundwater samples was collected from the confined aquifers across the study area (Figure 1(c)). All groundwaters were sampled from the boreholes at the depth of 150–700 m. The water in boreholes was pumped for more than three times of borehole volume before sampling to remove the stagnant water in the boreholes. In situ hydrochemical parameters, such as pH and electrical conductivity (EC), were monitored and sampling was conducted only after these parameters being stable. The sampled groundwaters were collected in the ultrapure water plastic buckets of 2.5 L which had been thoroughly rinsed with the target water three times before sampling. All groundwater samples were sent to the Laboratory for analysis with the aid

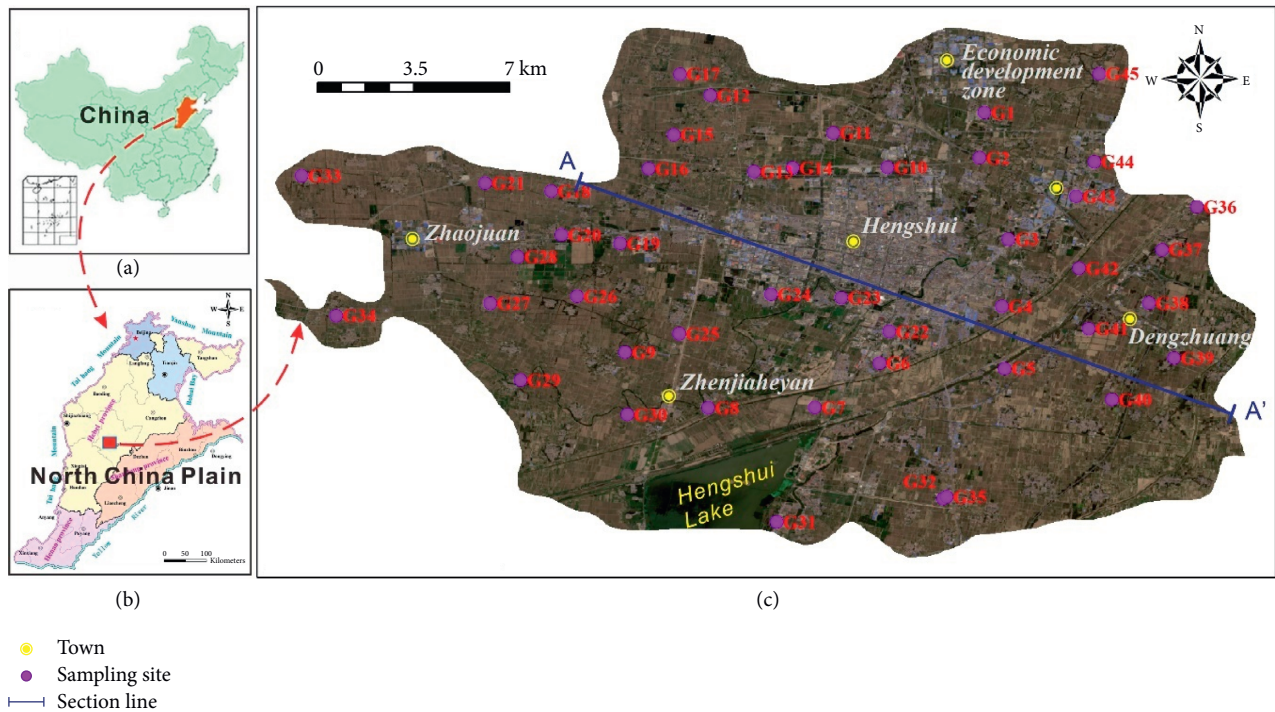


FIGURE 1: Location of the study area and sampling sites.

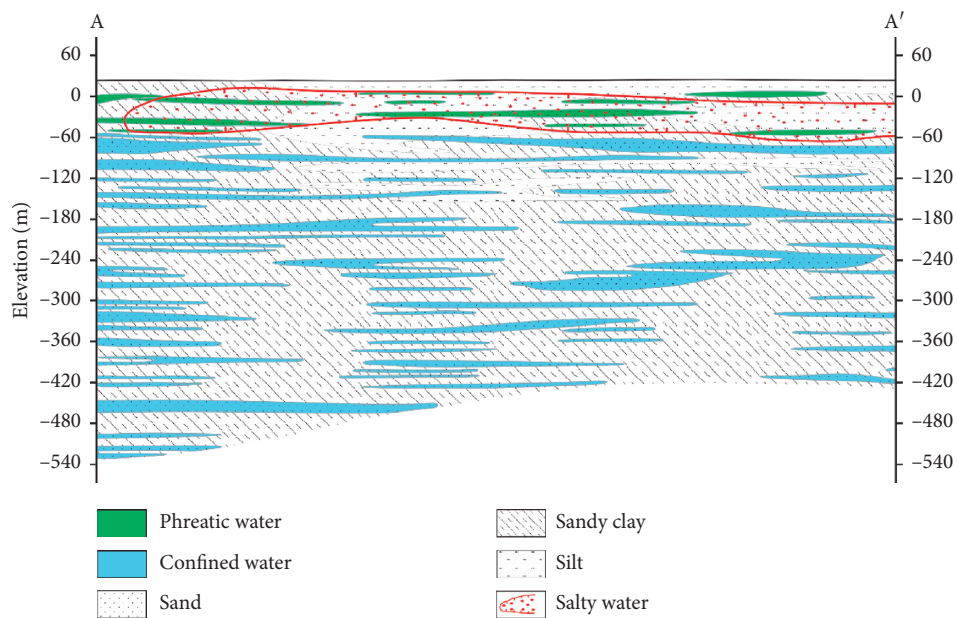


FIGURE 2: The hydrogeological cross section along the A-A'.

of incubators which could keep the samples in the condition of 4°C temperature.

The in situ parameters like pH and EC were obtained at the field with the aid of a multiparameter device (Multi 350i/SET, Munich, Germany). The analysis of other chemical parameters was conducted in the Laboratory of Groundwater Sciences and Engineering of the Institute of Hydrogeology and Environmental Geology, Chinese Academy of

Geological Sciences. Major cation ions (Ca^{2+} , Mg^{2+} , Na^+ , K^+) and trace elements (Zn, Mn, Fe) were determined using inductively coupled plasma-mass spectrometry (Agilent 7500ce ICP-MS, Tokyo, Japan). Ammonia-nitrogen (NH_4^+) and anions including Cl^- , SO_4^{2-} , NO_3^- , NO_2^- , F^- were measured by ion chromatography (Shimadzu LC-10ADvp, Kyoto, Japan). HCO_3^- and total dissolved solids (TDS) were obtained with the aid of acid-base titration. Ionic charge

balance was conducted to verify the accuracy of chemical analyses. The results showed the charge balance errors of all samples were within the permissible limit of $\pm 5\%$, demonstrating reasonably good measurement accuracy.

3.2. Human Health Risk Assessment. Contaminants in groundwater could potentially threaten the health of human beings if exposed to contaminated water. This potential health threat could be identified with the aid of a quantitative model, namely, the human health risk assessment model (HHRA model) established by the United States Environmental Protection Agency [60]. Generally, contaminants in water could pose threats through multiple pathways, such as drinking water intake, dermal contact, and inhalation. As reported by previous research, drinking water intake pathway has higher risks than other pathways regarding the high content of toxic elements in water [38, 39, 61, 62]. Thus, the pathway of drinking water intake should be paid significant attention regardless of age and gender.

The procedure of HHRA includes the following three steps:

Step 1: computation of the chronic daily intake dose of potential contaminants in target water:

$$CDI_i = \frac{(C_i \times IR \times EF \times ED)}{(BW \times AT)}, \quad (1)$$

$$AT = ED \times 365, \quad (2)$$

where CDI_i signifies the chronic daily intake dose of contaminant i ; C_i indicates the content of contaminant i in target water; IR is the rate of water oral intake; EF represents the exposure frequency; ED and AT refer to exposure duration and average exposure time, respectively; BW signifies the mean body weight of the consumer.

Step 2: identification of the hazard quotient:

$$HQ_i = \frac{CDI_i}{RfD_i}, \quad (3)$$

where HQ_i expresses the probabilistic health risk posed by single contaminant i ; RfD_i denotes the reference dose of contaminants i through the pathway of oral intake.

Step 3: synthetical assessment of the overall health risk:

$$HI = HQ_1 + HQ_2 + \dots + HQ_i, \quad (4)$$

where HI is the overall potential health risk posed by multiple contaminants in drinking water.

The parameters used in the HHRA model in the present study are listed in Table 1.

4. Results and Discussion

4.1. Physicochemical Characteristics of Groundwater. The physicochemical parameters of confined groundwater in the

study area were statistically demonstrated in the box plots of Figure 3. The desirable limit of various indices recommended by the WHO [65] and the Chinese guideline [66] was also presented.

The pH of the sampling water had a range from 7.26 to 10.32 with an average of 8.14, indicating a nearly neutral to slightly alkaline nature of confined groundwater. As shown in Figure 3(a), most of the groundwaters were with a pH value within the desirable range of 6.5–8.5 recommended by WHO [65]. About 22.2% of the total samples were found out of the pH desirable range and with a slightly more alkaline feature. A relatively large variation of EC values was observed from the sampled groundwaters with the range from 693 $\mu\text{S}/\text{cm}$ to 4,637 $\mu\text{S}/\text{cm}$ averaging at 1,128 $\mu\text{S}/\text{cm}$. The TDS also showed a relatively wide range from 467 mg/L to 3,122 mg/L with an average of 681 mg/L. Thus, groundwater had a large variation of salinity in the study area. However, most of the sampled waters had relatively low EC and TDS values, and only a small portion of samples had the EC and TDS beyond 2000 $\mu\text{S}/\text{cm}$ and 1000 mg/L, respectively (Figures 3(b) and 3(c)). The value of total hardness (TH) was in a wide range from 13 mg/L to 1,416 mg/L with an average of 121 mg/L. Groundwaters were dominantly with the TH value below the desirable limit of 450 mg/L and only 3 samples (6.7%) beyond this limit. According to the integrated water quality categories based on TDS and TH (Figure 4), confined groundwater in the study area was predominantly soft-fresh water. Four samples (8.9%) were observed falling in the moderately hard fresh category, one (2.2%) in the moderately hard brackish category and another (2.2%) in the hard brackish category. Only four groundwaters (8.9%) were under the very hard brackish category.

The solute chemistry of confined groundwater was dominated by Na^+ for cations (Figure 5) with a range from 162 mg/L to 591 mg/L and averaging at 203 mg/L. Ca^{2+} and Mg^{2+} ranked the second and third abundance in the major cations and varied from 4 mg/L to 221 mg/L and between 1 mg/L and 210 mg/L, respectively, with an average of 25 mg/L and 13 mg/L. K^+ was the least abundant ion in major cations and ranged from 0.41 mg/L to 8.88 mg/L with a mean of 1.12 mg/L. For all the major cations, only Mg^{2+} was found exceeding the desirable limit of 100 mg/L in three groundwater samples. It can be clearly seen from Figures 3(e)–3(h) that all these major cations of sampled groundwaters were concentrated in relatively low-value ranges, indicating desirable quality.

The major anions were dominated by Cl^- , followed by SO_4^{2-} and HCO_3^- (Figures 3(i)–3(k)). The concentration of these three anions was in the range of 108–1,353 mg/L for Cl^- , 109–659 mg/L for SO_4^{2-} , and 25–248 mg/L for HCO_3^- , with an average of 231 mg/L, 142 mg/L, and 113 mg/L, respectively. The portion of samples with Cl^- exceeding the desirable limit of 250 mg/L was large, accounting for approximately 42.2% of the total sampled waters (Figure 3(i)). For SO_4^{2-} , majority (88.9%) of the samples were observed within the desirable limit of 250 mg/L (Figure 3(j)). Thus, concerns on major anions should be focused on the relatively high content of Cl^- .

TABLE 1: The values of exposure parameters and RfD used in the HHAR model.

Exposure Parameter	Value				Contaminant	RfD _{oral} (mg/(kg × day))
	Infants	Children	Females	Males		
IR (L/day)	0.65*	1.5*	2.66*	3.62*	F ⁻	0.06***
EF (days/year)	365**	365**	365*	365**	Mn	0.14**
ED (years)	0.5*	6*	30*	30*	Fe	0.7**
BW (kg)	6.94*	25.9*	64.0*	73.0*		

*Zhai et al. [63]; **USEPA [60]; ***Zhang et al. [64].

Overall, groundwaters in the confined aquifers were predominantly of the Cl-Na type, with a few of the Mixed Cl-Mg-Ca type (2.2%) and Cl-Ca type (2.2%) (Figure 5). Generally, the relatively salty hydrochemical faces of groundwater like Cl-Na type are potentially formed by the natural hydrochemical evolution, or external salinity contamination input like seawater intrusion and anthropogenic pollutants input [9, 23]. Given the far away location from sea and poor water alternative ability in vertical, natural hydrochemical evolution was highly possible responsible for the salty Cl-Na type of confined groundwater in the study area. Those relatively fresh hydrochemical facies, that is, Mixed Cl-Mg-Ca type and Cl-Ca type, were the results of groundwater chemical evolution at different stages.

Some minor elements like nitrogen, F⁻, Zn, Mn, and Fe were detected to get insight into their contents in the confined groundwater and potential effects on safe water utilization. Nitrogen including NO₃⁻, NO₂⁻, and NH₄⁺ was all below the desirable limits (Figures 3(l)–3(n)), suggesting safe contents. Zn in all sampled groundwaters was also observed within the desirable limit of 1 mg/L. However, F⁻, Mn, and Fe were found beyond the desirable limits in some samples. The content of F⁻ varied from 0.40 mg/L to 1.97 mg/L, with an average of 0.74 mg/L. About 28.9% of samples were detected exceeding the desirable limit of 1 mg/L. The concentrations of Mn and Fe in groundwater were in the range of 0.001–0.361 mg/L and 0.02–30.96 mg/L, respectively, with an average of 0.014 mg/L and 1.09 mg/L. It can be clearly seen that only a small portion (15.6%) of samples had the Mn exceeding the desirable limit of 0.1 mg/L (Figure 3(q)), while high Fe groundwaters were widely distributed in the study area and 68.9% of the sampled groundwaters were observed beyond the desirable limit of 0.3 mg/L (Figure 3(r)). Thus, attention should be paid to the high F⁻, Mn, and Fe in confined water as their negative health effects on human beings.

4.2. Mechanisms Governing Groundwater Solute Chemistry.

To reveal the mechanisms controlling groundwater solute chemistry in confined aquifers of the study area, hydrochemical diagrams, correlation matrix, and hydrogeochemical simulation were introduced in the present study. Generally, the hydrochemical compositions of natural water were dominantly governed by three mechanisms, namely, precipitation, rock, and evaporation dominance, which could be visibly revealed by the Gibbs diagrams. As shown in Figure 6, all sampled confined groundwaters were situated in the rock dominance of Gibbs diagrams,

suggesting the solute chemistry of confined groundwater was naturally controlled by the rock-water interactions.

Besides the natural process, human activities are important external factors potentially regulating the hydrochemical composition of water. Nitrogen is an important indicator of pollution from the human community. As demonstrated in Figures 3(l)–3(n), all confined groundwaters in the study area had relatively low concentrations of nitrogen (including NO₃⁻, NO₂⁻, and NH₄⁺). Generally, the NO₃⁻ concentration in natural conditions is below 10 mg/L, and water with NO₃⁻ concentration below this natural limit is regarded as not influenced by human society. It can be clearly seen that almost all sampled groundwaters were dominantly with the NO₃⁻ concentration below 10 mg/L except for three samples slightly exceeding this natural limit, confirming nearly no anthropogenic pollutants input into the confined aquifers in the study area. Thus, the hydrochemistry of confined groundwater was only governed by the natural mechanism of rock-water interactions.

Various rocks can potentially be involved in the natural rock-water interactions during the groundwater circulation period. To constrain the potential contributed rocks, the end-member diagrams constructed by the ratio of Ca²⁺/Na⁺ versus Mg²⁺/Na⁺ and HCO₃⁻/Na⁺ were performed in the present study. Rocks involved in natural rock-water interactions can be revealed from three end-members of rock types, that is, carbonates, silicates, and evaporites [17, 43, 67]. As demonstrated in Figure 7, the sampled groundwaters were plotted in the dominance from the evaporites to the silicates, suggesting that the chemical solutes in the confined groundwater originated from the dissolution of evaporates and silicates. However, no sample was found located in the carbonates dominance, implying few contribution of carbonate minerals to groundwater chemistry.

The correlation matrix was introduced to further determine the contributions of evaporates and silicates to the hydrochemical components of confined aquifers. Significantly positive relations were observed between Na⁺ and Cl⁻, with the correlation coefficient of 0.96, implying the dissolution of halite (formula (1)) was one of the dominant processes controlling groundwater chemistry. This evidenced the aforementioned natural genesis of the salty hydrochemical face of Cl-Na in confined aquifers. Ca²⁺ also showed a significant positive relation to SO₄²⁻, suggesting the sulfate minerals dissolution (formulas (2) and (3)) dominantly contributed to the hydrochemical compositions in confined aquifers of the study area. These hydrochemical processes were evidenced by the saturation indexes (SI)

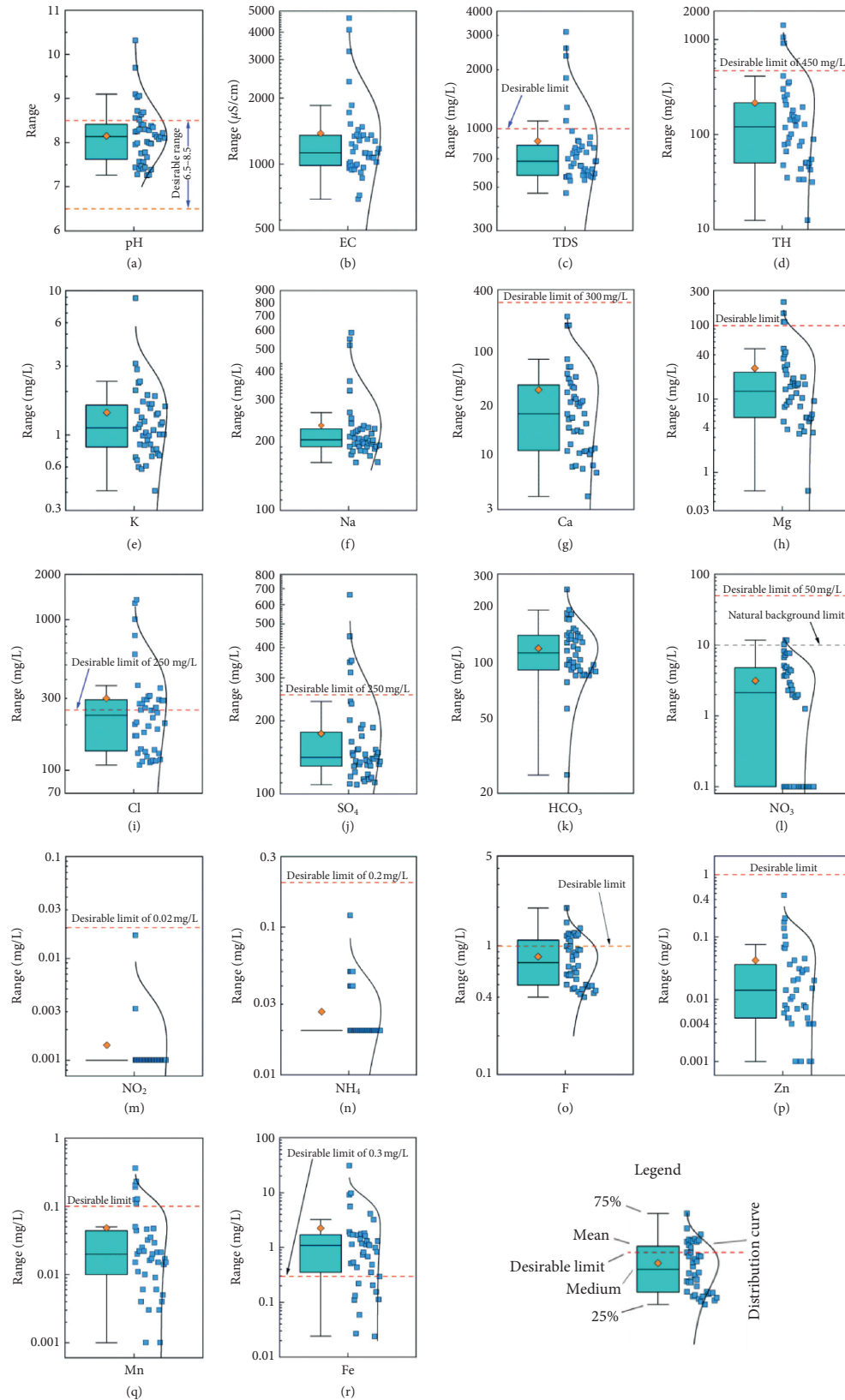


FIGURE 3: Box plots of physicochemical parameters of groundwater in the study area.

presented in Figure 8(a) that all sampled groundwaters were with unsaturated status ($SI < 0$) of halite, anhydrite, and gypsum minerals. Additionally, the dissolution of silicates

(formula (4)) was another dominant process contributing the major ions to groundwater, which was also demonstrated in Figure 7. The results of hydrochemical simulations

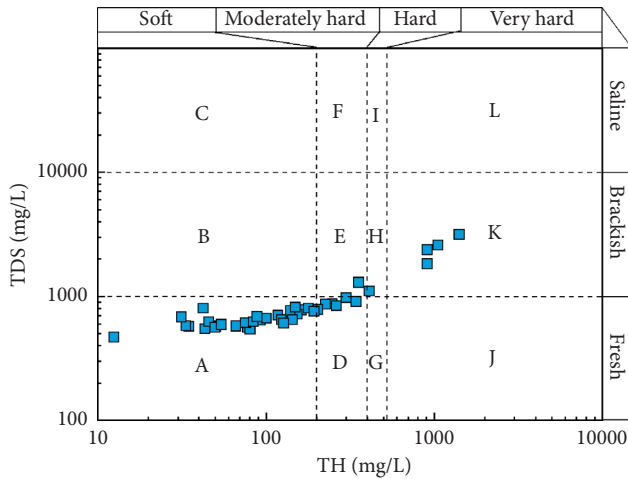


FIGURE 4: Scatter plots of total hardness (TH) versus total dissolved solids (TDS) showing the quality of groundwater.

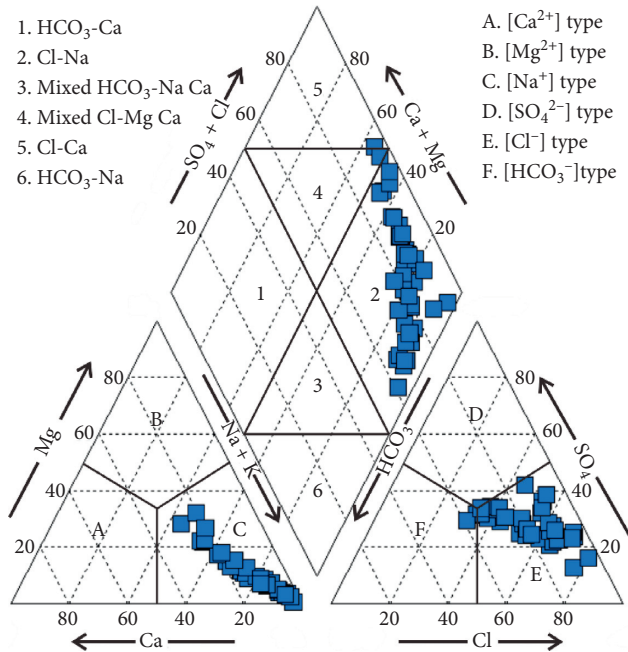
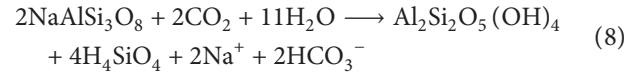
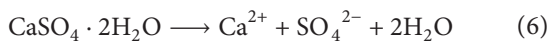
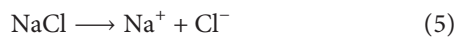


FIGURE 5: Piper diagrams demonstrating the hydrochemical compositions of groundwater in the study area.

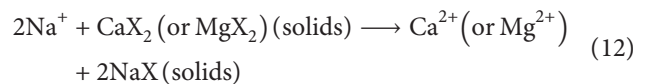
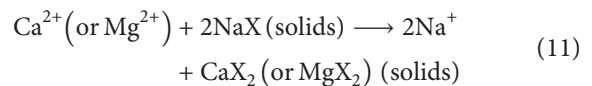
also showed that all fluoride-bearing, Fe-bearing, and Mn-bearing minerals were in the status of unsaturation (Figure 8(b)), suggesting the potential natural releasing of F^- , Mn, and Fe into groundwater from the aquifers' medium if these minerals exist. This was the reason for the relatively high contents of F^- , Mn, and Fe in some sampling groundwaters of the study area (Figures 3(o), 3(q), and 3(r)):



Ions exchange is a common rock-water interaction occurring in aquifers, especially that with fine mediums. As demonstrated in Figure 2, there occurs many fine aquifers' mediums in the study area, which could potentially provide the sources of ions for the ions exchange processes. The chloro-alkaline indices, which could be expressed by CAI-1 (formula (5)) and CAI-2 (formula (6)), were introduced to determine whether the ions exchange processes occurred and contributed to the hydrochemical compositions of groundwater. Generally, if one water having all the two chloro-alkaline indices below 0, indicating cation-exchange reaction (formula (7)) occurred; while, if reverse cation-exchange reaction (formula (8)) occurs, all chloro-alkaline indices would be positive. As shown in Figure 9(a), most (88.9%) of sampled groundwaters were with negative chloro-alkaline indices, implying a cation-exchange reaction there. The rest of the sampling groundwaters (G6, G29, G31, G39, G44) were found with positive negative chloro-alkaline indices, suggesting reverse cation-exchange reaction for these waters. These processes were examined using the relationship between $\text{Na}^+ + \text{K}^+ + \text{Cl}^-$ and $\text{Ca}^{2+} + \text{Mg}^{2+} - \text{HCO}_3^- - \text{SO}_4^{2-}$. Generally, if the cation-exchange reaction is the dominant process in the aquifers, groundwater should be plotted in the lower right dominance and along the $Y = -X$ line. If the reverse cation-exchange reaction is the predominant hydrochemical mechanism in the aquifer, water should be situated in the upper left dominance of the diagram and along the $Y = -X$ line. The bivariate diagram presented in Figure 9(b) evidenced the cation-exchange reaction for most groundwaters and reverse cation-exchange reaction for groundwaters of G6, G29, G31, G39, and G44:

$$\text{CAI} - 1 = \frac{\text{Cl}^- - (\text{Na}^+ + \text{K}^+)}{\text{Cl}^-} \quad (9)$$

$$\text{CAI} - 2 = \frac{\text{Cl}^- - (\text{Na}^+ + \text{K}^+)}{\text{HCO}_3^- + \text{SO}_4^{2-} + \text{CO}_3^{2-} + \text{NO}_3^-} \quad (10)$$



The correlation matrix (Table 2) also demonstrated that the EC, TH, and TDS had a significant positive relation to the ions of Na^+ , Ca^{2+} , Mg^{2+} , and Cl^- . Besides these four ions, the TH and TDS were also observed with significant positive relations to SO_4^{2-} . This evidenced that the hydrogeochemical processes discussed above predominantly contributed to the mineralization of confined groundwater in the study area. Overall, the solute chemistry of confined groundwater was dominantly controlled by the natural dissolution of evaporates (halite and sulfate) and silicates, cation-exchange

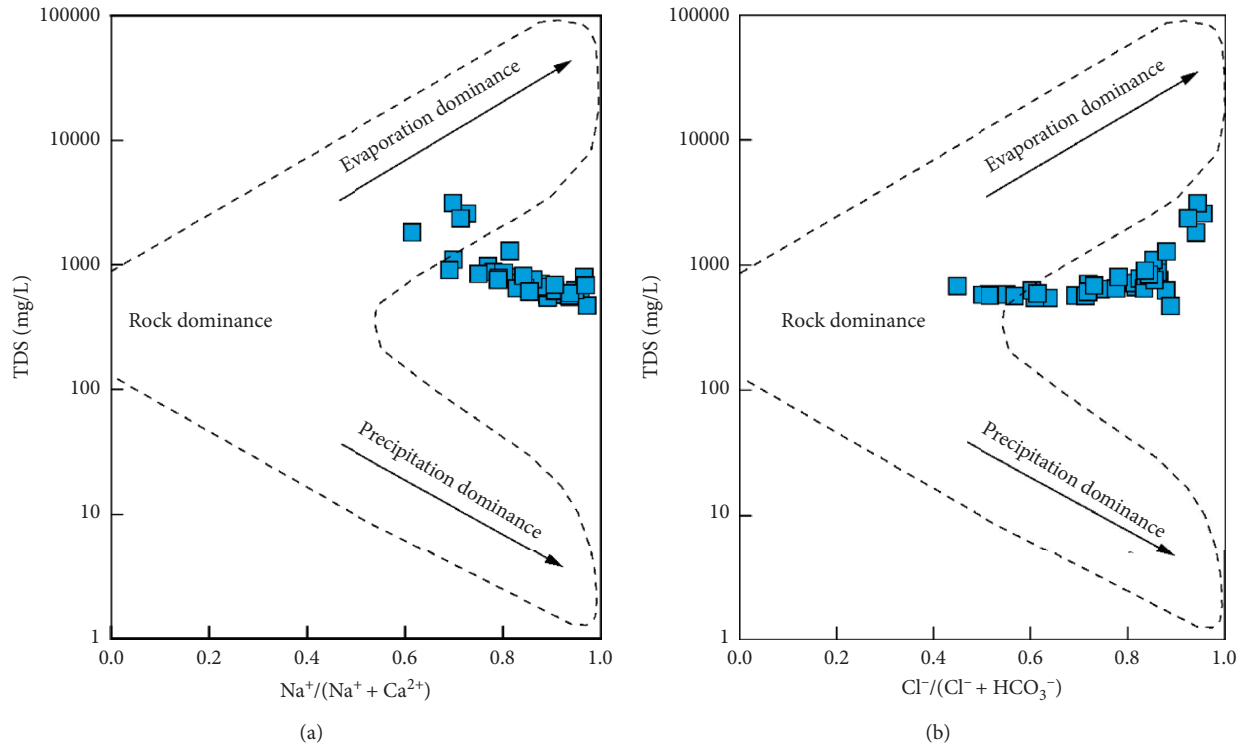


FIGURE 6: Gibbs diagrams demonstrating the natural mechanisms governing groundwater chemistry.

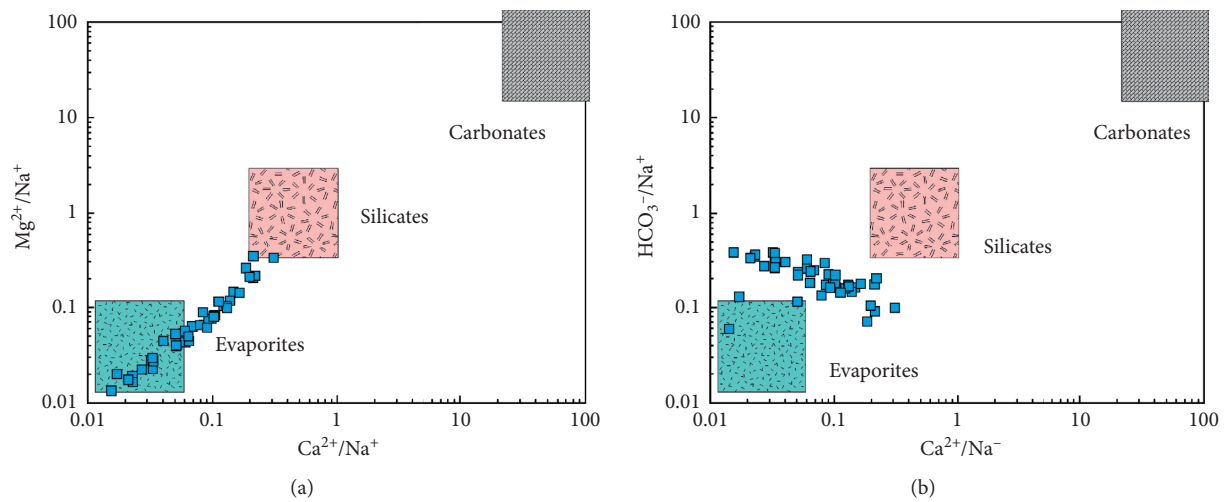


FIGURE 7: Scatter plots of (a) Na-normalized Ca versus Mg and (b) Na-normalized Ca versus HCO_3^- .

reaction. The ions releasing from fluoride-bearing, Fe-bearing, and Mn-bearing minerals contributed to the exceeding of F^- , Mn, and Fe in groundwater. Additionally, reverse cation-exchange reaction was also an important

process influencing the hydrochemistry of confined groundwater at some sampling locations. However, the hydrogeochemical compositions of confined groundwater were nearly out of the influence of anthropogenic factors.

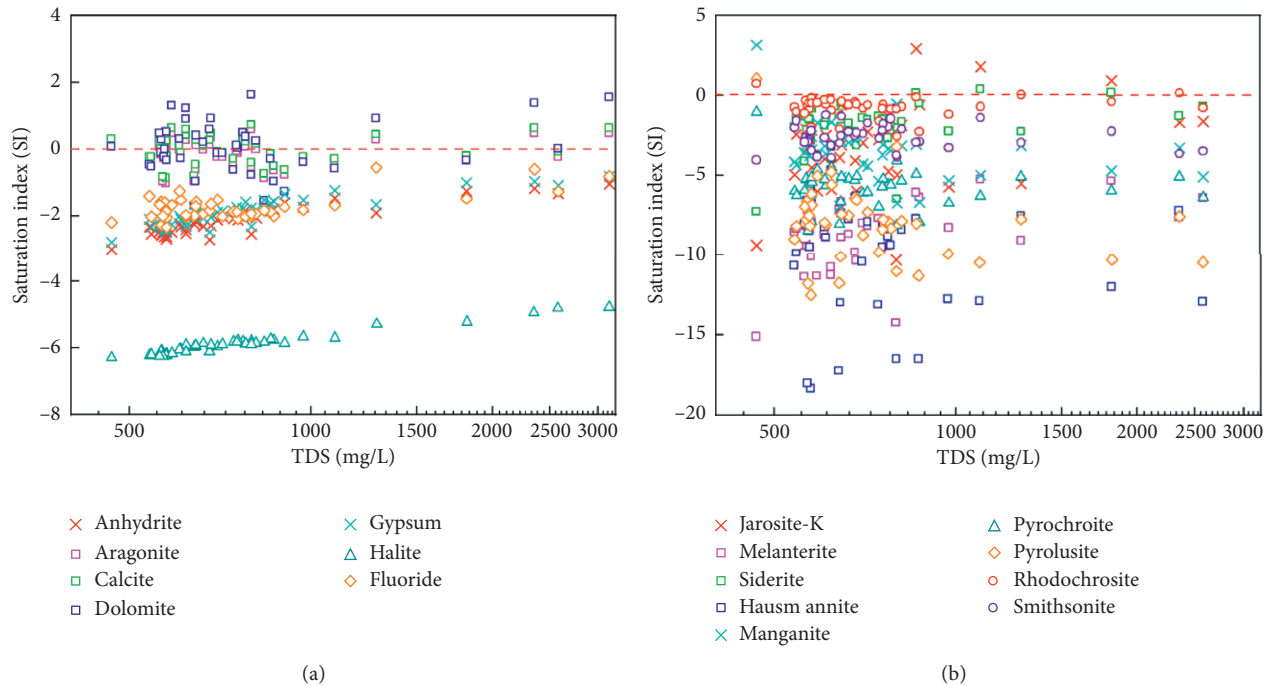


FIGURE 8: Saturation index of selected minerals in groundwater of the study area.

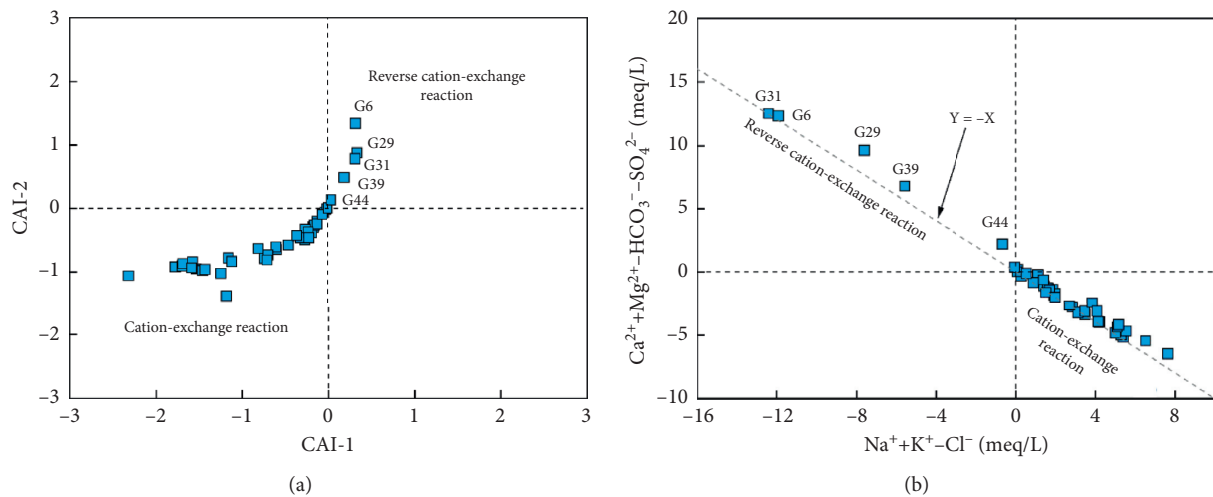


FIGURE 9: Scatter plots of (a) chloro-alkaline indices CAI-1 versus CAI-2 and (b) $\text{Na}^+ + \text{K}^+ - \text{Cl}^-$ versus $\text{Ca}^{2+} + \text{Mg}^{2+} - \text{HCO}_3^- - \text{SO}_4^{2-}$.

4.3. Potential Health Threats and Responsible Contaminants.

As discussed above, the F^- , Mn, and Fe were detected with relatively high contents in groundwater and may pose negative effects on human health. The human health risk assessment model (HHRA model) was introduced to reveal the potential negative effects of these contaminants on human health.

According to the assessment results, the HI values were in the range of 0.67–4.99 for infants, 0.42–3.08 for children, 0.30–2.21 for adult females and 0.36–2.64 for adult males, averaging at 1.60, 0.99, 0.71, and 0.85, respectively. It can be clearly seen that the overall health risks for various

populations were in the order of infants > children > males > females (Figure 10(a)). Similar results were also reported by many researchers [68–70]. The health risk can be classified into three categories, that is, low risk, medium risk, and high risk. Generally, an HI value less than 1 suggests the water with low and negligible health risk [71]. An HI value in the range of 1–4 is regarded as a medium health risk, and high health risk is implied if the HI value is beyond 4 [55, 72]. Thus, all populations were at health risk to some degree. Specifically, the potential health risk for infants varied from low to high risk category (Figure 10(a)), with 24.4% in the low chronic risk category, 73.4% in the medium

TABLE 2: Linear relationship (R2) between various chemical parameters of groundwater in the study area.

Index	pH	EC	TH	TDS	K ⁺	Na ⁺	Ca ²⁺	Mg ²⁺	Cl ⁻	SO ₄ ²⁻	HCO ₃ ⁻	NO ₃ ⁻	NO ₂ ⁻	NH ₄ ⁺	F ⁻	Zn	Mn	Fe	
pH	1																		
EC	-0.26	1																	
TH	-0.36	0.93*	1																
TDS	-0.28	0.97*	0.98*	1															
K ⁺	0.45	-0.05	-0.06	-0.01	1														
Na ⁺	-0.17	0.95*	0.91*	0.97*	0.02	1													
Ca ²⁺	-0.40	0.92*	0.99*	0.97*	-0.07	0.89*	1												
Mg ²⁺	-0.33	0.94*	0.99*	0.99*	-0.06	0.92*	0.97*	1											
Cl ⁻	-0.30	0.97*	0.98*	0.99*	-0.03	0.96*	0.96*	0.97*	1										
SO ₄ ²⁻	-0.24	0.81	0.93*	0.93*	0.08	0.86*	0.90*	0.93*	0.87*	1									
HCO ₃ ⁻	-0.10	-0.12	-0.12	-0.05	-0.41	0.06	-0.16	-0.08	-0.14	-0.01	1								
NO ₃ ⁻	-0.30	-0.24	-0.12	-0.18	0.12	-0.27	-0.07	-0.15	-0.15	-0.15	-0.42	1							
NO ₂ ⁻	0.34	-0.03	-0.10	-0.03	0.87*	0.04	-0.12	-0.09	-0.08	0.08	-0.08	-0.14	1						
NH ₄ ⁺	-0.07	-0.11	-0.14	-0.14	-0.01	-0.13	-0.14	-0.13	-0.14	-0.12	0.01	0.14	0.05	1					
F ⁻	0.36	0.09	0.04	0.13	-0.06	0.27	0.01	0.07	0.09	0.10	0.50*	-0.62*	0.16	-0.15	1				
Zn	-0.14	0.07	0.05	-0.01	-0.04	-0.09	0.09	0.03	-0.03	0.11	-0.13	0.07	-0.08	-0.11	-0.20	1			
Mn	-0.01	0.67*	0.48	0.44	-0.03	0.40	0.54*	0.43	0.45	0.36	-0.23	-0.25	-0.10	0.01	0.10	0.18	1		
Fe	0.11	0.01	-0.03	-0.05	0.02	-0.06	-0.01	-0.04	-0.05	-0.02	-0.14	-0.01	-0.07	0.20	-0.15	0.06	0.46	1	

*significant relation (absolute value of correlation coefficient >0.5).

chronic risk category, and 2.2% in the high risk category. For children, adult females, and males, the potential overall health risks only fell in the low risk and medium risk category, and no high risk was observed (Figure 10(a)). Most of the sampled waters had the HI value below 1 for these three populations, accounting for 60.0%, 91.1%, and 66.7% of the total sampled waters, respectively, suggesting negligible health risk in most of the area (Figure 11(b)–11(d)). Spatially, the potential health risk is distributed in the northern area surrounding the sampling site of G17 and the eastern area, as well as some sporadic areas adjacent to sampling sites like G22 and G4 (Figure 11).

For further illustrating the responsibility of each exceeding contaminant for the potential health risk, the HQ values of various contaminants for all populations are statistically presented in Figures 10(b)–10(d) with the aid of box plots. It can be seen that the HQ values of Mn for various populations were all below the permissible limit of 1 (Figure 10(c)), indicating negligible health threats from Mn in groundwater. For Fe in groundwater, the HQ values were dominantly (accounting for more than 90% of the sampled waters) below 1, and only very limited samples had the HQ value beyond the desirable limit of 1 (Figure 10(d)). For infants, one sample (2.2%) and two samples (4.4%) were found with high potential health risk and medium potential health risk from Fe in groundwater, respectively. Only one sample (2.2%), that is, G17, was observed with potential health threats to children, adult females, and males, and all ranked in the medium risk category. However, the potential health hazards of F⁻ were relatively higher than those of Mn and Fe in groundwater for all populations (Figures 10(b)–10(d)). Out of the sampled groundwater, 57.8%, 26.7%, 4.4%, and 17.8% were under the category of medium potential health risks to infants, children, adult females, and males, respectively, in terms of F⁻ in groundwater (Figure 10(b)). The statistic distribution of HQ posed by F⁻ was very similar to that of HI of multiple contaminants

(Figures 10(a) and 10(b)). All these indicated the exceeding F⁻ in groundwater had higher responsibilities to the overall potential health risk than other contaminants in the study area.

4.4. Implication for Sustainable Water Management. As discussed above, groundwater is essential for the development of various aspects in the North China Plain. Confined groundwater is more precious for the middle and lower reaches of the North China Plain due to the widespread distribution of salty water in the shallow aquifers. Thus, it is significantly crucial to realize the sustainable management of groundwater resources in confined aquifers although existing some potentially toxic elements in the water.

Most of the confined groundwater is fresh and soft in the study area, suggesting desirable water quality for the utilization by the human community in terms of the major solute chemistry. Although the quality of confined groundwater was not affected by the anthropogenic factors, the natural toxic elements including F⁻, Mn, and Fe exceeded the desirable limit for drinking purpose and would potentially pose threats to human society. Thus, these potential toxic elements should be paid attention to when the water is utilized as a domestic water resource. However, not all confined groundwater in the study area causes health threats to human beings, the attention should be concentratedly focused on the areas with potential threats by toxic elements. As aforementioned, the overall potential health threats mainly exist in the northern area surrounding the sampling site of G17 and the eastern area, as well as some sporadic areas adjacent to sampling sites like G22 and G4. Thus, other areas are safe for the utilization of confined groundwater resource.

For the potential risk areas mentioned above, the degree of health threats is different for various populations. Infants are more prone to the toxic elements in groundwater, and

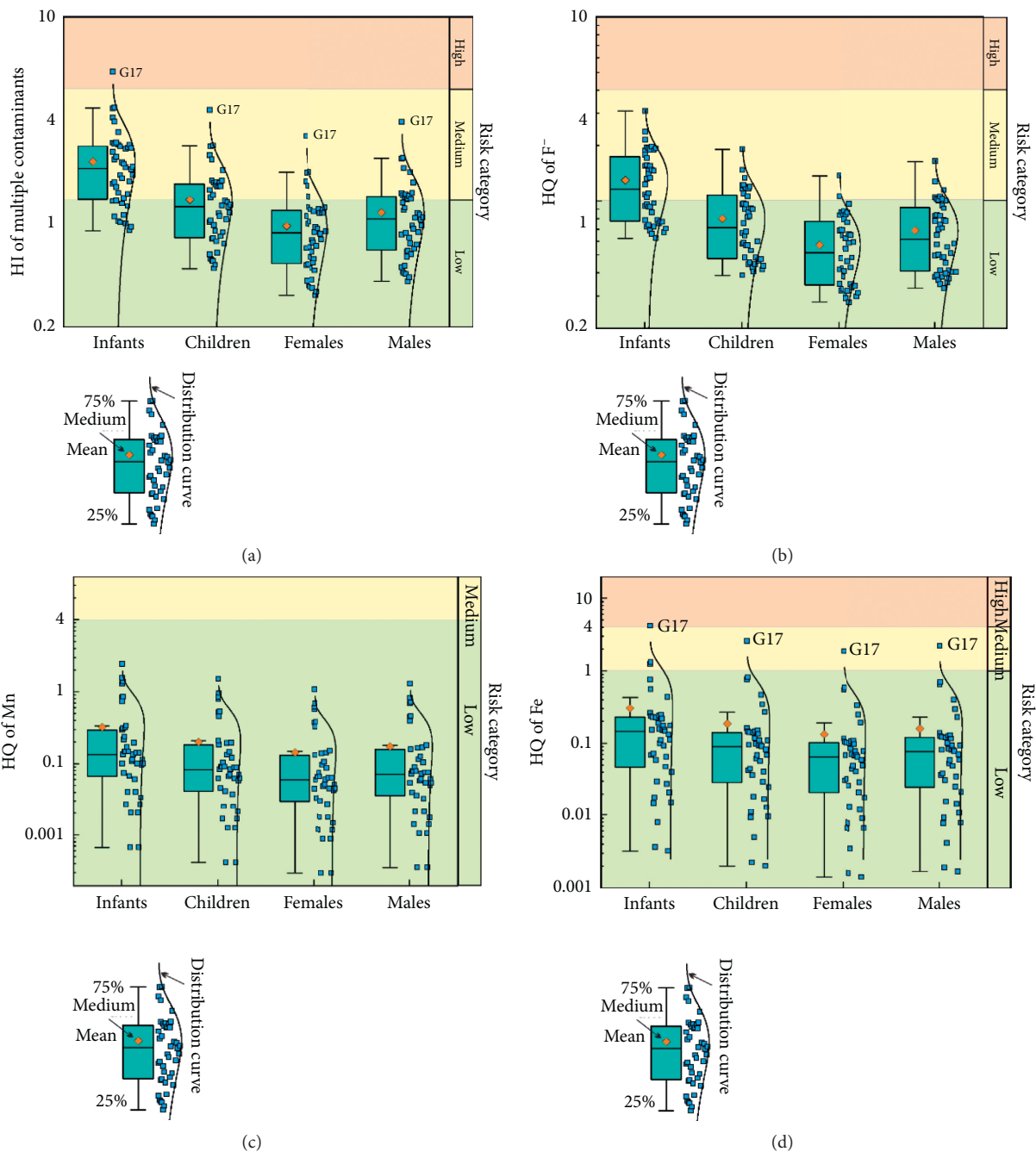


FIGURE 10: Box plots of (a) the overall noncarcinogenic health risk due to multiple contaminants and the hazard quotient of the noncarcinogenic health risk posed by a single contaminant of (b) F^- , (c) Mn, and (d) Fe.

the threats to children, adult females, and males are much less. Given the preciousness of confined groundwater resource, differential water supplies based on the potential health risk to various populations are recommended in the study area. Additionally, water quality improvement should be implemented in the potential risk area. Although Mn and

Fe are exceeding the desirable limit for water ingestion, their threats to human health are very limited and can be ignored. However, the health threat from the exceeding F^- in groundwater is significant. Considering the economic feasibility, the water improvement measures should be carried out aiming at exceeding F^- rather than other ions.

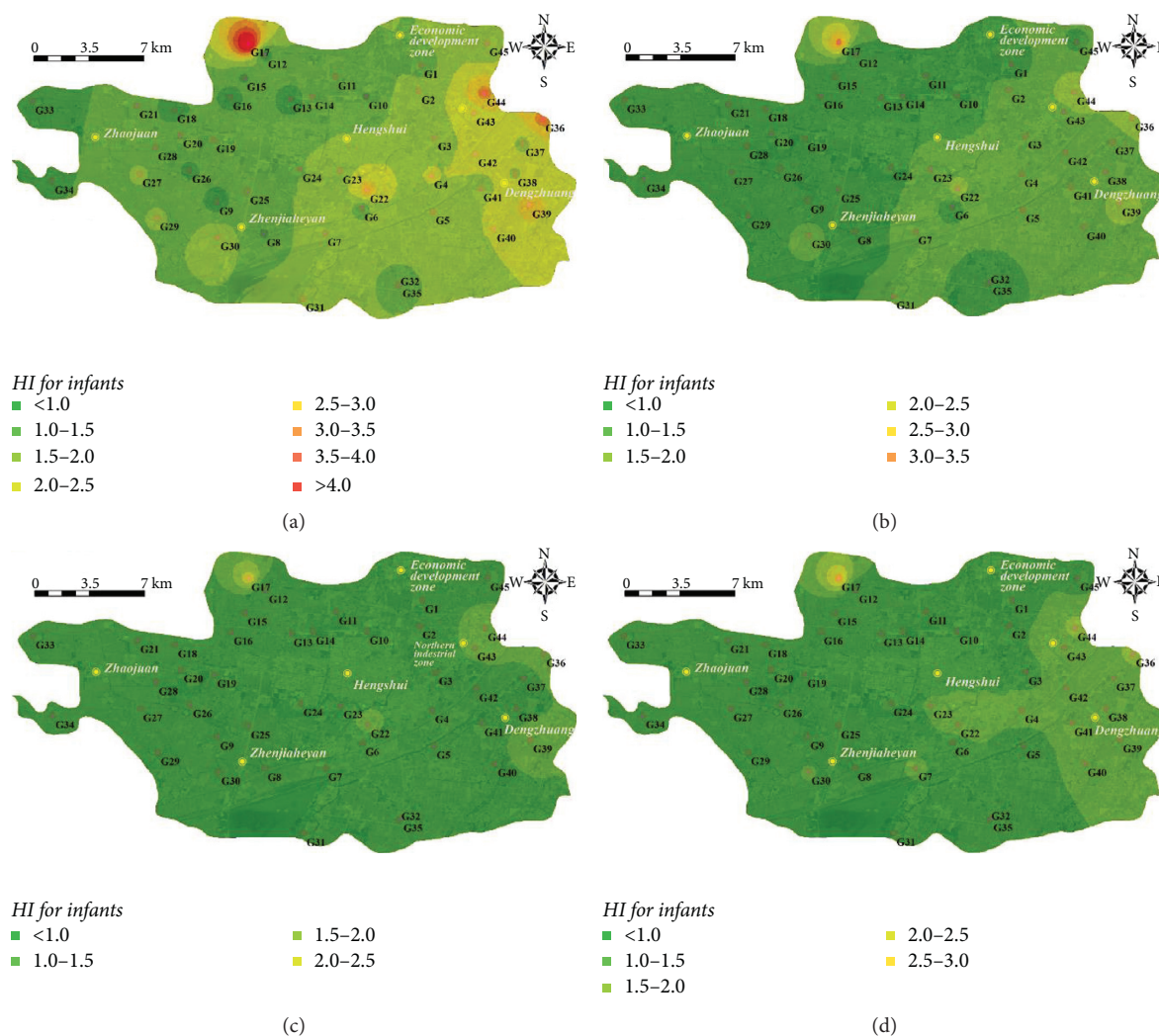


FIGURE 11: Distribution of the overall noncarcinogenic health risk to (a) infants, (b) children, (c) females, and (d) males.

5. Conclusions

Confined groundwater is the preferred water resource worldwide, especially in arid and semiarid regions with scarce surface water and poor quality of phreatic water. Hydrochemistry is the premise of available and sustainable confined groundwater and should be concerned preferentially. The urban area of Hengshui, North China Plain, was taken as the study area to get insight into the hydrochemistry and health perspective of confined groundwater in large sedimentary plains. The main findings are as follows:

- (1) Confined groundwater was of nearly neutral to slightly alkaline nature in the study area. Groundwater was predominantly soft-fresh water with average TH and TDS of 121 mg/L and 681 mg/L, respectively, and only a few samples in harder fresh or brackish categories. Hydrochemical facies were dominantly identified as Cl-Na type, with a few of the Mixed Cl-Mg-Ca type (2.2%) and Cl-Ca type (2.2%). The majority of the groundwater samples had the major ions within the desirable limit of WHO, except

for 6.7%, 11.1%, and 42.2% of Mg^{2+} , SO_4^{2-} , and Cl^- , respectively. Nitrogen (including NO_3^- , NO_2^- , and NH_4^+) and Zn were in a low and safe content, while F^- , Mn, and Fe were found exceeding the recommended limit of WHO in 28.9%, 15.6%, and 68.9% of the sampled groundwaters, respectively.

- (2) The solute chemistry of confined groundwater was governed by the natural rock-water interactions and out of the effects of anthropogenic activities. The major hydrochemical composition and mineralization were dominantly contributed by the dissolution of evaporates (halite and sulfate) and silicates, cation-exchange reaction. Reverse cation-exchange reaction also controlled the major chemistry in sporadic samples. The exceeding content of toxic elements of F^- , Mn, and Fe was a result of ions releasing of fluoride-bearing, Fe-bearing, and Mn-bearing minerals.
- (3) The overall chronic health risk posed by multiple contaminants was in the order of infants>children>males>females. The high health risk was only

potentially existing for infants. Majority of groundwater samples had the potential health risk negligible to children (60.0%), adult females (91.1%), and males (66.7%), but 73.4% of the sampled groundwater were with potential medium chronic health threats to infants. The exceeding F^- was highly responsible for the potential health risk to residents. The exceeding Fe in a few water samples can also pose health threats to some degree, while the potential risk from Mn was very low and negligible.

- (4) Most of the confined groundwaters had desirable hydrochemical quality for drinking purpose, but attention should also be paid to the exceeding geogenic toxic elements of F^- , Mn, and Fe. The potential chronic health risk was dominantly posed by F^- rather than Mn and Fe and at different levels. Differential water supplies based on the potential health risk to various populations are recommended. Water improvement measures should be conducted to eliminate the health threat from exceeding F^- , especially to the infants.

Data Availability

The data used to support the findings of the present study will be provided upon request by the corresponding author.

Conflicts of Interest

The authors declare that they have no conflicts of interest.

Acknowledgments

This research was funded by the National Natural Science Foundation of China (42007183), the Fundamental Research Funds for the Central Universities (2682019CX14), the National Basic Resources Survey Program of China (2017FY100405), the China Geological Survey (DD20160238 and DD20190303), the Student Research Training Program of Southwest Jiaotong University (201015), and the Research Project on Teaching Reform of Southwest Jiaotong University (20201023-04).

References

- [1] M. Ouarani, M. Bahir, D. J. Mulla et al., "Groundwater quality characterization in an overallocated semi-arid coastal area using an integrated approach: case of the essaouira basin, Morocco," *Water*, vol. 12, no. 11, 2020.
- [2] T. Gleeson, K. Villholth, R. Taylor, D. Perrone, and D. Hyndman, "Groundwater: a call to action," *Nature*, vol. 576, no. 7786, p. 213, 2019.
- [3] S. Jasechko, D. Perrone, K. M. Befus et al., "Global aquifers dominated by fossil groundwaters but wells vulnerable to modern contamination," *Nature Geoscience*, vol. 10, no. 6, pp. 425–429, 2017.
- [4] B. Wang, Y. Teng, H. Wang et al., "Entropy weight method coupled with an improved DRASTIC model to evaluate the special vulnerability of groundwater in Songnen Plain, Northeastern China," *Hydrology Research*, vol. 51, no. 5, pp. 1184–1200, 2020.
- [5] E. W. Banks, P. G. Cook, M. Owor et al., "Environmental tracers to evaluate groundwater residence times and water quality risk in shallow unconfined aquifers in sub Saharan Africa," *Journal of Hydrology*, 2020.
- [6] M. Alqadi, A. Margane, M. Al Raggad et al., "Implementation of simple strategies to improve wellfield management in arid regions: the case study of wadi Al arab wellfield, Jordan," *Sustainability*, vol. 11, p. 21, 2019.
- [7] S. Yin, Y. Xiao, X. Gu et al., "Geostatistical analysis of hydrochemical variations and nitrate pollution causes of groundwater in an alluvial fan plain," *Acta Geophysica*, vol. 67, no. 4, pp. 1191–1203, 2019.
- [8] Y. Xiao, J. Shao, S. K. Frappe et al., "Groundwater origin, flow regime and geochemical evolution in arid endorheic watersheds: a case study from the Qaidam Basin, northwestern China," *Hydrology and Earth System Sciences*, vol. 22, no. 8, pp. 4381–4400, 2018.
- [9] P. Li, S. He, N. Yang, and G. Xiang, "Groundwater quality assessment for domestic and agricultural purposes in Yan'an City, northwest China: implications to sustainable groundwater quality management on the Loess Plateau," *Environmental Earth Sciences*, vol. 77, no. 23, 2018.
- [10] W. Wang, Y. Chen, and W. Wang, "Groundwater recharge in the oasis-desert areas of northern Tarim Basin, Northwest China," *Hydrology Research*, vol. 51, no. 6, pp. 1506–1520, 2020.
- [11] N. Subba Rao, B. Ravindra, and J. Wu, "Geochemical and health risk evaluation of fluoride rich groundwater in Sattenapalle Region, Guntur district, Andhra Pradesh, India," *Human and Ecological Risk Assessment*, vol. 26, no. 9, pp. 2316–2348, 2020.
- [12] D. de Andrade Costa, J. P. Soares de Azevedo, M. A. dos Santos, and R. dos Santos Facchetti Vinhaes Assumpção, "Water quality assessment based on multivariate statistics and water quality index of a strategic river in the Brazilian Atlantic Forest," *Scientific Reports*, vol. 10, no. 1, 2020.
- [13] F. Bouteldjaoui, M. Bessenasse, J.-D. Taupin, and A. Kettab, "Mineralization mechanisms of groundwater in a semi-arid area in Algeria: statistical and hydrogeochemical approaches," *Journal of Water Supply: Research and Technology-Aqua*, vol. 69, no. 2, pp. 173–183, 2019.
- [14] K.-J. Lee, S.-T. Yun, S. Yu, K.-H. Kim, J.-H. Lee, and S.-H. Lee, "The combined use of self-organizing map technique and fuzzy c-means clustering to evaluate urban groundwater quality in Seoul metropolitan city, South Korea," *Journal of Hydrology*, vol. 569, pp. 685–697, 2019.
- [15] S. Hajji, B. Ayed, I. Riahi, N. Allouche, E. Boughariou, and S. Bouri, "Assessment and mapping groundwater quality using hybrid PCA-WQI model: case of the Middle Miocene aquifer of Hajeb Layoun-Jelma basin (Central Tunisia)," *Arabian Journal of Geosciences*, vol. 11, no. 20, 2018.
- [16] X. Gu, Y. Xiao, S. Yin et al., "Hydrogeochemical characterization and quality assessment of groundwater in a long-term reclaimed water irrigation area, north China plain," *Water*, vol. 10, no. 9, 2018.
- [17] S. Venkatramanan, S. Y. Chung, S. Selvam, S. Y. Lee, and H. E. Elzain, "Factors controlling groundwater quality in the Yeonjegu District of Busan City, Korea, using the hydrogeochemical processes and fuzzy GIS," *Environmental Science and Pollution Research*, vol. 24, no. 30, pp. 23679–23693, 2017.
- [18] X. Zhang, J. Miao, B. X. Hu, H. Liu, H. Zhang, and Z. Ma, "Hydrogeochemical characterization and groundwater quality assessment in intruded coastal brine aquifers (Laizhou Bay,

- China),” *Environmental Science and Pollution Research*, vol. 24, no. 26, pp. 21073–21090, 2017.
- [19] P. J. S. Kumar and L. Kuriachan, “Chemometric appraisal of groundwater quality for domestic, irrigation and industrial purposes in Lower Bhavani River basin, Tamil Nadu, India,” *International Journal of Environmental Analytical Chemistry*, 2020.
- [20] Y. Li, J. Liu, Z. Gao, M. Wang, and L. Yu, “Major ion chemistry and water quality assessment of groundwater in the Shigaze urban area, Qinghai-Tibetan Plateau, China,” *Water Supply*, vol. 20, no. 1, pp. 335–347, 2019.
- [21] Y. Li, S. Hu, X. Cui et al., “The distribution and influencing factors of chromium in regional groundwater at Sanmenxia Basin north-central China,” *Desalination and Water Treatment*, vol. 150, pp. 114–123, 2019.
- [22] J. Li, Z. Shi, G. Wang, and F. Liu, “Evaluating spatiotemporal variations of groundwater quality in northeast Beijing by self-organizing map,” *Water*, vol. 12, no. 5, 2020.
- [23] C. Li, X. Gao, S. Li, and J. Bundschuh, “A review of the distribution, sources, genesis, and environmental concerns of salinity in groundwater,” *Environmental Science and Pollution Research*, vol. 27, no. 33, pp. 41157–41174, 2020.
- [24] A. Shakoor, Z. Mahmood Khan, M. Arshad et al., “Regional groundwater quality management through hydrogeological modeling in LCC, west faisalabad, Pakistan,” *Journal of Chemistry*, vol. 2017, Article ID 2041648, 16 pages, 2017.
- [25] J. Pu, M. Cao, Y. Zhang, D. Yuan, and H. Zhao, “Hydrochemical indications of human impact on karst groundwater in a subtropical karst area, Chongqing, China,” *Environmental Earth Sciences*, vol. 72, no. 5, pp. 1683–1695, 2014.
- [26] X. Gao, X. Li, W. Wang, and C. Li, “Human activity and hydrogeochemical processes relating to groundwater quality degradation in the yuncheng basin, northern China,” *International Journal of Environmental Research and Public Health*, vol. 17, no. 3, 2020.
- [27] X. Gu, Y. Xiao, S. Yin et al., “Natural and anthropogenic factors affecting the shallow groundwater quality in a typical irrigation area with reclaimed water, North China Plain,” *Environmental Monitoring and Assessment*, vol. 189, no. 10, 2017.
- [28] C. P. S. Ahada and S. Suthar, “Groundwater nitrate contamination and associated human health risk assessment in southern districts of Punjab, India,” *Environmental Science and Pollution Research*, vol. 25, no. 25, pp. 25336–25347, 2018.
- [29] Y. Jia, B. Xi, Y. Jiang et al., “Distribution, formation and human-induced evolution of geogenic contaminated groundwater in China: a review,” *Science of The Total Environment*, vol. 643, pp. 967–993, 2018.
- [30] Y. Wang, X. Song, B. Li et al., “Temporal variation in groundwater hydrochemistry driven by natural and anthropogenic processes at a reclaimed water irrigation region,” *Hydrology Research*, vol. 49, no. 5, pp. 1652–1668, 2018.
- [31] P. Li, D. Karunanidhi, T. Subramani, and K. Srinivasamoorthy, “Sources and consequences of groundwater contamination,” *Archives of Environmental Contamination and Toxicology*, vol. 80, no. 1, pp. 1–10, 2021.
- [32] Y. Xiao, J. Shao, Y. Cui, G. Zhang, and Q. Zhang, “Groundwater circulation and hydrogeochemical evolution in Nomhon of Qaidam Basin, northwest China,” *Journal of Earth System Science*, vol. 126, no. 2, 2017.
- [33] S. Wang, X. Song, Q. Wang et al., “Shallow groundwater dynamics and origin of salinity at two sites in salinated and water-deficient region of North China Plain, China,” *Environmental Earth Sciences*, vol. 66, no. 3, pp. 729–739, 2012.
- [34] S. Tweed, M. Leblanc, I. Cartwright, G. Favreau, and C. Leduc, “Arid zone groundwater recharge and salinisation processes; an example from the Lake Eyre Basin, Australia,” *Journal of Hydrology*, vol. 408, no. 3–4, pp. 257–275, 2011.
- [35] S. Chen, Z. Tang, J. Wang et al., “Multivariate analysis and geochemical signatures of shallow groundwater in the main urban area of chongqing, southwestern China,” *Water*, vol. 12, no. 10, 2020.
- [36] S. Melki and M. Gueddari, “Impact assessment of phosphogypsum leachate on groundwater of sfax-agareb (south-east of Tunisia): using geochemical and isotopic investigation,” *Journal of Chemistry*, vol. 2018, Article ID 2721752, 10 pages, 2018.
- [37] K. K. Singh, G. Tewari, and S. Kumar, “Evaluation of groundwater quality for suitability of irrigation purposes: a case study in the udham singh nagar, uttarakhand,” *Journal of Chemistry*, vol. 2020, Article ID 6924026, 15 pages, 2020.
- [38] Y. Xiao, S. Yin, Q. Hao, X. Gu, Q. Pei, and Y. Zhang, “Hydrogeochemical appraisal of groundwater quality and health risk in a near-suburb area of North China,” *Journal of Water Supply: Research and Technology-Aqua*, vol. 69, no. 1, pp. 55–69, 2020.
- [39] S. Yin, Y. Xiao, P. Han et al., “Investigation of groundwater contamination and health implications in a typical semiarid basin of north China,” *Water*, vol. 12, no. 4, 2020.
- [40] J. Wu, P. Li, D. Wang, X. Ren, and M. Wei, “Statistical and multivariate statistical techniques to trace the sources and affecting factors of groundwater pollution in a rapidly growing city on the Chinese Loess Plateau,” *Human and Ecological Risk Assessment: An International Journal*, vol. 26, no. 6, pp. 1603–1621, 2020.
- [41] N. Subba Rao, B. Sunitha, N. Adimalla, and M. Chaudhary, “Quality criteria for groundwater use from a rural part of Wanaparthy District, Telangana State, India, through ionic spatial distribution (ISD), entropy water quality index (EWQI) and principal component analysis (PCA),” *Environmental Geochemistry and Health*, vol. 42, no. 2, pp. 579–599, 2019.
- [42] G. A. Stefania, M. Rotiroti, I. J. Buerge et al., “Identification of groundwater pollution sources in a landfill site using artificial sweeteners, multivariate analysis and transport modeling,” *Waste Management*, vol. 95, pp. 116–128, 2019.
- [43] O. A. Adeyeye, C. Xiao, Z. Zhang, A. S. Yawe, and X. Liang, “Groundwater fluoride chemistry and health risk assessment of multi-aquifers in Jilin Qianan, Northeastern China,” *Ecotoxicology and Environmental Safety*, vol. 211, pp. 1–14, 2021.
- [44] O. Rahmati, A. N. Samani, N. Mahmoodi, and M. Mahdavi, “Assessment of the contribution of N-fertilizers to nitrate pollution of groundwater in western Iran (case study: ghorveh-dehgelan aquifer),” *Water Quality, Exposure and Health*, vol. 7, no. 2, pp. 143–151, 2015.
- [45] S. Wang, S. Wei, H. Liang et al., “Nitrogen stock and leaching rates in a thick vadose zone below areas of long-term nitrogen fertilizer application in the North China Plain: a future groundwater quality threat,” *Journal of Hydrology*, vol. 576, pp. 28–40, 2019.
- [46] D. Marghade, D. B. Malpe, and N. Subba Rao, “Applications of geochemical and multivariate statistical approaches for the evaluation of groundwater quality and human health risks in a semi-arid region of eastern Maharashtra, India,” *Environmental Geochemistry and Health*, vol. 43, no. 2, pp. 683–703, 2019.

- [47] M. Qasemi, M. Afsharnia, M. Farhang, A. Bakhshizadeh, M. Allahdadi, and A. Zarei, "Health risk assessment of nitrate exposure in groundwater of rural areas of Gonabad and Bajestan, Iran," *Environmental Earth Sciences*, vol. 77, no. 15, 2018.
- [48] Y. Wang, J. Li, T. Ma, X. Xie, Y. Deng, and Y. Gan, "Genesis of geogenic contaminated groundwater: as, F and I," *Critical Reviews in Environmental Science and Technology*, pp. 1–39, 2020.
- [49] J. Li, Y. Wang, C. Zhu et al., "Hydrogeochemical processes controlling the mobilization and enrichment of fluoride in groundwater of the North China Plain," *Science of The Total Environment*, vol. 730, 2020.
- [50] H. Liu, H. Guo, L. Yang et al., "Occurrence and formation of high fluoride groundwater in the Hengshui area of the North China Plain," *Environmental Earth Sciences*, vol. 74, no. 3, pp. 2329–2340, 2015.
- [51] C. Zhi, H. Chen, P. Li et al., "Spatial distribution of arsenic along groundwater flow path in Chaobai River alluvial-proluvial fan, North China Plain," *Environmental Earth Sciences*, vol. 78, no. 8, 2019.
- [52] M. Yousefi, V. Kazemi Moghaddam, S. Maghsoudi Nasab et al., "Northwest of Iran as an endemic area in terms of fluoride contamination: a case study on the correlation of fluoride concentration with physicochemical characteristics of groundwater sources in Showt," *Desalination and Water Treatment*, vol. 155, pp. 183–189, 2019.
- [53] J. Podgorski and M. Berg, "Global threat of arsenic in groundwater," *Science*, vol. 368, p. 6493, 2020.
- [54] X. He, P. Li, J. Wu, M. Wei, X. Ren, and D. Wang, "Poor groundwater quality and high potential health risks in the Datong Basin, northern China: research from published data," *Environmental Geochemistry and Health*, vol. 43, no. 2, pp. 791–812, 2021.
- [55] Q. Hao, Y. Xiao, K. Chen, Y. Zhu, and J. Li, "Comprehensive understanding of groundwater geochemistry and suitability for sustainable drinking purposes in confined aquifers of the wuyi region, Central North China plain," *Water*, vol. 12, no. 11, 2020.
- [56] P. Li and L. Ren, "Evaluating the effects of limited irrigation on crop water productivity and reducing deep groundwater exploitation in the North China Plain using an agro-hydrological model: II. Scenario simulation and analysis," *Journal of Hydrology*, vol. 574, pp. 715–732, 2019.
- [57] L. Xing, H. Guo, and Y. Zhan, "Groundwater hydrochemical characteristics and processes along flow paths in the North China Plain," *Journal of Asian Earth Sciences*, vol. 71, pp. 250–264, 2013.
- [58] X. Xue, J. Li, X. Xie, K. Qian, and Y. Wang, "Impacts of sediment compaction on iodine enrichment in deep aquifers of the North China Plain," *Water Research*, vol. 159, pp. 480–489, 2019.
- [59] P. Li, "To make the water safer," *Exposure and Health*, vol. 12, no. 3, pp. 337–342, 2020.
- [60] USEPA, Risk Assessment Guidance for Superfund, Volume I: Human Health Evaluation Manual (Part A), Interim Final, 1989.
- [61] N. Adimalla and H. Qian, "Groundwater chemistry, distribution and potential health risk appraisal of nitrate enriched groundwater: a case study from the semi-urban region of South India," *Ecotoxicology and Environmental Safety*, vol. 207, pp. 1–10, 2021.
- [62] M. Yousefi, M. Ghoochani, and A. Hossein Mahvi, "Health risk assessment to fluoride in drinking water of rural residents living in the Poldasht city, Northwest of Iran," *Ecotoxicology and Environmental Safety*, vol. 148, pp. 426–430, 2018.
- [63] Y. Zhai, Y. Lei, J. Wu et al., "Does the groundwater nitrate pollution in China pose a risk to human health? A critical review of published data," *Environmental Science and Pollution Research*, vol. 24, no. 4, pp. 3640–3653, 2017.
- [64] Y. Zhang, J. Wu, and B. Xu, "Human health risk assessment of groundwater nitrogen pollution in Jinghui canal irrigation area of the loess region, northwest China," *Environmental Earth Sciences*, vol. 77, no. 7, 2018.
- [65] WHO, *Guidelines for Drinking-Water Quality*, World Health Organization, Geneva, Switzerland, 2011.
- [66] GAQS, *Standards for Groundwater Quality (GB/T 14848-2017)*, General Administration of Quality Supervision., Beijing, China, 2017.
- [67] J. Siddique, J. Menggui, M. H. Shah, A. Shahab, F. Rehman, and U. Rasool, "Integrated approach to hydrogeochemical appraisal and quality assessment of groundwater from sargodha district, Pakistan," *Geofluids*, vol. 2020, Article ID 6621038, 15 pages, 2020.
- [68] P. Li, X. He, and W. Guo, "Spatial groundwater quality and potential health risks due to nitrate ingestion through drinking water: a case study in Yan'an City on the Loess Plateau of northwest China," *Human and Ecological Risk Assessment*, vol. 25, no. 1-2, pp. 11–31, 2019.
- [69] N. Adimalla and P. Li, "Occurrence, health risks, and geochemical mechanisms of fluoride and nitrate in groundwater of the rock-dominant semi-arid region, Telangana State, India," *Human & Ecological Risk Assessment*, vol. 25, no. 1-2, pp. 81–103, 2018.
- [70] Y. Zhou, P. Li, M. Chen, Z. Dong, and C. Lu, "Groundwater quality for potable and irrigation uses and associated health risk in southern part of Gu'an County, North China Plain," *Environmental Geochemistry and Health*, vol. 43, no. 2, pp. 813–835, 2020.
- [71] P. Li, X. He, Y. Li, and G. Xiang, "Occurrence and health implication of fluoride in groundwater of loess aquifer in the Chinese loess plateau: a case study of tongchuan, northwest China," *Exposure and Health*, vol. 11, no. 2, pp. 95–107, 2018.
- [72] B. U. Ukah, J. C. Egbueri, C. O. Unigwe, and O. E. Ubido, "Extent of heavy metals pollution and health risk assessment of groundwater in a densely populated industrial area, Lagos, Nigeria," *International Journal of Energy and Water Resources*, vol. 3, no. 4, pp. 291–303, 2019.

Research Article

Hydrochemical Characteristics and Formation Mechanism of Strontium-Rich Groundwater in Shijiazhuang, North China Plain

Duo Li,¹ Shuang Gan,¹ Junfeng Li,² Zihan Dong,¹ Qi Long,¹ Shuwei Qiu,¹ Yahong Zhou ¹,
and Changyu Lu¹

¹School of Water Resources and Environment, Hebei Province Key Laboratory of Sustained Utilization and Development of Water Resources, Hebei Province Collaborative Innovation Center for Sustainable Utilization of Water Resources and Optimization of Industrial Structure, Hebei GEO University, Shijiazhuang 050031, China
²Hebei Institute of Hydrological Engineering Geology Investigation, Shijiazhuang 050031, China

Correspondence should be addressed to Yahong Zhou; zhyh327@163.com

Received 11 January 2021; Revised 16 February 2021; Accepted 13 March 2021; Published 25 March 2021

Academic Editor: Chengcheng Li

Copyright © 2021 Duo Li et al. This is an open access article distributed under the Creative Commons Attribution License, which permits unrestricted use, distribution, and reproduction in any medium, provided the original work is properly cited.

Strontium is a kind of trace element. Groundwater containing strontium is called mineral water when its content reaches a level that is beneficial for human physiology. Some groundwater resources in Shijiazhuang are rich in strontium. In this study, groundwater samples collected from 103 sites were studied for the hydrochemical characteristics of strontium and its formation mechanism in the groundwater system in Shijiazhuang City. The methods of source provenance analysis, factor correlation analysis, and runoff condition analysis were carried out in the study. The results showed that the content of strontium in eastern Shijiazhuang is higher than 0.229 mg/L, with a maximum content of 1.942 mg/L. The source of strontium is the dissolution of strontium-containing minerals in carbonate rock, sheet hemp rock, clastic rock, and granite in the Taihang Mountain area of the Hutuo River Basin. Strontium is positively correlated with total dissolved solids, bicarbonate, calcium magnesium, and free carbon dioxide. The erosion ability of groundwater strengthens the dissolution of strontium, and the geochemical action is mainly due to the dissolution. The enrichment and distribution of strontium are related to the conditions of groundwater runoff. Areas with good runoff conditions and strong mining are low in strontium, while areas with poor runoff conditions have high strontium content.

1. Introduction

Strontium is an alkaline-earth element, and its average abundance in the continental crust is 350 ppm [1]. Its elemental abundance varies among different types of magmatic rocks and sedimentary rocks. Among carbonate rocks, gypsum and phosphorous block rocks have the highest abundance of Sr. There are more than 30 kinds of strontium-bearing minerals in nature. The most important one is strontianite [2]. The strontium content of mineral water containing strontium is more than 0.2 mg/L. Strontium mineral water, metasilicate mineral water, and carbonated mineral water are the main types of natural mineral water

used for drinking in China. Strontium mineral water is distributed all over the country and is mainly found in Jilin, Shanxi, Jiangsu, Sichuan, and other regions. The function of strontium in the human body is mainly related to the formation of bones, and it is a normal component of human bones and teeth. It is also related to the function and structure of blood vessels. Excessive sodium in the body can cause hypertension and cardiovascular diseases, while strontium can reduce the absorption of sodium in the human body. Therefore, strontium has the effect of preventing these diseases [3]. Thus, the exploitation of natural strontium mineral water from available sources is of great importance.

Shijiazhuang is a border area between the Shanxi Block and the sags of the Bohai Basin. On the western part of Shijiazhuang are the Taihang Mountains, with an altitude of about 1000 m. The eastern part of Shijiazhuang is the alluvial proluvial plain of the Taihang Mountains, which is generally 30–100 m above sea level. Natural mineral water is widely distributed in Shijiazhuang and its surrounding areas, in which the indexes of strontium are up to the standard. This means the natural mineral water in these areas has enormous potential economic value. However, due to the lack of reasonable and unified planning for the development, utilization, and protection of mineral water resources in this area, such as unlicensed disordered mining and mixed layer mining, a large number of valuable resources are used for industrial, agricultural, and urban domestic water, which cannot be used with high quality, and the large-scale exploitation of groundwater leads to various environmental problems such as aquifer drainage and groundwater pollution, resulting in the waste of resources and environmental pollution. The rich and valuable mineral water resources in the study area have not been well developed, utilized, and protected. Therefore, the distribution characteristics, sources, migration, and enrichment trends and other hydrochemical characteristics of strontium in the study area should be analyzed [4, 5]. It can provide scientific basis for the development and protection of natural mineral water resources and give full play to the value of mineral water [6, 7]. The distribution, enrichment, and migration of strontium in groundwater are affected by many factors. At present, scholars have studied the influence of silty clay, groundwater, and various factors on the adsorption of Sr^{2+} . For example, the effects of contact time, solid-liquid ratio, and tracer concentration on the adsorption ratio of strontium on silty clay were studied by the static indicator method [8]. Through static experiments, the relationships among strontium adsorption and conventional anions and cations in groundwater were obtained [9–11]. The adsorption ability of strontium ions in the soil is related to lithology [12, 13], calcium ions, and other single ions [14, 15]. At the same time, loess [16] and different wetting media [17] also affect the migration ability of strontium ions. With the rapid development of the national economy, the demand for groundwater quality has forced us to analyze the influencing factors of groundwater quality in more detail. For example, the analysis of effects of carbon dioxide [18], groundwater system [19–21], groundwater chemical environment [22–24], and geological conditions [25] on strontium ions, the analysis of elements in mineral water [26, 27], and the evaluation of natural mineral water [28] have been reported in recent years. These previous research results have laid a solid foundation for the development of this study.

The main objectives of this research are to (1) characterize the depth, lithology, water abundance, and other aspects of the aquifers in the study area; (2) assess the distribution characteristics of strontium in groundwater; (3) analyze the correlation between strontium and other components; and (4) investigate the origin of Sr in groundwater. This study is designed to support local

decision makers in decision making related to sustainable development and utilization of groundwater mineral water.

2. Materials and Methods

2.1. Field Studies- Study Area. The study area is a part of the piedmont alluvial fan area in front of the Taihang Mountains. It is situated at latitude $37^{\circ}58'30''\text{N}\sim 38^{\circ}08'45''\text{N}$ and longitude $114^{\circ}25'30''\text{E}\sim 114^{\circ}48'35''\text{E}$ in the southeastern part of Hebei covering an area of 650 km^2 . The geological formation comprises a thick sequence of Quaternary deposits of mid-Pleistocene to recent age, which is composed of unconsolidated sand, silt, clay and kankar in various proportions. The climate in this region belongs to the warm temperate semihumid semiarid continental monsoon climate zone. It is characterized by dry and windy spring, hot and rainy summer, cool autumn, and cold winter. The average temperature ranges from 11 to 23° . The total annual rainfall is 493.3 mm . Corn and wheat are the major crops of the district.

2.2. Collection of Groundwater Samples. A total of 44 shallow groundwater samples and 29 deep groundwater samples were collected from the study area (Figure 1). The sample collection, processing, and storage methods were undertaken as per the standard procedures stipulated by the ministry of water resources in China to ensure data quality and consistency. In the study, the following physical and chemical parameters were analyzed: total dissolved solids (TDS), major cations (Mg^{2+} , Ca^{2+} , and Sr^{2+}), major anions (Cl^{-} , SO_4^{2-} , and HCO_3^{-}), and trace compounds such as free carbon dioxide (CO_2) and metasilicate (H_2SiO_3). Ca^{2+} and Mg^{2+} concentrations were determined using titration. The conductivity analyzer was used to measure EC and TDS. Sr^{2+} concentration was measured by ICP-AES.

3. Results and Discussion

3.1. The Characteristics of Water-Containing Media in the Study Area. The study area is located in the eastern part of Shijiazhuang, at the top and middle of the alluvial fan of the Hutuo River, covering 650 km^2 . According to the type of the water-containing medium, geological age, and other factors, the fourth system in the study area is divided into shallow aquifer and deep aquifer.

The shallow aquifer is formed by Q_3 and Q_4 , called a submerged aquifer. The western part of the study area is affected by the exploitation of groundwater for many years. The areas of Zhengding Zhuhe-Xi Zhaotong-Century Park-Jia village west of the first line have been dewatering. The water table of water-bearing layers in the eastern area is buried at the depth of 40 m to 90 m. The thickness of the aquifer is 20 m to 50 m. The main rocks are gravel, gravel containing, medium sand, water conducting, and water rich, with a permeability coefficient of 100 to 200 m/d. The amount of water per unit is generally between 30 and $80\text{ m}^3/\text{h}\cdot\text{m}$.

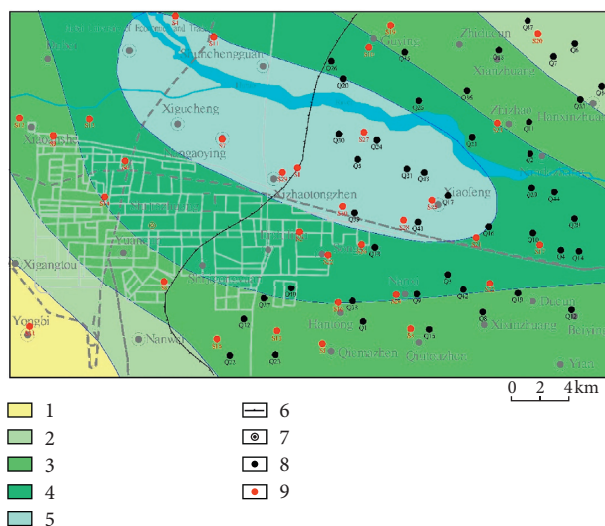


FIGURE 1: Study area and sampling locations: (1) water abundance of groundwater $< 10 \text{ m}^3/\text{h}\cdot\text{m}$; (2) water abundance of groundwater is between 10 and $30 \text{ m}^3/\text{h}\cdot\text{m}$; (3) water abundance of groundwater is between 30 and $50 \text{ m}^3/\text{h}\cdot\text{m}$; (4) water abundance of groundwater is between 50 and $70 \text{ m}^3/\text{h}\cdot\text{m}$; (5) water abundance of groundwater $> 70 \text{ m}^3/\text{h}\cdot\text{m}$; (6) boundary of the drainage area; (7) villages; (8) sampling points of shallow groundwater; and (9) sampling points of deep groundwater.

The deep aquifer is formed by Q_1 and Q_2 . The western part of the Sanlitun-Xi Zhaotong-Remain village is phreatic water. There is no stable aquiclude between it and the overlying shallow aquifer. The west of the line is confined water. The water table is buried between 80 m and 480 m. The thickness of the aquifer is 45 to 180 m. The main rock is gravel pebble, gravel-containing coarse sand, water conducting, and water rich, with a permeability coefficient of 30 to 130 m/d. The amount of water per unit is generally 40 to $110 \text{ m}^3/\text{h}\cdot\text{m}$.

3.2. Distribution Characteristics of Strontium in Groundwater.

Statistical summary of various parameters of strontium measured in groundwater is presented in Table 1. The abundance of Sr in the shallow groundwater ranges from 0.396 mg/L~1.942 mg/L, and that in the deep groundwater ranges from 0.229 mg/L~1.837 mg/L. The mode and standard deviation of strontium concentration in shallow and deep groundwater are, respectively, 1.092 mg/L, 0.368 and 0.460 mg/L, 0.326, with the average values of 1.023 mg/L and 0.771 mg/L. Significantly, the average strontium concentration in shallow groundwater is higher than that in deep groundwater [29]. Histograms are drawn according to the frequency of strontium values in shallow and deep groundwater (Figure 2). As can be seen from the figure, the concentration of Sr in the shallow layer and deep layer presents a normal distribution and is mainly concentrated around the mean values of 1.023 and 0.771.

The contour map of Sr (Figure 3) is drawn according to the strontium concentration values at the sampling points. As shown in Figure 3, the surface distribution of strontium in shallow and deep groundwater has the same characteristics: the strontium content in groundwater varies in different parts of the alluvial-diluvial fan. The content of

strontium increases gradually from the top to the middle parts and both sides of the bottom of the alluvial fan. The low-value zone of strontium content is located in the fan axis of Shijiazhuang City-High-tech zone-the oil refinery, and the high-value zone is located in the north and south. The Sr content in the south is higher than that in the north.

3.3. Correlation with Other Ions

3.3.1. Correlation between Strontium and Free CO_2 .

The abundance of Sr in the geological environment determines the strontium content in groundwater. High strontium abundance is conducive to the enrichment of strontium. Carbonate formations are the most suitable for Sr enrichment, and the clastic environments are the second most favorable. The content of strontium is abundant in the carbonate aquifer. SrCO_3 is a constituent mineral of carbonate salts and is insoluble in groundwater environment. Contact with corrosive water increases the solubility of the mineral. The lithology of the Taihang Mountains in the west of Shijiazhuang is mainly carbonate rock and gneisses which contain a large amount of strontium minerals, such as SrCO_3 and SrSO_4 . The formation of Sr mineral water occurs because the Sr-containing minerals are easily dissolved in water. Sr in groundwater in the study zone is derived from the dissolution of carbonate minerals. Hence, the concentration of strontium has a certain correlation with the concentration of free CO_2 . The relationship between the concentration of Sr and free CO_2 in shallow and deep groundwater is shown in Figure 4. The results verify that there is a positive correlation between Sr and free CO_2 . Specifically, the strontium content in groundwater rises gradually with the increase in the content of free carbon dioxide.

TABLE 1: Mathematical statistics of strontium in shallow and deep groundwater.

The concentration of Sr	Shallow aquifer	Deep aquifer
Mean value	1.023	0.771
Median	1.001	0.747
Mode	1.092	0.460
Standard deviation	0.368	0.326
Variance	0.136	0.128
Range	1.546	1.608
Min	0.396	0.229
Max	1.942	1.837

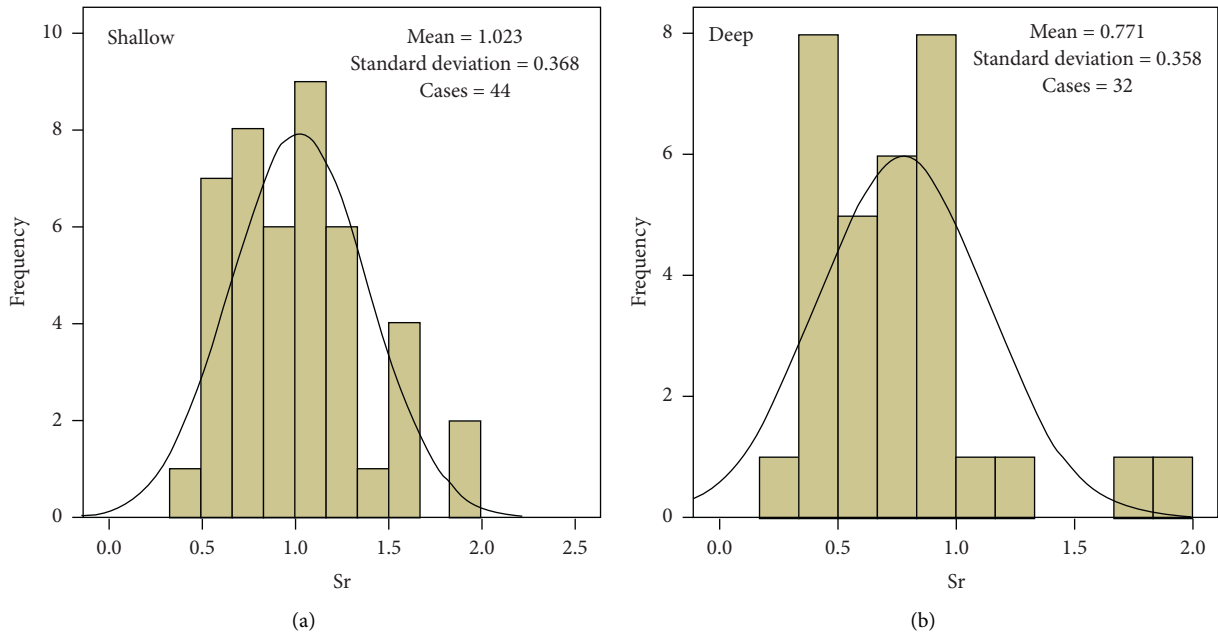


FIGURE 2: Frequency histogram of strontium concentration in shallow and deep groundwater.



FIGURE 3: Strontium distribution in shallow and deep groundwater: (1) contour lines of strontium content in shallow water; (2) contour lines of strontium content in deep water; (3) boundary of the drainage area; and (4) villages.

3.3.2. *Correlation between Strontium and Conventional Factors.* Piper diagram is drawn based on the contents of major negative ions and cations (Figure 5) [30]. The figure suggests that the main hydrochemical types in the study area are $\text{SO}_4\text{-Cl-Ca-Mg}$ and $\text{HCO}_3\text{-Ca-Mg}$. Most of the

groundwater in the study area is low salinity bicarbonate water, and Mg^{2+} , Ca^{2+} , and HCO_3^- are the most common ions. It can be seen from Figure 6 that Sr is positively correlated with TDS and TH. Lixiviation is the chief geochemistry action that controls strontium content [31, 32].

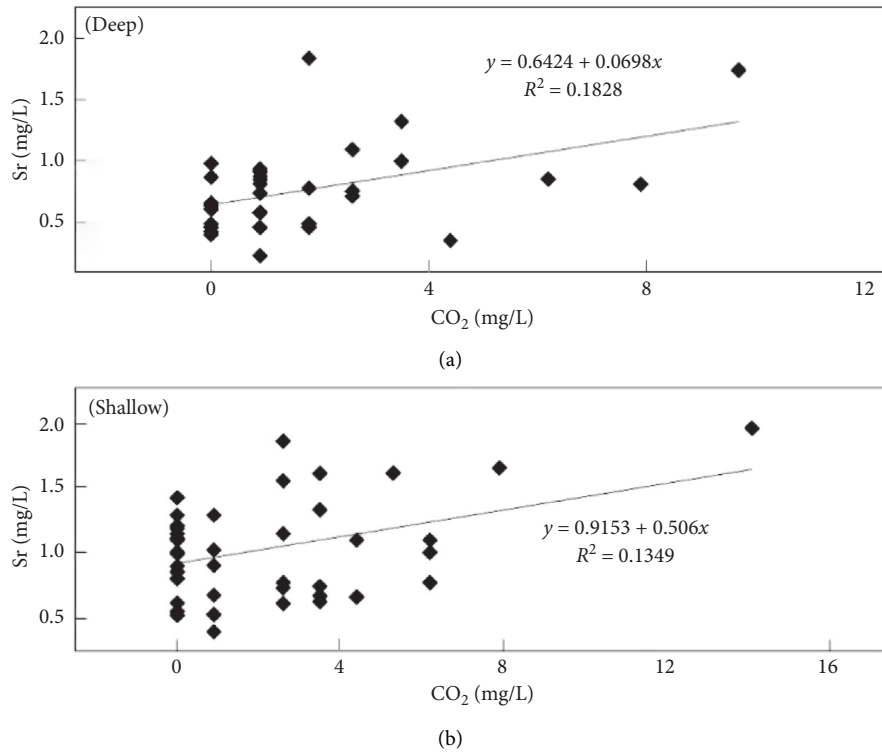


FIGURE 4: Relationship between strontium and free carbon dioxide in shallow and deep groundwater.

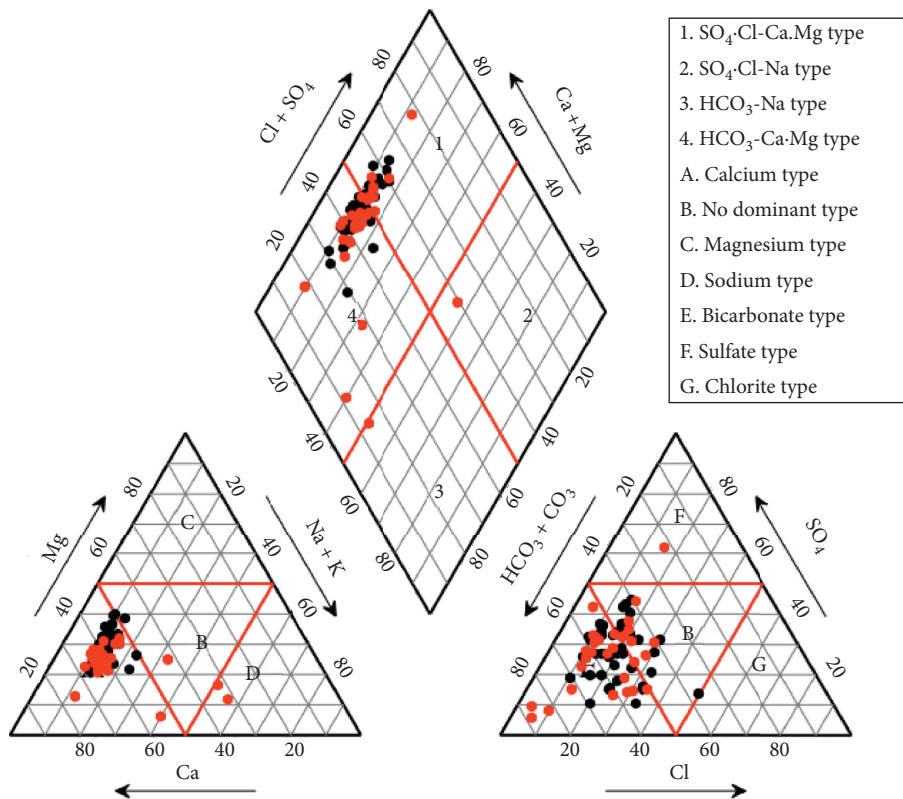


FIGURE 5: Piper diagram of groundwater samples.

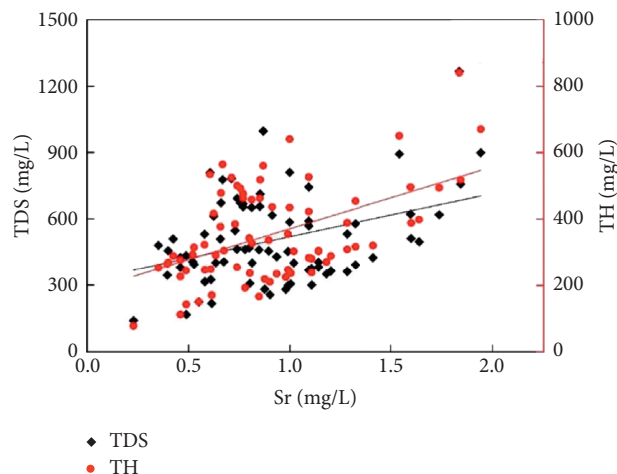


FIGURE 6: Relationship between groundwater strontium, TDS, and TH.

Studies have shown that mineral waters containing strontium are primarily of HCO_3^- type and secondarily of $\text{HCO}_3^-/\text{SO}_4^{2-}$ type [33]. Consequently, it can be speculated that the concentration of bicarbonate ions and sulfate ions in groundwater has a certain correlation with the concentration of strontium in groundwater. The relationship between strontium concentration and bicarbonate ion concentration in groundwater was plotted (Figure 7). As shown in the figure, the concentration of strontium in groundwater is positively correlated with the concentration of bicarbonate ions. It can be seen from Figure 8 that the concentration of strontium in groundwater is also positively correlated with the concentrations of Ca^{2+} and Mg^{2+} , which indicates that the main components of the rocks that undergo leaching are carbonate minerals.

3.4. Analysis of Strontium Enrichment

3.4.1. Sources of Strontium. Strontium is a trace element in the lithosphere, but its abundance is the highest in the upper lithosphere. It is distributed widely with an average of 3.75×10^{-4} . The formation, enrichment, and distribution of Sr have certain regularity. They are affected by the geological background of the formation area, groundwater movement, and geochemical environment.

As a widely distributed trace element in nature, strontium is highly resolutive. Therefore, the content of strontium in natural water is slightly higher than that of other trace elements. In carbonate rock, gypsiferous clastic rock, and salt rock, minerals such as strontium carbonate and celestite are easily soluble in water. The rocks containing Sr are magmatic rocks, clastic rocks, and metamorphic rocks, which are formed by thermal metamorphism. These rocks are conducive to the dissolution of strontium. The strontium content in groundwater depends largely on its geochemical environment and the properties of strontium. During the weathering of rock, especially the decomposition of feldspar, the interaction between strontium salt and water rich in

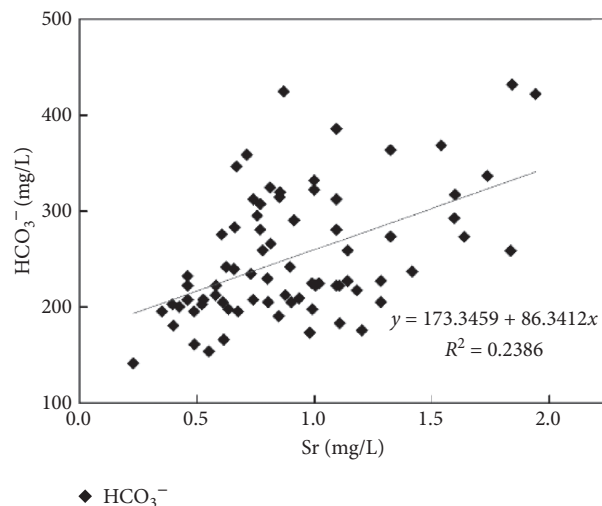


FIGURE 7: Relationship between groundwater strontium and bicarbonate.

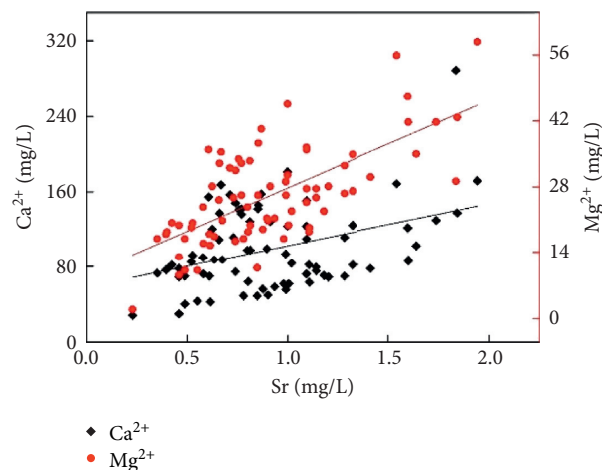


FIGURE 8: Relationship between strontium, calcium, and magnesium contents in groundwater.

carbon dioxide is beneficial to the precipitation of strontium. It dissolves in water and causes strontium enrichment.

The strontium content in groundwater is closely related to the geochemical environment such as the lithology of the aquiferous medium and strontium content. The content of strontium is the highest in carbonate rocks, followed by clastic strata, and also high in granite and granodiorite. The study area is located on the top and middle belt of Hutuo River alluvial fans. The stratigraphic distribution of the Hutuo River Basin upstream region mainly consists of the archaean group, fuping group, Wutai group, lower palaeozoic group, Hutuo group of gneiss and other metamorphic rocks, carbonate rock, clastic rock, upper palaeozoic, Cambrian Ordovician carbonate rocks, carboniferous Permian clastic rock, and granite, granite diorite vein, etc., as shown in Figure 9. There are many strontium-bearing minerals in the rocks, such as strontianite, which easily dissolve in water. The dissolution of strontium-bearing

- (3) The strontium content in the groundwater in most of the study area is more than 0.4 mg/L. The enrichment and distribution of strontium in the groundwater are related to groundwater runoff conditions. Moreover, the strontium content is lower at the axial part of the alluvial-diluvial fan and the descending funnel. The area with poor runoff conditions is high in strontium content.

In summary, the results of this work help to identify the conditions and factors responsible for Sr enrichment in groundwater, which can be useful for the exploitation of Sr-containing mineral water. This study can provide a scientific basis for the development and protection of natural mineral water resources for drinking and the management planning of the relevant departments, to ensure that the abundant mineral water resources can be used rationally and continuously and to improve the drinking water quality in Shijiazhuang.

Data Availability

The data supporting the conclusions in this work are included in this manuscript. Other datasets generated and analyzed during the current work are available from the corresponding author on reasonable request.

Conflicts of Interest

The authors declare no conflicts of interest.

Acknowledgments

This work was supported by the Open Fund of the Key Laboratory of Subsurface Hydrology and Ecological Effects in the Arid Region of the Ministry of Education (300102299505) and the Natural Science Foundation of Education Department in Hebei Province (D2019403194).

References

- [1] S. R. Taylor, and M. M. Scott, *The Continental Crust: Its Composition and Evolution*, 1985.
- [2] F. Ehya, B. Shakouri, and M. Rafi, "Geology, mineralogy, and isotope (Sr, S) geochemistry of the Likak celestite deposit, SW Iran," *Carbonates and Evaporites*, vol. 28, pp. 419–431, 2013.
- [3] K. S. An, "Development status and main problems of drinking natural mineral water in China," *North China Journal of Geology and Mineral Resources*, vol. 4, pp. 341–346, 1994, in Chinese.
- [4] Y. Gao, H. Qian, W. Ren, H. Wang, F. Liu, and F. Yang, "Hydrogeochemical characterization and quality assessment of groundwater based on integrated-weight water quality index in a concentrated urban area," *Journal of Cleaner Production*, vol. 260, 2020.
- [5] Y. H. Zhou, P. Y. Li, L. L. Xue, Z. H. Dong, and D. Li, "Solute geochemistry and groundwater quality for drinking and irrigation purposes: a case study in Xinle city," *North China Geochemistry*, vol. 80, no. 4, 2020.
- [6] S. H. Wang, L. Zhao, W. Huang et al., "Solvothermal synthesis of CoO/BiVO₄ p-n heterojunction with micro-nano spherical structure for enhanced visible light photocatalytic activity towards degradation of tetracycline," *Materials Research Bulletin*, vol. 135, pp. 111161–111169, 2021.
- [7] W. L. Shi, M. Y. Li, X. L. Huang et al., "Construction of CuBi₂O₄/Bi₂MoO₆ p-n heterojunction with nanosheets-on-microrods structure for improved photocatalytic activity towards broad-spectrum antibiotics degradation," *Chemical Engineering Journal*, vol. 394, pp. 125009–125018, 2020.
- [8] X. Zhou, K. Zeng, R. R. Zhang, Y. Wang, and T. Q. Ma, "Study on adsorption distribution coefficient of Sr on silty clay," *Nuclear Electronics and Detection Technology*, vol. 33, no. 3, pp. 301–304, 2013.
- [9] Y. Xie, Z. K. Shi, T. Wu, and D. Zhang, "Study on the influence of site groundwater characteristic factors on uranium and strontium adsorption," *Chemical Research and Application*, vol. 24, no. 11, pp. 1685–1690, 2012, in Chinese.
- [10] K. Berninger and J. Pennanen, "Heavy metals in perch (*Perca fluviatilis* L.) from two acidified lakes in the Salpausselkä Esker area in Finland," *Water, Air, and Soil Pollution*, vol. 81, no. 3–4, pp. 283–294, 1995.
- [11] S. Li, S. J. Ni, C. J. Zhang, M. G. Ding, and H. J. Wu, "Sorption kinetics of strontium in soil," *Journal of Nuclear and Radiochemistry*, vol. 29, no. 2, pp. 90–95, 2007.
- [12] Y. E. Yang, Y. Li, W. Pan, Z. M. Wang, and S. W. Ni, "Migration of stable element Sr in soil columns," *Atomic Energy Science and Technology*, vol. 40, no. 3, pp. 292–296, 2006.
- [13] L. Wu, S. J. Wang, and L. Li, "Adsorption characteristics of strontium on soil around a petrochemical wastewater reservoir in Xinjiang," *Chemical Research and Application*, vol. 3, pp. 12–16, 2012, in Chinese.
- [14] J. Solecki, "Investigation of ⁸⁵Sr adsorption in the presence of Na⁺, K⁺ and Cs⁺ on selected soils from different horizons," *Journal of Radioanalytical and Nuclear Chemistry*, vol. 268, no. 2, pp. 357–364, 2006.
- [15] J. Solecki and S. Michalik, "Studies of ⁸⁵Sr adsorption on grain fractions of soil," *Journal of Radioanalytical and Nuclear Chemistry*, vol. 267, no. 2, pp. 271–278, 2006.
- [16] L. J. Huo, T. W. Qian, J. T. Hao, and D. Y. Zhao, "Sorption and retardation of strontium in saturated Chinese loess: experimental results and model analysis," *Journal of Environmental Radioactivity*, vol. 116, pp. 19–27, 2013.
- [17] A. Boyer, P. Ning, D. Killely et al., "Strontium adsorption and desorption in wetlands: role of organic matter functional groups and environmental implications," *Water Research*, vol. 133, pp. 27–36, 2018.
- [18] K. E. Pit'eva, M. A. Fortygina, and A. V. Mikheev, "Formation of the composition and quality of carbonate mineral water of the Elburgan water bearing complex (Essentuki Town)," *Moscow University Geology Bulletin*, vol. 62, pp. 277–285, 2007.
- [19] M. Pennisi, R. Gonfiantini, S. Grassi, and P. Squarci, "The utilization of boron and strontium isotopes for the assessment of boron contamination of the Cecina river alluvial aquifer (central-western Tuscany, Italy)," *Applied Geochemistry*, vol. 21, no. 4, pp. 643–655, 2006.
- [20] O. Alhassanieh, O. Mrad, and Z. Ajji, "Sorption and migration of Cs, Sr, and Eu in gypsum-groundwater system," *Nukleonika*, vol. 57, pp. 125–131, 2012.
- [21] N. I. Ivanova, "Strontium distribution patterns in groundwater and aquifer host rocks in the southeastern part of the Severnaya Dvina artesian basin," *Moscow University Geology Bulletin*, vol. 69, no. 4, pp. 258–266, 2014.
- [22] C. P. Petalas, "A preliminary assessment of hydrogeological features and selected anthropogenic impacts on an alluvial fan

- aquifer system in Greece,” *Environmental Earth Sciences*, vol. 70, no. 1, pp. 439–452, 2013.
- [23] Y. X. Wang, Z. L. Shen, and S. G. Moisevich, “Strontium hydrogeochemistry of thermal groundwaters from Baikal and Xinzhou,” *Science in China Series E: Technological Sciences*, vol. 44, no. 1, pp. 138–143, 2001.
- [24] Z. Rui, Y. G. Teng, and J. S. Wang, “Modeling migration of strontium in sand and gravel aquifer in the candidate VLLW disposal site,” *Journal of Radioanalytical and Nuclear Chemistry*, vol. 281, no. 3, pp. 653–662, 2009.
- [25] B. Christophe, M. V. Bocxstaele, E. Ponzevera, and C. R. Quénel, “Fit for purpose validated method for the determination of the strontium isotopic signature in mineral water samples by multi-collector inductively coupled plasma mass spectrometry,” *Spectrochimica Acta Part B: Atomic Spectroscopy*, vol. 64, no. 3, pp. 229–234, 2009.
- [26] K. Usuda, K. Kono, T. Dote et al., “Survey of strontium in mineral waters sold in Japan,” *Biological Trace Element Research*, vol. 112, no. 1, pp. 77–86, 2006.
- [27] B. Z. Yan, C. L. Xiao, X. J. Liang, R. C. Wei, and S. L. Wu, “Characteristics and genesis of mineral water from Changbai mountain, Northeast China,” *Environmental Earth Sciences*, vol. 73, no. 8, pp. 4819–4829, 2015.
- [28] L. J. Liu, H. Z. Xu, Q. P. Cui, and J. Wang, “Evaluation of deep underground natural drinking mineral water field in eastern Shijiazhuang city,” *South-to-North Water Transfers and Water Science & Technology*, vol. 6, pp. 106–109, 2010, in Chinese.
- [29] Y. H. Zhou, P. Y. Li, M. J. Chen, Z. H. Dong, and C. Y. Lu, “Groundwater quality for potable and irrigation uses and associated health risk in southern part of Gu’an county,” *North China Plain. Environ Geochem Health*, vol. 43, no. 2, pp. 813–835, 2020.
- [30] Y. H. Zhou, P. Y. Li, L. L. Xue, Z. H. Dong, and D. Li, “Solute geochemistry and groundwater quality for drinking and irrigation purposes: a case study in Xinle City,” *North China Geochemistry*, vol. 80, no. 4, 2020.
- [31] Y. Gao, H. Qian, C. Huo, and J. Chen, “Assessing natural background levels in shallow groundwater in a large semiarid drainage basin,” *Journal of Hydrology*, vol. 584, Article ID 124638, 2020.
- [32] P. Y. Li, X. D. He, and W. Y. Guo, “Spatial groundwater quality and potential health risks due to nitrate ingestion through drinking water: a case study in Yan’an city on the Loess Plateau of northwest China,” *Human and Ecological Risk Assessment*, vol. 25, no. 1-2, pp. 11–31, 2019.
- [33] Y. H. Zhou, J. Ning, L. X. Li, Q. Long, and A. H. Wei, “Health risk assessment of groundwater in Gaobeidian, North China: distribution, source, and chemical species of the main contaminants,” *Exposure and Health*, vol. 12, no. 1-2, pp. 427–446, 2020.